AD-A118 264 CALIFORNIA UNIV IRVINE F/G 8/13
TWO-DIMENSIONAL NUMERICAL MODEL OF COUPLED HEAT AND MOISTURE TR--ETC(U)
AUG 82 G L GUYMON, T V HROMADKA DAAG29-79-C-0080
UNCLASSIFIED ARO-16278.25-GS NL

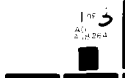

ARO 16278.25-GS

2

TWO-DIMENSIONAL NUMERICAL MODEL OF COUPLED HEAT AND MOISTURE TRANSPORT IN FROST HEAVING SOILS

FINAL REPORT

Gary L. Guymon

T. V. Hromadka II

August 1982

U.S. ARMY RESEARCH OFFICE

CONTRACT DAAG29-79-C-0080

CIVIL ENGINEERING
UNIVERSITY OF CALIFORNIA
IRVINE CA 92717

Approved for Public Release
Distribution Unlimited

DISCLAIMER NOTICE

THIS DOCUMENT IS BEST QUALITY PRACTICABLE. THE COPY FURNISHED TO DTIC CONTAINED A SIGNIFICANT NUMBER OF PAGES WHICH DO NOT REPRODUCE LEGIBLY.

UNCLASSIFIED

SECURITY CLASSIFICATION OF THIS PAGE (When Data Entered)

REPORT DOCUMENTATION PAGE	READ INSTRUCTIONS BEFORE COMPLETING FORM
1. REPORT NUMBER	2. GOVT ACCESSION NO. AD-A118264 / 3. RECIPIENT'S CATALOG NUMBER
4. TITLE (and Subtitle) TWO-DIMENSIONAL NUMERICAL MODEL OF COUPLED HEAT AND MOISTURE TRANSPORT IN FROST HEAVING SOILS	5. TYPE OF REPORT & PERIOD COVERED / 6. PERFORMING ORG. REPORT NUMBER
7. AUTHOR(s) Gary L. Guymon, T. V. Hromadka II	8. CONTRACT OR GRANT NUMBER(s) DAAG29-79-C-0080
9. PERFORMING ORGANIZATION NAME AND ADDRESS Civil Engineering, University of California, Irvine, IRvine, CA 92717	10. PROGRAM ELEMENT, PROJECT, TASK AREA & WORK UNIT NUMBERS
11. CONTROLLING OFFICE NAME AND ADDRESS U. S. Army Research Office, Post Office Box 12211, Research Triangle Park, NC 27709	12. REPORT DATE August 1982 / 13. NUMBER OF PAGES
14. MONITORING AGENCY NAME & ADDRESS (if different from Controlling Office)	15. SECURITY CLASS. (of this report) Unclassified / 15a. DECLASSIFICATION/ DOWNGRADING SCHEDULE

16. DISTRIBUTION STATEMENT (of this Report)

Approved for public release; distribution unlimited.

17. DISTRIBUTION STATEMENT (of the abstract entered in Block 20, if different from Report)

NA

18. SUPPLEMENTARY NOTES

The view, opinions, and/or findings contained in this report are those of the author(s) and should not be construed as an official Department of the Army position, policy, or decision, unless so designated by other documentation.

19. KEY WORDS (Continue on reverse side if necessary and identify by block number)

Numerical model, coupled heat and moisture transport, freezing soils, frost heave, thaw consolidation, cold regions, geothermal analysis.

20. ABSTRACT (Continue on reverse side if necessary and identify by block number)

A two-dimensional numerical model of coupled heat and moisture transport in freezing and thawing soils is developed and tested. For simple but useful geometries the model permits estimation of frost heave and thaw consolidation. The model is coded in FORTRAN IV and is designed to run on mini-class computers.

DD FORM 1 JAN 73 1473 EDITION OF 1 NOV 65 IS OBSOLETE

UNCLASSIFIED

SECURITY CLASSIFICATION OF THIS PAGE (When Data Entered)

TABLE OF CONTENTS

PROBLEM STUDIED

The problem studied was the thermal and moisture regime of freezing and thawing soils. The objective was to provide additional technology for analysis and design of geotechnical structures in cold climates. Such structures include roadway embankments, river levees, airfields, and embankment dams. Specific regions of emphasis were Alaska and Canada.

The basic approach taken was based upon development of a two-dimensional model of coupled heat and moisture transport in soils undergoing phase change. While several widely used two-dimensional models of heat transport alone existed, there was no model of the coupled process of heat and moisture transport. Although one has the luxury of assuming static moisture conditions in a number of important geotechnical studies of freezing or thawing soils, there is a significant class of problems where moisture transport plays an important role; e.g. long-term moisture migration may change bulk thermal parameters and frost heave is entirely dependent on moisture transport.

SUMMARY OF IMPORTANT RESULTS

The results of this three-year research effort have been published in a number of refereed journals which are included in the Appendix. Additionally, three theses/dissertations have been prepared by students who were partially funded by this research project. Their work may be obtained through University microfilms.

Important results can be categorized into four main areas: numerical techniques, model strategy, development of a two-dimensional deterministic model, and probabilistic/uncertainty concepts.

Advances in domain numerical techniques were achieved during the course of the research. The impetus for this advance was the need to accurately calculate the temperature of a soil system so that the freezing/thawing isotherm could be precisely positioned. The need for a high degree of precision is that there is a substantial difference in the strength of unfrozen and frozen soil. Our research has lead to a unification of domain methods into a single mass lumping matric. Through the specification of a single mass lumping factor Galerkin finite element, integrated finite difference, or an infinity of mass lumped domain procedures may be selected.

The second area of advance achieved during the course of the research was the verification of the concept that well established physics-based equations of heat and mass transport could be employed for processes that are well understood. Secondly, less well established processes, such as the dynamic behavior in soil zones undergoing water phase change, can be modeled by phenomenological relationships. However, such an approach necessarily leads to a multiparameter model in which certain phenomenological parameters can only be determined by calibration. In constructing such models care must be exercised in the manner ancillary processes are incorporated into the model. As an example we found that the use of the widely used apparent heat capacity approach led to model inconsistencies and undesirable parameter restraints when incorporating both simultaneous heat and moisture transport into a single model. For this reason we use a modeling approximation based upon an isothermal control volume approach.

A two-dimensional coupled heat and moisture transport model, FROST2B, written in FORTRAN IV, was successfully developed for arbitrary shaped domains.

Components of the model have been verified against linearized analytical simple domain problems, laboratory data, and field data. The model has been applied to several on-going prototype geothermal analysis problems. The model includes a "front-end" data loader and is written to run on the now widespread mini-computers. Some "back-end" graphics capability have also been prepared. Because of the problem of soil interaction-structure interaction during freezing or thawing soils in arbitrarily and possibly complex domains, frost heave calculations are not permitted in the B-version of the program. A second version, FROST2D, for simple but useful geometries (e.g. roadways) has been prepared for frost heave and thaw consolidation estimates. This program includes an internal mesh generator and is applicable to problems where it may be assumed that soil interaction forces are negligible. Both programs are written for variable layer soils and include the ability to deal with surcharge loading. The model is only applicable to low surcharge loadings (i.e. less than 60 kPa).

In the course of our research, it has become quite clear that deterministic models by themselves may not be adequate. Frost heave is apparently highly sensitive to the deterministic parameters that govern moisture flow, in particular, and heat flow, to some extent. The difficulty is in the wide variation in parameters. For example, determination of the hydraulic conductivity in carefully controlled field situations for homogeneous and uniform soils may involve a coefficient of variation of 500 percent. Estimated frost heave may vary over 100 percent with such potential errors in parameter selection. We have developed and applied a point probability estimate technique to evaluating the probabilistic nature of key model parameters, such as hydraulic conductivity, and these concepts have been incorporated into a one-dimensional version of the model (primarily developed with CRREL funding). In the future, these same concepts should be combined with the two-dimensional model.

AVAILABILITY OF COMPUTER CODE

Line printer listings and/or magnetic tapes of the computer code may be obtained from the principal author or from U.S.Army--Cold Regions Research and Laboratory, Hanover, New Hampshire 03755.

LIST OF PUBLICATIONS

Journal Papers

Hromadka II, T. V. and G. L. Guymon, 1980, Numerical Mass Balance for Soil-Moisture Transport Problems, Advances in Water Resources, 3, 107-114.

Hromadka II, T. V. and G. L. Guymon, 1980, A Note on Time Integration of Unsaturated Soil-Moisture Transport, Advances in Water Resources, 3, 181-186.

Hromadka II, T. V. and G. L. Guymon, 1981, Some Approaches to Modeling Phase Change in Freezing Soils, Cold Regions Science and Technology, 4, 137-145.

Hromadka II, T. V. and G. L. Guymon, 1981, Subdomain Integration Model of Ground-Water Flow, ASCE, Irrigation and Drainage Journal, 107(IR2), 187-195.

Hromadka II, T. V. and G. L. Guymon, 1981, Improved Linear Trial Function Finite Element Model of Soil Moisture Transport, Water Resources Research, 17(3), 504-512.

Hromadka II, T. V. and G. L. Guymon, 1981, Nodal Domain Integration Model of One-Dimensional Advection-Diffusion, Advances in Water Resources, 5, 9-16.

Guymon, G. L., R. L. Berg, T. C. Johnson, and T. V. Hromdka II, 1981, Results from a Mathematical Model of Frost Heave, Transportation Research Record, 809, 2-6.

Hromadka II, T. V. and G. L. Guymon, 1982, Numerical Approximation of Linear Two-Dimensional Davection-Diffusion Processes in Rectangular Spatial Domains, Advances in Water Resources, 5, 56-60.

Hromadka II, T. V., G. L. Guymon, G. C. Pardoen, 1981, Nodal Domain Integration Model of Unsaturated Two-Dimensional Soil-Water Flow: Development, Water Resources Research, 17(5), 1425-1430.

Guymon, G. L., M. E. Harr, R. L. Berg, and T. V. Hromadka II, 1981, A Probabilistic-Deterministic Analysis of One-Dimensional Ice Segretation in A Freezing Soil Column, Cold Regions Science and Technology, 5, 127-140.

Hromadka II, T. V. and G. L. Guymon, 1982, Sensitivity of a Frost Heave Model to the Method of Numerical Simulation, Cold Regions Science and Technology, in-press.

Hromadka II, T. V. and G. L. Guymon, 1982, A Note on Approximation of One-Dimensional Heat Transfer With and Without Phase Change, Numerical Heat Transfer, 5, 223-232.

Hromadka II, T. V. and G. L. Guymon, 1982, Mass Lumping Models of the Linear Diffusion Equation, Advances in Water Resources, accepted for publication.

Hromadka II, T. V. and G. L. Guymon, 1982, Application of A Boundary Integral Equation to Prediction of Freezing Fronts in Soil, Cold Regions Science and Technology, accepted for publication.

Guymon, G. L. and T. V. Hromadka II, 1982, Two-Dimensional Model of Coupled Heat and Moisture Transport in Frost Heaving Soils, Canadian Geotechnical Journal, submitted for possible publication.

Theses - Dissertations

Hromadka II, T. V., 1980, Mathematical Model of Frost Heave in Freezing Soils, A dissertation submitted in partial satisfaction of the Ph.D. degree, University of California, Irvine.

Yen, Chung-Cheng, 1981, Numerical Analog of Two-Dimensional Saturated-Unsaturated Flow in Porous Media with a Free Surface, A thesis submitted in partial satisfaction of the M.S. degree, University of California, Irvine.

Abdel-Latif, M., 1982, Some Aspects of Soil-Pile Interaction under Axially Static Loading - A Two-Dimensional Finite Element Approach, A thesis submitted in partial satisfaction of the M.S. degree, University of California, Irvine.

LIST OF SCIENTIFIC PERSONNEL

Gary L. Guymon, Professor of Civil Engineering, Principal Investigator

Gerard C. Pardoen, Associate Professor of Civil Engineering, Co-Principal Investigator

Theodore V. Hromadka II, Ph.D. received 1980.

Chung-Cheng Yen, M.S. received 1981.

Mohamed Abdel-Latif, M.S. received 1982.

APPENDIX

JOURNAL REPRINTS AND MANUSCRIPTS

Numerical mass balance for soil-moisture transport problems

T. V. HROMADKA II and G. L. GUYMON
School of Engineering, University of California, Irvine, CA. 92717, USA

The Galerkin finite element method coupled with the Crank–Nicolson time advance procedure is often used as a numerical analog for unsaturated soil-moisture transport problems. The Crank–Nicolson procedure leads to numerical mass balance problems which results in instability. A new temporal and spatial integration procedure is proposed that exactly satisfies mass balance for the approximating function used. This is accomplished by fitting polynomials continuously throughout the time and space domain and integrating the governing differential equations. To reduce computational effort, the resulting higher order polynomials are reduced to quadratic and linear piece-wise continuous polynomial approximation functions analogous to the finite element approach. Results indicate a substantial improvement in accuracy over the combined Galerkin and Crank–Nicolson methods when comparing to simplified problems where analytical solutions are available.

INTRODUCTION

Finite element techniques have been applied to numerical solutions of moisture transfer in soils by a number of investigators[1–7]. A substantial amount of work has been done on the efficiency and accuracy of finite element Galerkin techniques[3,5,8]. In the case of moisture transfer in unsaturated soils, the equation of state is non-linear and generally in order to apply the finite element method the governing differential equation of state is linearized by forcing parameters to be constant within each finite element. Hromadka and Guymon[6] investigate the numerical effects of various approximations for determining the constant parameters, but assume that the time derivative term is approximated by the Crank–Nicolson time advancement routine. In this paper the coupled numerical analogs based upon the Galerkin finite element method and Crank–Nicolson method are examined in respect to satisfaction of mass balance in the governing equation of state. A numerical modification to the finite element analog of moisture transfer in a horizontal soil column is presented, and extensions to moisture transfer in a vertical soil column and a two-dimensional soil system are included.

TRANSPORT ANALOG

Horizontal infiltration of water into a homogeneous soil column of length L having an initial water content θ_0 and suddenly subjected for time $t>0$ to a greater constant water content θ_1 at $x=0$ is described by:

$$\frac{\partial}{\partial x}\left[D(\theta)\frac{\partial\theta}{\partial x}\right]=\frac{\partial\theta}{\partial t} \tag{1}$$

$$\theta=\theta_0 \quad t=0 \quad 0\leq x\leq L$$

$$\theta=\theta_1 \quad t>0 \quad x=0 \tag{2}$$

where θ is the dimensionless soil volumetric water content; x is the horizontal spatial coordinate; t is time; and $D(\theta)$ is the soil water diffusivity.

The finite element approach used to solve equations (1) and (2) is the Galerkin version of the weighted residual process[2]. The solution domain is discretized into the union of n finite elements by:

$$L=\bigcup_{i=1}^{n} L_i \tag{3}$$

The water content is utilized as the state variable and is approximated within each finite element by:

$$\theta(x,t)=\sum N_j(x,t)\theta_j \tag{4}$$

where N_j is the appropriate linearly independent shape functions; θ_j is the state variable values at elemental-nodal points designated by the general summation index j.

The Galerkin technique utilizes the set of shape functions as the weighting functions, which indicates that the corresponding finite element representation for the infiltration process is

$$\int_L\left\{\frac{\partial}{\partial x}\left[D(\theta)\frac{\partial\theta}{\partial x}\right]-\frac{\partial\theta}{\partial t}\right\}N_i\,dx=0 \tag{5}$$

Integration by parts expands equation (5) into the form:

$$\sum_{i=1}^{n}\left\{D(\theta)\frac{\partial\theta}{\partial x}N_i\Big|_S-\int_L\left[D(\theta)\frac{\partial\theta}{\partial x}\frac{\partial N_i}{\partial x}-N_i\frac{\partial\theta}{\partial t}\right]dx\right\}=0 \tag{6}$$

where S_i is the external endpoints of the one-dimensional finite element, L. The first term within the braces negates to zero for interior elements and also satisfies the usual

0309-1708/80/030107-08$02.00

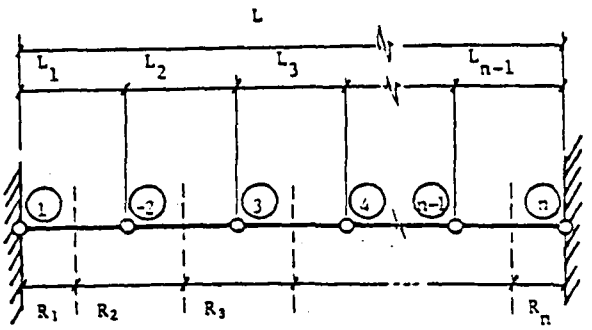

Figure 1. One-dimensional nodal domain. (1) = nodal point number 1; R_1 = nodal domain number 1; L = column length

specified (or flux type) boundary conditions of the problem for exterior finite elements. The remaining integral term is solved by substituting the appropriate element approximations and shape functions into the integrand and solving by numerical integration. The non-linear nature of the partial differential equation, however, generally introduces difficulties in integrating equation (6). It is customary to deal with this problem by assuming the diffusivity function to be constant within each finite element during a finite time interval, Δt (e.g. Guymon and Luthin[4]). The Crank–Nicolson time advancement approximation has been widely used[2,5] to solve the time derivation of equation (6). The time derivative could also be approximated by the Galerkin technique[1]; however, it does not appear to be advantageous[9].

The Crank–Nicolson formulation reduces equation (6), where values of soil–water diffusivity are assumed constant within each finite element, into a system of linear equations expressed in matrix form as:

$$\left\{\mathbf{P}+\frac{\Delta t}{2}\mathbf{S}\right\}\theta^{t-1}=\left\{\mathbf{P}-\frac{\Delta t}{2}\mathbf{S}\right\}\theta^{t} \tag{7}$$

where **P** is a symmetrical capacitance matrix and is a function of element nodal global coordinates; **S** is a symmetrical stiffness matrix and is a function of element nodal global coordinates and constant finite element diffusivity coefficients (during time step Δt); Δt is the finite time step increment; and θ^k is the vector of nodal state variable approximations (volumetric water content) at time steps $k = t, t-1$.

Hromadka and Guymon[6] show that the numerical expressions of the combined equations (6) and (7) results in an incorrect balance of mass for each nodal solution. To correct the mass-balance relations, the time-integrated influx of moisture was equated to the net integrated spatial variation of moisture content. For the special case of a Galerkin linear shape-function approximation (with the Crank–Nicolson time advancement procedure), a modified finite element capacitance matrix was developed; however, a detailed mathematical analysis of the matrix modification was not presented. The following discussion addresses the mathematical development of the modified finite element capacitance matrix (for solution of equation (1)) and extends the modifications to include the so-called convection–diffusion class of equations (i.e., a vertical soil column problem), and finally develops a two-dimensional horizontal moisture transport analog.

MATHEMATICAL DEVELOPMENT

Assume the soil column is discretized into n nodal domains by n nodal points as shown in Fig. 1 where:

$$\left.\begin{aligned} R_1 &\equiv \{x : 0 \le x \le \tfrac{L_1}{2}\} \\ R_j &\equiv \{x : x(\theta_j) - \tfrac{L_{j-1}}{2} < x \le x(\theta_j) + \tfrac{L_j}{2}\} \\ R_n &\equiv \{x : x(\theta_n) - \tfrac{L_{n-1}}{2} < x \le L\} \\ R &\equiv \bigcup_{j=1}^{n} R_j \end{aligned}\right\} \tag{8}$$

where θ_j is the value of state variable at spatial increment j and L_j is the redefined spatial length between nodal points (θ_j, θ_{j-1}).

The solution of equation (1) within each nodal domain determines n equations:

$$\left.\begin{aligned} &\frac{\partial}{\partial x}\left[D(\theta)\frac{\partial\theta}{\partial x}\right]=\frac{\partial\theta}{\partial t} : x\in R_1 \\ &\frac{\partial}{\partial x}\left[D(\theta)\frac{\partial\theta}{\partial x}\right]=\frac{\partial\theta}{\partial t} : x\in R_2 \\ &\qquad\vdots \\ &\frac{\partial}{\partial x}\left[D(\theta)\frac{\partial\theta}{\partial x}\right]=\frac{\partial\theta}{\partial t} : x\in R_n \end{aligned}\right\} \tag{9}$$

Using a local coordinate system defined by:

$$\left.\begin{aligned} &\frac{dy}{dx}=1 \\ &R_j \equiv \{y : 0 < y < l_j\} \end{aligned}\right\} \tag{10}$$

the system defined by equations in (9) can be integrated to give:

$$\begin{bmatrix} \int_{\Delta t}\int_{R_1}\frac{\partial}{\partial y}\left[D(\theta)\frac{\partial\theta}{\partial y}\right]dy\,dt \\ \int_{\Delta t}\int_{R_2}\frac{\partial}{\partial y}\left[D(\theta)\frac{\partial\theta}{\partial y}\right]dy\,dt \\ \vdots \\ \int_{\Delta t}\int_{R_n}\frac{\partial}{\partial y}\left[D(\theta)\frac{\partial\theta}{\partial y}\right]dy\,dt \end{bmatrix} = \begin{bmatrix} \int_{\Delta t}\int_{R_1}\frac{\partial\theta}{\partial t}\,dy\,dt \\ \int_{\Delta t}\int_{R_2}\frac{\partial\theta}{\partial t}\,dy\,dt \\ \vdots \\ \int_{\Delta t}\int_{R_n}\frac{\partial\theta}{\partial t}\,dy\,dt \end{bmatrix} \tag{11}$$

where the temporal integration is assumed to occur over a time-step increment of Δt. Equation (11) can be rewritten as:

$$\begin{bmatrix} \int_{k\Delta t}^{(k+1)\Delta t} \left\{ D\frac{\partial \theta}{\partial y} \Big|_{0}^{l_1} \right\} dt \\ \int_{k\Delta t}^{(k+1)\Delta t} \left\{ D\frac{\partial \theta}{\partial y} \Big|_{0}^{l_2} \right\} dt \\ \vdots \\ \int_{k\Delta t}^{(k+1)\Delta t} \left\{ D\frac{\partial \theta}{\partial y} \Big|_{0}^{l_n} \right\} dt \end{bmatrix} = \begin{bmatrix} \int_{0}^{l_1} \left\{ \theta \Big|_{k\Delta t}^{(k+1)\Delta t} \right\} dy \\ \int_{0}^{l_2} \left\{ \theta \Big|_{k\Delta t}^{(k+1)\Delta t} \right\} dy \\ \vdots \\ \int_{0}^{l_n} \left\{ \theta \Big|_{k\Delta t}^{(k+1)\Delta t} \right\} dy \end{bmatrix} \tag{12}$$

where k is the temporal time step increment.

The state variable, θ, can be approximated spatially throughout R by the Ritz formulation; i.e.

$$\hat{\theta}(x, t_0) = \sum_{j=1}^{n} N_j(x)\theta_j \tag{13}$$

where N_j is the appropriate polynomial spatial shape function and θ_j is the state variable value at nodal points designated by the general summation index j. Additionally, let θ be approximated temporally by:

$$\theta^*(x_0, t) = \sum_{m=-1}^{k-1} M_m \theta^m \tag{14}$$

where M_m is the appropriate polynomial temporal shape function and θ^m is the state variable value at nodal points designated by the general summation index m; $m=0$ indicates the initial condition, $m=-1$ indicates the condition at time step $(-\Delta t)$.

Equations (13) and (14) can be combined as:

$$\left.\begin{aligned} \hat{\theta}(x, t) &= \sum_{j=1}^{n} N_j(x)\theta_j^* \\ \theta_j^* &= \sum_{m=-1}^{k-1} M_m \theta_n^m \end{aligned}\right\} \tag{15}$$

where the θ_n^m are known values of the state variable for time steps $(-1, 0, 1, \ldots, k)$.

Combining equations (12) and (15) yields:

$$\begin{bmatrix} \int_{k\Delta t}^{(k+1)\Delta t} \left\{ D\frac{\partial \hat{\theta}}{\partial y} \Big|_{0}^{l_1} \right\} dt \\ \int_{k\Delta t}^{(k+1)\Delta t} \left\{ D\frac{\partial \hat{\theta}}{\partial y} \Big|_{0}^{l_2} \right\} dt \\ \vdots \\ \int_{k\Delta t}^{(k+1)\Delta t} \left\{ D\frac{\partial \hat{\theta}}{\partial y} \Big|_{0}^{l_n} \right\} dt \end{bmatrix} = \begin{bmatrix} \int_{0}^{l_1} \left\{ \hat{\theta} \Big|_{k\Delta t}^{(k+1)\Delta t} \right\} dy \\ \int_{0}^{l_2} \left\{ \hat{\theta} \Big|_{k\Delta t}^{(k+1)\Delta t} \right\} dy \\ \vdots \\ \int_{0}^{l_n} \left\{ \hat{\theta} \Big|_{k\Delta t}^{(k+1)\Delta t} \right\} dy \end{bmatrix} \tag{16}$$

The solution of equation (16) where water content is approximated by equation (15) results in increasing computational effort as the time solution progresses. By approximating water content both spatially and temporally by sets of piecewise continuous polynomials, the numerical effort is considerably reduced.

For discussion purposes, let the l_i be uniform throughout R, and soil-water diffusivity held constant during time step Δt.

$$\left.\begin{aligned} &l_i = \Delta x;\ i = 1, 2, \ldots, n \\ &l_1 = l_n = \Delta x/2 \\ &\frac{\partial D}{\partial t} = 0;\ k\Delta t < t < (k+1)\Delta t \end{aligned}\right\} \tag{17}$$

Then for water content characterized by parabolas both spatially and temporally:

$$\left.\begin{aligned} \hat{\theta}(y, t_0) &= \left[\frac{\theta_0 - 2\theta_1 + \theta_2}{2(\Delta x)^2}\right]y^2 + \left[\frac{4\theta_1 - 3\theta_0 - \theta_2}{2\Delta x}\right]y + \theta_0 \\ \hat{\theta}(y_0, t) &= \left[\frac{\theta^0 - 2\theta^1 + \theta^2}{2(\Delta t)^2}\right]t^2 + \left[\frac{4\theta^1 - 3\theta^0 - \theta^2}{2\Delta x}\right]t + \theta^0 \end{aligned}\right\} \tag{18}$$

where $(\theta_0, \theta_1, \theta_2)$ represent typical nodal points separated by the constant spatial increment Δx; and $(\theta^0, \theta^1, \theta^2)$ represent typical nodal points separated by the constant temporal increment Δt. The spatial gradient of water content is evaluated by:

$$\left.\begin{aligned} \frac{\partial \theta}{\partial y}\Big|_0 &= (\theta_1^* - \theta_0^*)/\Delta x \\ \frac{\partial \theta}{\partial y}\Big|^{\Delta x} &= (\theta_2^* - \theta_1^*)/\Delta x \\ \theta\left(y = \frac{\Delta x}{2}\right) &= \theta_1^* \end{aligned}\right\} \tag{19}$$

where the starred terms represent functions of time as defined by equation (18). In order to coincide interpolating parabolas between nodal points, the average of all interpolating parabolas within a nodal domain are used. Accordingly, interior nodal points may have up to five nodal points contributing to each nodal point's numerical solution.

NUMERICAL MODEL VERIFICATION

The proposed numerical scheme was applied to the normalized soil moisture transfer problem:

$$\frac{\partial^2 \theta}{\partial x^2} = \frac{\partial \theta}{\partial t} \qquad 0 \leqslant x \leqslant 1 \tag{20}$$

with boundary conditions

$$\theta(0, t) = (1, t) = 0 \qquad t > 0 \tag{21}$$

and initial condition

$$\theta(x, 0) = 1 \tag{22}$$

The exact solution is the well-known series expansion:

$$\theta(x, t) = \frac{4}{\pi}\left(\sin \pi x e^{-\pi^2 t} + \frac{\sin 3\pi x}{3} e^{-9\pi^2 t} + \dots\right) \tag{23}$$

For the normalized soil moisture transfer problem, the numerical approach of equations (16) and (18) reduces to the following set of linear equations:

$$\frac{\Delta t}{12(\Delta x)}\{-(\theta_1^0 - 2\theta_2^0 + 3\theta_3^0) + 8(\theta_1^1 - 2\theta_2^1 + \theta_3^1) +$$

$$5(\theta_1^2 - 2\theta_2^2 + \theta_3^2)\} = \frac{\Delta x}{48}\{-(\theta_0^2 + 6\theta_1^2 - 38\theta_2^2 + 6\theta_3^2 - \theta_4^2) -$$

$$(-\theta_0^1 - 6\theta_1^1 + 38\theta_2^1 - 6\theta_3^1 - \theta_4^1)\} \tag{24}$$

The first set of braces equals the net integrated influx of moisture between time steps Δt and $2\Delta t$ (superscripts 1 and 2, respectively); the second set of braces is the integrated variation of water content during the time advancement. For $\beta = 4(\Delta t)/(\Delta x)^2$, equation (24) may be rewritten as:

$$-\theta_0^2 - \theta_1^2(6 - 5\beta) - \theta_2^2(38 + 10\beta) + \theta_3^2(6 - 5\beta) - \theta_4^2$$

$$= -\beta(\theta_1^0 - 2\theta_2^0 - \theta_3^0) + \theta_1^1(6 + 8\beta) + \theta_2^1(38 - 16\beta) -$$

$$\theta_3^1(6 + 8\beta) - (\theta_0^1 - \theta_4^1) \tag{25}$$

where superscripts and subscripts refer to temporal and spatial coordinates. Appropriate integration with respect to space and time on column-end nodal domains gives for the global matrix system (with specified boundary conditions)

$$\begin{bmatrix} 1 & 0 & 0 & 0 & \dots & \dots & \dots & 0 \\ (3-5\beta) & (41+10\beta) & (5-5\beta) & -1 & 0 & \dots & \dots & 0 \\ -1 & (6-5\beta) & (38-10\beta) & (6-5\beta) & -1 & 0 & \dots & 0 \\ 0 & -1 & (6-5\beta) & (38+10\beta) & (6-5\beta) & -1 & \dots & 0 \\ \vdots & & & & & & & \\ 0 & 0 & -1 & (5-5\beta) & (41-10\beta) & (3-5\beta) & & \\ 0 & 0 & & 0 & 0 & 1 & & \end{bmatrix} \theta^{j+1} =$$

$$\begin{bmatrix} 1 & 0 & 0 & & 0 & 0 & \dots & 0 \\ (3+5\beta) & (-16\beta+41) & (8\beta+5) & -1 & 0 & 0 & \dots & 0 \\ -1 & (6+8\beta) & (38-16\beta) & (6+8\beta) & -1 & 0 & \dots & 0 \\ 0 & -1 & (6+8\beta) & (38-16\beta) & (6+8\beta) & -1 & \dots & 0 \\ \vdots & & & & & & & \\ 0 & 0 & & -1 & (5+8\beta) & (41-16\beta) & & (3+8\beta) \\ 0 & 0 & & & 0 & 0 & & 1 \end{bmatrix} \theta^j -$$

$$\begin{bmatrix} 0 & 0 & 0 & 0 & 0 \\ 1 & -2 & 1 & 0 & 0 \\ 0 & 1 & -2 & 1 & 0 \\ \vdots & & & & \\ 0 & 0 & & 1 & -2 & 1 \\ 0 & 0 & & 0 & 0 & 0 \end{bmatrix} \theta^{j-1} \tag{26}$$

where θ^j is the vector of nodal water content values at time steps $j = 0, 1, 2$ of Δt increments.

Equation (26) can be simplified by assuming all interpolating parabolas within a defined nodal domain to be coincident. Thus, for interior nodal domains the appropriate integrated relations become:

$$\frac{\Delta t}{12(\Delta x)}\{-(\theta_1^0 - 2\theta_2^0 + \theta_3^0) + 8(\theta_1^1 - 2\theta_2^1 + \theta_3^1) +$$

$$5(\theta_1^2 - 2\theta_2^2 + \theta_3^2)\} = \frac{\Delta x}{24}\{(\theta_1^2 - 22\theta_2^2 + \theta_3^2) -$$

$$(\theta_1^1 + 22\theta_2^1 + \theta_3^1)\} \tag{27}$$

where the first and second set of braces represent the integrated moisture influx and integrated variation of water content, respectively, between time steps Δt and $2\Delta t$ (superscripts $j = 1, 2$). For $\gamma = 2(\Delta t)/(\Delta x)^2$ and appropriate integration with respect to space and time on column-end nodal domains, the global matrix system corresponding to the numerical approximations of equation (20) by equations (16) and (18) is:

$$\begin{bmatrix} 1 & 0 & 0 & 0 & \dots & 0 \\ (1-5\gamma) & (22+10\gamma) & (1-5\gamma) & 0 & \dots & 0 \\ 0 & (1-5\gamma) & (22+10\gamma) & (1-5\gamma) & \dots & 0 \\ \vdots & & & & & \\ 0 & \dots & 0 & 0 & (1-5\gamma) & (22+10\gamma) & (1-5\gamma) \\ 0 & \dots & 0 & 0 & 0 & 0 & 1 \end{bmatrix} \theta^j -$$

$$\begin{bmatrix} 1 & 0 & 0 & 0 & 0 & \dots & 0 \\ (1-6\gamma) & (22-16\gamma) & (1-8\gamma) & 0 & \dots & & 0 \\ 0 & (1-8\gamma) & (22-16\gamma) & (1-8\gamma) & \dots & & 0 \\ \vdots & & & & & & \\ 0 & 0 & 0 & 0 & (1-8\gamma) & (22-16\gamma) & (1-6\gamma) \\ 0 & 0 & 0 & 0 & 0 & 0 & 1 \end{bmatrix} \theta^{j-1} -$$

$$\begin{bmatrix} 0 & & & & & 0 \\ 1 & -2 & 1 & 0 & \dots & 0 \\ 0 & 1 & -2 & 1 & 0 & \dots & 0 \\ \vdots & & & & & & \\ 0 & \dots & & 0 & 1 & -2 & 1 \\ 0 & \dots & & 0 & 0 & 0 & 0 \end{bmatrix} \theta^{j-2} \tag{28}$$

where specified boundary conditions are included.

Equation (28) can be further simplified temporally by letting:

$$\frac{\partial \theta}{\partial t} = \frac{\theta^{j+1} - \theta^j}{\Delta t} \tag{29}$$

Then, combining equations (27) and (29):

$$\frac{1}{2\Delta x}[(\theta_2^2 - \theta_1^2) - (\theta_1^2 - \theta_0^2) + (\theta_2^1 - \theta_1^1) - (\theta_1^1 - \theta_0^1)]$$

$$= \frac{\Delta x}{24}[(\theta_1^2 - 22\theta_2^2 + \theta_3^2) - (\theta_1^1 + 22\theta_2^1 + \theta_3^1)] \tag{30}$$

which results in the modified capacitance matrix formulation[6]:

$$\hat{\mathbf{P}}\ (\text{modified}) \equiv \frac{\Delta x}{24}\begin{bmatrix} 11 & 1 \\ 1 & 11 \end{bmatrix} \tag{31}$$

To determine the numerical effectiveness of solving the normalized soil-water transfer problem by the formu-

Table 1. Comparison of numerical model results at x = 0.50*

Time	Finite element method†	Nodal domain integration‡	Exact solution	Finite element error (%)	Nodal integration error (%)
0.01	0.887	0.901	0.999	11	9
0.02	0.786	0.833	0.975	19	15
0.03	0.697	0.763	0.918	24	17
0.04	0.618	0.700	0.846	27	17
0.05	0.548	0.641	0.772	29	17
0.06	0.486	0.588	0.702	28	16
0.07	0.431	0.538	0.637	32	16
0.08	0.382	0.493	0.578	34	15
0.09	0.339	0.452	0.524	35	14
0.10	0.301	0.414	0.474	36	13
0.11	0.267	0.380	0.430	38	12
0.12	0.237	0.348	0.390	39	11
0.13	0.210	0.319	0.353	40	10
0.14	0.186	0.292	0.320	42	9
0.15	0.165	0.268	0.290	43	8
0.16	0.146	0.246	0.262	44	6
0.17	0.130	0.225	0.238	46	5
0.18	0.115	0.206	0.215	47	4
0.19	0.102	0.189	0.195	48	3
0.20	0.091	0.173	0.177	49	2

* Three nodal point discretization.
† Equation (32).
‡ Simplified version of nodal integration using equation (28).

lations of equations (24), (27), and (30), a Galerkin finite element analog to equation (20) was also determined for comparison. The Galerkin finite element-matrix formulation (for a linear polynomial shape function approximation) numerically approximates the normalized problem of equation (20) within each finite element by:

$$\hat{\mathbf{S}}\begin{Bmatrix}\theta_i\\ \theta_j\end{Bmatrix}+\hat{\mathbf{P}}\begin{Bmatrix}\dot{\theta}_i\\ \dot{\theta}_j\end{Bmatrix}=\frac{1}{\Delta x}\begin{bmatrix}1 & -1\\ -1 & 1\end{bmatrix}\begin{Bmatrix}\theta_i\\ \theta_j\end{Bmatrix}+\frac{\Delta x}{6}\begin{bmatrix}2 & 1\\ 1 & 2\end{bmatrix}\begin{Bmatrix}\dot{\theta}_i\\ \dot{\theta}_j\end{Bmatrix} \tag{32}$$

where $\hat{\mathbf{S}}$ and $\hat{\mathbf{P}}$ are element stiffness and capacitance matrices and (θ_i, θ_j) and $(\dot{\theta}_i, \dot{\theta}_j)$ refer to the element nodal and dynamic nodal moisture content values for an element of length Δx.

By comparison, the modified finite element-matrix system for equation (31) is:

$$\hat{\mathbf{S}}\begin{Bmatrix}\theta_i\\ \theta_j\end{Bmatrix}+\hat{\mathbf{P}}\ (\text{modified})\begin{Bmatrix}\dot{\theta}_i\\ \dot{\theta}_j\end{Bmatrix}=\frac{1}{\Delta x}\begin{bmatrix}1 & -1\\ -1 & 1\end{bmatrix}\begin{Bmatrix}\theta_i\\ \theta_j\end{Bmatrix}+\frac{\Delta x}{24}\begin{bmatrix}11 & 1\\ 1 & 11\end{bmatrix}\begin{Bmatrix}\dot{\theta}_i\\ \dot{\theta}_j\end{Bmatrix} \tag{33}$$

Results from application of equation (11) to the problem defined by equation (20) are shown in Table 1. The matrix system of equation (28) is used to better compare numerical results to the linear approximating function results of the Galerkin approximation (linear polynomial shape function) of equations (7) and (32). The numerical approximation was based on a three nodal discretization of the one-dimensional domain in which two of the nodal points are specified as boundary conditions; thus the matrix systems reduce to a single linear equation for both numerical approximations. From Table 1, it is seen that for this problem the numerical approach of equation (28) provides increasingly accurate results whereas the finite element approximation progressively gives poorer approximations for the same level of spatial discretization. Additionally, the numerical approach of equation (28) produces similar approximations to those obtained by revising the Galerkin capacitance matrix in accordance with equations (7) and (33).

For further comparison, the nodal domain of equation (20) was discretized by five nodal points. Comparison of numerical solutions by the Galerkin finite element approach, equations (7) and (32); the revised finite element capacitance matrix approach, equations (7) and (33); and the numerical approximation given by equation (26) to the exact solution at $x = 0.50$ are shown in Table 2. Again, the nodal integration approach provides significant improvement over the finite element method. From Table 2, the finite element matrix system revised by equation (31) gives similar results to the model of equation (26) for time greater than 0.06. However, for the initial instability to the numerical system (due to the boundary conditions) the numerical approach of equation (26) provides better approximations.

EXTENSION TO ONE-DIMENSIONAL CONVECTION-DIFFUSION EQUATION

The second order linearized partial differential equation:

$$\frac{\partial}{\partial x}k_1\frac{\partial\theta}{\partial x}-k_2\frac{\partial\theta}{\partial x}=k_3\frac{\partial\theta}{\partial t};\quad x\in R \tag{34}$$

applies to a vertical unsaturated soil column problem where the k_i are the appropriate hydraulic parameters. Discretizing the domain into uniform nodal domains R_j in accordance with equation (8), equation (34) can be integrated spatially within each nodal domain to give:

$$k_1\frac{\partial\theta}{\partial x}\Big|_1^*-\int_R^* k_2\frac{\partial\theta}{\partial x}\,dx=\int_R^* k_3\frac{\partial\theta}{\partial t}\,dx \tag{35}$$

Table 2. Comparison of numerical model results at x = 0.50*

Time	Finite element method†	Revised capacitance matrix‡	Nodal integration per (26)	Exact solution
0.01	1.041	0.989	1.023	0.999
0.02	0.970	0.941	0.956	0.975
0.03	0.881	0.876	0.887	0.918
0.04	0.796	0.807	0.812	0.846
0.05	0.718	0.739	0.741	0.772
0.06	0.647	0.674	0.674	0.702
0.07	0.583	0.614	0.613	0.637
0.08	0.525	0.558	0.557	0.578
0.09	0.472	0.508	0.506	0.524
0.10	0.427	0.461	0.460	0.474
0.11	0.385	0.419	0.418	0.430
0.12	0.347	0.381	0.379	0.390
0.13	0.312	0.346	0.345	0.353
0.14	0.282	0.314	0.313	0.320
0.15	0.254	0.285	0.284	0.290
0.16	0.229	0.259	0.258	0.262
0.17	0.207	0.235	0.235	0.238
0.18	0.186	0.214	0.213	0.215
0.19	0.167	0.194	0.194	0.195
0.20	0.151	0.176	0.176	0.177

* Five nodal point discretization.
† Equation (32).
‡ Equation (33).

Table 3 Comparison of numerical model results for a vertical column

Solution	$x=0$	$x=50$	Error	$x=100$
Exact	1	0.276	0%	0
Finite element method	1	0.429	55%	0
Integration	1	0.342	24%	0

Assuming the k_i to be constant within each nodal domain during a time step Δt, and integrating with respect to time gives:

$$\int_{\Delta t}\left(k_1\frac{\partial\theta}{\partial x}\right)_{\Gamma}dt+\int_{\Delta t}\left(k_2\theta\right)_{\Gamma_t}dt=\left(\int_{R_i}k_3\theta\,dx\right)_{\Gamma} \tag{36}$$

where Γ_x and Γ_t are the spatial and temporal boundaries. For θ approximated spatially and temporally by equation (18), and assuming coincident parabolic interpolation functions within each nodal domain R_i, the resulting expression for an interior nodal point θ_1 between nodal points (θ_0, θ_2) is:

$$A_1\theta_0^2-A_2\theta_1^2+A_3\theta_2^2=B_1\theta_0^1+B_2\theta_1^1+B_3\theta_2^1+C_1\theta_0^0+C_2\theta_1^0+C_3\theta_2^0 \tag{37}$$

where

$$A_1=k_3+5k_2(\Delta t/\Delta x)-5\alpha k_1$$

$$A_2=22k_3+10\alpha k_1$$

$$A_3=k_3-5k_2(\Delta t/\Delta x)-5\alpha k_1$$

$$B_1=8\alpha k_1-8k_2(\Delta t/\Delta x)+k_3$$

$$B_2=-16\alpha k_1+22k_3$$

$$B_3=8\alpha k_1+8k_2(\Delta t/\Delta x)+k_3$$

$$C_1=-k_1\alpha+k_2(\Delta t/\Delta x)$$

$$C_2=2\alpha k_1$$

$$C_3=-k_1\alpha-k_2(\Delta t/\Delta x)$$

and where $\alpha=2(\Delta t)/(\Delta x)^2$.

Disregarding the coincident parabolic interpolation function assumption, a soil-moisture transfer mass balance would occur by averaging all possible parabolic interpolations within each R_i. Accordingly, for a typical nodal point θ_2 interior to the sequence of nodal points (θ_0, θ_1, θ_3, θ_4),

$$\theta_{R\,\mathrm{adj}_2}=\frac{1}{16}\theta_0-\frac{5}{8}\theta_1-\frac{5}{8}\theta_3-\frac{1}{16}\theta_4 \tag{38}$$

whereby equation (38) can be appropriately combined with equation (28) to give the complete mass balance formulation.

A numerical advantage of equation (37) to a linear shape function finite element (Galerkin) formulation with a Crank-Nicolson time step advancement process was found. The two methods were compared to the exact solution of the problem

$$k_1\frac{\partial^2\theta}{\partial x^2}-k_2\frac{\partial\theta}{\partial x}=\frac{\partial\theta}{\partial t} \tag{39}$$

with conditions,

$$\theta(0,t)=\theta_0, \qquad t>0$$

$$\theta(\infty,t)=0, \qquad t>0$$

$$\theta(x,0)=0, \qquad 0\leqslant x\leqslant\infty$$

The well known solution to equation (39) is the expression:

$$\frac{\theta}{\theta_0}=\frac{1}{2}\left\{\operatorname{erfc}\left[\frac{x-k_2t}{(4k_1t)^{1/2}}\right]+\exp\left[\frac{xk_2}{k_1}\right]\operatorname{erfc}\left[\frac{x-k_2t}{(4k_1t)^{1/2}}\right]\right\} \tag{40}$$

where k_1 and k_2 are assumed constant. Equation (39) was solved for arbitrarily selected values of $k_1=2.5$, $k_2=0.0625$. A time step $\Delta t=25$ was used and equation (39) was modelled by assuming that

$$\theta(100,t)=0, \qquad 0\leqslant t\leqslant 250 \tag{41}$$

in order to obtain a finite one-dimensional domain. For comparison purposes, a two element discretization of element size equal to 50 was used. A linear shape function *Galerkin approximation in* accordance with equations (6) and (7) was used for comparison purposes. For a total time equal to 250, the numerical results are shown in Table 3. Comparison of both numerical methods indicates consistent approximation improvement by using a model based on equation (37).

EXTENSION TO TWO-DIMENSIONS

The two-dimensional mathematical model for horizontal soil water transport in a rectangular domain R, where water content is the state variable is given by:

$$\frac{\partial}{\partial x}\left[D(\theta)\frac{\partial\theta}{\partial x}\right]+\frac{\partial}{\partial y}\left[D(\theta)\frac{\partial\theta}{\partial y}\right]=\frac{\partial\theta}{\partial t};\ (x,y)\in R \tag{42}$$

Analogous to the one-dimensional case, the domain is discretized into n rectangular nodal domains by n nodal points as shown in Fig. 2.

$$R=\bigcup_{i=1}^{n}R_i \tag{43}$$

Application of equation (42) to each R_i gives

$$\frac{\partial}{\partial x}\left[D(\theta)\frac{\partial\theta}{\partial x}\right]+\frac{\partial}{\partial y}\left[D(\theta)\frac{\partial\theta}{\partial y}\right]=\frac{\partial\theta}{\partial t};\ (x,y)\in R_i,\ \forall \tag{44}$$

Integrating spatially and temporally on each R_i gives

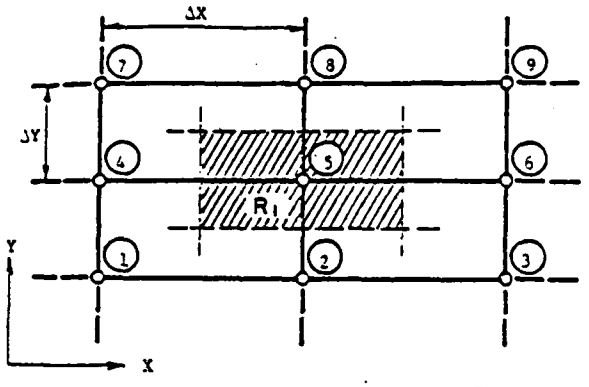

Figure 2. Two-dimensional nodal domain. (i) = *nodal point i;* R_i = *nodal domain number i;* $\Delta X \sim x$-*direction increment;* $\Delta Y \sim y$-*direction increment;* $R = \bigcup_{i=1}^{n} R_i$

$$\int_{\Delta t}\int_{R_i}\int\frac{\partial}{\partial x}\left[D(\theta)\frac{\partial\theta}{\partial x}\right]dx\,dy\,dt+\int_{\Delta t}\int_{R_i}\int\frac{\partial}{\partial y}\left[D(\theta)\frac{\partial\theta}{\partial y}\right]dy\,dx\,dt = \int_{R_i}\int_{\Delta t}\int\frac{\partial\theta}{\partial t}dt\,dx\,dy \qquad i=1,2,\ldots,n \tag{45}$$

or

$$\int_{\Delta t}\int_{\Delta y}\int\left\{D(\theta)\frac{\partial\theta}{\partial x}\right\}_{\Gamma_x}dy\,dt+\int_{\Delta t}\int_{\Delta x}\int\left\{D(\theta)\frac{\partial\theta}{\partial y}\right\}_{\Gamma_y}dx\,dt = \int_{\Delta x}\int_{\Delta y}\int\{\theta\}_{\Gamma_t}dx\,dy \qquad i=1,2,\ldots,n \tag{46}$$

where (ΔX, ΔY, Δt) are the spatial and temporal increments respectively and (Γ_x, Γ_y, Γ_t) are the spatial and temporal boundaries respectively. For a finite element domain discretization, assuming soil water diffusivity constant within each finite element during a time step Δt, equation (46) can be written as:

$$\int_{\Delta t}\left(\int_{0}^{\Delta Y/2}\left\{D\frac{\partial\theta}{\partial x}\right\}_{\Gamma_x}dy+\int_{\Delta Y/2}^{\Delta Y}\left\{D\frac{\partial\theta}{\partial x}\right\}_{\Gamma_x}dy\right)dt+$$

$$\int_{\Delta t}\left(\int_{0}^{\Delta x/2}\left\{D\frac{\partial\theta}{\partial y}\right\}_{\Gamma_y}dx+\int_{\Delta x/2}^{\Delta x}\left\{D\frac{\partial\theta}{\partial y}\right\}_{\Gamma_y}dx\right)dt = \int_{\Delta x}\int_{\Delta y}\{\theta\}_{\Gamma_t}dy\,dx \tag{47}$$

A numerical analog can be derived by considering the normalized two-dimensional horizontal moisture transfer model similar to equations (20), (21), (22),

$$\frac{\partial^2\theta}{\partial x^2}+\frac{\partial^2\theta}{\partial y^2}=\frac{\partial\theta}{\partial t}; \qquad 0\leq x\leq 1,\ 0\leq y\leq 1 \tag{48}$$

Assume θ to be approximated spatially by parabolic interpolating functions, and temporally by a linear interpolating function. The temporal term of (46) is given numerically by considering Fig. 2; i.e.

$$\int_{\Delta x}\int_{\Delta y}\theta\,dx\,dy=\frac{\Delta X\Delta Y}{576}(\theta_1+\theta_3+\theta_7+\theta_9+22\theta_2+22\theta_4+22\theta_6+22\theta_8+484\theta_5) \tag{49}$$

The integrated x-direction influx is:

$$\frac{\Delta Y}{24\Delta X}(\theta_1-2\theta_2+\theta_3+22\theta_4-44\theta_5+22\theta_6+\theta_7-2\theta_8+\theta_9) \tag{50}$$

Similarly, the integrated y-direction influx is:

$$\frac{\Delta X}{24\Delta Y}(\theta_1+\theta_3+\theta_7+\theta_9+22\theta_2+22\theta_8-2\theta_4-2\theta_6-44\theta_5) \tag{51}$$

Combining equations (50) and (51), the net integrated influx is, for $\Delta X=\Delta Y$:

$$\frac{1}{12}(\theta_1+10\theta_2+\theta_3+10\theta_4-44\theta_5+10\theta_6+\theta_7+10\theta_8+\theta_9) \tag{52}$$

For identical constant spatial increments, the solution of equation (46) reduces to the one-dimensional problem of equation (20) for zero y-directional influx. From Fig. 2 and equations (49) and (52), the problem simplifying assumptions are:

$$\left.\begin{aligned}&\frac{\partial\theta}{\partial y}=0\\&\Delta X=\Delta Y\\&\theta_1=\theta_4=\theta_7\\&\theta_2=\theta_5=\theta_8\\&\theta_3=\theta_6=\theta_9\end{aligned}\right\} \tag{53}$$

By substitution, the matrix system defined by equations (49) and (52) reduce to the matrix system defined by equation (30).

CONCLUSIONS

The mathematical analysis leading to numerical analogs that preserve mass balance in a horizontal soil transport problem is presented. Extensions from the one-

dimensional horizontal soil-transport model to the so-called linearized convection diffusion equation is also presented. Comparison of numerical results to the appropriate finite element numerical solutions indicate significant improvement when utilizing the mass balanced schemes.

Extension of the one-dimensional approach to two dimensions is additionally included. Although only the rectangular domain is analysed, application of the improved model to irregular domains is accomplished by using the usual finite element matrices for non-rectangular regions, and including the mass-balanced matrix systems for the remaining rectangular regions.

ACKNOWLEDGEMENTS

This research was supported by an U.S. Army Research Office Contract No. DAAG 29-79-C-0080.

REFERENCES

1. Bruen, J. C. Jr. and Zvsoloski, G. Solution of vertical unsaturated flow of soil water. *Soil Sci.* 1974, 116, 41.
2. Desai, C. S. *Elementary Finite Element Method*. Prentice-Hall, Englewood Cliffs, 1979.
3. Douglas, J. Jr., and Dupont, T. Galerkin methods for parabolic equations. *SIAM J. Numer. Anal.* 1970, 7, 575.
4. Guymon, G. L. and Luthin, J. N. A coupled heat and moisture transport model for artic soils. *Water Resour. Res.* 1974, 10, 995.
5. Haynoe, H. M. Studs of relative efficiency of finite difference Galerkin techniques for modeling soil water transfer. *Water Resour. Res.* 1978, 14, 97.
6. Hromadka, T. V. and Guymon, G. L. Some effects of linearizing the unsaturated soil-moisture transfer diffusion model. *Water Resour. Res.* in press.
7. Newman, S. P., Feddes, R. A. and Bresler, E. Finite element analysis of two-dimensional flow in soils considering water uptake by roots. I. Theory. *Soil Sci. Soc. Am. Proc.* 1975, 39.
8. Price, H. S., Cavendish, J. C. and Varga, R. S. Numerical methods of higher-order accuracy for diffusion convection equations. *Soc. Pet. Eng.* 1968, 243, 293.
9. Yoon, Y. S. and Yeh, W. W.-G. The Galerkin method for nonlinear parabolic equations of unsteady groundwater flow. *Water Resour. Res.* 1975, 11, 751.

A note on time integration of unsaturated soil–moisture transport

T. V. HROMADKA II and G. L. GUYMON
School of Engineering, University of California, Irvine, Ca 92717, USA
(Received 29 February 1980)

The non-linear soil-moisture diffusivity model can be approximately linearized by using values of diffusivity assumed constant for small intervals of space and time. By a series expansion of the diffusivity function and integrating the resulting series of differential equations with respect to time, an improved numerical model is developed. Results from application of this new approach to a sharp wetting-front soil infiltration problem indicates that a 67% saving in numerical effort is achieved at comparable estimation accuracy levels when using the traditional finite timestep Crank–Nicolson approach.

INTRODUCTION

The study of numerical methods for the approximation of non-linear soil–moisture transport in a horizontal column has received recent attention. Hayhoe[2] compared the numerical effectiveness between the finite element and finite difference numerical methods in modelling a sharp wetting-front soil infiltration problem. A special finite difference analog was advanced as the best numerical approach to the problem studied. Hromadka and Guymon[5] further studied the sharp wetting-front problem and developed a modification to the finite element method which resulted in an increase in model accuracy for a linear soil–water diffusivity problem. For a non-linear diffusivity problem, the traditional finite element formulation gave superior results to Hayhoe's finite difference approach when the finite element analog used constant element diffusivity values as determined by a spatial estimation procedure[6].

In this paper, the non-linear soil–water diffusivity problem is re-examined with respect to the finite element modified procedure which we call the 'nodal integration method'. By expanding the diffusivity function as a Taylor series time expansion, the governing equations can be temporally integrated. This procedure results in a numerical analog similar to the nodal integration formulation, but with a constant element diffusivity value determined by a temporal integration. This new numerical approach enables the finite timestep increment to be increased and yet retain similar numerical approximation accuracy. Although the quasi-constant values of diffusivity used to linearize the mathematical model require additional computational effort, the overall computer execution costs are reduced. Reduced costs are achieved because of reduction in the number of finite timestep advancements of the problem's global matrices.

The mathematical development of this numerical procedure is presented herein. As a case study, the integration procedure is used to approximate the numerically difficult problem previously studied by Hayhoe[2] and Hromadka and Guymon[4].

MATHEMATICAL DEVELOPMENT

The one-dimensional horizontal soil–moisture transport model for an unsaturated soil column is:

$$\frac{\partial}{\partial x}\left[D\frac{\partial\theta}{\partial x}\right]=\frac{\partial\theta}{\partial t};\quad x\in R$$
$$R\equiv\{x;0\leqslant x\leqslant L\} \tag{1}$$

where θ is the volumetric water content (θ less than the soil's porosity); x is the spatial coordinate; t is time; D is the soil–water diffusivity and is a function of soil–water content; and R is the spatial domain of definition.

The domain R can be discretized by n nodal points $\theta_j (j=1, 2, \ldots, n)$ into n disjoint subsets:

$$\begin{aligned}
R_1&\equiv\{x;0\leqslant x\leqslant(x(\theta_1)-x(\theta_2))/2\}\\
R_2&\equiv\{x;(x(\theta_1)-x(\theta_2))/2<x\leqslant(x(\theta_2)-x(\theta_3))/2\}\\
&\vdots\\
R_n&\equiv\{x;(x(\theta_{n-1})-x(\theta_n))/2<x\leqslant x(\theta_n)=L\}
\end{aligned} \tag{2}$$

where $x(\theta_j)$ is the spatial coordinate associated to nodal point θ_j, and

$$R=\bigcup_{j=1}^{n} R_j \tag{3}$$

Equation (1) must be satisfied on each R_j. Therefore, n equations are generated by solving:

$$\frac{\partial}{\partial x}\left[D\frac{\partial\theta}{\partial x}\right]=\frac{\partial\theta}{\partial t};\quad x\in R_j,\ \forall_j \tag{4}$$

0309-1708/80/0403-0181/$02.00/0

where

$$D = D(\theta)$$
$$\theta = \theta(x,t) \tag{5}$$

Integrating equation (4) with respect to space gives:

$$\left\{D\frac{\partial\theta}{\partial x}\right\}\Big|_{\Gamma_j} = \frac{\partial}{\partial t}\int_{R_j}\theta\,dx; \qquad x\in R_j,\ \forall_j \tag{6}$$

where Γ_j is the spatial boundary of region R_j. Integrating equation (6) with respect to time gives:

$$\int_{k\Delta t}^{(k+1)\Delta t}\left\{D\frac{\partial\theta}{\partial x}\right\}\Big|_{\Gamma_j} dt = \int_{R_j}\{\theta\}\Big|_{\Gamma_t} dx \tag{7}$$

where Γ_t is the limits of temporal integration between timesteps $k\Delta t$ and $(k+1)\Delta t$. Equation (7) can be simplified by using the linear transformation:

$$t = k\Delta t + \varepsilon$$
$$0 \leqslant \varepsilon \leqslant \Delta t \tag{8}$$

Thus,

$$\int_0^{\Delta t}\left\{D(k\Delta t+\varepsilon)\frac{\partial\theta(k\Delta t+\varepsilon)}{\partial x}\right\}\Big|_{\Gamma_j} d\varepsilon = \int_{R_j}\{\theta\}\Big|_{\Gamma_t} dx \tag{9}$$

The soil-water diffusivity function can be expressed with respect to time by the Taylor series:

$$D(x=x_0,\ k\Delta t-\varepsilon) = \sum_{i=0}^{r}\frac{D^{(i)}(x=x_0,\ k\Delta t)\varepsilon^i}{i!} \tag{10}$$

where i is the ith order temporal differential operator; and x_0 is a specified spatial coordinate. Combining equations (9) and (10) gives:

$$\int_0^{\Delta t}\left\{\left(\sum_{i=0}^{r}\frac{D^{(i)}(k\Delta t)\varepsilon^i}{i!}\right)\frac{\partial\theta(k\Delta t+\varepsilon)}{\partial x}\right\}\Big|_{\Gamma_j} d\varepsilon = \int_{R_j}\{\theta\}\Big|_{\Gamma_t} dx \tag{11}$$

For a spatial local coordinate system defined by:

$$y = x - (x(\theta_j) + x(\theta_{j-1}))/2 \qquad x\in R_j$$
$$dy = dx$$
$$l_j = (x(\theta_{j-1}) - x(\theta_{j-1}))/2 \tag{12}$$

Equation (11) can be expanded as:

$$\sum_{i=0}^{r}\frac{D^{(i)}(y=l_j,\ k\Delta t)}{i!}\int_0^{\Delta t}\varepsilon^i\left\{\frac{\partial\theta(k\Delta t+\varepsilon)}{\partial y}\right\}\Big|_{y=l_j} d\varepsilon -$$
$$\sum_{i=0}^{r}\frac{D^{(i)}(y=0,\ k\Delta t)}{i!}\int_0^{\Delta t}\varepsilon^i\left\{\frac{\partial\theta(k\Delta t+\varepsilon)}{\partial y}\right\}\Big|_{y=0} d\varepsilon$$
$$= \int_{R_j}\{\theta\}\Big|_{\Gamma_t} dy \tag{13}$$

The soil-water content function is approximated spatially and temporally by:

$$\theta \simeq \hat{\theta}$$
$$\hat{\theta} = \sum_{r=1}^{n} N_r\left(\sum_{m=0}^{k+1} M_m\,\theta_r^m\right) \tag{14}$$

where N_r and M_m are the linearly independent spatial and temporal shape functions, and

$$\theta_r^m = \hat{\theta}(x = x(\theta_r),\ t = m\,\Delta t) \tag{15}$$

where the θ_r^m are known values for time steps $m = 0, 1, \ldots, k$. The spatial gradient of the soil-water content function is approximated by:

$$\frac{\partial\theta}{\partial x} \simeq \frac{\partial\hat{\theta}}{\partial x} = \sum_{r=1}^{n}\frac{\partial N_r}{\partial x}\left(\sum_{m=0}^{k+1} M_m\,\theta_r^m\right) \tag{16}$$

Substituting equations (14) and (16) into equation (13) gives the numerical approximation:

$$\sum_{i=0}^{r}\frac{D^{(i)}(y=l_j,\ k\Delta t)}{i!}\int_0^{\Delta t}\varepsilon^i\left\{\sum_{r=1}^{n}\frac{\partial N_r}{\partial x}\left(\sum_{m=0}^{k+1} M_m\,\theta_r^m\right)\right\}\Big|_{y=l_j} d\varepsilon -$$
$$\sum_{i=0}^{r}\frac{D^{(i)}(y=0,\ k\Delta t)}{i!}\int_0^{\Delta t}\varepsilon^i\left\{\sum_{r=1}^{n}\frac{\partial N_r}{\partial x}\left(\sum_{m=0}^{k+1} M_m\,\theta_r^m\right)\right\}\Big|_{y=0} d\varepsilon$$
$$= \int_0^{l_j}\left\{\sum_{r=1}^{n} N_r\left(\sum_{m=0}^{k+1} M_m\,\theta_r^m\right)\right\}\Big|_{\Gamma_t} dy \tag{17}$$

The unknown values of nodal points θ_r^{k+1} can be solved by equating:

$$\sum_{i=0}^{r}\frac{D^{(i)}(y=l_j,\ k\Delta t)}{i!}\int_0^{\Delta t}\varepsilon^i\left\{\sum_{r=1}^{n}\frac{\partial N_r}{\partial x}M_{k+1}\,\theta_r^{k+1}\right\}\Big|_{y=l_j} d\varepsilon -$$
$$\sum_{i=0}^{r}\frac{D^{(i)}(y=0,\ k\Delta t)}{i!}\int_0^{\Delta t}\varepsilon^i\left\{\sum_{r=1}^{n}\frac{\partial N_r}{\partial x}M_{k+1}\,\theta_r^{k+1}\right\}\Big|_{y=0} d\varepsilon -$$
$$\int_0^{l_j}\sum_{r=1}^{n} N_r\,\theta_r^{k+1}\,dx =$$
$$\sum_{i=0}^{r}\frac{D^{(i)}(y=0,\ k\Delta t)}{i!}\int_0^{\Delta t}\varepsilon^i\left\{\sum_{r=1}^{n}\frac{\partial N_r}{\partial x}\left(\sum_{m=0}^{k} M_m\,\theta_r^m\right)\right\}\Big|_{y=0} d\varepsilon -$$

$$\sum_{i=0}^{r} \frac{D^{(i)}(y=l,\ k\Delta t)}{i!} \int_0^{\Delta t} \varepsilon^i \left\{ \sum_{r=1}^{n} \frac{\partial N_r}{\partial x} \left(\sum_{m=0}^{k} M_m\, \theta_r^{(m)} \right) \right\}_{l,\,k\Delta t} \mathrm{d}\varepsilon - \int_0^{l} \sum_{r=1}^{n} N_r\, \theta_r^{k}\, \mathrm{d}x \qquad (18)$$

NUMERICAL MODEL

The space-time surface approximated by equation (14) can be simplified by assuming that the functional surface can be described by sets of piecewise continuous polynomials. For a parabolic spatial shape function approximation for θ between nodal points $(\theta_{j-1},\ \theta_j,\ \theta_{j+1})$,

$$\left.\frac{\partial\theta}{\partial x}\right|_{y=l} = (\theta_{j-1} - \theta_j)/l$$

$$\left.\frac{\partial\theta}{\partial x}\right|_{y=0} = (\theta_j - \theta_{j-1})/l \qquad (19)$$

$$\int_{y=0}^{l} \theta\, \mathrm{d}y = \frac{l}{24}[\theta_{j-1} + 22\theta_j - \theta_{j-1}]$$

where for discussion purposes it is assumed that in equation (19)

$$x(\theta_{j-1}) - x(\theta_j) = x(\theta_j) - x(\theta_{j-1}) = l$$

$$\mathrm{d}x = \mathrm{d}y$$

For a linear polynomial function approximation for the time curves between time-steps $(k,\ k+1)$ where $(k+1)$ is the time step to be evaluated,

$$\theta_j(k\Delta t - \varepsilon) = (\theta_j^{k\Delta t})\left(\frac{\Delta t - \varepsilon}{\Delta t}\right) - (\theta_j^{(k-1)\Delta t})\frac{\varepsilon}{\Delta t}$$

$$k\Delta t \leqslant t \leqslant (k-1)\ \Delta t \qquad (20)$$

$$\mathrm{d}\varepsilon = \mathrm{d}t$$

Combining equations (19) and (20), the spatial gradient approximation during the time-step Δt is given by:

$$\left.\frac{\partial\theta}{\partial x}\right|_{y=l} = (\theta_{j-1}^2 - \theta_{j-1}^1 - \theta_j^2 + \theta_j^1)\varepsilon\ l\Delta t + (\theta_{j-1}^1 - \theta_j^1)\ l$$

$$\left.\frac{\partial\theta}{\partial x}\right|_{y=l} = (\theta_j^2 - \theta_j^1 - \theta_{j-1}^2 - \theta_{j-1}^1)\varepsilon\ l\Delta t + (\theta_j^1 - \theta_{j-1}^1)\ l$$

$$0 \leqslant \varepsilon \leqslant \Delta t \qquad (21)$$

where superscripts 1 and 2 refer to timesteps $k\Delta t$ and $(k-1)\Delta t$, respectively. Combining equations (18), (19) and (21) gives:

$$\sum_{i=0}^{r} \frac{D^{(i)}(y=l)}{i!} \int_0^{\Delta t} \left\{ (\theta_{j-1}^2 - \theta_{j-1}^1 - \theta_j^2 - \theta_j^1)\frac{\varepsilon^{i+1}}{l\Delta t} - (\theta_{j-1}^1 - \theta_j^1)\frac{\varepsilon^i}{l} \right\} \mathrm{d}\varepsilon -$$

$$\sum_{i=0}^{r} \frac{D^{(i)}(y=0)}{i!} \int_0^{\Delta t} \left\{ (\theta_j^2 - \theta_j^1 - \theta_{j-1}^2 - \theta_{j-1}^1)\frac{\varepsilon^{i+1}}{l\Delta t} - (\theta_j^1 - \theta_{j-1}^1)\frac{\varepsilon^i}{l} \right\} \mathrm{d}\varepsilon$$

$$= \frac{l}{24}[(\theta_{j-1}^2 + 22\theta_j^2 + \theta_{j-1}^2) - (\theta_{j-1}^1 + 22\theta_j^1 - \theta_{j-1}^1)] \qquad (22)$$

The temporal integration of equation (22) is evaluated by isolating the time-integrated function as:

$$\sum_{i=0}^{r} \frac{D^{(i)}(y=l)}{i!} \left[\frac{(\theta_{j-1}^2 - \theta_j^2) - (\theta_{j-1}^1 - \theta_j^1)}{l\Delta t} \right] \int_0^{\Delta t} \varepsilon^{i+1}\, \mathrm{d}\varepsilon -$$

$$\sum_{i=0}^{r} \frac{D^{(i)}(y=l)}{i!} \left[\frac{\theta_{j-1}^1 - \theta_j^1}{l} \right] \int_0^{\Delta t} \varepsilon^i \mathrm{d}\varepsilon -$$

$$\sum_{i=0}^{r} \frac{D^{(i)}(y=0)}{i!} \left[\frac{(\theta_j^2 - \theta_{j-1}^2) - (\theta_j^1 - \theta_{j-1}^1)}{l\Delta t} \right] \int_0^{\Delta t} \varepsilon^{i+1}\, \mathrm{d}\varepsilon -$$

$$\sum_{i=0}^{r} \frac{D^{(i)}(y=0)}{i!} \left[\frac{\theta_j^1 - \theta_{j-1}^1}{l} \right] \int_0^{\Delta t} \varepsilon^i \mathrm{d}\varepsilon =$$

$$\frac{l}{24}[(\theta_{j-1}^2 - 22\theta_j^2 + \theta_{j-1}^2) - (\theta_{j-1}^1 - 22\theta_j^1 + \theta_{j-1}^1)] \qquad (23)$$

Rearranging terms, the nodal point expressions can be isolated by:

$$[\theta_{j-1}^2 - \theta_j^2] \sum_{i=0}^{r} \frac{D^{(i)}(y=l)}{i!l\Delta t} \int_0^{\Delta t} \varepsilon^{i+1}\, \mathrm{d}\varepsilon -$$

$$[\theta_j^2 - \theta_{j-1}^2] \sum_{i=0}^{r} \frac{D^{(i)}(y=0)}{i!l\Delta t} \int_0^{\Delta t} \varepsilon^{i+1}\, \mathrm{d}\varepsilon -$$

$$[\theta_{j-1}^1 - \theta_j^1] \sum_{i=0}^{r} \frac{D^{(i)}(y=l)}{i!l\Delta t} \int_0^{\Delta t} (\Delta t\varepsilon^i - \varepsilon^{i+1})\, \mathrm{d}\varepsilon -$$

$$[\theta_j^1 - \theta_{j-1}^1] \sum_{i=0}^{r} \frac{D^{(i)}(y=0)}{i!l\Delta t} \int_0^{\Delta t} (\Delta t\varepsilon^i - \varepsilon^{i+1})\, \mathrm{d}\varepsilon =$$

$$\frac{l}{24}[\theta_{j-1}^2 - 22\theta_j^2 - \theta_{j-1}^2] - \frac{l}{24}[\theta_{j-1}^1 + 22\theta_j^1 - \theta_{j-1}^1] \qquad (24)$$

Carrying out the indicated integration in equation (24) gives:

$$[\theta_{j-1}^2-\theta_j^2]\sum_{i=0}^{r}\frac{D^{(i)}(y=0)(\Delta t)^{i-1}}{i!}\frac{l}{(i+2)}-$$

$$[\theta_j^2-\theta_{j-1}^2]\sum_{i=0}^{r}\frac{D^{(i)}(y=0)(\Delta t)^{i-1}}{i!}\frac{l}{(i+2)}+$$

$$[\theta_{j-1}^1-\theta_j^1]\sum_{i=0}^{r}\frac{D^{(i)}(y=l)}{i!}\frac{(\Delta t)^{i-1}}{(i+1)(i+2)}-$$

$$[\theta_j^1-\theta_{j-1}^1]\sum_{i=0}^{r}\frac{D^{(i)}(y=0)}{i!}\frac{(\Delta t)^{i-1}}{(i+1)(i+2)}=$$

$$\frac{l}{24}[\theta_{j-1}^2+22\theta_j^2+\theta_{j-1}^2]-\frac{l}{24}[\theta_{j-1}^1+22\theta_j^1+\theta_{j-1}^1] \qquad (25)$$

In a different notation, equation (25) can be rewritten as:

$$\bar{D}_1[\theta_{j-1}^2-\theta_j^2]-\bar{D}_0[\theta_j^2-\theta_{j-1}^2]-\frac{l}{24}[\theta_{j-1}^2+22\theta_j^2+\theta_{j-1}^2]$$

$$=-\bar{D}_1[\theta_{j-1}^1-\theta_j^1]+\bar{D}_0[\theta_j^1-\theta_{j-1}^1]-\frac{l}{24}[\theta_{j-1}^1+22\theta_j^1+\theta_{j-1}^1] \qquad (26)$$

where

$$\bar{D}_\eta=\sum_{i=0}^{r}\frac{D^{(i)}(y=\eta)(\Delta t)^{i-1}}{i!(i+2)}\frac{l}{l}; \qquad \eta=0,\ l$$

$$\bar{D}_\eta=\sum_{i=0}^{r}\frac{D^{(i)}(y=\eta)(\Delta t)^{i-1}}{(i+2)!}\frac{l}{l}; \qquad \eta=0,\ l \qquad (27)$$

Since the space–time surface is assumed to be linear with respect to time, the temporal differentials of soil–water diffusivity in equation (27) are given by:

$$D^{(N)}\equiv\frac{\partial^N D}{\partial t^N}=\frac{\partial^N D}{\partial\theta^N}\left(\frac{\partial\theta}{\partial t}\right)^N \qquad (28)$$

where the temporal water content gradient can be approximated from values of water content during time step k.

Hromadka and Guymon[6] determine a complete formulation for a parabolic spatial interpolation function which involved five nodal points rather than three in order to estimate nodal point values; however, the additional computational effort did not significantly increase the approximation accuracy. In their study, the (linear interpolation shape function) Galerkin analog to equation (1), was determined and modified to correspond to equation (26) for the special case of $i=0$.

The Galerkin version of the weighted residual process can be used to approximate equation (1) by the finite element method. The solution domain is discretized into the union of n finite elements by:

$$L=\bigcup_{i=1}^{n}L_i \qquad (29)$$

The water content is utilized as the state variable and is approximated within each finite element by:

$$\theta(x)=\Sigma N_j(x)\theta_j \qquad (30)$$

where N_j = the appropriate linearly independent shape functions; θ_j = state variable values at element-nodal points designated by the general summation index j.

The Galerkin technique utilizes the set of shape functions as the weighting functions, which indicates that the corresponding finite element representation for the infiltration process is:

$$\int_{L_e}\left\{\frac{\partial}{\partial x}\left[D(\theta)\frac{\partial\theta}{\partial x}\right]-\frac{\partial\theta}{\partial t}\right\}N_j\,dx=0 \qquad (31)$$

Integration by parts expands equation (31) into the form:

$$\sum_{i=1}^{n}\left\{D(\theta)\frac{\partial\theta}{\partial x}N_j\Big|_{S_i}-\int_{L_e}\left[D(\theta)\frac{\partial\theta}{\partial x}\frac{\partial N_j}{\partial x}-N\frac{\partial\theta}{\partial t}\right]dx\right\}=0 \qquad (32)$$

where S_i = external endpoints of the one-dimensional finite element, L_e. The first term within the braces sums to zero for interior elements, and also satisfies the usual specified (or flux type) boundary conditions of the problem for exterior finite elements. The remaining integral term is solved by substituting the appropriate element approximations and shape functions into the integrand and solving by numerical integration. A convenient approach to deal with the non-linearity of equation (32) is to assume the diffusivity function to be constant within each finite element during a finite time interval, Δt, in order to carry out the integration. The Crank–Nicolson time advancement approximation has been widely used[1,2] to solve the time derivative of equation (32).

The Crank–Nicolson formulation reduces equation (32), where values of soil–water diffusivity are assumed constant within each finite element, into a system of linear equations expressed in matrix form as:

$$\left\{\mathbf{P}+\frac{\Delta t}{2}\mathbf{S}\right\}\theta^{i+1}=\left\{\mathbf{P}-\frac{\Delta t}{2}\mathbf{S}\right\}\theta^{i} \qquad (33)$$

where $\mathbf{P}$ is a symmetrical capacitance matrix and is a function of element nodal global coordinates; $\mathbf{S}$ is a symmetrical stiffness matrix and is a function of element nodal global coordinates and constant finite element diffusivity coefficients (during time step Δt); Δt is the finite time step increment; and θ^k is the vector of nodal state variable approximations (volumetric water content) at time steps $k=i,\ i+1$.

For a linear polynomial shape function, the element matrices determined from equation (32) are given by:

$$\hat{\mathbf{S}}\begin{pmatrix}\theta_i\\ \theta_j\end{pmatrix}-\hat{\mathbf{P}}\begin{pmatrix}\dot{\theta}_i\\ \dot{\theta}_j\end{pmatrix}=\frac{D_i}{l_i}\begin{bmatrix}1 & -1\\ -1 & 1\end{bmatrix}\begin{pmatrix}\theta_i\\ \theta_j\end{pmatrix}-\frac{l_i}{6}\begin{bmatrix}2 & 1\\ 1 & 2\end{bmatrix}\begin{pmatrix}\dot{\theta}_i\\ \dot{\theta}_j\end{pmatrix} \qquad (34)$$

where D_i is the quasi-constant diffusivity within element i; $\hat{\mathbf{S}}$ and $\hat{\mathbf{P}}$ are element stiffness and capacitance matrices, respectively; and $(\theta_i,\ \theta_j)$ and $(\dot{\theta}_i,\ \dot{\theta}_j)$ refer to the element nodal and dynamic nodal moisture content values, respectively, for an element of length l_i.

For the linear temporal interpolation function, equations (26) and (27) can be written analogously to equations (33) and (34) as:

$$[\mathbf{P}-\bar{\mathbf{S}}]\theta^{i+1}=[\mathbf{P}-\bar{\mathbf{S}}]\theta^{i} \qquad (35)$$

Table 1. Comparison of numerical efficiency at time $t = 16.5$ minutes (values of water content)

x (cm)	Exact (Hayhoe)	$\Delta t = 0.1$ min $r = 0$	$\Delta t = 0.1$ min $r = 2$	$\Delta t = 0.1$ min $r = 5$	$\Delta t = 0.3$ min $r = 0$	$\Delta t = 0.3$ min $r = 2$	$\Delta t = 0.3$ min $r = 5$
0.0	1.0	1.0	1.0	1.0	1.0	1.0	1.0
0.5	0.99	0.99	0.99	0.99	0.98	0.99	0.99
1.0	0.97	0.97	0.97	0.97	0.97	0.97	0.97
1.5	0.95	0.95	0.95	0.95	0.94	0.95	0.95
2.0	0.92	0.93	0.92	0.92	0.92	0.93	0.93
2.5	0.88	0.90	0.89	0.89	0.88	0.90	0.90
3.0	0.84	0.87	0.85	0.85	0.84	0.87	0.86
3.5	0.78	0.82	0.78	0.78	0.82	0.82	0.82
4.0	0.67	0.39	0.63	0.64	0.05	0.37	0.40
4.5	0.0	0.0	0.0	0.0	0.0	0.0	0.0
5.0	0.0	0.0	0.0	0.0	0.0	0.0	0.0

r: number of temporal Taylor series terms (diffusivity function) included
Δt: time step magnitude

where the element matrices composing the global S matrices of equation (35) are given by:

$$\bar{S} \equiv \bar{D}_\eta \begin{bmatrix} 1 & -1 \\ -1 & 1 \end{bmatrix}$$

$$\bar{S} \equiv \bar{D}_\eta \begin{bmatrix} 1 & -1 \\ -1 & 1 \end{bmatrix} \tag{36}$$

and

$$\bar{P} \equiv \frac{l}{24} \begin{bmatrix} 11 & 1 \\ 1 & 11 \end{bmatrix} \tag{37}$$

MODEL APPLICATION

The numerical model given by equations (35), (36) and (37) was applied to a sharp wetting-front problem of soil-water infiltration into an air-dry horizontal column[2,5]. The analytic value of soil-water diffusivity for Hanford sandy loam[4] was selected in order to provide a sharp wetting front through the soil column, causing the numerical analysis of moisture flow in the soil to be difficult. The quasi-analytic solution advanced by Philip and Knight[3] and utilized by Hayhoe[2] was used for this study.

Equation (1) was solved subject to the initial condition:

$$\theta(x,t) = 0;\ t = 0,\ 0 \leqslant x \leqslant L \tag{38}$$

and the boundary conditions:

$$\theta(0,\ t) = 1,\ \theta(L,\ t) = 0;\ t > 0 \tag{39}$$

where the soil-water diffusivity ($cm^2\ min^{-1}$) is given by:

$$D(\theta) = \begin{cases} 0.9 \times 10^{-3} \exp(8.36\theta),\ \theta > 0 \\ 0.9 \times 10^{-3},\ \theta = 0 \end{cases} \tag{40}$$

and θ is the dimensionless volumetric water content.

Owing to the nature of the soil-water diffusivity function of (40), the temporal variation of diffusivity is extremely important during the Δt time step. As such, the temporal diffusivity Taylor series finds good use in sharp wetting front infiltration problems as presented herein. For moisture transport problems where the diffusivity function causes less difficulty in numerical estimation, the model represented by equation (35) can be used to reduce execution time by approximately two-thirds. That is, by expanding the time series of equation (27), the time step magnitude Δt was found to be capable of a 300% increase and yet retain the same level of approximation accuracy. Table 1 contains various values of time step magnitudes Δt (in min) and time series expansion terms in the numerical model of equation (1) by (35) at time $t = 16.5$ min. For the numerical model, a spatial discretization of 0.5 cm was used where the total column length was set at 5.0 cm to correspond to the model results of Hayhoe[2].

The test results indicate that the numerical accuracy achieved for $\Delta t = 0.1$ min (without the temporal Taylor series expansion for diffusivity) is also matched for a $\Delta t = 0.3$ min time step where the temporal Taylor series is included through the fifth term. Since the integration of the diffusivity series expansion involves negligible computer execution time when compared to the solution of matrices during the time advancement, further increases in time step sizes may be possible for less difficult models.

CONCLUSIONS

A new numerical approach to soil water (diffusivity) infiltration problems is advanced. By use of a modified finite element analog to the governing equations, a Taylor series of soil water diffusivity with respect to time can be integrated. Application to a case study indicates a reduction in execution costs due to the capability of increasing the finite time step and yet retain comparable numerical accuracy.

The inclusion of the Taylor series expansion for diffusivity (30) in the traditional finite element matrix formulation (34) was found to produce less desirable results. Using the numerical model for equation (1) given in Hromadka and Guymon[5], the addition of the temporal Taylor series modification produced an increasing over-estimation of the wetting front advancement into the horizontal soil column. That is, as the number of the diffusivity function Taylor series terms were increased in equation (34), the numerical solution indicated an increasingly inaccurate penetration of moisture into the horizontal soil column. This numerical behaviour is probably due to the finite element capacitance matrix over-estimation of mean moisture content within the nodal domains[5].

A sophistication of the proposed integration technique is to use higher order polynomial interpolation functions

for the time variable. For a parabolic interpolating function, the increase in numerical accuracy was found to be negligible[6]. However, some advantage was found when using a parabolic interpolation for time in order to estimate the temporal gradient of the diffusivity function (28). For the horizontal soil column, the timestep increase (at comparable numerical accuracy) was found to be approximately 330%, whereas the linear estimation procedure enabled a 300% increase in timestep magnitude. The additional computer memory and computation requirements involving a parabolic temporal interpolation, however, somewhat offsets the advantage of the additional timestep increase in magnitude.

ACKNOWLEDGEMENT

This research was supported by the U.S. Army Research Office (Grant No. DAAG29-79-C-0080).

REFERENCES

1 Desai, C. S. *Elementary Finite Element Method*. Prentice-Hall, Englewood Cliffs, 1979
2 Hayhoe, H. N. Study of relative efficiency of finite difference and Galerkin techniques for modeling soil-water transfer. *Water Resourc. Res.* 1978, 14(1), 97
3 Philip, J. R. and Knight, J. H. On solving the unsaturated flow equation: 3. New quasi-analytic technique. *Soil Sci.* 1974, 117, 1
4 Reichardt, K., Nielsen, D. R. and Biggar, J. W. Scaling of horizontal infiltration into homogeneous soils. *Proc. Soil Sci. Soc. Am.* 1972, 36, 241
5 Hromadka II, T. V. and Guymon, G. L. Some effects of linearizing the unsaturated soil-moisture transfer diffusion model. *Water Resourc. Res.* in press
6 Hromadka II, T. V. and Guymon, G. L. Numerical mass balance for soil-moisture transfer problems. *Adv. Water Resourc.* 1980, 3, 107

Cold Regions Science and Technology, 4(1981)137–145
Elsevier Scientific Publishing Company, Amsterdam – Printed in The Netherlands

SOME APPROACHES TO MODELING PHASE CHANGE IN FREEZING SOILS

T.V. Hromadka II and G.L. Guymon
School of Engineering, University of California, Irvine, CA (U.S.A.)

R.L. Berg
Geotechnical Research Branch, U.S. Army, CRREL, Hanover, NH (U.S.A.)

(Received January 7, 1980; accepted November 6, 1980)

ABSTRACT

Phase change effects associated with freezing soils dominate the thermal state of the soil regime. Furthermore, freezing of soil water influences the soil moisture regime by providing a moisture sink which tends to draw mobile soil moisture to freezing fronts. Consequently, it is critical to general purpose models that soil water phase change effects and the interrelated problem of estimating the moisture sink effects (i.e., conversion of liquid water to ice) be accurately modeled. The choice of such a model will not only influence the precision of simulated temperatures and water contents in a freezing soil, but also have a significant impact on computational efficiency. A review of several current models that assume unfrozen water content is functionally related to subfreezing temperatures indicate that within a freezing soil the soil water flow model and heat transport model parameters are restricted in spatial gradients according to the spatial gradient of modeled unfrozen water content. A freezing soil model based on the concept of isothermal phase change of soil water is proposed as an alternative approach.

INTRODUCTION

The possibility of numerically modeling the complex processes which occur in simultaneous heat and soil-moisture transport in a freezing soil has received much attention during the last decade. Early mathematical models for simulating the soil freezing process were proposed by Harlan (1973), and Guymon and Luthin (1974). More recent modeling efforts of coupled heat and soil-moisture transport in freezing soils include Sheppard et al. (1977), Jame (1978), Taylor and Luthin (1978), and Guymon et al. (1980). A comparison of these various modeling efforts indicates that the approaches used to simulate the soil freezing process differ. Guymon et al. use a so-called "isothermal" approach where the governing heat and moisture flow equations are solved independently and soil-water phase change is modeled within freezing soil by returning below freezing temperatures to the freezing point until the available soil water is frozen. The other referenced modeling efforts all assume that volumetric water content, θ, and temperature, T, are functionally related within a freezing region of soil

$$\theta = \theta(T), \quad T < 0°C \tag{1}$$

and numerically iterate between the coupled heat and moisture transport relations until values of θ and T are within a selected tolerance to the soil water freezing characteristic curve approximation; if temperatures are above freezing and the soil is ice free, then the functional relation of eqn. (1) is discontinued (Taylor and Luthin). Sheppard et al., however, used an alternative statement of eqn. (1) to eliminate the soil-moisture variable component by a volumetric water content to temperature gradient, and mathematically combined the coupled equations into a single relation based on temperature. This reduced formulation incorporated the so-called apparent heat capacity defined by

$$C_a = C_m + L_f \partial\theta/\partial T \tag{2}$$

0165-232X/81/0000–0000/$02.50

where C_a is the volumetric apparent heat capacity; C_m is the volumetric heat capacity of the soil-water–ice mixture; L_a is the volumetric latent heat of fusion of water; and the density of water, ρ_W, is assumed to be unity. Equation (2) was apparently originally presented in terms of volumetric ice content, but more commonly volumetric water content is used in eqn. (2) (Williams 1968 and Anderson et al. 1973).

Although Jame, and Taylor and Luthin numerically iterate and adjust solutions of the governing heat and moisture flow equations until eqn. (1) is satisfied, the underlying mathematical result is the solution of a single differential equation incorporating an appropriate apparent heat capacity term.

The Sheppard et al. mathematical model assumes negligible gravity effects in their vertical soil-water flow model, and relates soil-water pore pressure head to absolute temperature in order to combine both transport equations into an apparent heat capacity formulation including eqn. (2). Jame, and Taylor and Luthin, however, simulate coupled heat and moisture flow in a horizontal freezing soil column and use volumetric water content as the governing moisture transport variable.

In this paper, the two governing heat and soil-water flow mathematical models used in a horizontal freezing soil column problem will be combined into a single transport model similar to the vertical column model of Sheppard et al. Using the volumetric water content to temperature functional relationship assumption, the resulting combined transport model can be written in terms of either the moisture transport or heat transport variables (i.e. volumetric water content or temperature), with the apparent heat capacity term (or equivalent) included in the formulation. From the resulting combined model, it will be shown that severe limitations on the transport conduction parameters of thermal conductivity and soil-water diffusivity must be satisfied in order for the model to describe the soil-water freezing process.

The objective of this paper is twofold. The first objective is to evaluate the mathematical consistency of combining the assumptions in eqns. (1) and (2) with coupled heat and moisture transport models. A number of investigators assumes that soil-moisture transport in freezing soils can be modeled by an analogy to unsaturated soil-water flow theory where soil moisture driven by hydraulic gradients dominates, and the usual soil-water diffusivity can be modified by an ice-content correction or scaling factor in order to accommodate ice formation and its effect on soil-water flow. Additionally, the classical heat transport relation is assumed for heat flow within freezing soils, and heat transport due to convection by soil-water flow is assumed negligible in several models. Ice formation within freezing soils is modeled by an appropriate soil-moisture sink and heat source term based on the time rate of change of volumetric ice content within the freezing soil.

The second objective of this paper is to present an alternative modeling approach based on the previously mentioned isothermal concept. This second approach is based on the assumptions of an analogy to unsaturated soil-water flow theory and the classical heat transport relation (with convection), but somewhat relaxes the volumetric water content to temperature functional requirement. Soil water in excess of that predicted by the soil-water freezing characteristic curve is permitted, but further soil freezing is modeled isothermally until the soil-water content corresponds to the freezing characteristic curve.

SOIL-WATER PHASE CHANGE EFFECTS MODELED AS AN APPARENT HEAT CAPACITY

A horizontal freezing soil column will be discussed due to the extensive numerical model development and laboratory parameter estimations given in the literature (e.g. Jame 1978).

Soil water flow in freezing soils is generally assumed modeled by an analogy to unsaturated soil-water flow theory by

$$\frac{\partial}{\partial x}\left(D\,\frac{\partial \theta}{\partial x}\right) = \frac{\partial \theta}{\partial t} + \frac{\rho_I \partial \theta_I}{\rho_W \partial t} \tag{3}$$

where D is the appropriate freezing soil-water diffusivity. Equation (3) is based upon the assumption that soil water primarily moves as a liquid, driven by hydraulic gradients. Vapor movement and thermally driven moisture flow is assumed negligible (Fuchs 1978, for example).

Neglecting convected heat effects, heat flow in freezing soils is generally modeled by

$$\frac{\partial}{\partial x}\left(K_T\,\frac{\partial T}{\partial x}\right) = C_m\,\frac{\partial T}{\partial t} - L_a\,\frac{\rho_I}{\rho_W}\,\frac{\partial \theta_I}{\partial t} \tag{4}$$

where K_T is the thermal conductivity; θ_I is the volumetric ice content; L_a is the volumetric latent heat of fusion for liquid water; and ρ_I is the density of ice. A third major assumption in several current models is that water content and temperature are functionally related for below freezing temperatures (Sheppard et al., Taylor and Luthin, Jame)

$$\theta = \theta(T), \quad \theta \in R(T) \tag{5}$$

where $R(T)$ is the domain of functional definition for subfreezing temperatures.

From eqn. (5), the thermal gradient of water content is defined by (Jame, Sheppard et al.)

$$\hat{\theta} = \partial\theta/\partial T, \quad \theta \in R(T) \tag{6}$$

Therefore, eqns. (3), (4), (5) and (6) may be combined into one governing equation similar to the formulation of Sheppard et al.

$$\frac{\partial}{\partial x}\left[L_a D \frac{\partial \theta}{\partial x} + \frac{K_T}{\hat{\theta}} \frac{\partial \theta}{\partial x}\right] = \left[L_a + \frac{C_m}{\hat{\theta}}\right] \frac{\partial \theta}{\partial t}, \theta \in R(T) \tag{7}$$

or in simpler notation,

$$\left.\begin{aligned} &\frac{\partial}{\partial x}\left(\alpha_1 \frac{\partial \theta}{\partial x}\right) = \alpha_3 \frac{\partial \theta}{\partial t} \\ &\theta = \theta(T) \\ &\alpha_1 = L_a D + K_T/\hat{\theta} \\ &\alpha_3 = L_a + C_m/\hat{\theta} \end{aligned}\right\} \tag{8}$$

where α_3 is the corresponding apparent heat capacity term equivalent to eqn. (2) for volumetric water content used as the primary variable in eqn. (7). Thus, the $\theta = \theta(T)$ assumption leads to one equation incorporating an apparent heat capacity term (or equivalent) and ancillary relationships between parameters. Although from the above it is necessary to numerically solve only one equation, Jame (1978) and Taylor and Luthin (1978), for example, numerically solve each equation of state separately, and adjust solutions by an iteration procedure for an assumed $\theta = \theta(T)$.

To determine the ice content profile, considerations of mass transport may be used as outlined in Hromadka and Guymon (1980). Thus, eqn. (3) can be temporally and spatially discretized for numerical solution as follows:

$$\left\{\int_{\Omega_j} \theta_I \, dx\right\}_{\Delta t}^{2\Delta t} = \frac{\rho_W}{\rho_I} \int_{\Delta t}^{2\Delta t} \left\{D \frac{\partial \theta}{\partial x}\Big|_{\Gamma_j}\right\} dt - \frac{\rho_W}{\rho_I}\left\{\int_{\Omega_j} \theta \, dx\right\}_{\Delta t}^{2\Delta t} \tag{9}$$

where Δt is a numerical time step increment, Ω_j and Γ_j are spatial domains and boundaries respectively of soil column region, j. Appropriate basis or trial functions are substituted into eqn. (9) and indicated mathematical operations are carried out, yielding a matrix system very similar to that resulting from using the well-known finite-element method.

Some theoretical implications and problem limitations as posed by eqn. (7) can best be developed by examining a simulation of horizontal freezing in a soil column. Laboratory data obtained by Jame (1978) are used as a case study. Unsaturated soil-water diffusivity, $D(\theta)$, is assumed described as shown in Fig. 1, and water content is assumed to be a function

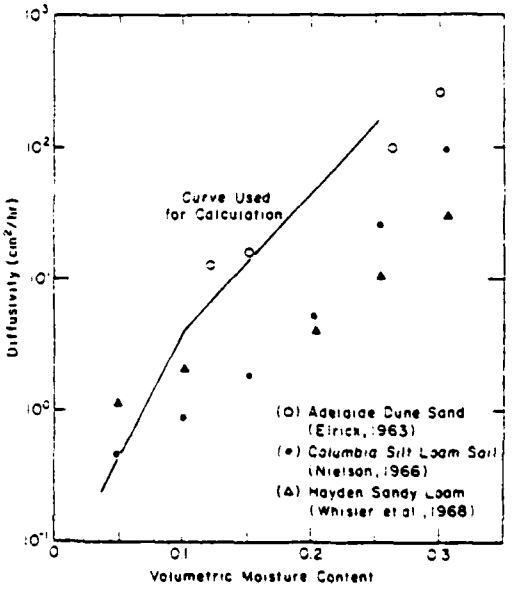

Fig. 1. Soil-water diffusivity versus unfrozen moisture content (Jame 1978).

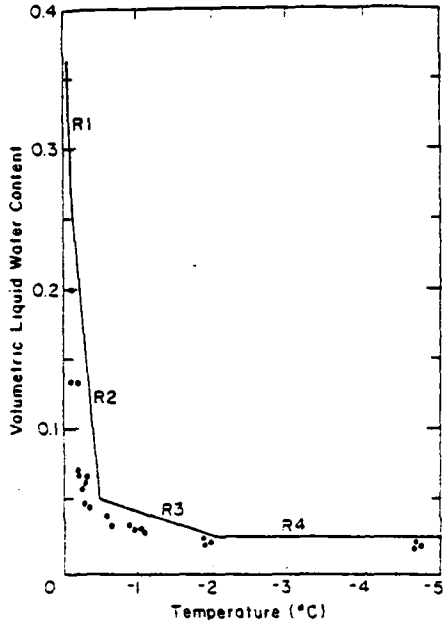

Fig. 2. Liquid water content versus temperature relationship showing experimental data and the approximate curve used in the computations (Jame 1978).

of temperature as shown in Fig. 2. These data are generally similar to data from frost susceptible soils. From Figs. 1 and 2, it can be shown that within region R_1 of the diffusivity curve, the magnitudes of $(C_m/\dot{\theta})$ and $(K_T/\dot{\theta})$ are less than one-half of one percent of the magnitudes of (L_a) and (DL_a), respectively. Accordingly, within region R_1 eqn. (7) may be numerically approximated for the given assumptions by

$$\left.\begin{aligned} &\frac{\partial}{\partial x}\left(D\,\frac{\partial \theta}{\partial x}\right) = \frac{\partial \theta}{\partial t} \\ &D = D(\theta,\theta_I) = D(\theta)/10^{10\theta_I} \\ &x \in R_1 \end{aligned}\right\} \qquad (10)$$

where $D(\theta,\theta_I)$ is assumed defined by an adjustment to unsaturated diffusivity as described by Taylor and Luthin. Because data on hydraulic conductivity of frozen soil are not generally available, an estimate of frozen soil hydraulic conductivity is usually assumed for most models. The approach used by Taylor and Luthin which is based upon unfrozen soil water diffusivity is arbitrarily selected for study purposes. For region R_4 (Fig. 1), eqn. (7) may be examined in the limit to be

$$\lim_{\dot{\theta}\to 0}\left\{\frac{\partial}{\partial x}\left[\left(\frac{K_T}{\dot{\theta}} + DL_a\right)\frac{\partial \theta}{\partial x}\right] = \left(\frac{C_m}{\dot{\theta}} + L_a\right)\frac{\partial \theta}{\partial t}\right\}$$

$$= \left\{\frac{\partial}{\partial x}\left(K_T\,\frac{\partial T}{\partial x}\right) = C_m\,\frac{\partial T}{\partial t}\right\}, \quad x \in R_4 \qquad (11)$$

where the thermal parameters are functions of soil, water and ice fractions. Within regions R_2 and R_3, the magnitudes of (DL_a) and $(K_T/\dot{\theta})$ generally are such that neither term can be eliminated from the formulation.

For significant diffusivity values, difficulties may arise in attempting to model a zero moisture flux boundary condition while maintaining a freezing thermal gradient: that is, for $\theta = \theta(T)$,

$$\left.\begin{aligned} &D\,\frac{\partial \theta}{\partial x} = (D\dot{\theta})\frac{\partial T}{\partial x} = 0 \\ &K_T\,\frac{\partial T}{\partial x} = 0 \end{aligned}\right\} \qquad (12)$$

would be the boundary condition. Accordingly, diffusivity must be set to zero at the column boundary.

Another difficulty is possible accumulation of soil moisture above the water content value predicted by the characteristic curve, $\theta(T)$. For the horizontal freezing column problem (Jame, for example) where zero moisture flux occurs at the column boundaries at $x = (0, L)$, the $\theta = \theta(T)$ assumption necessarily implies that the thermal and moisture gradients are positive, for the freezing front advancing from $x = 0$. Also, a closed system freezing column problem can only have a depletion of unfrozen soil moisture, since an increase of moisture implies an increase of temperature by the $\theta(T)$ assumptions and eqns. (3) and (4). Hence, the governing relations within regions of freezing soil become

$$\left.\begin{aligned} &\frac{\partial}{\partial x}\left[\left(\frac{K_T}{\dot{\theta}} + DL_a\right)\frac{\partial \theta}{\partial x}\right] = \left(\frac{C_m}{\dot{\theta}} + L_a\right)\frac{\partial \theta}{\partial t}, \quad 0 < x < L \\ &\partial\theta/\partial t \leqslant 0, \quad t \geqslant 0 \\ &\theta = \theta(T) \end{aligned}\right\} \qquad (13)$$

For $\partial\theta/\partial t = 0$,

$$-\frac{\partial}{\partial x}\left(K_T \frac{\partial T}{\partial x}\right) = L_a \frac{\partial}{\partial x}\left(D \frac{\partial \theta}{\partial x}\right) \tag{14}$$

which results in a specific formulation for thermal conductivity in a steady-state moisture content region for the models considered

$$\left.\begin{aligned} K_T &= \frac{A_0}{(\partial T/\partial x)} - DL_a \frac{\partial \theta}{\partial T} \\ \theta &= \theta(T) \\ \partial\theta/\partial t &= 0 \end{aligned}\right\} \tag{15}$$

For some region, $\hat{R}$, of the soil column where $\hat{\theta}$ is set to the constant value $\hat{\theta}_0$, A_0 can be evaluated such that eqn. (18) becomes

$$K_T = \frac{(K_T' + L_a \hat{\theta}_0 D')\left(\frac{\partial T}{\partial x}\right)'}{\left(\frac{\partial T}{\partial x}\right)} - L_a \hat{\theta}_0 D;\ x \in \hat{R} \tag{16}$$

where primes indicate known values. An approximate spatial gradient relationship is given by

$$\left.\begin{aligned} \frac{\partial}{\partial x}\hat{K}_T &\approx -L_a \hat{\theta}_0 \frac{\partial D}{\partial x};\quad x \in \hat{R} \\ \theta &= \theta(T) \\ \partial\theta/\partial t &\approx 0 \\ (\partial T/\partial x)'/(\partial T/\partial x) &\approx 1 \end{aligned}\right\} \tag{17}$$

where $\hat{K}_T$ denotes that thermal conductivity function which satisfies the steady-state moisture content relationship of eqn. (16).

For the dynamic case, in a freezing soil, eqn. (13) can be rewritten as

$$\left.\begin{aligned} &\frac{\partial}{\partial x}\left[\left(\frac{K_T}{\hat{\theta}} + L_a D\right)\frac{\partial \theta}{\partial x}\right] = \left(\frac{C_m}{\hat{\theta}} + L_a\right)\frac{\partial \theta}{\partial t} \\ &\frac{\partial \theta}{\partial t} < 0,\quad 0 < x < L \end{aligned}\right\} \tag{18}$$

where for unidirectional freezing in a soil-column (freezing front advancing from $x = 0$) the various gradients are generally given by

$$\left.\begin{aligned} &\partial\theta/\partial t \leqslant 0 \\ &\partial\theta/\partial x > 0 \\ &\partial^2\theta/\partial x^2 \leqslant 0 \\ &\partial K_T/\partial x \leqslant 0 \\ &\partial D/\partial x \geqslant 0 \end{aligned}\right\} \tag{19}$$

From eqns. (18) and (19)

$$\frac{\partial}{\partial x}\left[\left(\frac{-K_T}{\hat{\theta}}\right)\frac{\partial \theta}{\partial x}\right] > \frac{\partial}{\partial x}\left[(L_a D)\frac{\partial \theta}{\partial x}\right] \tag{20}$$

which when expanded gives (for below freezing temperatures)

$$\frac{\partial}{\partial x}(DL_a) < -\frac{\partial}{\partial x}\left(\frac{K_T}{\hat{\theta}}\right) - \left(\frac{K_T}{\hat{\theta}} + L_a D\right)\frac{\partial^2 \theta}{\partial x^2}\Big/\frac{\partial \theta}{\partial x} \tag{21}$$

In order to avoid moisture accumulation at a constant temperature and preserve the $\theta(T)$ assumption, eqn. (21) must be satisfied for every water content profile. Thus, for the given model assumptions, the transport parameters are limited in spatial gradients according to the spatial gradient of water content. Especially important are the initial conditions of the problem which also bound the parameter spatial gradients as given in eqn. (21).

For example purposes, consider a strictly freezing horizontal soil-column problem with initial conditions given below (Fig. 3):

$$\left.\begin{aligned} &\theta = \theta(T)\ \text{(Fig. 2)} \\ &\theta(x = 0,\ t \geqslant 0) = \theta_b \\ &\theta(x = L,\ t = 0) = \theta_0;\ \theta_b < \theta_0 < \eta \\ &\theta(x, t = 0) = (\theta_0 - \theta_b)x/L + \theta_b \\ &\frac{\partial \theta}{\partial x}(x = L,\ t > 0) = 0 \\ &\frac{\rho_I}{\rho_W}\theta_I + \theta = \theta_0;\ t = 0,\ 0 < x < L \\ &\hat{\theta} > 0,\ 0 < x < L \\ &T(x) < 0\,^\circ\text{C},\ 0 \leqslant x \leqslant L \end{aligned}\right\} \tag{22}$$

where η is the porosity. Thermal conductivity is assumed given by the DeVries (1966) equation

$$K_T = K_W\theta + K_I\theta_I + K_S\theta_S \tag{23}$$

where (K_W, K_I, K_S) are the thermal conductivities of

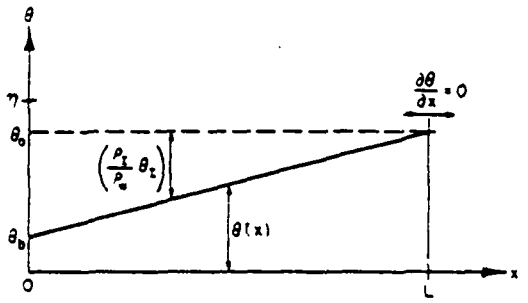

Fig. 3. Geometry for example initial condition problem.

water, ice and soil. Other pertinent parameter estimations are obtained from the laboratory data shown in Figs. (1) and (2). The unsaturated diffusivity shown in Fig. (1) is estimated by

$$D(\theta, \theta_I = 0) = 0.278e^{25.58\theta}, \quad 0.11 \leq \theta \leq 0.26 \quad (24)$$

Taylor and Luthin propose an ice accumulation correction factor, I, for freezing soils, such that

$$\left.\begin{aligned} D(\theta,\theta_I) &= D(\theta)/I \\ I &= 10^{10\theta_I} \end{aligned}\right\} \quad (25)$$

Thus, for below freezing temperatures

$$D(\theta,\theta_I) = 0.278e^{(25.58\theta - 23.03\theta_I)}, \quad 0.11 \leq \theta \leq 0.26 \quad (26)$$

The spatial gradient of diffusivity for below freezing temperatures is given by the chain rule

$$\frac{\partial D(\theta,\theta_I)}{\partial x} = \frac{\partial D}{\partial \theta}\frac{\partial \theta}{\partial x} + \frac{\partial D}{\partial \theta_I}\frac{\partial \theta_I}{\partial x} \quad (27)$$

From eqn. (23)

$$\frac{\partial K_T}{\partial x} = K_W \frac{\partial \theta}{\partial x} + K_I \frac{\partial \theta_I}{\partial x} \quad (28)$$

From Fig. 2,

$$\theta(T) = 0.325 + 0.55T, \quad 0.11 \leq \theta \leq 0.26 \quad (29)$$

thus,

$$\dot{\theta} = \frac{\partial \theta}{\partial T} = 0.55 \equiv \dot{\theta}_0, \quad 0.11 \leq \theta \leq 0.26 \quad (30)$$

For the initial conditions of eqn. (22) and $0.11 \leq \theta \leq 0.26$,

$$\left.\begin{aligned} \frac{\partial \theta_I}{\partial x} &= -\frac{\rho_W}{\rho_I}\frac{\partial \theta}{\partial x} = -1.1\frac{\partial \theta}{\partial x} \\ \frac{\partial K_T}{\partial x} &= (K_W - 1.1K_I)\frac{\partial \theta}{\partial x} < 0 \\ \frac{\partial D(\theta,\theta_I)}{\partial x} &= 50.91\, D\frac{\partial \theta}{\partial x} \end{aligned}\right\} \quad (31)$$

For the initial conditions of eqn. (22), the statement of eqn. (7) is rewritten in terms of temperature as

$$\frac{\partial}{\partial x}\left[\left(L_a D\dot{\theta} + K_T\right)\frac{\partial T}{\partial x}\right] = \left[L_a \dot{\theta} + C_m\right]\frac{\partial T}{\partial t} \quad (32)$$

and from eqn. (2),

$$\left[L_a \dot{\theta} + C_m\right]\frac{\partial T}{\partial t} = C_a \frac{\partial T}{\partial t} \quad (33)$$

Equation 32 is expanded as

$$\left(L_a D\dot{\theta} + K_T\right)\frac{\partial^2 T}{\partial x^2} + \left[\frac{\partial}{\partial x}\left(L_a D\dot{\theta} + K_T\right)\right]\frac{\partial T}{\partial x} = C_a \frac{\partial T}{\partial t} \quad (34)$$

For $\dot{\theta}$ equal to the constant $\dot{\theta}_0$ per eqn. (30), the initial condition modeled temperature profile is linear and

$$\left.\begin{aligned} \frac{\partial}{\partial x}\left(L_a D\dot{\theta}_0 + K_T\right) &= \frac{C_a \dfrac{\partial T}{\partial t}}{\dfrac{\partial T}{\partial x}} \\ \partial T/\partial x &> 0 \end{aligned}\right\} \quad (35)$$

but from eqn. (4), the initial condition of the test problems implies

$$\frac{\partial K_T}{\partial x}\frac{\partial T}{\partial x} = C_m \frac{\partial T}{\partial t} - L_a \frac{\rho_I}{\rho_W}\frac{\partial \theta_I}{\partial t} \quad (36)$$

Thus,

$$\left.\begin{aligned} 0 &> C_m \frac{\partial T}{\partial t} - L_a \frac{\rho_I}{\rho_W}\frac{\partial \theta_I}{\partial t} \\ \frac{\partial K_T}{\partial x} &< 0 \end{aligned}\right\} \quad (37)$$

Since convected heat is assumed negligible in this example, it can be assumed that initially

$$\partial T/\partial t \leq 0 \tag{38}$$

but

$$\frac{\partial T}{\partial t} = \frac{\partial T}{\partial \theta}\frac{\partial \theta}{\partial t}, \quad T<0°C \tag{39}$$

Thus, for the initial condition of the test problem

$$\partial \theta/\partial t \leq 0 \tag{40}$$

Therefore, from eqns. (18), (35), (38) and (40)

$$\frac{\partial DL_a}{\partial x} \leq -\frac{\partial}{\partial x}\frac{K_T}{\dot{\theta}_0} \tag{41}$$

is a necessary condition to preserve the $\theta(T)$ assumption for the freezing soil test problem. From eqn. (34), the restrictions of eqn. (41) also apply in a freezing soil where temperature (or moisture) gradients are linear. The conditions of eqn. (41) can also be determined from eqn. (7) by a development similar to the above.

For thermal parameters assumed given by

$$\left.\begin{aligned} K_W &= 4.8 \text{ cal/h cm °C} \\ K_I &= 19 \text{ cal/h cm °C} \\ L_a &= 80 \text{ cal/cm}^3 \end{aligned}\right\} \tag{42}$$

eqn. (41) can be evaluated for the initial conditions of the test problem as

$$\left.\begin{aligned} \frac{\partial DL_a}{\partial x} &= 4072.8\, D\,\frac{\partial \theta}{\partial x} \text{ cal/h cm}^2 \\ \frac{\partial}{\partial x}\left(\frac{K_T}{\dot{\theta}}\right) &= -29.3\,\frac{\partial \theta}{\partial x} \text{ cal/h cm}^2 \end{aligned}\right\} \tag{43}$$

but $\partial\theta/\partial x > 0$ by Fig. 3. Thus, from the initial condition of the test problem and eqns. (41) and (43), a necessary requirement for preserving the $\theta(T)$ assumption is

$$\left.\begin{aligned} &D(\theta,\theta_I) \leq 0.0072 \text{ cm}^2/\text{m} \\ &0 < x < L \end{aligned}\right\} \tag{44}$$

The conditions of eqn. (44) cannot generally be satisfied for the considered domain $0.11 < \theta < 0.26$.

For modeling purposes, it is assumed that eqn. (41) must be satisfied for any moisture content profile. The results of eqn. (41) can also be derived from eqn. (21) by considerations of linear water content profiles. A major implication of eqn. (41) is that for the $\theta(T)$ assumption to remain valid, the soil freezing front must essentially continually advance into the soil column. The requirement of eqn. (20) implies that the net heat efflux must never be exceeded by the net influx of latent heat (influx due to moisture transport). Since the assumed initial condition ice and water content profile are arbitrary for the problem of Fig. 3, the $\theta(T)$ assumption and resulting apparent heat capacity term formulation indicates that the models that incorporate these are restricted to a limited class of soil freezing problems.

SOIL-WATER PHASE CHANGE EFFECTS MODELED AS AN ISOTHERMAL PROCESS

Guymon et al. (1980) propose a model of simultaneous flux of heat and moisture in freezing and thawing soils that assumes latent heat effects can be modeled as an isothermal process. The concepts employed in this model are discussed below.

Consider the heat budget ΔQ required to alter a unit volume soil-water–ice mixture by a temperature change of dT in a time interval of dt,

$$\Delta Q = C_m\,dT - L_a\frac{\rho_I}{\rho_W}\frac{\partial \theta_I}{\partial t}\,dt \tag{45}$$

Equation (45) can be rewritten as

$$\Delta Q = C_m\frac{\partial T}{\partial t}\,dt - L_a\frac{\rho_I}{\rho_W}\frac{\partial \theta_I}{\partial t}\,dt \tag{46}$$

where temperature is a differentiable function of time.

Application of eqn. (46) to problems where the water content of the soil can also be assumed to be a differentiable function of temperature permits the rewriting

$$\Delta Q = \left(C_m + L_a\frac{\partial \theta}{\partial T}\right)\frac{\partial T}{\partial t}\,dt \tag{47}$$

which establishes the apparent heat capacity formulation of eqn. (2), where applicable.

Assuming that the convected moisture enters the soil system at approximately the temperature of the freezing point depression, a small drop in temperature ΔT (in time Δt) of the soil-ice–water mixture is modeled by a heat budget of

$$\Delta Q = L_a [\theta' - \theta(T_0)] - L_a \frac{\partial \theta}{\partial T} \Delta T - C_m \Delta T \quad (48)$$

where θ' is the volumetric moisture content at the beginning of the process; $\theta(T_0)$ is the volumetric water content described by the thermal soil-water characteristic curve for temperature T_0, T_0 is the initial temperature of the system, ΔT is the temperature drop (assumed negative), and ΔQ is the heat lost from the system during time step Δt.

From eqn. (48), three macroscopic thermodynamic cases are accommodated in the lumped isothermal model for a strictly freezing process

$$L_a [\theta' - \theta(T_0)] = \Delta Q \quad (49)$$

$$L_a [\theta' - \theta(T_0)] > \Delta Q \quad (50)$$

$$L_a [\theta' - \theta(T_0)] < \Delta Q \quad (51)$$

Equation (49) is associated with isothermal freezing in a static thermal and moisture regime. Relation (50) also indicates isothermal freezing (i.e. no temperature variation) but additionally indicates possible moisture accumulation. Equation (51) occurs with a temperature change of the system ΔT (during time step Δt) determined from eqn. (48)

$$\Delta T = \frac{L_a[\theta' - \theta(T_0)] - \Delta Q}{L_a \frac{\partial \theta}{\partial T} + C_m} \quad (52)$$

The ice accumulation term is calculated by

$$\frac{\rho_I}{\rho_W} \frac{\partial \theta_I}{\partial t} dt = \begin{cases} \dfrac{\Delta Q}{L_a}, & \text{if } \Delta Q \leq L_a [\theta' - \theta(T_0)] \\ [\theta' - \theta(T_0)] - \dfrac{\partial \theta}{\partial T} \Delta T, & \\ \text{if } \Delta Q > L_a[\theta' - \theta(T_0)] & \end{cases} \quad (53)$$

Assume $\theta(T)$ approximated by a set of linear functions defined on a discretized thermal domain per Fig. 2. Then for an appropriate temperature subdomain for $T_a \leq T \leq T_b$

$$\theta(T) = \beta_0 + \beta_1 T \quad (54)$$

where β_0, β_1 are constant soil parameters, and

$$\partial \theta(T)/\partial T = \beta_1 \quad (55)$$

Thus, for a small change in temperature ΔT (ΔT negative), eqn. (48) and eqn. (55) are modeled by

$$\Delta Q = \{L_a[\theta' - \theta(T_0)] - L_a \beta_1 \Delta T\} - C_m \Delta T \quad (56)$$

where the term in brackets represents an isothermal freezing process.

The terms within the braces of eqn. (56) may be approximated numerically by decoupling the ice formation terms from the general heat transfer equation and allocating the subsequent heat evolution to a latent heat budget. As the ice content increases, the thermal and moisture parameters are adjusted. Ice formation is interpreted as a moisture sink in the moisture transfer relation. Only when the necessary heat evolution has occurred, is a soil mixture's temperature allowed to recede below the freezing point depression, hence modeling the isothermal phase change process.

DISCUSSION

Although there are no apparent theoretical problems in applying the apparent heat capacity concept to numerical models that deal only with the thermal regime of freezing soils, there may be problems when using this concept to numerically model simultaneous thermal and moisture states of freezing soils. This is particularly true in regions where the thermal (or moisture content) spatial gradients are approximately linear, resulting in invalidation of the water content to temperature functional relationship as shown herein. In the literature, numerical models employing this approach require small time-steps (on the order of centimeters). Using currently proposed numerical modeling approaches shows that assumptions imbedded in these models lead to inconsistencies when these models use the apparent heat capacity approach in its present form. Either an apparent heat capacity formulation based upon open freezing situations where moisture is mobile will have to be prepared or alternative means of accounting for latent heat effects are required.

An alternative modeling approach is proposed which is based on an isothermal soil-water freezing submodel. Such an approach leads to a self-consistent model. From a practical standpoint, time-step sizes can be relatively large, of the order of hours, and spatial discretization can also be relatively large, of the order of 0.5 meters. Models that have been developed and employed are able to accurately simulate thermal and moisture states of freezing soils over long time spans, of the order of years. The ability to use large discretization and achieve stable, accurate results over a long simulation period will become increasingly important as more complex problems are attempted which require two or three spatial dimensions. It is emphasized that the proposed isothermal approach is a lumped thermodynamic assumption used for predictive modeling. No claim is made that such a modeling assumption describes the microscopic thermodynamic behavior of water freezing or thawing in a soil.

REFERENCES

Anderson, D.M., Tice, A.R. and McKim, H.L. (1973), The unfrozen water and the apparent specific heat capacity of frozen ground. In: Second International Permafrost Conference, Yakutsk, USSR, North Amer. Conf., National Acad. of Sci., pp. 289–294.

DeVries, D.A. (1966), Thermal properties of soils. In: W.E. van Wijk (Ed.), Physics of Plant Environment. North-Holland Pub. Co., Amsterdam, pp. 210–235.

Fuchs, M., Campbell, G.S. and Papendick, R.I. (1978), An analysis of sensible and latent heat flow in a partially frozen unsaturated soil. Soil Sci. Soc. Am. J., 42: 379–385.

Guymon, G.L. and Luthin, J.N. (1974), A coupled heat and moisture transport model for arctic soils. Water Resources Res., 10(5): 995–1001.

Guymon, G.L., Hromadka, T.V. II and Berg, R.L. (1980), A one-dimensional frost heave model based upon simulation of simultaneous heat and water flux. Cold Regions Sci. Technol., 3: 253–262.

Harlan, R.L. (1973), Analysis of coupled heat-fluid transport in partially frozen soil. Water Resources Res., 9(5): 1314–1323.

Hromadka, T.V. II and Guymon, G.L. (1980), Some effects of linearizing the unsaturated soil-moisture transfer diffusivity model. Water Resources Res., 16(4): 643–650.

Jame, Y.W. (1978), Heat and mass transfer in freezing unsaturated soil. Ph.D. Dissertation, Univ. of Saskatchewan, Saskatoon, Canada.

Sheppard, M.I., Kay, B.O. and Loch, J.P.C. (1977), Development and testing of a computer model for heat and mass flow in freezing soils. In: Proc. Third Int. Permafrost Conf., Edmonton, Canada, National Research Council of Canada, Vol. 1, pp. 76–81.

Taylor, G.S. and Luthin, J.N. (1978), A model for coupled heat and moisture transfer during soil freezing, Canadian Geotech. J., 15: 548–555.

Williams, P.J. (1968), Properties and behavior of freezing soils. Norwegian Geotechnical Inst. Pub. No. 72.

SUBDOMAIN INTEGRATION MODEL OF GROUND-WATER FLOW

By T. V. Hromadka II[1] and G. L. Guymon,[2] M. ASCE

INTRODUCTION

Numerical solution of the governing differential equations describing one-dimensional ground-water flow has received substantial attention since the advent of modern computers. Generally, numerical models are developed which employ the well-known finite-difference or Galerkin finite element methods (1,2) to approximate the governing equations, resulting in a model which can be solved generally only with computers of at least the minicomputer class. Recently, the "method-of-lines" (3) was used to solve the nonlinear unconfined ground-water flow equations resulting in a numerical model which can be accommodated by a programmable hand-held calculator. The algorithm used a "shooting method" which required an iteration process to obtain the desired accuracy. The main purpose of this paper is to present another approach to solving nonlinear (and linear) problems such as ground-water flow processes which also may be accommodated by programmable calculators. The numerical approach used is the subdomain integration version of the weighted residual methods as applied to solving for spatial coordinates as a function of the ground-water (or piezometric) surface.

The objectives of this paper are threefold. The first objectives is to present the subdomain integration numerical method as applied to a specific class of one-dimensional transport problems. Hromadka and Guymon (6,7,8) developed this numerical modeling procedure in detail and compare modeling efficiency to the well known finite difference and Galerkin finite element methods, and conclude that the subdomain integration procedure leads to a more accurate numerical model for the various problems tested. Extension of the modeling method to one-dimensional and two-dimensional linear and nonlinear advection-diffusion problems are the subject of current papers (9,10,11).

The second objective of this paper is to determine a subdomain integration

[1]Asst. Research Engr. and Lect., School of Engrg., University of California, Irvine, Calif. 92717.

[2]Assoc. Prof. of Civ. Engrg., School of Engrg., Univ. of California, Irvine, Calif. 92717.

Note. Discussion open until June 1, 1981. To extend the closing date one month, a written request must be filed with the Manager of Technical and Professional Publications, ASCE. Manuscript was submitted for review for possible publication on October 15, 1980. This paper is part of the Journal of the Irrigation and Drainage Division, Proceedings of the American Society of Civil Engineers, ©ASCE, Vol. 107, No. IR2, June, 1981. ISSN 0044-7978/81/0002-0187/$01.00.

numerical model which solves for spatial coordinates rather than solving for the governing flow equation's state variable. This approach somewhat eliminates nonlinearity (due to state variable dependent parameters) because the nonlinear parameters are evaluated at a constant value of the state variable along the boundaries of each subdomain.

The third objective is to simplify the resulting subdomain integration numerical model into an approximation which can be accommodated by programmable calculators. For the specialized problems tested, the simplified subdomain integration approximation produced good results when compared to available analytic solutions.

Governing One-Dimensional Ground-Water Flow Equations

One dimensional, unsteady ground-water flow in a confined homogeneous aquifer of a nearly uniform thickness is generally described by a linear partial differential equation of the form

$$\alpha \frac{\partial^2 h}{\partial x^2} = \frac{\partial h}{\partial t} \qquad (1)$$

subject to appropriate boundary and initial conditions. In Eq. 1, h = a convenient reference of piezometric head (Fig. 3); *x and t = spatial and temporal coordinates;* and α = the quotient of transmissivity T, and effective porosity, n. Examples of approximately one-dimensional ground-water flow include the movement of water between a stream and the aquifer in response to a change in stage, and aquifer recharge from streams, canals, and irrigation ditches due to a sudden increase in stage.

The nonlinear partial differential equation describing *one-dimensional unconfined* ground-water flow is the well known Boussinesq equation

$$\frac{\partial}{\partial x}\left(K_s h \frac{\partial h}{\partial x}\right) = n \frac{\partial h}{\partial t} \qquad (2)$$

in which K_s = the saturated *hydraulic conductivity; and h* = the hydraulic head. Due to the nonlinearity of Eq. 2, only a few quasianalytical solutions exist for select problems (4,5).

Numerical Model

The subdomain integration method (6-10) is applied to the governing flow equation of unconfined (and confined) ground-water flow. The boundary and initial conditions are assumed defined such that the spatial coordinate x can be described as a function of h (Fig. 1). The h-axis domain Ω is discretized by n nodal points into n subdomains Ω_j such that

$$\Omega = \bigcup_{j=1}^{n} \Omega_j \qquad (3)$$

in which $\Omega_j \cap \Omega_{j+1} = \frac{1}{2}(h_j + h_{j+1})$; $j = 1, 2, \ldots, n-1$ (4)

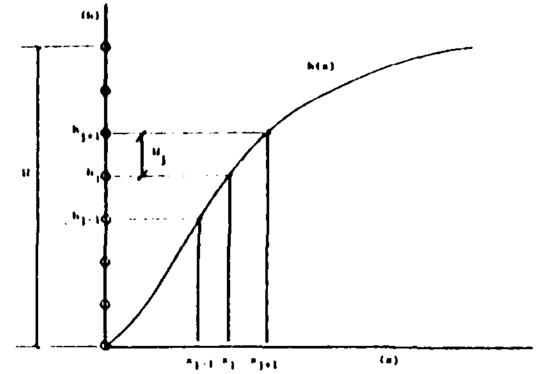

FIG. 1.—Nodal Point Distribution on *h*-Axis Global Domain Ω

For an interior subdomain Ω_j, $1 < j < n$, let

$$h' = \Omega_{j-1} \cap \Omega_j = \frac{1}{2}(h_{j-1} + h_j); \quad h'' = \Omega_j \cap \Omega_{j+1} = \frac{1}{2}(h_j + h_{j+1}) \qquad (5)$$

$$x' = x(h'); \quad x'' = x(h'') \qquad (6)$$

The integration of the nonlinear Eq. 2 over Ω_j is modeled by

$$\left(K_s h \frac{dh}{dx}\right)\Big|_{x''} - \left(K_s h \frac{dh}{dx}\right)\Big|_{x'} = n \frac{d}{dt}\int_{x'}^{x''} h\,dx + n h' \frac{dx'}{dt} - n h'' \frac{dx''}{dt} \qquad (7)$$

For a linear trial function approximation on subdomain Ω_j (Fig. 2)

$$\int_{x'}^{x''} h\,dx = \frac{1}{8}\left[(x_j - x_{j-1})(h_{j-1} + 3h_j) + (x_{j+1} - x_j)(h_{j+1} + 3h_j)\right] \qquad (8)$$

in which each h_j is constant and $x_j = x_j(t)$. Thus

$$\frac{d}{dt}\int_{x'}^{x''} h\,dx = \frac{1}{8}\left[(h_{j-1} + 3h_j)\left(\frac{dx_j}{dt} - \frac{dx_{j-1}}{dt}\right) + (h_{j+1} + 3h_j)\left(\frac{dx_{j+1}}{dt} - \frac{dx_j}{dt}\right)\right] \qquad (9)$$

$$\frac{dx'}{dt} = \frac{1}{2}\left(\frac{dx_{j-1}}{dt} + \frac{dx_j}{dt}\right); \quad \frac{dx''}{dt} = \frac{1}{2}\left(\frac{dx_j}{dt} + \frac{dx_{j+1}}{dt}\right) \qquad (10)$$

Equation 9 can be rewritten as

$$\frac{d}{dt}\int_{x'}^{x''} h\,dx = \frac{dx_{j-1}}{dt}\left(-\frac{h_{j-1} + 3h_j}{8}\right) + \frac{dx_j}{dt}\left(\frac{h_{j-1} - h_{j+1}}{8}\right)$$

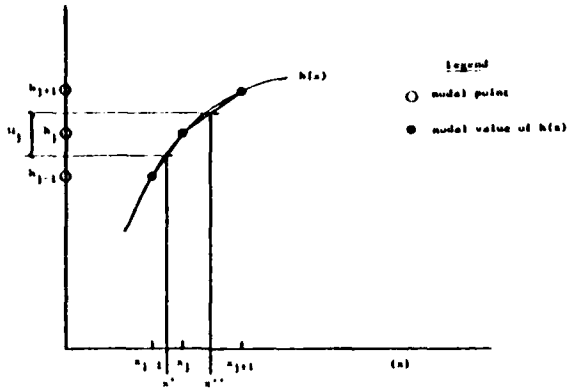

FIG. 2.—Linear Trial Function Approximation on Subdomain Ω_i

$$+\frac{dx_{i+1}}{dt}\left(\frac{h_{i+1}+3h_i}{8}\right) \quad (11)$$

$$\text{and}\quad h'\frac{dx'}{dt}-h''\frac{dx''}{dt}=\frac{dx_{i-1}}{dt}\left(\frac{h_{i-1}+h_i}{4}\right)+\frac{dx_i}{dt}\left(\frac{h_{i-1}-h_{i+1}}{4}\right)$$

$$\frac{dx_{i+1}}{dt}\left(\frac{h_i+h_{i+1}}{4}\right) \quad (12)$$

From the preceding linear trial function approximations, Eq. 7 is rewritten as

$$\frac{d}{dt}\int_{x_{i-1}}^{x_{i+1}} h\,dx+h'\frac{dx'}{dt}-h''\frac{dx''}{dt}=\frac{dx_{i-1}}{dt}\left(\frac{h_{i-1}-h_i}{8}\right)$$

$$+\frac{dx_i}{dt}\left(\frac{3h_{i-1}-3h_{i+1}}{8}\right)+\frac{dx_{i+1}}{dt}\left(\frac{h_i-h_{i+1}}{8}\right) \quad (13)$$

For the linear trial function approximation for h on Ω_i,

$$\left(K_i h\frac{\partial h}{\partial x}\right)\Big|_{x_{i-1}}=K_i h'\frac{(h_i-h_{i-1})}{(x_i-x_{i-1})} \quad (14)$$

$$\left(K_i h\frac{\partial h}{\partial x}\right)\Big|_{x_{i+1}}=K_i h''\frac{(h_{i+1}-h_i)}{(x_{i+1}-x_i)} \quad (15)$$

in which $K_i h'\,(h_i - h_{i-1})$ and $K_i h''\,(h_{i+1} - h_i)$ are constant for all time due to the numerical approximation solving for specified spatial coordinates x_i (Fig. 2). Combining Eqs. 7, 13, 14, and 15 gives the subdomain integration numerical model for Eq. 2 on Ω_i:

$$\frac{8\hat{K}_i h''(h_{i+1}-h_i)}{(x_{i+1}-x_i)}-\frac{8\hat{K}_i h'(h_i-h_{i-1})}{(x_i-x_{i-1})}=\frac{dx_{i-1}}{dt}(h_{i-1}-h_i)$$

$$+3\frac{dx_i}{dt}(h_{i-1}-h_{i+1})+\frac{dx_{i+1}}{dt}(h_i-h_{i+1}) \quad (16)$$

in which $\hat{K}_i = K_i/n$.

For problems where

$$h_{i+1}-h_i=h_i-h_{i-1}=\Delta h \quad (17)$$

$$\text{and}\quad \frac{dx_{i-1}}{dt}+\frac{dx_{i+1}}{dt}=2\frac{dx_i}{dt} \quad (18)$$

the numerical statement of Eq. 16 can be simplified as

$$\frac{\hat{K}_i h''\Delta h}{(x_{i+1}-x_i)}-\frac{\hat{K}_i h'\Delta h}{(x_i-x_{i-1})}=\Delta h\frac{dx_i}{dt} \quad (19)$$

It may be noted that the K_i parameter has not been assumed constant in the numerical model derivations, i.e., due to the approach of solving for spatial coordinates x_i, nonlinear terms such as $hK(h)$ will be constant on the boundaries of Ω_i.

Equation 17 is integrated with respect to time to give the model approximation for Eq. 2 on Ω_i,

$$\int_{t=k\Delta t}^{t=(k+1)\Delta t}\left[\frac{\hat{K}_i h''}{(x_{i+1}-x_i)}-\frac{\hat{K}_i h'}{(x_i-x_{i-1})}\right]dt+x_i(k\Delta t)=x_i[(k+1)\Delta t] \quad (20)$$

Integrating Eq. 20 over a small Δt timestep gives

$$\frac{\hat{K}_i h''\Delta t}{(x_{i+1}^2-x_i^2)-(x_{i+1}^1-x_i^1)}\ln\left(\frac{x_{i+1}^2-x_i^2}{x_{i+1}^1-x_i^1}\right)$$

$$-\frac{\hat{K}_i h'\Delta t}{(x_i^2-x_{i-1}^2)-(x_i^1-x_{i-1}^1)}\ln\left(\frac{x_i^2-x_{i-1}^2}{x_i^1-x_{i-1}^1}\right)+x_i^1=x_i^2 \quad (21)$$

in which in Eq. 21 the superscripts 1 and 2 designate x-coordinate values at time $k\Delta t$ and $(k + 1)\,\Delta t$, respectively. Equation 21 can be further simplified by letting

$$\frac{\hat{K}_i h''\Delta t}{(\bar{x}_{i+1}-\bar{x}_i)}-\frac{\hat{K}_i h'\Delta t}{(\bar{x}_i-\bar{x}_{i-1})}+x_i^1=x_i^2 \quad (22)$$

in which it is assumed that (12)

$$\bar{x}_i=\frac{1}{2}[3x_i(t=k\Delta t)-x_i(t=k\Delta t-\Delta t)] \quad (23)$$

Therefore, an explicit formulation for the approximation of Eq. 2 is developed whereby each future x-coordinate, e.g., x_i^2, can be determined from previously determined data. The development of an equivalent numerical model for Eq. 1 follows analogously to the preceding derivation (6,7,8).

Model Applications

To demonstrate the accuracy of the proposed numerical method, the first

problem presented is an idealization of ground-water flow from a confined aquifer that forms the banks of a stream. It is assumed that drawdown is sufficiently small so that Eq. 1 describes the flow process. The initial and boundary conditions assumed in order to simulate an instantaneous step change in the piezometric profile of the aquifer are (Fig. 3)

$$h(x,0) = h_o; \quad h(\infty,t) = h_o, t \geq 0; \quad h(0,t) = 0, t > 0 \quad \ldots\ldots\ldots\ldots (24)$$

The analytical solution to Eqs. 1 and 24 is given by

$$h = h_o \operatorname{erf}\left(\frac{x}{\sqrt{4\alpha t}}\right)$$

in which h_o = the assumed constant step change of stage. For example purposes, the substitutions of a unit step change in stage and $\alpha = 0.25$ (units of L^2/T) were used.

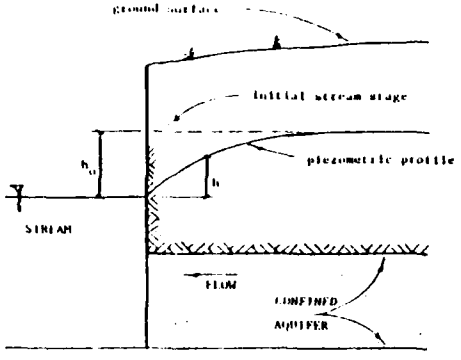

FIG. 3.—Flow from Confined Aquifer to Stream Due to Drop in Stage

Due to the several simplifying assumptions used to reduce the complexity of Eq. 16 to the approximation of Eq. 22, small timestep increments were required. The assumption of Eq. 17 is met by suitable discretization of Ω by equally spaced nodal points. The assumption of Eq. 18, however, limits the time rate of change of the state variable profile, i.e., in the initial portions of the problem solution when the piezometric profile changes relatively rapidly, much smaller timestep increments were required than when the piezometric profile varied more slowly. In order to keep the program size small, several simulations were made using various constant timestep sizes. The resulting modeled profiles were compared until negligible differences in the computed piezometric profiles were observed with decreasing timestep size. The resulting piezometric profile at various intervals of time are compared to model results in Fig. 4. From the figure, good results were obtained in the use of Eq. 22 to model the linear formulation of Eq. 1.

The second problem presented is the application of the model of Eq. 22 to solution of the nonlinear formulation of Eq. 2. The problem considered is

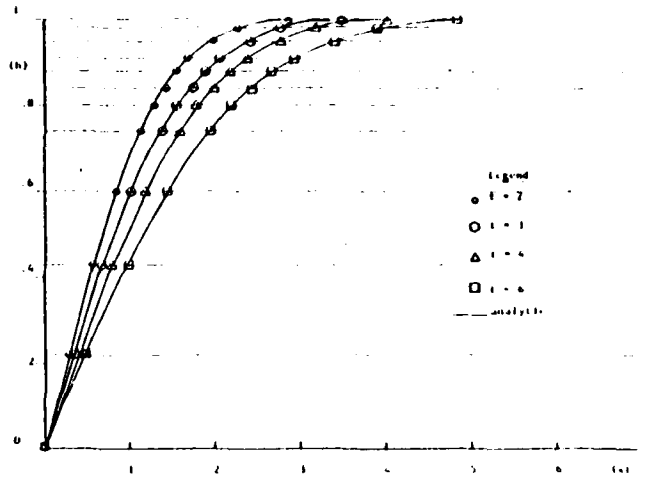

FIG. 4.—Model Results in Predicting Piezometric Profile

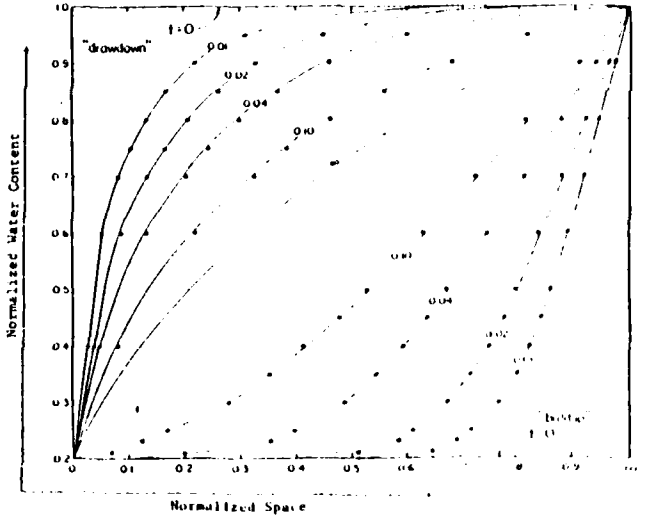

FIG. 5.—Model Results in Predicting Free Water Surface [Dots Represent Modeled Results; Solid Line Represents Analytic Solution to Equation 2 (3)]

the estimation of unconfined ground-water surface profiles for an instantaneous step change in elevation between two reservoirs separated by a given length of soil. Figure 5 shows dimensionless water surface profiles and computed results. For the normalized problems considered, time steps of .000125 were used requiring a total of 720 cycles to advance the profiles from normalized time of 0.01 0.10. As can be seen from Fig. 5, good results are achieved. As with the previous test problems, several simulations were made reducing constant timestep sizes until negligible differences in the computed ground-water surface profiles were observed.

The computational algorithm can be accommodated on current programmable calculators when the simplifying assumptions of Eqs. 18 and 19 are used. A further simplication of the model is the elimination of the time-step approximation of Eq. 23, further reducing calculator memory requirements.

Conclusions

The subdomain integration version of the weighted residuals method is applied to the linear and nonlinear equations of one dimensional confined and unconfined ground water flow, respectively. The approach used is to determine the spatial coordinates as a function of piezometric or free ground-water surface profiles. A simplified version of the numerical model can be accommodated by current programmable calculators. Good results were obtained when applying the proposed numerical model to the problems considered. However, several simulations were required for each problem tested, progressively reducing timestep sizes until negligible differences in computed results were observed.

Acknowledgments

This research was supported by the United States Army, Research Office, Triangle Park, N. C., Grant No. DAAG29-79-C-0080.

Appendix I.—References

1. McWhorter, D. B., and Sunada, D. K., *Ground-Water Hydrology and Hydraulics*, WPR Publications, Fort Collins, Colo., 1977.
2. Freeze, R. A., and Cheery, J. A., *Groundwater*, Prentice-Hall, Inc., Englewood Cliffs, N.J., 1979.
3. Koussis, A. D., and Watson, R. W., "Ground-Water Flow Computations by Method of Lines," *Journal of the Irrigation and Drainage Division*, ASCE, Vol. 106, No. IR1, Proc. Paper 15238, Mar., 1980, pp. 1-8.
4. Van Schilfgaarde, J., "Design of Tile Drainage for Falling Water Tables," *Journal of the Irrigation and Drainage Division*, ASCE, Vol. 89, No. IR2, Proc. Paper 3543, June, 1963, pp. 1-11.
5. McWhorter, D. B., and Duke, H. R., "Transient Drainage with Nonlinearity and Capillarity," *Journal of the Irrigation and Drainage Division*, ASCE, Vol. 102, No. IR2, Proc. Paper 12185, June, 1976, pp. 193-204.
6. Hromadka, T. V. II, and Guymon, G. L., "Numerical Mass Balance for Soil Moisture Transport Problems," *Advances in Water Resources Research*, Vol. 3, 1980, p. 107.
7. Hromadka, T. V. II, and Guymon, G. L., "Some Effects in Linearizing the Unsaturated Soil Moisture Transfer Diffusion Model," *Water Resources Research*, Vol. 16, 1980, pp. 643-650.
8. Hromadka, T. V. II, and Guymon, G. L., "Time Integration of Soil Water Diffusivity

Problems," *Advances in Water Resources Research*, 1980.
9. Hromadka, T. V. II, and Guymon, G. L., "Improved Linear Shape Function Model of Soil Moisture Transport," *Water Resources Research*, 1980.
10. Hromadka, T. V. II, and Guymon, G. L., "Nodal Domain Integration Model of One-Dimensional Advection-Diffusion," *Advances in Water Resources Research*, 1980.
11. Hromadka, T. V. II, and Guymon, G. L., "A Note on Numerical Approximation of Two-Dimensional Advection-Diffusion Process in Rectangular Spatial Domains," *Advances in Water Resources Research*, 1980.
12. Ahuja, L. R., and Swartzendruber, D., "Horizontal Soil-Water Intake Through a Thin Zone of Reduced Permeability," *Journal of Hydrology*, Vol. 19, 1973, pp. 71-89.

Appendix II.—Notation

The following symbols are used in this paper:

h = piezometric or free water surface elevation;
h_j = nodal point value of h;
K_s = saturated hydraulic conductivity;
$\hat{K}_s$ = K_s/n;
n = specific porosity;
x, t = space and time coordinates;
erf = error function;
α = hydraulic diffusivity;
Δt = time step;
Ω = domain of definition; and
Ω_j = subdomain j.

16323 MODEL OF GROUNDWATER FLOW

KEY WORDS: Calculators; **Computation; Equations; Ground water; Groundwater flow; Mathematical programming;** Nonlinear systems, Numerical calculations; Seepage

ABSTRACT: The subdomain numerical integration method is applied to the nonlinear one-dimensional saturated groundwater flow equation (Boussinesq equation). Because the state variable of the resulting numerical analog can be cast in terms of spatial coordinates, nonlinearity can be eliminated, greatly increasing accuracy and simplifying the numerical code. As a result, the solution can be performed on hand held programmable calculators. Good results were obtained when applying the method to confined and unconfined (nonlinear) aquifer examples.

REFERENCE: Hromadka, T. V., II, and Guymon, G. L., "Subdomain Integration Model of Ground-Water Flow," *Journal of the Irrigation and Drainage Division*, ASCE, Vol. 107, No. IR2, Proc. Paper 16323, June, 1981, pp. 187-195.

WATER RESOURCES RESEARCH, VOL. 17, NO. 3, PAGES 504–512, JUNE 1981

Improved Linear Trial Function Finite Element Model of Soil Moisture Transport

T. V. HROMADKA II AND G. L. GUYMON

School of Engineering, University of California, Irvine, California 92717

Two methods of modeling a higher-order approximation function of soil moisture transport by an improved linear trial function approximation are presented. The first approach considered is based upon use of the alternation theorem and a finite element capacitance matrix that incorporates the Galerkin finite element, subdomain, finite difference, and proposed nodal domain integration methods. The second approach extends the first approach by developing a temporal relationship for element matrices such that a higher-order approximation function can be modeled by a linear approximation function. Comparison of model results produced from a nodal domain integration model incorporating these improved linear trial function approximations to the finite element, subdomain, and finite difference methods indicates that this approach may lead to a generalized modeling method for soil moisture transport problems.

INTRODUCTION

The study of numerical methods for the approximation of linear and nonlinear soil moisture transport in a one-dimensional domain has received some recent attention. *Hayhoe* [1978] compared the numerical effectiveness between the finite element and finite difference numerical methods in modeling a sharp wetting front soil infiltration problem. A special finite difference analog was advanced as the best numerical approach to the problem studied. *Hromadka and Guymon* [1980*a*] further studied the sharp wetting front problem and developed a modification to the finite element method which resulted in an increase in model accuracy for a linear soil water diffusivity problem. For a nonlinear diffusivity problem the traditional finite element formulation gave comparable results to *Hayhoe*'s [1978] finite difference approach when the finite element analog used constant element diffusivity values as determined by a spatial estimation procedure. A procedure to determine which numerical (domain) method to use for simulation of all moisture transport problems, however, is not advanced.

In this paper, two approaches for increasing numerical model accuracy by modeling a higher-order or a more complex family of trial functions by linear trial functions are presented. Such modeling procedures would benefit from the lower computational effort associated with smaller matrix arrays and yet incorporate some of the increase in numerical accuracy usually provided by higher-order trial function approximation sets.

By use of the alternation theorem for determining a 'best' approximation of a lower-order polynomial estimator to a higher-order polynomial or function, an adjustment error distribution is determined which is a function of the discretized domain nodal point set. Use of this error distribution function in a subdomain integration procedure aids in incorporating some benefits of a higher-order approximation function set into a lower-order approximation function set.

Another possibility is to define appropriate correction factors (as a function of time) which equate the various soil moisture transport terms as modeled by a family of higher-order trial functions to the first-order trial function model approximations. Like the alternation theorem approach, the resulting numerical model has the reduced matrix computer memory requirements but incorporates some of the benefits of a higher-order trial function approximation set.

We call this extension of the subdomain version of the finite element weighted residuals method the 'nodal domain integration method.' For the class of problems considered, the resulting element matrix system determined from the nodal domain integration procedure is a function of a single parameter η, which may be variable with respect to both space and time. Thus η may vary between finite elements and also change as the numerical simulation progresses in time. As special cases of the nodal domain integration element matrix system, specified constant values of η correspond to the Galerkin finite element, subdomain, and finite difference approximations. Consequently, a computer algorithm based on the resulting element matrix system derived from the nodal domain integration method will also represent these other specified numerical approaches for certain specified values of the parameter η.

MATHEMATICAL DEVELOPMENT

The one-dimensional horizontal soil moisture transport model for an unsaturated soil column is

$$\frac{\partial}{\partial x}\left(D\frac{\partial\theta}{\partial x}\right)=\frac{\partial\theta}{\partial t} \qquad x\in\Omega$$
$$\Omega=\{x:0\le x\le L\} \tag{1}$$

where θ is the volumetric water content (θ less than the soil's porosity), x is the spatial coordinate, t is time, D is the soil water diffusivity and is a function of soil water content, and Ω is the spatial domain of definition.

The domain Ω can be discretized by n nodal points into n disjoint subdomains:

$$\begin{aligned}\Omega_1&=\{x:0\le x\le (x_1+x_2)/2\}\\ \Omega_2&=\{x:(x_1+x_2)/2<x\le (x_2+x_3)/2\}\\ &\vdots\\ \Omega_n&=\{x:(x_{n-1}+x_n)/2<x\le x_n=L\}\end{aligned} \tag{2}$$

where x_i is the spatial coordinate associated to nodal point value θ_i and

$$\Omega=\bigcup_{i=1}^{n}\Omega_i \tag{3}$$

Paper number 0043-1397/81/008W-0504$01.00

Equation (1) must be satisfied on each Ω_r. Therefore n equations are generated by solving

$$\frac{\partial}{\partial x}\left[D\frac{\partial\theta}{\partial x}\right] = \frac{\partial\theta}{\partial t} \qquad x \in \Omega_r \tag{4}$$

where

$$D = D(\theta)$$
$$\theta = \theta(x, t) \tag{5}$$

Integrating (4) with respect to space gives

$$\left\{D\frac{\partial\theta}{\partial x}\right\}\Big|_{\Gamma_r} = \frac{\partial}{\partial t}\int_{\Omega_r}\theta\,dx \qquad x \in \Omega_r \tag{6}$$

where Γ_r is the spatial boundary of region Ω_r. Integrating (6) with respect to time gives

$$\int_{k\Delta t}^{(k+1)\Delta t}\left\{D\frac{\partial\theta}{\partial x}\right\}\Big|_{\Gamma_r} dt = \int_{\Omega_r}\{\theta\}\Big|_{\Gamma_r} dx \tag{7}$$

where Γ_t is the limits of temporal integration between time steps $k\Delta t$ and $(k+1)\Delta t$. Equation (7) can be simplified by using the linear transformation

$$t = k\Delta t + \epsilon$$
$$0 \le \epsilon \le \Delta t \tag{8}$$

Thus

$$\int_0^{\Delta t}\left\{D(k\Delta t+\epsilon)\frac{\partial\theta(k\Delta t+\epsilon)}{\partial x}\right\}\Big|_{\Gamma_r} d\epsilon = \int_{\Omega_r}\{\theta\}\Big|_{\Gamma_r} dx \tag{9}$$

The soil water diffusivity function can be expressed with respect to time by the Taylor series

$$D(x = x_0, k\Delta t + \epsilon) = \sum_{i=0}^{\infty}\frac{D^{(i)}(x = x_0, k\Delta t)\epsilon^i}{i!} \tag{10}$$

where (i) is the ith order temporal partial differential operator, and x_0 is a specified spatial coordinate. Combining (9) and (10) gives

$$\int_0^{\Delta t}\left\{\left(\sum_{i=0}^{\infty}\frac{D^{(i)}(k\Delta t)\epsilon^i}{i!}\right)\frac{\partial\theta(k\Delta t+\epsilon)}{\partial x}\right\}\Big|_{\Gamma_r} d\epsilon = \int_{\Omega_r}\{\theta\}\Big|_{\Gamma_r} dx \tag{11}$$

For a spatial local coordinate system defined by

$$y = \{x | 0 \le y \le l_r\} \qquad x \in \Omega_r$$
$$dy = dx \tag{12}$$
$$l_r = (x_{r+1} - x_{r-1})/2$$

(11) can be expanded as

$$\sum_{i=0}^{\infty}\frac{D^{(i)}(y = l_r, k\Delta t)}{i!}\int_0^{\Delta t}\epsilon^i\left\{\frac{\partial\theta(k\Delta t+\epsilon)}{\partial x}\right\}\Big|_{x=l_r} d\epsilon - \sum_{i=0}^{\infty}\frac{D^{(i)}(y = 0, k\Delta t)}{i!}\int_0^{\Delta t}\epsilon^i\left\{\frac{\partial\theta(k\Delta t+\epsilon)}{\partial x}\right\}\Big|_{x=0} d\epsilon = \int_{\Omega_r}\{\theta\}\Big|_{\Gamma_r} dx \tag{13}$$

The soil water content function is approximated spatially and temporally by

$$\theta(x, t) \simeq \hat{\theta}(x, t)$$

$$\hat{\theta}(x, t) = \sum_{r=1}^{\hat{n}} N_r(x)\left(\sum_{m=0}^{\hat{k}+1} M_m(t)\theta_r^m\right) \tag{14}$$

where N_r and M_m are the linearly independent spatial and temporal shape functions and

$$\theta_r^m = \theta(x = x_r, t = m\Delta t) \tag{15}$$

where the θ_r^m are known values for time steps $m = \{0, 1, \cdots, k\}$ and x_r is the spatial coordinate of node r. The spatial gradient of the soil water content function is approximated by

$$\frac{\partial\theta}{\partial x} \simeq \frac{\partial\hat{\theta}}{\partial x} = \sum_{r=1}^{\hat{n}}\frac{\partial N_r}{\partial x}\left(\sum_{m=0}^{\hat{k}+1} M_m\theta_r^m\right) \tag{16}$$

Substituting (14) and (16) into (13) gives the numerical approximation of the governing flow equation in Ω_r:

$$\sum_{i=0}^{\hat{n}}\frac{D^{(i)}(y = l_r, k\Delta t)}{i!}\int_0^{\Delta t}\epsilon^i\left\{\sum_{r=1}^{\hat{n}}\frac{\partial N_r}{\partial x}\left(\sum_{m=0}^{\hat{k}+1} M_m\theta_r^m\right)\right\}\Big|_{x=l_r} d\epsilon - \sum_{i=0}^{\hat{n}}\frac{D^{(i)}(y = 0, k\Delta t)}{i!}\int_0^{\Delta t}\epsilon^i\left\{\sum_{r=1}^{\hat{n}}\frac{\partial N_r}{\partial x}\left(\sum_{m=0}^{\hat{k}+1} M_m\theta_r^m\right)\right\}\Big|_{x=0} d\epsilon = \int_0^{l_r}\left\{\sum_{r=1}^{\hat{n}} N_r\left(\sum_{m=0}^{\hat{k}+1} M_m\theta_r^m\right)\right\}\Big|_{\Gamma_r} dy \tag{17}$$

The unknown values of nodal points θ_r^{k+1} can be solved by equating

$$\sum_{i=0}^{\hat{n}}\frac{D^{(i)}(y = l_r, k\Delta t)}{i!}\int_0^{\Delta t}\epsilon^i\left\{\sum_{r=1}^{\hat{n}}\frac{\partial N_r}{\partial x}M_{k+1}\theta_r^{k+1}\right\}\Big|_{x=l_r} d\epsilon - \sum_{i=0}^{\hat{n}}\frac{D^{(i)}(y = 0, k\Delta t)}{i!}\int_0^{\Delta t}\epsilon^i\left\{\sum_{r=1}^{\hat{n}}\frac{\partial N_r}{\partial x}M_{k+1}\theta_r^{k+1}\right\}\Big|_{x=0} d\epsilon - \int_0^{l_r}\sum_{r=1}^{\hat{n}} N_r\theta_r^{k+1}\,dx$$
$$= \sum_{i=0}^{\hat{n}}\frac{D^{(i)}(y = 0, k\Delta t)}{i!}\int_0^{\Delta t}\epsilon^i\left\{\sum_{r=1}^{\hat{n}}\frac{\partial N_r}{\partial x}\left(\sum_{m=0}^{\hat{k}} M_m\theta_r^m\right)\right\}\Big|_{x=0} d\epsilon - \sum_{i=0}^{\hat{n}}\frac{D^{(i)}(y = l_r, k\Delta t)}{i!}\int_0^{\Delta t}\epsilon^i\left\{\sum_{r=1}^{\hat{n}}\frac{\partial N_r}{\partial x}\left(\sum_{m=0}^{\hat{k}} M_m\theta_r^m\right)\right\}\Big|_{x=l_r} d\epsilon - \int_0^{l_r}\sum_{r=1}^{\hat{n}} N_r\theta_r^k\,dx \tag{18}$$

Approximation Improvement by Use of Alternation Theorem (Nodal Domain Integration Method)

The space-time surface approximated by (14) can be simplified by assuming that the functional surface $\hat{\theta}(x, t)$ can be described by sets of piecewise continuous functions. For a first-order polynomial spatial trial function approximation $\hat{\theta}$ for θ between nodal point values $(\theta_{r-1}, \theta_r, \theta_{r+1})$,

$$\frac{\partial\theta}{\partial x}\Big|_{r-1} = (\theta_{r-1} - \theta_r)/l$$
$$\frac{\partial\theta}{\partial x}\Big|_{r} = (\theta_r - \theta_{r-1})/l$$

$$\int_{x=0}^{l} \theta \, dy = \frac{l}{8}\left[\theta_{j-1} + 6\theta_j + \theta_{j+1}\right] \tag{19}$$

where for discussion purposes it is assumed that in (19),

$$x_{j+1} - x_j = x_j - x_{j-1} = l$$
$$dx = dy$$

A major problem in the linear spatial approximation of θ between neighboring nodal points is that θ curvature is *not* modeled. Thus a higher-order polynomial approximation or a more complex family of trial functions may be useful. However, additional computer memory is usually required due to the increase in the resulting matrix bandwidth incorporating additional nodal points (degrees of freedom) in the higher-order approximation. Another possibility is to approximate the more complex or higher-order trial function approximations θ for ϑ with linear trial functions $\hat{\theta}$. That is, determine the best linear approximation $\hat{\theta}$ to ϑ between consecutive nodal points. For example, let

$$\hat{\vartheta} = \theta_j + \frac{(\theta_{j+1} - \theta_j)}{\sin(\pi/2\alpha)} \sin\left(\frac{\pi Z}{2l'\alpha}\right) \qquad Z \in \Omega \tag{20}$$

where a local coordinate Z is defined by

$$\Omega = x | x_j \le x \le x_{j+1}$$
$$\Omega = Z | 0 \le Z \le l' \tag{21}$$

and

$$l' = x_{j+1} - x_j$$
$$\alpha \ge 1 \tag{22}$$

The best linear approximation $\hat{\theta}$ for ϑ on Ω is given from the alternation theorem [*Cheney*, 1966, p. 75] by setting

$$\vartheta(0) - \hat{\theta}(0) = +e \tag{23a}$$
$$\vartheta(\mu) - \hat{\theta}(\mu) = -e \tag{23b}$$
$$\vartheta(l') - \hat{\theta}(l') = -e \tag{23c}$$

where e equals a constant error and

$$\hat{\theta}(Z) = \lambda Z + \beta \qquad 0 \le Z \le l'$$
$$0 < \mu < l' \tag{24}$$

Solution of condition (23*a*) gives

$$\vartheta(0) - \hat{\theta}(0) = \beta - \theta_j = +e \tag{25}$$

Solution of condition (23*c*) gives

$$\vartheta(l') - \hat{\theta}(l') = \lambda l' + \beta - \theta_{j+1} = +e \tag{26}$$

From (25) and (26),

$$\hat{\theta}(Z) = \frac{(\theta_{j+1} - \theta_j)}{l'} Z + \theta_j + e \qquad Z \in \Omega \tag{27}$$

Solving for e, (23*b*) is differentiated and set to zero:

$$\frac{d}{dZ}(\vartheta(Z) - \hat{\theta}(Z)) = 0 \qquad Z \in \Omega \tag{28}$$

giving

$$\mu = \frac{2l'\alpha}{\pi} \cos^{-1}\left[\frac{2\alpha \sin(\pi/2\alpha)}{\pi}\right] \tag{29}$$

Combining (23*b*) and (29) gives

$$e = \frac{(\theta_{j+1} - \theta_j)}{2\pi}\left\{\frac{(\pi^2 - 4\alpha^2 \sin^2(\pi/2\alpha))^{1/2}}{\sin(\pi/2\alpha)} - 2\alpha \cos^{-1}\left[\frac{2\alpha \sin(\pi/2\alpha)}{\pi}\right]\right\} \tag{30}$$

In (30), $\alpha = 1$ corresponds to a quarter cycle of the general sinusoidal curve, whereas $\alpha \to \infty$ corresponds to a zero-curvature approximation (straight line). For a given value of $\alpha = \alpha_0$,

$$e(\theta_j, \theta_{j+1}, \alpha_0) = e(\theta_j, \theta_{j+1}) \tag{31}$$

Therefore for $Z \in \Omega$

$$\hat{\theta}(Z) = (\theta_{j+1} - \theta_j)\frac{Z}{l'} + \theta_j + e(\theta_j, \theta_{j+1}) \tag{32}$$

Comparison of (32) to (19) indicates that the spatial gradient terms remain similar, but the integration of $\hat{\theta}$ differs from that of θ in (19) due to the e term. Thus anagolous to (19),

$$\left.\frac{\partial\theta}{\partial x}\right|_{x=l} = (\theta_{j+1} - \theta_j)/l$$
$$\left.\frac{\partial\theta}{\partial x}\right|_{x=0} = (\theta_j - \theta_{j-1})/l \tag{33}$$
$$\int_{x=0}^{l} \theta \, dy = \int_{x=0}^{x_e} \hat{\theta} \, dy + \int_{x=x_e}^{l} \theta \, dy$$

The selection of the approximation in (20) is arbitrary. Another possibility is to fit a polynomial to all nodal values in Ω and solve for $e(\theta_j, \theta_{j+1})$ for each Δt time step.

TIME INTEGRATION APPROXIMATION

For Δt time steps a linear polynomial function approximation may be used to model the time variation of $\vartheta(x, t)$ between time steps $(k, k+1)$, where $(k+1)$ is the time step to be evaluated; thus

$$\theta_j(k\Delta t + \epsilon) = (\theta_j^{k\Delta t})\left(\frac{\Delta t - \epsilon}{\Delta t}\right) + (\theta_j^{(k+1)\Delta t})\frac{\epsilon}{\Delta t} \tag{34}$$
$$k\Delta t \le t \le (k+1)\Delta t \qquad 0 \le \epsilon \le \Delta t$$

Combining (33) and (34), the spatial gradient approximation during the time step Δt is given by

$$\left.\frac{\partial\theta}{\partial x}\right|_{x=l} = (\theta_{j+1}^2 - \theta_{j-1}^1 - \theta_j^2 + \theta_j^1)\epsilon/l\Delta t + (\theta_{j+1}^1 - \theta_j^1)/l$$
$$\left.\frac{\partial\theta}{\partial x}\right|_{x=0} = (\theta_j^2 - \theta_j^1 - \theta_{j-1}^2 + \theta_{j-1}^1)\epsilon/l\Delta t + (\theta_j^1 - \theta_{j-1}^1)/l \tag{35}$$

where superscripts 1 and 2 refer to time steps $k\Delta t$ and $(k+1)\Delta t$, respectively. Combining (13), (33), and (35) gives

$$\sum_{n=1}^{m} \frac{D^n(y=l, k\Delta t)}{l^n} \int_0^{\Delta t} \left\{(\theta_{j+1}^2 - \theta_{j-1}^1 - \theta_j^2 + \theta_j^1)\frac{\epsilon^{n-1}}{l\Delta t} + (\theta_{j-1}^1 - \theta_j^1)\frac{\epsilon^{n-1}}{l}\right\} d\epsilon - \sum_{n=1}^{m} \frac{D^n(y=0, k\Delta t)}{l^n} \int_0^{\Delta t} \left\{(\theta_j^2 - \theta_{j-1}^2 + \theta_{j-1}^1 - \theta_j^1)\frac{\epsilon^{n-1}}{l\Delta t} + (\theta_j^1 - \theta_{j-1}^1)\frac{\epsilon^{n-1}}{l}\right\} d\epsilon$$

$$= \int_0^{l} (\theta)\Big|_{t_r} dy \tag{36}$$

The temporal integration of (36) is evaluated by isolating the time integrable functions as

$$\sum_{i=0}^{\infty} \frac{D^{(i)}(y=l)}{i!} \left[\frac{(\theta_{j+1}^{i+2} - \theta_j^{i+2}) - (\theta_{j+1}^{i+1} - \theta_j^{i+1})}{l\Delta t}\right] \int_0^{\Delta t} \epsilon^{i+1}\, d\epsilon$$
$$+ \sum_{i=0}^{\infty} \frac{D^{(i)}(y=l)}{i!} \left[\frac{\theta_{j+1}^{i+1} - \theta_j^{i+1}}{l}\right] \int_0^{\Delta t} \epsilon^{i}\, d\epsilon$$
$$- \sum_{i=0}^{\infty} \frac{D^{(i)}(y=0)}{i!} \left[\frac{(\theta_j^{i+2} - \theta_{j-1}^{i+2}) - (\theta_j^{i+1} - \theta_{j-1}^{i+1})}{l\Delta t}\right]$$
$$\cdot \int_0^{\Delta t} \epsilon^{i+1}\, d\epsilon - \sum_{i=0}^{\infty} \frac{D^{(i)}(y=0)}{i!} \left[\frac{\theta_j^{i+1} - \theta_{j-1}^{i+1}}{l}\right] \int_0^{\Delta t} \epsilon^{i}\, d\epsilon$$
$$= \int_0^{l} (\theta)\Big|_{t_r} dy \tag{37}$$

Rearranging terms, the nodal point water content values can be isolated by

$$[\theta_{j+1}^{i+2} - \theta_j^{i+2}] \sum_{i=0}^{\infty} \frac{D^{(i)}(y=l)}{i!l\Delta t} \int_0^{\Delta t} \epsilon^{i+1}\, d\epsilon$$
$$- [\theta_j^{i+2} - \theta_{j-1}^{i+2}] \sum_{i=0}^{\infty} \frac{D^{(i)}(y=0)}{i!l\Delta t} \int_0^{\Delta t} \epsilon^{i+1}\, d\epsilon$$
$$+ [\theta_{j+1}^{i+1} - \theta_j^{i+1}] \sum_{i=0}^{\infty} \frac{D^{(i)}(y=l)}{i!l\Delta t} \int_0^{\Delta t} (\Delta t\epsilon^{i} - \epsilon^{i+1})\, d\epsilon$$
$$- [\theta_j^{i+1} - \theta_{j-1}^{i+1}] \sum_{i=0}^{\infty} \frac{D^{(i)}(y=0)}{i!l\Delta t} \int_0^{\Delta t} (\Delta t\epsilon^{i} - \epsilon^{i+1})\, d\epsilon$$
$$= \int_0^{l} (\theta)\Big|_{t_r} dy \tag{38}$$

Carrying out the indicated integration in (38) gives

$$[\theta_{j+1}^{i+2} - \theta_j^{i+2}] \sum_{i=0}^{\infty} \frac{D^{(i)}(y=l)}{i!l} \frac{(\Delta t)^{i+1}}{(i+2)} - [\theta_j^{i+2} - \theta_{j-1}^{i+2}]$$
$$\cdot \sum_{i=0}^{\infty} \frac{D^{(i)}(y=0)}{i!l} \frac{(\Delta t)^{i+1}}{(i+2)} + [\theta_{j+1}^{i+1} - \theta_j^{i+1}] \sum_{i=0}^{\infty} \frac{D^{(i)}(y=l)}{i!l}$$
$$\cdot \frac{(\Delta t)^{i+1}}{(i+1)(i+2)} - [\theta_j^{i+1} - \theta_{j-1}^{i+1}] \sum_{i=0}^{\infty} \frac{D^{(i)}(y=0)}{i!l} \frac{(\Delta t)^{i+1}}{(i+1)(i+2)}$$
$$= \int_0^{l} (\theta)\Big|_{t_r} dy \tag{39}$$

In a simplified notation, (39) can be rewritten as

$$\bar{\bar{D}}_l[\theta_{j+1}^{i+2} - \theta_j^{i+2}] - \bar{\bar{D}}_0[\theta_j^{i+2} - \theta_{j-1}^{i+2}] =$$
$$- \bar{D}_l[\theta_{j+1}^{i+1} - \theta_j^{i+1}] + \bar{D}_0[\theta_j^{i+1} - \theta_{j-1}^{i+1}] + \int_0^{l} (\theta)\Big|_{t_r} dy \tag{40}$$

where

$$\bar{\bar{D}}_i = \sum_{i=0}^{\infty} \frac{D^{(i)}(y=\xi)}{i!(i+2)} \frac{(\Delta t)^{i+1}}{l} \qquad \xi = 0, l$$
$$\bar{D}_i = \sum_{i=0}^{\infty} \frac{D^{(i)}(y=\xi)(\Delta t)^{i+1}}{(i+2)!l} \qquad \xi = 0, l \tag{41}$$

For the Δt duration space-time surface assumed linear with respect to time the temporal differentials of soil water diffusivity in (41) are given by

$$D^{(N)} = \frac{\partial^N D}{\partial t^N} = \frac{\partial^N D}{\partial \theta^N} \left|\frac{\partial \theta}{\partial t}\right|^N \tag{42}$$

where N denotes the order of the differential operator.

MODEL APPLICATIONS (ALTERNATION THEOREM)

The normalized moisture transport problem for constant diffusivity [*Hromadka and Guymon*, 1980*a*, *b*] is given by

$$\frac{\partial^2 \theta}{\partial x^2} = \frac{\partial \theta}{\partial t} \qquad x \in \Omega \tag{43}$$

where

$$\Omega = \{x | 0 \le x \le 1\}$$
$$\theta(x, t=0) = 1 \qquad x \in \Omega \tag{44}$$
$$\theta(x = 0, 1; t > 0) = 0$$

The problem domain Ω is assumed discretized into two finite elements (Ω_1, Ω_2) of equal length by three nodal values (θ_1, θ_2, θ_3) where (x_1, x_2, x_3) = (0, 0.5, 1.). Because of the boundary conditions of (44) the resulting system of modeled linear equations reduces to a single equation of one unknown, θ_2. In order to evaluate the effectiveness of using the alternation theorem approach to modeling (43) and (44) the finite element, finite difference, and nodal domain integration solutions will also be determined for comparison purposes.

The Galerkin version of the weighted residual process can be used to approximate (1) and (43) by the finite element method. The solution domain is discretized into the union of $(n-1)$ finite elements (21) by

$$\Omega = \bigcup_{i=1}^{n-1} \Omega_i \tag{45}$$

The water content is utilized as the state variable and is approximated within each finite element by

$$\hat{\theta}(x, t) = \sum_{j=1}^{2} N_j(x)\, \theta_j(t) \tag{46}$$

where N_j is the appropriate linearly independent shape functions and θ_j is the state variable values at element-nodal points designated by the general summation index j.

The Galerkin technique utilizes the set of shape functions as the weighting functions, which indicates that the corresponding finite element representation for the infiltration process is

$$\int \left\{\frac{\partial}{\partial x}\left[D(\theta)\frac{\partial \theta}{\partial x}\right] - \frac{\partial \theta}{\partial t}\right\} N_i\, dx = 0 \tag{47}$$

Integration by parts expands (47) into the form

$$\sum_{i=1}^{2} \left\{D(\theta)\frac{\partial \theta}{\partial x} N_i\Big|_S - \int_{\Omega_i} \left[D(\theta)\frac{\partial \theta}{\partial x}\frac{\partial N}{\partial x} + N\frac{\partial \theta}{\partial t}\right] dx\right\} = 0 \tag{48}$$

where S_i represents the external end points of the one-dimensional finite element Ω_i. The first term within the braces sums to zero for interior elements and also satisfies the usual specified (flux) boundary conditions of the problem for exterior finite elements. The remaining integral term is solved by sub-

stituting the appropriate element approximations and shape functions into the integrand and solving by numerical integration. A convenient approach for dealing with the nonlinearity of (48) is to assume the diffusivity function to be constant within each finite element during a finite time interval Δt in order to carry out the integration [*Guymon and Luthin*, 1974]. *Hromadka and Guymon* [1980*a*] examined some approaches in determining appropriate values of diffusivity for use in this method of linearizing. The Crank-Nicolson time advancement approximation has been widely used [*Hayhoe*, 1974; *Desai*, 1979] to perform the time integration of (1) and (43).

The Crank-Nicolson formulation reduces (48), where values of soil water diffusivity are assumed constant within each finite element, into a system of linear equations expressed in matrix form as

$$\left\{\mathbf{P} + \frac{\Delta t}{2}\mathbf{S}\right\}\theta^{k+1} = \left\{\mathbf{P} - \frac{\Delta t}{2}\mathbf{S}\right\}\theta^{k} \tag{49}$$

where $\mathbf{P}$ is a symmetrical capacitance matrix and is a function of element nodal global coordinates, $\mathbf{S}$ is a symmetrical stiffness matrix and is a function of element nodal global coordinates and constant finite element diffusivity coefficients (during timestep Δt), Δt is the finite time step increment, and θ^k is the vector of nodal state variable approximations (volumetric water content) at time step k.

For a linear polynomial trial function the element matrices determined from (48) are given by

$$\mathbf{S}\begin{Bmatrix}\theta_i\\ \theta_j\end{Bmatrix} + \hat{\mathbf{P}}\begin{Bmatrix}\dot{\theta}_i\\ \dot{\theta}_j\end{Bmatrix} = \frac{D_i}{l_i'}\begin{bmatrix}1 & -1\\ -1 & 1\end{bmatrix}\begin{Bmatrix}\theta_i\\ \theta_j\end{Bmatrix} + \frac{l_i'}{6}\begin{bmatrix}2 & 1\\ 1 & 2\end{bmatrix}\begin{Bmatrix}\dot{\theta}_i\\ \dot{\theta}_j\end{Bmatrix} \tag{50}$$

where D_i is the quasi-constant diffusivity within element i, $\mathbf{S}$ and $\hat{\mathbf{P}}$ are element stiffness and capacitance matrices, respectively, and (θ_i, θ_j) and $(\dot{\theta}_i, \dot{\theta}_j)$ refer to the element nodal and time derivative of nodal moisture content values, respectively, for an element of length l_i'.

For the linear temporal trial function the nodal domain integration approximation of (40) and (41) can be written analogously to (49) and (50) as

$$\{\hat{\mathbf{P}} + \bar{\mathbf{S}}\}\,\theta^{k+1} = \{\hat{\mathbf{P}} - \bar{\mathbf{S}}\}\,\theta^{k} \tag{51}$$

where the element matrices composing the global $\mathbf{S}$ matrices of (51) are given by

$$\bar{\mathbf{S}} = \bar{D}_i\begin{bmatrix}1 & -1\\ -1 & 1\end{bmatrix}$$
$$\mathbf{S} = \bar{D}_i\begin{bmatrix}1 & -1\\ -1 & 1\end{bmatrix} \tag{52}$$

and for $\alpha \to \infty$

$$\hat{\mathbf{P}} = \frac{l}{8}\begin{bmatrix}3 & 1\\ 1 & 3\end{bmatrix} \tag{53}$$

Hromadka and Guymon [1980*a*] rewrite the capacitance matrix $\hat{\mathbf{P}}$ in (50) as

$$\hat{\mathbf{P}}(\eta) = \frac{l}{2(\eta - 1)}\begin{bmatrix}\eta & 1\\ 1 & \eta\end{bmatrix} \tag{54}$$

where the Galerkin approximation in (49) leads to

$$\hat{\mathbf{P}}(2) = \frac{l}{6}\begin{bmatrix}2 & 1\\ 1 & 2\end{bmatrix} \tag{55}$$

The nodal integration approximation with $\alpha \to \infty$ leads to a type of subdomain approximation

$$\hat{\mathbf{P}}(3) = \frac{l}{8}\begin{bmatrix}3 & 1\\ 1 & 3\end{bmatrix} \tag{56}$$

The finite difference approach is given by

$$\lim_{\eta \to \infty}\hat{\mathbf{P}}(\eta) = \frac{l}{2}\begin{bmatrix}1 & 0\\ 0 & 1\end{bmatrix} \tag{57}$$

Application of the alternation theorem to the sinusoidal estimate of (20) for θ in the normalized problem of (43) is made for $\alpha = 1$, where

$$\hat{\theta} = \theta_2 \sin \pi x \qquad 0 \le x \le 1 \tag{58}$$

The best linear approximation $\hat{\theta}$ for $\hat{\theta}$ in subdomain Ω_1 is found from (32). For $0 < \mu < 0.5$ and $x \in \Omega_1$, solution of (29) gives (for $\alpha = 1$)

$$\mu = \frac{1}{\pi}\cos^{-1}\left[\frac{2}{\pi}\right] \simeq 0.28 \tag{59}$$

Thus the maximum error e in the linear approximation $\hat{\theta}$ for $\hat{\theta}$ on Ω_1 occurs at $x = (0, \mu, \frac{1}{2})$. This error is evaluated from (23*b*) as

$$e = \theta_2\left(\tfrac{1}{2}\sin \pi\mu - \mu\right) \simeq 0.105\theta_2 \tag{60}$$

Thus the best linear approximation $\hat{\hat{\theta}}$ for $\hat{\theta}$ on (Ω_1, Ω_2) is

$$\begin{aligned}\hat{\hat{\theta}}(x) &= 2\theta_2 x + 0.105\theta_2 \qquad x \in \Omega_1\\ \hat{\hat{\theta}}(x) &= 2\theta_2(1 - x) + 0.105\theta_2 \qquad x \in \Omega_2\end{aligned} \tag{61}$$

Selection of other values of α in (20) would result in a different linear approximation $\hat{\hat{\theta}}$ in (61).

From (19), solution of (43) and (44) gives

$$\left.\frac{\partial\hat{\theta}}{\partial x}\right|_{\Gamma} = -4\theta_2 \tag{62}$$

$$\frac{\partial}{\partial t}\int_{\Omega_2}\hat{\theta}\,dx = \left(\frac{e}{2} + \frac{3}{8}\right)\frac{\partial\theta_2}{\partial t} \simeq 0.4275\,\frac{\partial\theta_2}{\partial t} \tag{63}$$

where the e term in (63) serves as a type of weighting factor to the θ_2 nodal point approximation in the nodal integration formulation of (19).

For the study problem of (43) and (44) the presented domain numerical solutions result in the expression [*Hromadka and Guymon*, 1980*a*, *b*]

$$\lim_{\Delta x \to 0}\theta_2(t) = \exp\left[-8\left(\frac{\eta - 1}{\eta}\right)t\right] \qquad t \ge 0 \tag{64}$$

where η is the entry in the capacitance matrix $\mathbf{P}(\eta)$ of (54). Solution of (62) and (63) gives

$$-4\theta_2(t) = 0.4275\,\frac{\partial\theta_2}{\partial t} \tag{65}$$

therefore

$$\theta_2(t) = \exp\left[(-9.357)t\right] \qquad t \ge 0 \tag{66}$$

TABLE 1 Domain Solution η Values for Test Problem

Approximation	Equation	Equivalent η*
Nodal integration–linear shape function	(56)	3
Galerkin-linear shape function	(55)	2
Finite difference	(57)	∞
Linear approximation to parabola	(72)	7
Linear approximation to sinusoidal estimate	(66)	5.9

Reference text equations (43) and (44).
*Reference text equation (54).

As a second selection for the θ approximation, a second-order polynomial for θ on Ω in the solution of (43) and (44) is

$$\hat{\theta}(x) = 4\theta_2(x - x^2) \qquad x \in \Omega \tag{67}$$

Analogous to the sinusoidal approximation, the best linear approximation for the parabola $\hat{\theta}$ function on Ω_1 is

$$\hat{\theta}(x) = 2\theta_2 + e \qquad x \in \Omega_1 \tag{68}$$

where μ and e are

$$\begin{aligned} \mu &= \tfrac{1}{2} \\ e &= \theta_2/8 \end{aligned} \tag{69}$$

The maximum $\hat{\theta}$ error to the parabola $\hat{\theta}$ in Ω_1 occurs at $x = (0, \frac{1}{2}, \frac{1}{2})$. Therefore

$$\begin{aligned} \hat{\theta}(x) &= 2\theta_2 x + \frac{\theta_2}{8} \qquad x \in \Omega_1 \\ \hat{\theta}(x) &= 2\theta_2(1 - x) + \frac{\theta_2}{8} \qquad x \in \Omega_2 \end{aligned} \tag{70}$$

Combination of (6) and (70) gives

$$-4\theta_2(t) = \frac{7}{16}\frac{\partial \theta_2}{\partial t} \tag{71}$$

$$\lim_{\Delta x \to 0} \theta_2(t) = \exp\left[-\left(\frac{64}{7}\right)t\right] \qquad t \geq 0 \tag{72}$$

Table 1 summarizes computed or equivalent values of η corresponding to (64) for the various domain approximations of (43) and (44). Table 2 gives values of the tested domain solutions for comparison to the analytical solution of the example problem at $x = 0.50$.

From Table 2 it can be seen that a numerical model using the alternation theorem to approximate a higher-order trial function approximation $\hat{\theta}$ for θ increases numerical model accuracy (for the problem studied) in comparison to the standard Galerkin finite element and linear nodal domain integration approaches. The finite difference numerical approximation, however, gives the best numerical estimates for θ during the initial test problem solution. After normalized time $t = 0.12$, however, the finite difference approximation increasingly overestimates the analytic solution for θ.

The above results suggest that the parameter η of the element capacitance matrix in (54) should vary as a function of time in order to obtain a more accurate numerical approximation. The following section develops such a numerical model which determines η as a function of time for each finite element.

Approximation Improvement by Use of Adjusted Linear Model (Nodal Domain Integration Method)

In this section a second method of modeling a higher-order or more complex family of trial functions by a linear trial function approximation is presented. For the one-dimensional soil water transport problem studied, this approach assumes that the matrix diagonal entry η (54) is a function of time and that the spatial integration and gradient evaluation of a higher-order approximation $\hat{\theta}$ of θ can be equated on Ω_j to an approximation based on an adjusted linear trial function system $\hat{\theta}$.

Let $\hat{\theta}$ be an approximation function of a higher-order approximation $\hat{\theta}$ of θ, where the spatial gradients of $\hat{\theta}$ on Γ_j are defined by

$$\left\{\frac{\partial \hat{\theta}}{\partial x}\right\}\Big|_{\Gamma_j} = \frac{(\theta_{j+1} - \theta_j)}{l_j'} - \frac{(\theta - \theta_{j-1})}{l_{j-1}'} \tag{73}$$

where l_j' is the length of finite element j.

A spatial gradient adjustment function $c(x, t)$ is defined by

$$\begin{aligned} c(x, t) &= (\partial\hat{\theta}/\partial x)/(\partial\theta/\partial x) \qquad 0 < c < \infty \\ c(x, t) &= 1 \qquad \text{otherwise} \end{aligned} \tag{74}$$

Therefore it is assumed that

$$D\frac{\partial \hat{\theta}}{\partial x} = Dc\frac{\partial \hat{\theta}}{\partial x} \tag{75}$$

where

$$\left\{D\frac{\partial \hat{\theta}}{\partial x}\right\}_{j\Gamma} = \left\{Dc\frac{\partial \hat{\theta}}{\partial x}\right\}_{j\Gamma} \tag{76}$$

TABLE 2. Numerical Solution of Normalized Soil Moisture Transport Problem

Time	$\eta = 2$	$\eta = 3$	$\eta = 5.9$	$\eta = 7$	$\eta = \infty$	Exact
0.01	0.887	0.889	0.911	0.913	0.923	0.999
0.02	0.787	0.808	0.829	0.833	0.852	0.975
0.03	0.698	0.726	0.755	0.760	0.787	0.918
0.04	0.619	0.653	0.688	0.694	0.726	0.846
0.05	0.549	0.587	0.626	0.633	0.670	0.772
0.10	0.301	0.344	0.392	0.401	0.449	0.474
0.15	0.165	0.202	0.246	0.254	0.301	0.290
0.20	0.091	0.118	0.154	0.161	0.202	0.177
0.25	0.050	0.069	0.096	0.102	0.135	0.108
0.30	0.027	0.041	0.060	0.064	0.091	0.066

One variable nodal point.

On Γ_j, define

$$Dc = A(t) \qquad k\Delta t \le t \le (k+1)\Delta t \tag{77}$$

such that

$$A(k\Delta t + \epsilon) = \sum_{i=0}^{\infty} A^{(i)}(k\Delta t)\,\frac{\epsilon^i}{i!} \qquad 0 \le \epsilon \le \Delta t \tag{78}$$

where (i) represents the ith order temporal partial differential operator. Then

$$\left\{ D\,\frac{\partial\theta}{\partial x} \right\}\Big|_{\Gamma_j} = \left\{ \sum_{i=0}^{\infty} A^{(i)}(k\Delta t)\,\frac{\epsilon^i}{i!}\,\frac{\partial\theta}{\partial x} \right\}\Big|_{\Gamma_j} \tag{79}$$

A function $\eta(t)$ is defined by

$$\int_{\Omega_j} \theta\,dx = \frac{l_j}{2[\eta(t)+1]}\left[\theta_{j-1} + 2\theta_j\,\eta(t) + \theta_{j+1}\right] \tag{80}$$

where for modeling purposes $\eta(t)$ is restricted to values

$$\eta(t) \ge 2 \tag{81}$$

The value of 3 in (81) corresponds to a first-order polynomial subdomain approximation for θ, whereas $\eta(t) = 2$ corresponds to a finite element (Galerkin) approach, and $\eta(t) \to \infty$ corresponds to a finite difference approximation.

The $\hat{\theta}$ approximator is also defined to have the property

$$\int_{\Omega_j} \hat{\theta}\,dx = \int_{\Omega_j} \theta\,dx \qquad \eta(t) \ge 2 \tag{82a}$$

as defined by (80).

$$\int_{\Omega_j} \theta\,dx = \frac{l_j}{8}\left[\theta_{j-1} + 6\theta_j + \theta_{j+1}\right] \qquad \eta(t) < 2 \tag{82b}$$

Substituting (79) and (82) into (36) gives the nodal domain integration statement

$$\int_{\Delta t}\left\{ \sum_{i=0}^{\infty} A^{(i)}(k\Delta t)\,\frac{\epsilon^i}{i!}\,\frac{\partial\theta}{\partial x} \right\}\Big|_{\Gamma_j} = \frac{l_j\left[\theta_{j-1} + 2\theta_j\,\eta(k\Delta t + \Delta t) + \theta_{j+1}\right]}{2[\eta(k\Delta t + \Delta t) + 1]} - \frac{l_j\left[\theta_{j-1} + 2\theta_j\,\eta(k\Delta t) + \theta_{j+1}\right]}{2[\eta(k\Delta t) + 1]} \tag{83}$$

where

$$\eta(k\Delta t + \epsilon) = \sum_{i=0}^{\infty} \eta^{(i)}(k\Delta t)\,\frac{\epsilon^i}{i!} \qquad 0 \le \epsilon \le \Delta t \tag{84}$$

Analogous to the development leading to (41),

$$\bar{A}(\xi) = \frac{1}{l_j}\sum_{i=0}^{\infty} A_i\,\frac{(\xi)(\Delta t)^{i+1}}{i!(i+2)} \qquad \xi = (0, l)$$
$$\hat{A}(\xi) = \frac{1}{l_j}\sum_{i=0}^{\infty} A_i\,\frac{(\xi)(\Delta t)^{i+1}}{(i-2)!} \qquad \xi = (0, l) \tag{85}$$

where for modeling purposes it is assumed that second-order (and higher) temporal differentials are negligible and

$$A_0 = [cD]|_{k\Delta t}$$
$$A_1 = \left[c\,\frac{\partial D}{\partial\theta}\,\frac{\partial\theta}{\partial t} + D\,\frac{\partial c}{\partial t} \right]_{k\Delta t} \tag{86}$$
$$A_2 = \left[c\,\frac{\partial^2 D}{\partial\theta^2}\left(\frac{\partial\theta}{\partial t}\right)^2 + 2\,\frac{\partial c}{\partial t}\,\frac{\partial D}{\partial\theta}\,\frac{\partial\theta}{\partial t} \right]_{k\Delta t}$$

and for small Δt, $(\partial^2\theta/\partial t^2) = (\partial c^2/\partial t^2) = 0$. Thus analogous to (51), (52), and (53),

$$\bar{s} = \bar{A}\begin{bmatrix} 1 & -1 \\ -1 & 1 \end{bmatrix}$$
$$\hat{s} = \hat{A}\begin{bmatrix} 1 & -1 \\ -1 & 1 \end{bmatrix}$$
$$\bar{p} = \frac{l_j}{2(\bar{\eta}+1)}\begin{bmatrix} \eta & 1 \\ 1 & \eta \end{bmatrix} \tag{87}$$
$$\hat{p} = \frac{l_j}{2(\hat{\eta}+1)}\begin{bmatrix} \hat{\eta} & 1 \\ 1 & \hat{\eta} \end{bmatrix}$$

where $\bar{\eta} = \eta(k\Delta t + \Delta t)$ and $\hat{\eta} = \eta(k\Delta t)$.

From the above the soil water transport problem may be modeled by an appropriately defined linear trial function approximation set which incorporates some of the benefits of a higher-order family of approximations. Thus additional numerical accuracy may be achieved while retaining the symmetric matrix formulation characteristic of a linear polynomial approximation of θ.

Model Applications (Linear Approximation Adjustment)

The normalized transport problem of (43) and (44) is reanalyzed using a five nodal point discretization of Ω with $(x_1, x_2, x_3, x_4, x_5) = (0, \frac{1}{4}, \frac{1}{2}, \frac{3}{4}, 1)$. A Galerkin finite element or finite difference numerical approximation model for this problem follows from the preceding sections.

For θ assumed to be described by a second-order polynomial such that

$$\theta = N_1\theta_{j-1} + N_2\theta_j + N_3\theta_{j+1} \qquad x \in \Omega_j \tag{88}$$

then from (74) and (82)

$$c(t) = 1$$
$$\eta(t) = 11 \tag{89}$$

As another example of a higher-order approximation $\hat{\theta}$ of θ on Ω, a fourth-order polynomial approximation of θ is given by

$$\theta = \sum_{i=1}^{5} N_i\theta_i \qquad x \in \Omega \tag{90}$$

For the fourth-order approximation, (37) is determined for each Δt time step by solving (74), (80), and (82). For a normalized time step of $\Delta t = 0.01$, $n(t)$ and $c(t)$ were modeled as a constant during each time step, ignoring the time variation of both adjustment terms.

Computer simulation results for numerical models based on the Galerkin finite element method ($\eta = 2$), linear subdomain method ($\eta = 3$), finite difference method ($\eta = \infty$), nodal domain integration using (89) ($\eta = 11$), nodal domain integration using an adjusted linear approximation of a fourth-order polynomial approximation, and a fourth-order polynomial subdomain approximation for the test problem are given in Table 3. From Table 3 the true fourth-order subdomain approximation gave the most accurate results, but the

TABLE 3. Numerical Solution of Normalized Moisture Transport Problem

	η = 2*		η = 3†		η = 11‡		η = ∞§		Fourth Order†		Adjusted Linear†		Analytic	
Time	x = 0.25	x = 0.5	x = 0.25	x = 0.5	x = 0.25	x = 0.5	x = 0.25	x = 0.5	x = 0.25	x = 0.5	x = 0.25	x = 0.5	x = 0.25	x = 0.5
0.01	0.802	1.041	0.823	1.017	0.851	0.989	0.861	0.981	0.864	1.003	0.864	1.013	0.923	0.999
0.02	0.701	0.970	0.716	0.960	0.743	0.941	0.755	0.933	0.760	0.961	0.761	0.967	0.789	0.975
0.03	0.627	0.881	0.637	0.882	0.660	0.876	0.671	0.873	0.676	0.898	0.678	0.902	0.690	0.918
0.04	0.564	0.796	0.572	0.802	0.592	0.807	0.602	0.807	0.606	0.828	0.608	0.830	0.615	0.846
0.05	0.508	0.718	0.515	0.727	0.533	0.739	0.543	0.743	0.546	0.758	0.548	0.759	0.553	0.772
0.10	0.302	0.427	0.310	0.439	0.327	0.461	0.335	0.472	0.331	0.469	0.331	0.468	0.336	0.474
0.15	0.179	0.254	0.187	0.264	0.202	0.285	0.209	0.295	0.202	0.287	0.201	0.285	0.205	0.290
0.20	0.107	0.151	0.113	0.159	0.125	0.176	0.131	0.185	0.123	0.175	0.123	0.174	0.125	0.177
0.25	0.063	0.090	0.068	0.096	0.077	0.109	0.082	0.116	0.075	0.107	0.075	0.106	0.076	0.018
0.30	0.038	0.053	0.041	0.058	0.048	0.067	0.051	0.072	0.046	0.065	0.046	0.064	0.047	0.066

Three variable nodal points.
*Galerkin finite element analog.
†Subdomain approximation.
‡Nodal domain integration method.
§Finite difference method.

nodal domain integration model closely matched these results. Thus the numerical accuracy produced by a fourth-order approximation is closely matched by a first-order approximation, significantly reducing computer memory requirements. Additionally, the computer computation requirements in solving (74) and (82) are offset by the reduction in a higher-order approximation matrix computational effort. Values of $\eta(t)$ and $c(t)$ computed for the (fourth order) linear adjusted model were approximately 10.5 and 1.0, respectively. This may explain the good results obtained by the linear adjusted model using (88) and (89).

Application of Linear Approximation Adjustment Approach to a Nonlinear Problem

The numerical model given by (83), (87), and (89) was applied to a sharp wetting front problem of soil water infiltration into an air dry horizontal column [*Hayhoe*, 1978; *Hromadka and Guymon*, 1980*c*]. The analytical value of soil water diffusivity for Hanford sandy loam [*Reichardt et al.*, 1972] was selected in order to provide a sharp wetting front through the soil column, causing the numerical analysis of moisture flow in the soil to be difficult. The quasi-analytic solution advanced by *Philip and Knight* [1974] and utilized by *Hayhoe* [1978] was used for this study.

Equation (1) was solved subject to the initial condition

$$\theta(x, t) = 0 \qquad t = 0 \qquad 0 \le x \le L \tag{91}$$

and the boundary conditions

$$\theta(0, t) = 1 \qquad \theta(L, t) = 0 \qquad t > 0 \tag{92}$$

where the soil water diffusivity (cm² min⁻¹) is given by

$$\begin{aligned} D(\theta) &= 0.9 \times 10^{-1} \exp(8.36\theta) \qquad \theta > 0 \\ D(\theta) &= 0.9 \times 10^{-3} \qquad \theta = 0 \end{aligned} \tag{93}$$

and θ is the volumetric water content.

Because of the nature of the soil water diffusivity function of (93) the temporal variation of diffusivity is extremely important during the Δt time step. Table 4 contains various values of time step magnitudes Δt (in minutes) and time series expansion terms in the numerical model of (1) by (83) at time t = 16.5 min. For the numerical model a spatial discretization of 0.5 cm was used where the total column length was set at 5.0 cm to correspond to the model results of *Hayhoe* [1978].

Conclusions

Two techniques of modeling a higher-order trial function approximation of soil moisture transport using an improved linear trial function approximation set have been developed. Both techniques retain the smaller symmetrical matrix systems associated with numerical models of soil moisture transport based on a linear polynomial trial function but increase the numerical accuracy of the model by incorporating some of the benefits of a higher-order approximation.

Because the various numerical methods considered (finite difference, Galerkin finite element, subdomain method) are available in the proposed model, it is concluded that the proposed numerical approach may lead to a generalized modeling method for all soil moisture transport problems. The computer code used for each simulation is identical except for a variation in the capacitance matrix entry η. Therefore a comparison of numerical efficiency between the finite differ-

TABLE 4 Comparison of Numerical Model Results at Time t = 1 to 5 Minutes

x, cm	Analytic*	Δt = 0.1 min, i = 0	Δt = 0.1 min, i = 2	Δt = 0.1 min, i = 5	Δt = 0.3 min, i = 0	Δt = 0.3 min, i = 2	Δt = 0.3 min, i = 5
0.0	1.0	1.0	1.0	1.0	1.0	1.0	1.0
0.5	0.99	0.99	0.99	0.99	0.98	0.99	0.99
1.0	0.97	0.97	0.97	0.97	0.97	0.97	0.97
1.5	0.95	0.95	0.95	0.95	0.94	0.95	0.95
2.0	0.92	0.93	0.92	0.92	0.92	0.93	0.93
2.5	0.88	0.90	0.89	0.89	0.88	0.90	0.90
3.0	0.84	0.87	0.85	0.85	0.84	0.87	0.86
3.5	0.78	0.82	0.78	0.78	0.82	0.82	0.82
4.0	0.67	0.39	0.63	0.64	0.05	0.37	0.40
4.5	0.0	0.0	0.0	0.0	0.0	0.0	0.0
5.0	0.0	0.0	0.0	0.0	0.0	0.0	0.0

Values of water content. The i is the number of temporal Taylor series terms (diffusivity function) included, and Δt is the time step magnitude.

*Results from *Hayhoe* [1978].

ence, Galerkin finite element, subdomain method, and the proposed nodal domain integration approach is provided.

NOTATION

- A flux adjustment factor.
- α sinusoidal curve trial function adjustment factor.
- D soil water diffusivity.
- (λ, β) coefficients of $\bar{\theta}$ linear function approximation for θ.
- c gradient adjustment factor.
- ϵ local time coordinate $0 \leq \epsilon \leq \Delta t$.
- e alternation theorem error of $\bar{\theta}$ approximation for θ.
- μ point of relative maximum error of $\bar{\theta}$ approximation for θ in Ω_j.
- (i) partial differential operator (order).
- k time step increment number.
- L length of one-dimensional domain.
- l_j length of nodal domain j.
- l' length of finite element spatial domain.
- l length of nodal domain for constant element discretization.
- M_m temporal shape function.
- N_i spatial shape function.
- n number of nodal points in Ω.
- $\eta(t)$ integration adjustment factor as a function of time.
- θ unsaturated volumetric water content.
- θ_j value of θ at node j.
- $\hat{\theta}$ trial function approximation for θ.
- θ_i^m $\hat{\theta}(x = x_i, t = m\Delta t)$.
- $\bar{\theta}$ linear polynomial approximation for $\hat{\theta}$.
- η element capacitance matrix diagonal entry.
- x_j spatial coordinate of node j.
- Δt time step (constant).
- t time.
- Γ_t limits of time step integration.
- Z local spatial coordinate in finite element spatial domain.
- Ω domain of problem definition.
- Ω_j nodal domain j.
- $\hat{\Omega}_j$ finite element domain j.
- Γ_j boundary of Ω_j.
- $\mathbf{P}$ global capacitance matrix.
- $\hat{\mathbf{P}}$ finite element capacitance matrix.
- $\bar{\mathbf{P}}$ nodal domain capacitance matrix.
- $\hat{\mathbf{P}}(\eta)$ finite element capacitance matrix as a function of η.
- $\mathbf{S}$ global stiffness matrix.
- $\hat{\mathbf{S}}$ finite element stiffness matrix.
- $\bar{\mathbf{S}}, \overline{\mathbf{S}}$ nodal domain stiffness matrices.

REFERENCES

Desai, C. S., *Elementary Finite Element Methods*, Prentice-Hall, Englewood Cliffs, N. J., 1979.

Cheney, E. W., *Introduction to Approximation Theory*, McGraw-Hill, New York, 1966.

Guymon, G. L., and J. N. Luthin, A coupled heat and moisture transport model for arctic soils, *Water Resour. Res.*, *10*(5), 995–1001, 1974.

Hayhoe, H. N., Study of relative efficiency of finite difference and Galerkin techniques for modeling soil water transfer, *Water Resour. Res.*, *14*(1), 97–102, 1978.

Hromadka, T. V., II, and G. L. Guymon, Some effects of linearizing the unsaturated soil moisture transfer diffusivity model, *Water Resour. Res.*, *16*(4), 643–650, 1980*a*.

Hromadka, T. V., II, and G. L. Guymon, Numerical mass balance soil-moisture transfer problems, *Advan. Water Resour.*, 1980*b*.

Hromadka, T. V., II, and G. L. Guymon, A note on time integration of unsaturated soil moisture transport, *Advan. Water Resour.*, 181–186, 1980*c*.

Philip, J. R., and J. H. Knight, On solving the unsaturated flow equation, 3, New quasi-analytic technique, *Soil Sci.*, *117*(1), 1–13, 1974.

Reichardt, K., D. R. Nielsen, and J. W. Biggar, Scaling of horizontal infiltration into homogeneous soils, *Soil Sci. Soc. Am. J.*, *36*, 241–245, 1972.

(Received July 16, 1980;
revised November 10, 1980;
accepted November 27, 1980.)

Nodal domain integration model of one-dimensional advection–diffusion

T. V. HROMADKA II and G. L. GUYMON
Department of Civil Engineering, School of Engineering, University of California, Irvine, Ca 92717, USA

The nodal domain integration method is applied to a one-dimensional advection–diffusion mathematical model without a source term. Comparison of the resulting numerical model to the well known Galerkin finite element, subdomain, and finite difference domain models indicates that a single numerical statement can be developed which includes the Galerkin finite element, subdomain, and finite difference models as special cases.

INTRODUCTION

The determination of an optimum numerical method to model problems analogous to soil-moisture transport in a one-dimensional domain has received some recent attention. The primary numerical modelling (domain) approaches has generally been either the Galerkin finite element or finite difference methods. Pinder and Gray[10] present a comparison of these two modelling approaches for a linear, one-dimensional advection–diffusion problem where the advection component is large; the finite element method is concluded as superior. Hayhoe[4] demonstrated that a finite difference analog produced better numerical accuracy than a finite element model for a non-linear soil–water diffusion model problem in which a highly sensitive soil–water diffusivity parameter caused a sharp wetting front, making a numerical modelling effort difficult. Hromadka and Guymon[5] re-examined the sharp wetting front problem with a finite element numerical model using a quasi-constant element soil–water diffusivity computation scheme; the numerical model results were found to be comparable to Hayhoe's finite difference analog results, but gave a better prediction of the wetting front penetration. In a more detailed study, Hromadka and Guymon[9] integrated the soil–water diffusivity parameter with respect to time and determined another modelling approach (nodal domain integration) to the sharp wetting front problem. In this later study, other comparable numerical methods (finite difference, Galerkin finite element, subdomain integration) were rewritten into a single matrix system modelling statement of nodal point values and equation parameters similar to the element matrix system generated by the Galerkin finite element method. This resulting element matrix formulation is strictly a function of the element capacitance (time derivative) matrix diagonal entry as determined for a linear polynomial trial function approximation between nodal points. Consequently, numerical 'efficiency'[1–3,7,10] in modelling a one-dimensional diffusivity model of soil–water transport could be viewed as a function of a single element matrix system parameter. In order to better estimate the soil–water content function spatially, Hromadka and Guymon[9], examined two methods of approximating a higher order or more complex family of trial functions between nodal points by a linear polynomial trial function approximation. This technique would incorporate some of the benefits provided by a higher order state variable approximation between nodal points and yet retain the symmetry and smaller matrix bandwidths resulting from a linear trial function approximation. Both approaches resulted in the combined matrix system statement identified above but with the element capacitance matrix diagonal component variable with respect to time and space.

The purpose of this paper is twofold. First, the advection–diffusion equation is analysed to determine an appropriate element matrix modelling statement which incorporates the finite element, finite difference, and subdomain integration modelling approaches. The second objective is to model a higher order spatial trial function approximation between nodal points with a linear trial function approximation in a diffusion dominated process. This linear approximation effort is based upon determining a higher order trial function approximation of the state variable between nodal points using information provided by the spatial distribution of the time derivative of the state variable. For numerical model development, a Fickian dispersion process of a conservative dissolved species with solute concentration C within pure water is considered as a case study.

NODAL DOMAIN INTEGRATION MODEL DEVELOPMENT

The one-dimensional form of the advection–diffusion equation for non-reactive dissolved constituents in saturated, homogeneous, isotropic materials under steady-state uniform flow is:

$$\left.\begin{aligned} \frac{\partial}{\partial x}\left[D\frac{\partial C}{\partial x}\right]-\frac{\partial}{\partial x}[UC]=\frac{\partial C}{\partial t},\ x\in\Omega \\ \Omega\equiv\{x\,|\,0\leqslant x\leqslant L\} \end{aligned}\right\} \quad (1)$$

where x is the spatial coordinate taken along the flowline direction in spatial domain Ω; U is the mean linear flow

velocity, D is the coefficient of hydrodynamic dispersion in the x-direction; and C is the solute concentration. Chemical, biological and radioactive effects are neglected. In equation (1), the parameters D and U are left within the spatial gradient terms in order to provide a more general numerical model development.

The domain Ω can be discretized by n nodal points C_j ($j = 1,2,\ldots,n$) into n disjoint subdomains:

$$\begin{aligned}\Omega_1 &\equiv \{x | 0 \leqslant x \leqslant (x_1 + x_2)/2\}\\ \Omega_2 &\equiv \{x | (x_1 + x_2)/2 < x \leqslant (x_2 + x_3)/2\}\\ &\vdots\\ \Omega_n &\equiv \{x | (x_{n-1} + x_n)/2 < x \leqslant x_n = L\}\end{aligned} \tag{2}$$

where x_j is the spatial coordinate associated to nodal point value C_j, and

$$\Omega = \bigcup_{i=1}^{n} \Omega_i \tag{3}$$

Equation (1) must be satisfied on each Ω_j. Therefore, n equations are generated by solving:

$$\frac{\partial}{\partial x}\left[D\frac{\partial C}{\partial x}\right] = \frac{\partial C}{\partial t} - \frac{\partial}{\partial x}[UC];\ x \in \Omega_j,\ \forall_j \tag{4}$$

where it is assumed

$$\left.\begin{aligned} D &= D(C)\\ C &= C(x,t)\end{aligned}\right\} \tag{5}$$

Integrating equation (4) with respect to space gives the subdomain model:

$$\left\{D\frac{\partial C}{\partial x}\right\}_{\Gamma} = \frac{\partial}{\partial t}\int_{\Omega} C\,dx - \{UC\}_{\Gamma};\ x \in \Omega_j,\ \forall_j \tag{6}$$

where Γ is the spatial boundary of region Ω_j. Integrating equation (6) with respect to time gives:

$$\int_{k\Delta t}^{(k+1)\Delta t}\left\{D\frac{\partial C}{\partial x}\right\}_{\Gamma} dt = \int_{\Omega}\{C\}_{\Gamma}\,dx + \int_{k\Delta t}^{(k+1)\Delta t}\{UC\}_{\Gamma}\,dt \tag{7}$$

where Γ_t is the limits of temporal integration between timesteps $k\Delta t$ and $(k+1)\Delta t$. Equation (7) can be rewritten by using the linear transformation:

$$\left.\begin{aligned} t &= k\Delta t + \varepsilon\\ 0 &\leqslant \varepsilon \leqslant \Delta t\end{aligned}\right\} \tag{8}$$

Thus,

$$\int_0^{\Delta t}\left\{D(k\Delta t+\varepsilon)\frac{\partial C(k\Delta t+\varepsilon)}{\partial x}\right\}_{\Gamma} d\varepsilon = \int_{\Omega}\{C\}_{\Gamma}\,dx - \int_0^{\Delta t}\{U(k\Delta t+\varepsilon)C(k\Delta t+\varepsilon)\}_{\Gamma}\,d\varepsilon \tag{9}$$

The diffusivity and advection parameters can be expressed with respect to time by the Taylor series:

$$\xi(x = x_0,\ k\Delta t + \varepsilon) = \sum_{i=0}^{r}\frac{\xi^{(i)}(x = x_0,\ k\Delta t)\varepsilon^i}{i!} + \cdots,\quad \xi = U,\ D \tag{10}$$

where (i) is the ith order temporal partial differential operator; and x_0 is a specified spatial coordinate. Combining equations (9) and (10) gives:

$$\int_0^{\Delta t}\left\{\left(\sum_{i=0}^{r}\frac{D^{(i)}(k\Delta t)\varepsilon^i}{i!}\right)\frac{\partial C(k\Delta t+\varepsilon)}{\partial x}\right\}_{\Gamma} d\varepsilon = \int_{\Omega}\{C\}_{\Gamma}\,dx - \int_0^{\Delta t}\left\{\left(\sum_{i=0}^{r}\frac{U^{(i)}(k\Delta t)\varepsilon^i}{i!}\right)C(k\Delta t+\varepsilon)\right\}_{\Gamma} d\varepsilon \tag{11}$$

For a spatial local coordinate system defined by:

$$\left.\begin{aligned} y &\equiv \{y | 0 \leqslant y \leqslant l_j,\ x \in \Omega_j\}\\ dy &= dx\\ l_j &= |\Omega_j|\end{aligned}\right\} \tag{12}$$

Equation (11) can be expanded as:

$$\sum_{i=0}^{r}\frac{D^{(i)}(y = l_j, k\Delta t)}{i!}\int_0^{\Delta t}\varepsilon^i\left\{\frac{\partial C(k\Delta t+\varepsilon)}{\partial y}\right\}_{y=l_j} d\varepsilon - \sum_{i=0}^{r}\frac{D^{(i)}(y = 0, k\Delta t)}{i!}\int_0^{\Delta t}\varepsilon^i\left\{\frac{\partial C(k\Delta t+\varepsilon)}{\partial y}\right\}_{y=0} d\varepsilon = \int_{\Omega}\{C\}_{\Gamma}\,dy - \sum_{i=0}^{r}\frac{U^{(i)}(y = l_j, k\Delta t)}{i!}\int_0^{\Delta t}\varepsilon^i\{C(k\Delta t+\varepsilon)\}_{y=l_j} d\varepsilon - \sum_{i=0}^{r}\frac{U^{(i)}(y = 0, k\Delta t)}{i!}\int_0^{\Delta t}\varepsilon^i\{C(k\Delta t+\varepsilon)\}_{y=0} d\varepsilon \tag{13}$$

To this point, equation (13) is an exact statement of equation (1), and to proceed to a solvable numerical algorithm the following inexact approximation is made:

$$\left.\begin{aligned} C &\simeq \hat{C}\\ \hat{C} &= \sum_{i=1}^{n} N_i\left(\sum_{m=1}^{k+1} M_m C_i^m\right)\end{aligned}\right\} \tag{14}$$

where the solute-concentration function is approximated spatially and temporally and where N_i and M_m are the linearly independent spatial and temporal shape functions, and

$$C_i^m = \hat{C}(x = x_i,\ t = m\,\Delta t) \tag{15}$$

where the C_i^m are known values for timesteps m

$= 0,1,\ldots,k$), and x_r is the spatial coordinate of node r. The spatial gradient of the soil-water content function is approximated by:

$$\frac{\partial C}{\partial x} \simeq \frac{\partial \hat{C}}{\partial x} = \sum_{r=1}^{n} \frac{\partial N_r}{\partial x}\left(\sum_{m=0}^{k+1} M_m C_r^m\right) \tag{16}$$

Substituting equations (14) and (16) into equation (13) gives the numerical approximation:

$$\begin{aligned}
&\sum_{i=0}^{r} \frac{D^{(i)}(y=l_r,k\Delta t)}{i!} \int_0^{\Delta t} \varepsilon^i \left\{\sum_{r=1}^{n} \frac{\partial N_r}{\partial x}\left(\sum_{m=0}^{k+1} M_m C_r^m\right)\right\}_{y=l_r} \mathrm{d}\varepsilon - \\
&\sum_{i=0}^{r} \frac{D^{(i)}(y=0,k\Delta t)}{i!} \int_0^{\Delta t} \varepsilon^i \left\{\sum_{r=1}^{n} \frac{\partial N_r}{\partial x}\left(\sum_{m=0}^{k+1} M_m C_r^m\right)\right\}_{y=0} \mathrm{d}\varepsilon \\
&\quad = \int_0^{l_r} \left\{\sum_{r=1}^{n} N_r\left(\sum_{m=0}^{k+1} M_m C_r^m\right)\right\}_{t=\Delta t} \mathrm{d}y + \\
&\sum_{i=0}^{r} \frac{U^{(i)}(y=l_r,k\Delta t)}{i!} \int_0^{\Delta t} \varepsilon^i \left\{\sum_{r=1}^{n} N_r\left(\sum_{m=0}^{k+1} M_m C_r^m\right)\right\}_{y=l_r} \mathrm{d}\varepsilon - \\
&\sum_{i=0}^{r} \frac{U^{(i)}(y=0,k\Delta t)}{i!} \int_0^{\Delta t} \varepsilon^i \left\{\sum_{r=1}^{n} N_r\left(\sum_{m=0}^{k+1} M_m C_r^m\right)\right\}_{y=0} \mathrm{d}\varepsilon
\end{aligned} \tag{17}$$

The unknown values of nodal points C_r^{k+1} can be solved by:

$$\begin{aligned}
&\sum_{i=0}^{r} \frac{D^{(i)}(y=l_r,k\Delta t)}{i!} \int_0^{\Delta t} \varepsilon^i \left\{\sum_{r=1}^{n} \frac{\partial N_r}{\partial x} M_{k+1} C_r^{k+1}\right\}_{y=l_r} \mathrm{d}\varepsilon - \\
&\sum_{i=0}^{r} \frac{D^{(i)}(y=0,k\Delta t)}{i!} \int_0^{\Delta t} \varepsilon^i \left\{\sum_{r=1}^{n} \frac{\partial N_r}{\partial x} M_{k+1} C_r^{k+1}\right\}_{y=0} \mathrm{d}\varepsilon \\
&\quad = \int_0^{l_r} \sum_{r=1}^{n} N_r C_r^{k+1}\,\mathrm{d}x + \sum_{i=0}^{r} \frac{U^{(i)}(y=0,k\Delta t)}{i!} \times \\
&\qquad \int_0^{\Delta t} \varepsilon^i \left\{\sum_{r=1}^{n} N_r M_{k+1} C_r^{k+1}\right\}_{y=0} \mathrm{d}\varepsilon - \\
&\sum_{i=0}^{r} \frac{U^{(i)}(y=l_r,k\Delta t)}{i!} \int_0^{\Delta t} \varepsilon^i \left\{\sum_{r=1}^{n} N_r M_{k+1} C_r^{k+1}\right\}_{y=l_r} \mathrm{d}\varepsilon \\
&= \sum_{i=0}^{r} \frac{D^{(i)}(y=0,k\Delta t)}{i!} \int_0^{\Delta t} \varepsilon^i \left\{\sum_{r=1}^{n} \frac{\partial N_r}{\partial x}\left(\sum_{m=0}^{k} M_m C_r^m\right)\right\}_{y=0} \mathrm{d}\varepsilon - \\
&\sum_{i=0}^{r} \frac{D^{(i)}(y=l_r,k\Delta t)}{i!} \int_0^{\Delta t} \varepsilon^i \left\{\sum_{r=1}^{n} \frac{\partial N_r}{\partial x}\left(\sum_{m=0}^{k} M_m C_r^m\right)\right\}_{y=l_r} \mathrm{d}\varepsilon - \\
&\int_0^{l_r} \sum_{r=1}^{n} N_r C_r^{k}\,\mathrm{d}x - \sum_{i=0}^{r} \frac{U^{(i)}(y=l_r,k\Delta t)}{i!} \times \\
&\int_0^{\Delta t} \varepsilon^i \left\{\sum_{r=1}^{n} N_r\left(\sum_{m=0}^{k} M_m C_r^m\right)\right\}_{y=l_r} \mathrm{d}\varepsilon - \\
&\sum_{i=0}^{r} \frac{U^{(i)}(y=0,k\Delta t)}{i!} \int_0^{\Delta t} \varepsilon^i \left\{\sum_{r=1}^{n} N_r\left(\sum_{m=0}^{k} M_m C_r^m\right)\right\}_{y=0} \mathrm{d}\varepsilon
\end{aligned} \tag{18}$$

DISCRETIZED DOMAIN NUMERICAL MODEL

The space-time surface approximated by equation (14) can be simplified by assuming that the functional surfaces $C(x,t)$ can be described by sets of piecewise continuous functions. For a first order polynomial spatial trial function approximation $\hat{C}$ for C between nodal points (C_{j-1}, C_j, C_{j+1})

$$\left.\begin{aligned}
\left(\frac{\partial \hat{C}}{\partial x}\right)_{y=l} &= (C_{j-1} - C_j)/l \\
\left(\frac{\partial \hat{C}}{\partial x}\right)_{y=0} &= (C_j - C_{j-1})/l \\
\int_0^{l} \hat{C}\,\mathrm{d}y &= \frac{l}{6}[C_{j-1} + 6C_j + C_{j+1}] \\
\{\hat{C}\}_{\Gamma} &= \frac{1}{2}(C_{j-1} - C_{j+1})
\end{aligned}\right\} \tag{19}$$

where for discussion purposes it is assumed that $l_r = l$.

For Δt timesteps of equation (18) small, a linear polynomial function approximation may be used for the time curves between timesteps $(k, k-1)$ where $(k-1)$ is the timestep to be evaluated, thus

$$\left.\begin{aligned}
C_j(k\Delta t - \varepsilon) &= (C_j^{k\Delta t})\left(\frac{\Delta t - \varepsilon}{\Delta t}\right) - (C_j^{(k-1)\Delta t})\frac{\varepsilon}{\Delta t} \\
k\Delta t &\leq t \leq (k+1)\Delta t \\
\mathrm{d}\varepsilon &= \mathrm{d}t
\end{aligned}\right\} \tag{20}$$

Combining equations (19) and (20), the spatial gradient approximation during the time-step Δt as a function of time is:

$$\left.\begin{aligned}
\left(\frac{\partial \hat{C}}{\partial x}\right)_{y=l} &= (C_{j-1}^{k} - C_{j-1}^{k-1} - C_j^{k} + C_j^{k-1})\varepsilon/l\Delta t + (C_{j-1}^{k-1} - C_j^{k-1})/l \\
\left(\frac{\partial \hat{C}}{\partial x}\right)_{y=0} &= (C_j^{k} - C_j^{k-1} - C_{j-1}^{k} + C_{j-1}^{k-1})\varepsilon/l\Delta t + (C_j^{k-1} - C_{j-1}^{k-1})/l \\
0 &\leq \varepsilon \leq \Delta t
\end{aligned}\right\} \tag{21}$$

where superscripts 1 and 2 refer to timesteps $k\Delta t$ and $(k+1)\Delta t$, respectively. Combining equations (18), (19), (20) and (21) gives a type of subdomain integration model incorporating the expansion of the non-linear terms $D(C)$ and $U(C)$ over the timestep Δt:

$$\sum_{i=0}^{\tau}\frac{D^{(i)}(y=l)}{i!}\int_0^{\Delta t}\left\{(C_{j+1}^2-C_{j-1}^1-C_j^2-C_j^1)\frac{\varepsilon^{i+1}}{l\Delta t}+\right.$$

$$\left.(C_{j+1}^1-C_j^1)\frac{\varepsilon^i}{l}\right\}d\varepsilon-\sum_{i=0}^{\tau}\frac{D^{(i)}(y=0)}{i!}\times$$

$$\int_0^{\Delta t}\left\{(C_j^2-C_j^1-C_{j-1}^2-C_{j-1}^1)\frac{\varepsilon^{i+1}}{l\Delta t}+(C_j^1-C_{j-1}^1)\frac{\varepsilon^i}{l}\right\}d\varepsilon$$

$$=\frac{l}{8}[C_{j-1}^2+6C_j^2+C_{j+1}^2]-\frac{l}{8}[C_{j-1}^1+6C_j^1+C_{j+1}^1]+$$

$$\sum_{i=0}^{\tau}\frac{U^{(i)}(y=l)}{i!}\int_0^{\Delta t}\frac{1}{2}\left\{C_{j+1}^1\varepsilon^i+(C_{j+1}^2-C_{j-1}^1)\frac{\varepsilon^{i+1}}{\Delta t}\right\}d\varepsilon-$$

$$\sum_{i=0}^{\tau}\frac{U^{(i)}(y=0)}{i!}\int_0^{\Delta t}\frac{1}{2}\left\{C_{j-1}^1\varepsilon^i+(C_{j-1}^2-C_{j-1}^1)\frac{\varepsilon^{i+1}}{\Delta t}\right\}d\varepsilon \qquad (22)$$

Carrying out the indicated integration in equation (22) gives:

$$[C_{j-1}^2-C_j^2]\sum_{i=0}^{\tau}\frac{D^{(i)}(y=l)(\Delta t)^{i+1}}{i!(i+2)}-$$

$$[C_j^2-C_{j-1}^2]\sum_{i=0}^{\tau}\frac{D^{(i)}(y=0)}{i!}\frac{(\Delta t)^{i+1}}{(i+2)}-$$

$$[C_{j-1}^1-C_j^1]\sum_{i=0}^{\tau}\frac{D^{(i)}(y=l)}{i!}\frac{(\Delta t)^{i+1}}{(i+1)(i+2)}-$$

$$[C_j^1-C_{j-1}^1]\sum_{i=0}^{\tau}\frac{D^{(i)}(y=0)}{i!}\frac{(\Delta t)^{i+1}}{(i+1)(i+2)} \qquad (23)$$

$$=\frac{l}{8}[C_{j-1}^2-6C_j^2-C_{j+1}^2]-\frac{l}{8}[C_{j-1}^1+6C_j^1+C_{j+1}^1]+$$

$$\frac{1}{2}C_{j-1}^2\sum_{i=0}^{\tau}\frac{U^{(i)}(y=l)(\Delta t)^{i+1}}{i!(i+2)}-\frac{1}{2}C_{j-1}^1\sum_{i=0}^{\tau}\frac{U^{(i)}(y=l)(\Delta t)^{i+1}}{i!(i+2)}-$$

$$\frac{1}{2}C_{j-1}^2\sum_{i=0}^{\tau}\frac{U^{(i)}(y=0)(\Delta t)^{i+1}}{i!(i+2)}-\frac{1}{2}C_{j-1}^1\sum_{i=0}^{\tau}\frac{U^{(i)}(y=0)(\Delta t)^{i+1}}{i!(i+2)}$$

In a different notation, equation (23) can be rewritten as:

$$\bar{D}_1[C_{j-1}^2-C_j^2]-\bar{D}_0[C_j^2-C_{j-1}^2]-\frac{1}{2}\bar{C}_1C_{j-1}^2-\frac{1}{2}\bar{C}_0C_{j-1}^2-$$

$$\frac{l}{8}[C_{j-1}^2-6C_j^2-C_{j+1}^2]=-\frac{l}{8}[C_{j-1}^1+6C_j^1+C_{j+1}^1]-$$

$$\bar{D}_1[C_{j-1}^1-C_j^1]-\bar{D}_0[C_j^1-C_{j-1}^1]-\frac{1}{2}\bar{C}_1C_{j-1}^1-\frac{1}{2}\bar{C}_0C_{j-1}^1 \qquad (24)$$

where

$$\left.\begin{aligned}\bar{D}_\lambda&=\sum_{i=0}^{\tau}\frac{D^{(i)}(y=\lambda l)(\Delta t)^{i+1}}{i!(i+2)l},\ \lambda=0,1\\ \bar{D}_\lambda&=\sum_{i=0}^{\tau}\frac{D^{(i)}(y=\lambda l)(\Delta t)^{i+1}}{(i+2)!l},\ \lambda=0,1\\ \bar{C}_\lambda&=\sum_{i=0}^{\tau}\frac{U^{(i)}(y=\lambda l)(\Delta t)^{i+1}}{i!(i+2)},\ \lambda=0,1\\ \bar{C}_\lambda&=\sum_{i=0}^{\tau}\frac{U^{(i)}(y=\lambda l)(\Delta t)^{i+1}}{(i+2)!},\ \lambda=0,1\end{aligned}\right\} \qquad (25)$$

For the advective and diffusivity parameters constant in Ω_e and for a linear polynomial trial function approximation of solute concentration between nodal points with respect to both space and time, equation (24) reduces to:

$$\frac{D_0}{2l}[C_{j+1}^2-2C_j^2-C_{j-1}^2-C_{j-1}^1-2C_j^1-C_{j+1}^1]-$$

$$\frac{U_0}{2}[(C_{j+1}^2-C_{j-1}^2)2-(C_{j+1}^1-C_{j-1}^1)2] \qquad (26)$$

$$=\frac{l}{\Delta t}[(C_{j-1}^2-6C_j^2-C_{j+1}^2)8-(C_{j-1}^1+6C_j^1+C_{j+1}^1)8]$$

Pinder and Gray[10] develop a finite difference and Galerkin finite element numerical analog for equation (1) in order to compare relative numerical efficiency between these two common modelling approaches. The finite element, finite difference, and subdomain integration formulation of equation (26) can be represented by a single modelling statement for a Crank–Nicolson time advancement approximation:

$$\frac{D_0}{2l}[C_{j+1}^2-2C_j^2-C_{j-1}^2-C_{j-1}^1-2C_j^1-C_{j+1}^1]-$$

$$\frac{U_0}{2}[(C_{j+1}^2-C_{j-1}^2)2-(C_{j+1}^1-C_{j-1}^1)2] \qquad (27)$$

$$=\frac{l}{2\Delta t(\eta-1)}[(C_{j-1}^2-2\eta C_j^2-C_{j+1}^2]-[C_{j-1}^1+2\eta C_j^1+C_{j+1}^1]$$

where in equation (27) the finite element, subdomain integration, and finite difference methods are determined by $\eta=(2,3,\infty)$ respectively. Equation (27) can be written in an element matrix system:

$$-\frac{D_0}{l}\begin{bmatrix}1&-1\\-1&1\end{bmatrix}\begin{Bmatrix}C_j^2\\C_{j+1}^2\end{Bmatrix}-\frac{U_0}{2}\begin{bmatrix}1&-1\\1&-1\end{bmatrix}\begin{Bmatrix}C_j^2\\C_{j+1}^2\end{Bmatrix}$$

$$=\frac{l}{2\Delta t(\eta-1)}\begin{bmatrix}-1&1\\1&-\eta\end{bmatrix}\begin{Bmatrix}C_{j-1}^2\\C_{j+1}^2\end{Bmatrix} \qquad (28)$$

where the so-called capacitance matrix (time derivative component) contains all η-term information similar to the soil water diffusivity model matrix system determined in Hromadka and Guymon[5]. For a Crank–Nicolson time advancement approximation equation (28) may be written as:

$$\left(\mathbf{P}+\frac{\Delta t}{2}\mathbf{S}\right)\{\mathbf{C}^2\}=\left(\mathbf{P}-\frac{\Delta t}{2}\mathbf{S}\right)\{\mathbf{C}^1\} \tag{29}$$

where $\{\mathbf{C}^k\}$ are the element nodal points at timestep k, and

$$\mathbf{S}=\frac{D_0}{l}\begin{bmatrix}1 & -1\\ -1 & 1\end{bmatrix}-\frac{U_0}{2}\begin{bmatrix}1 & -1\\ 1 & 1\end{bmatrix} \tag{30}$$

$$P=\frac{l}{2(\eta+1)}\begin{bmatrix}\eta & 1\\ 1 & \eta\end{bmatrix} \tag{31}$$

LINEAR MODEL OF HIGHER ORDER SHAPE FUNCTION (NODAL DOMAIN INTEGRATION MODEL)

Hromadka and Guymon[6] examined two methods of approximating a higher order or more complex family of trial functions by a linear polynomial trial function approximation. One method used the Alternation theorum in order to determine an 'optimum' linear polynomial estimate of a higher order approximator. A second approach was the definition of an element matrix system that approximated the integration and gradients of a higher order approximator $\hat{C}$ of C within each nodal domain, Ω_j. This second approach is reviewed in the following, and another technique of determining η as a function of time examined in a following section. A constant diffusivity diffusion process (without advection) is used for model development purposes.

Let $\bar{C}$ be an approximation function of a higher order approximation $\hat{C}$ of C, where the spatial gradients of $\bar{C}$ on Γ_j are defined by:

$$\left\{\frac{\partial\bar{C}}{\partial x}\right\}_{\Gamma_j}\equiv\frac{(C_{j+1}-C_j)}{l}-\frac{(C_j-C_{j-1})}{l} \tag{32}$$

A spatial gradient adjustment function $e(x,t)$ is defined by:

$$e(x,t)\equiv\begin{cases}\dfrac{\partial\hat{C}}{\partial x}\Big/\dfrac{\partial\bar{C}}{\partial x};\ 0<e<\infty\\ 1;\ \text{otherwise}\end{cases} \tag{33}$$

Therefore, it is assumed that:

$$D\frac{\partial\hat{C}}{\partial x}=eD\frac{\partial\bar{C}}{\partial x} \tag{34}$$

where

$$\left\{D\frac{\partial\hat{C}}{\partial x}\right\}_{\Gamma_j}=\left\{eD\frac{\partial\bar{C}}{\partial x}\right\}_{\Gamma_j} \tag{35}$$

On Γ_j, define

$$eD=A(t);\ k\Delta t\leqslant t\leqslant(k+1)\Delta t \tag{36}$$

such that:

$$A(k\Delta t+\varepsilon)=\sum_{i=0}^{r}A^{(i)}(k\Delta t)\frac{\varepsilon^i}{i!};\ 0\leqslant\varepsilon\leqslant\Delta t \tag{37}$$

where (i) represents the ith order temporal partial differential operator. Then

$$\left\{D\frac{\partial\hat{C}}{\partial x}\right\}_{\Gamma_j}=\left\{\sum_{i=0}^{r}A^{(i)}(k\Delta t)\frac{\varepsilon^i}{i!}\frac{\partial\bar{C}}{\partial x}\right\}_{\Gamma_j} \tag{38}$$

A function $\eta(t)$ is defined by

$$\int_{\Omega_j}\bar{C}\,dx=\frac{l}{2[\eta(t)-1]}[C_{j-1}+2C_j\eta(t)+C_{j+1}] \tag{39}$$

where

$$\eta(t)\neq-1 \tag{40}$$

The value of 3 in equation (40) corresponds to a first order polynomial $\bar{C}$ function subdomain approximation for C, whereas $\eta(t)=2$ corresponds to a Galerkin finite element model, and $\eta(t)=\infty$ determines a finite difference model.

The $\bar{C}$ approximator is also defined to have the property:

$$\int_{\Omega_j}\bar{C}\,dx\equiv\int_{\Omega_j}\hat{C}\,dx,\ \eta(t)=-1 \tag{41}$$

For a diffusion process without advection, $U_0=0$ in equation (1). Therefore, substituting equations (38) and (41) into equation (18) gives the modelling statement (for $U_0=0$):

$$\int_{\Delta t}^{\cdot}\left\{\sum_{i=0}^{r}A^{(i)}(k\Delta t)\frac{\varepsilon^i}{i!}\frac{\partial\bar{C}}{\partial x}\right\}_{\Gamma_j}d\varepsilon=\frac{l[C_{j-1}-2C_j\eta(k\Delta t-\Delta t)-C_{j+1}]}{2[\eta(k\Delta t-\Delta t)+1]}-$$

$$\frac{l[C_{j-1}-2C_j\eta(k\Delta t)-C_{j+1}]}{2[\eta(k\Delta t)+1]} \tag{42}$$

where

$$\eta(k\Delta t+\varepsilon)=\sum_{i=0}^{r}\eta^{(i)}(k\Delta t)\frac{\varepsilon^i}{i!};\ 0\leqslant\varepsilon\leqslant\Delta t \tag{43}$$

Analogous to the development leading to equations (24) and (25):

$$\left.\begin{aligned}\bar{A}(\lambda)&=\frac{1}{l}\sum_{i=0}^{r}\frac{A_i(\xi)(\Delta t)^{i+1}}{i!(i+2)}\\ \bar{\eta}(\lambda)&=\frac{1}{l}\sum_{i=0}^{r}\frac{\eta_i(\xi)(\Delta t)^{i+1}}{(i+2)!}\end{aligned}\right\}\ \lambda=(0,1) \tag{44}$$

The nodal domain integration element matrix system similar to equation (29) is written as:

$$\left(\bar{\mathbf{p}}+\frac{\Delta t}{2}\bar{\mathbf{s}}\right)\{C^2\}=\left(\bar{\mathbf{p}}-\frac{\Delta t}{2}\bar{\mathbf{s}}\right)\{C^1\} \tag{45}$$

where,

$$\left.\begin{aligned}\bar{\mathbf{s}}&=\bar{A}\begin{bmatrix}1&-1\\-1&1\end{bmatrix}\\ \bar{\mathbf{s}}&=\bar{A}\begin{bmatrix}1&-1\\-1&1\end{bmatrix}\\ \bar{\mathbf{p}}&=\frac{l}{2(\bar{\eta}+1)}\begin{bmatrix}\bar{\eta}&1\\1&\bar{\eta}\end{bmatrix}\\ \bar{\mathbf{p}}&=\frac{l}{2(\bar{\eta}+1)}\begin{bmatrix}\bar{\eta}&1\\1&\bar{\eta}\end{bmatrix}\end{aligned}\right\} \tag{46}$$

where $\bar{\eta}=\eta(k\Delta t+\Delta t)$, $\bar{\eta}=\eta(k\Delta t)$.

APPLICATION OF LINEAR MODEL

The approach to be used for determining a higher order approximation $\hat{C}$ of C in Ω is to determine C as a function of $\partial C/\partial t$ spatially distributed within each Ω_j. The problem of a one-dimensional diffusion process with constant parameters where the solute concentration is initially C_0 and the concentration is decreased in stepwise fashion to C_1 at both ends of the one-dimensional domain Ω is used in order to compare previous modelling results[3] to the proposed approach. The diffusion problem can be normalized as:

$$\frac{\partial^2 C}{\partial x^2}=\frac{\partial C}{\partial t},\quad x\in\Omega \tag{47}$$

where

$$\left.\begin{aligned}&\Omega\equiv\{x|0\leqslant x\leqslant 1\}\\ &C(x,t=0)=1,\quad x\in\Omega\\ &C(x=0,1;t>0)=0\end{aligned}\right\} \tag{48}$$

The problem domain Ω is assumed discretized into two finite elements $(\hat{\Omega}_1,\hat{\Omega}_2)$ of equal length by three nodal points (C_1,C_2,C_3) where $(x_1,x_2,x_3)=(0,0.5,1)$. Owing to the boundary conditions of equation (48), the resulting system of modelled linear equations reduces to a single equation of one unknown, C_2. In order to evaluate the effectiveness of the proposed numerical approach to modelling equations (47) and (48), the Galerkin finite element, finite difference, subdomain, and nodal domain integration solutions will also be presented for comparison purposes.

For the study problem of equations (47) and (48), the considered domain numerical solutions result in the expression[8]:

$$\lim_{\Delta t\to 0}C_2(t)=\exp\left[-8\left(\frac{\eta+1}{\eta}\right)t\right],\quad t\geqslant 0 \tag{49}$$

where η is the entry in the capacitance matrix $\mathbf{P}(\eta)$ of equation (31).

Within Ω_2, an approximation $\hat{C}$ of C can be determined from equation (47) by integrating twice (with respect to x) the time derivative of C. Thus, for some instant in time t_0 it may be assumed in Ω_2:

$$\frac{\partial C}{\partial t}(x,t=t_0)\simeq\dot{C}_2=\frac{\partial^2\hat{C}}{\partial x^2} \tag{50}$$

where $\dot{C}_2$ is a finite difference estimate of the time derivative of C at the variable nodal point. Integrating equation (50) with respect to space gives for Ω_2:

$$\frac{\partial\hat{C}}{\partial x}(x,t=t_0)\simeq\dot{C}_2x+\alpha \tag{51}$$

A finite difference estimate of $\partial C/\partial x$ at node 2 determines the value α. Integrating a second time,

$$\hat{C}(x,t=t_0)=\frac{1}{2}\dot{C}_2x^2-\frac{1}{2}\dot{C}_2x-\beta \tag{52}$$

Evaluating equation (52) for C_2 gives in Ω_2:

$$\hat{C}(x,t=t_0)=\frac{1}{2}\dot{C}_2\left(x^2-x-\frac{1}{4}\right)+C_2 \tag{53}$$

For the approximation $\hat{C}$ of C in Ω_2 given in equation (53),

$$\int_{\Omega_2}\hat{C}\,dx=\frac{\dot{C}_2}{192}+\frac{C_2}{2} \tag{54}$$

From equations (45) and (46), for $e=1$, the modelling statement similar to equation (49) is:

$$\left.\begin{aligned}&\frac{\partial}{\partial t}\left[\frac{\dot{C}_2}{192}+\frac{C_2}{2}\right]=-4C_2\\ &C_2(t)=(-0.11237)e^{-97.1918t}-(1.11237)e^{-8.8082t};\quad t>0\end{aligned}\right\} \tag{55}$$

Table 1 gives a comparison of the analytical solution to equations (47) and (48) to the considered domain solutions of 49 (for $\eta=2,3,\infty$) and the proposed model of equation (55). From Table 1, a significant increase in accuracy is provided by the proposed modelling

Table 1. Numerical solution of normalized diffusion problem (one variable nodal point)

Time	$\eta=2$*	$\eta=3$+	$\eta=\infty$‡	Linear model**	Analytic solution
0.01	0.887	0.889	0.923	0.972	0.999
0.02	0.787	0.808	0.852	0.913	0.975
0.03	0.698	0.726	0.787	0.846	0.918
0.04	0.619	0.653	0.726	0.779	0.846
0.05	0.549	0.587	0.670	0.715	0.772
0.10	0.301	0.344	0.449	0.461	0.474
0.15	0.165	0.202	0.301	0.297	0.290
0.20	0.091	0.118	0.202	0.191	0.171
0.25	0.050	0.069	0.135	0.123	0.108
0.30	0.027	0.041	0.091	0.080	0.066

* Galerkin finite element method
\+ Subdomain model
‡ Finite difference model
** Nodal domain integration model

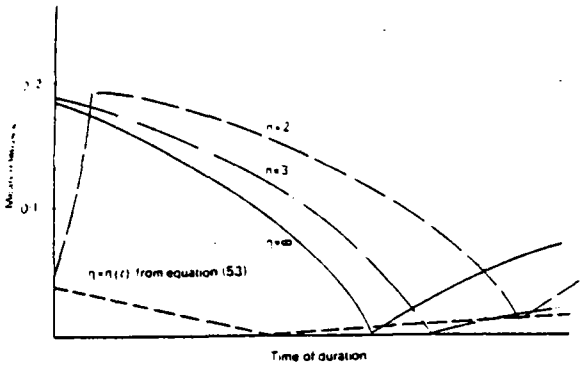

Figure 1. Typical mean relative error from numerical model of diffusion-dominated process ($D_0 = 1.0$; $U_0 = 0.05$)

approach. As another example, a second order polynomial estimate of $\hat{C}_2(x,t=t_0)$ is possible using the information provided at all three nodes. Thus in Ω_2,

$$\hat{C}_2(x,t=t_0)=\frac{\partial^2\hat{C}_2}{\partial x^2}=-4x^2\hat{C}_2+4x\hat{C}_2 \qquad (56)$$

Similar to equations (50)–(55), for $x\in\Omega_2$

$$\hat{C}(x,t=t_0)=\left(-\frac{1}{3}\hat{C}_2\right)\left[x^4-2x^3+x-\frac{5}{16}\right]-C_2 \qquad (57)$$

giving

$$C_2=(-0.1086)e^{-89.6^{-8}t}-(1.1086)e^{-9^{-8}36t};\ t\geq 0 \qquad (58)$$

Comparison of equations (55) and (58) shows that little advantage is gained by the extra computational effort in a higher order estimate of $\hat{C}$ in Ω_2 by the proposed technique.

APPLICATION TO ADVECTIVE-DIFFUSION PROBLEM

The advection–diffusion element matrix system statement of equation (29) is a function of the element capacitance matrix diagonal entry, η. For constant parameters, the following problem was analysed in order to evaluate the sensitivity of equation (29) to variations of η:

$$D_0\frac{\partial^2 C}{\partial x^2}-U_0\frac{\partial C}{\partial x}=\frac{\partial C}{\partial t};\ x\in\Omega \qquad (59)$$

with initial and boundary conditions

$$\left.\begin{aligned} C(x,t=0)&=0;\ x\in\Omega\\ C(1,t>0)&=1\\ C(\infty,t\geq 0)&=0\\ \Omega:&\ \{x;x\geq 0\}\end{aligned}\right\} \qquad (60)$$

For a linear trial function approximation of the state variable C with respect to time, the numerical analog reduces to the Crank–Nicolson time advancement approximation. Diffusivity (D_0) was set to 1.0 whereas the parameter U_0 was varied from 0.0 to 10.0. More than 200 separate simulations were made in order to evaluate η as a function of uniform element size Δx, timestep size Δt, and advective parameter U_0. Results of this sensitivity study indicates that with respect to relative error, the use of a constant η value throughout the simulation (e.g. $\eta=2,3,\infty$) provides varying qualities of accuracy (Fig. 1). That is, for each assumed constant η-value, the resulting numerical analog produced good results depending where in time and space the model solution is examined for error. It was noted, however, that for the smaller U_0 values tested, better results were obtained for small η values ($\eta=2,3$); whereas for large U_0 values, large η values ($\eta=\infty$) produced better results. Additionally, it is noted that these determinations are based on a specific advection–diffusion problem; another class of problems may produce different conclusions of modelling trends such as found in Hromadka and Guymon[5] where η was found to be somewhat dependent on the spatial gradient of the problem's solution profile. From the above, varying η as a function of time (and between elements) is suggested. Two methods of determining values of $\eta(t)$ are given in Hromadka and Guymon[8] where the approach used is to determine a linear polynomial trial function approximation of a higher order or more complex family of state variable approximation functions. A third approach in determining $\eta(t)$ is given in the previous section where a strict diffusion process is modelled.

CONCLUSIONS

A method of modelling a higher order trial function approximation of advection–diffusion by an improved linear trial function approximation set has been developed. This method retains the smaller symmetric matrix system associated to numerical models of advection–diffusion based on a linear polynomial trial function, but increase the numerical accuracy of the model by incorporating some of the benefits of a higher order approximation.

Since similarities between the various considered numerical methods (finite difference, Galerkin finite element, subdomain integration) are used in the proposed model, it is concluded that the proposed numerical approach may lead to a generalized modelling method for many classes of advection–diffusion problems. The computer code used for each simulation is identical except for a variation in the capacitance diagonal entry, η. Therefore, a comparison of numerical efficiency between the finite difference, Galerkin finite element, subdomain integration, and the proposed variable η term (nodal domain integration) approach is provided by the results obtained herein.

ACKNOWLEDGEMENT

This research was supported by the US Army Research Office (Grant No. DAAG29-79-C-0080).

REFERENCES

1. Desai, C. S. *Elementary Finite Element Method*. Prentice Hall, Englewood Cliffs, 1979.
2. Cheney, E. W. *Introduction to Approximation Theory*. McGraw-Hill, New York, 1966.
3. Guymon, G. L. and Luthin, J. N. A coupled heat and moisture

transport model for artic soils. *Water Resourc. Res.* 1974, 10, (5), 995

4 Hayhoe, H. N. Study of relative efficiency of finite difference and Galerkin techniques for modeling soil-water transfer. *Water Resourc. Res.* 1978, 14(1), 97

5 Hromadka II, T. V. and Guymon, G. L. Some effects of linearizing the unsaturated soil-moisture transfer diffusion model. *Water Resourc. Res.* 1980, 16, 643

6 Hromadka II, T. V. and Guymon, G. L. Numerical mass balance for soil-moisture transfer problems. *Adv. Water Resourc.* 1980, 3, 107

7 Hromadka II, T. V. and Guymon, G. L. A note on time integration of unsaturated soil moisture transport. *Adv. Water Resourc.* 1980, 3, 181

8 Hromadka II, T. V. and Guymon, G. L. Improved linear shape function model of soil moisture transport. *Water Resourc. Res.* 1981, 17, 504

9 Philip, J. R. and Knight, J. H. On solving the unsaturated flow equation: 3. New quasi-analytic technique. *Soil Sci.* 1974, 117, 1

10 Pinder, G. F. and Gray, W. G. *Finite Element Simulation in Surface and Subsurface Hydrology*. Academic Press, New York, 1977

Results from a Mathematical Model of Frost Heave

G.L. GUYMON, R.L. BERG, T.C. JOHNSON, AND T.V. HROMADKA II

A one-dimensional model for simulation of frost heave in a vertical soil column is presented. The model is based on simultaneous computation of heat and moisture transport in a freezing or thawing soil. Thermal processes at the freezing front are approximated by a lumped isothermal approach. The model accurately simulates frost heave, soil pore-water pressures, and temperatures when compared with a laboratory freezing column; however, to achieve adequate correlation certain model parameters must be determined by calibration. Because the model, like the frost-heave process itself, is highly sensitive to environmental and soil parameters that are variable in both time and space, purely deterministic simulations will not provide sufficiently accurate predictions. Consequently, further development of the model is required in order to include a statistical-probabilistic approach for estimating frost heave within specified confidence limits.

Since July 1975, the Federal Highway Administration (FHWA), the Federal Aviation Administration (FAA), and the U.S. Army Cold Regions Research and Engineering Laboratory (CRREL) have been engaged in a jointly funded project to develop a better understanding of freezing and thawing processes in soils. The main thrust of the research has been the development of more suitable methods for analyzing and simulating potential frost heave and thaw weakening in prototype embankments. The component of the research reported here is the development of a mathematical model of frost heave. The other components of the research are the development of a one-dimensional laboratory freezing and thawing soil column (1 and a paper by Ingersoll and Berg elsewhere in this Record), the collection of field data on frost heave and thaw weakening (2), an evaluation of soil frost-susceptibility index tests (see the paper by Chamberlain elsewhere in this Record), and an evaluation of thaw weakening of soils (see the paper by Cole, Irwin, and Johnson elsewnere in this Record).

It has been recognized for some time (2) that frost-heave-susceptibility criteria for soils and associated laboratory test methods in current use are unreliable. Soils that meet established criteria may experience frost heave while other soils that do not meet the criteria may be free from frost heave (3). The original purpose of the mathematical modeling research was to develop a tool to correlate results of laboratory tests of frost susceptibility with pavement frost heaves measured in the field. The development of a mathematical model was seen as a practical way to integrate most of the complex soil thermal and hydraulic characteristics with the environmental factors that influence a given soil profile. Part of our initial objective was to identify the most significant parameters that influence frost heave in a given soil in order to assess and develop improved laboratory tests of frost-heave susceptibility. As our study progressed, it became apparent that the mathematical model has usefulness beyond the original objective and can probably be applied directly as a design aid or tool. It is emphasized, however, that laboratory tests will still be required to characterize the parameters of the mathematical model.

BASIS OF MATHEMATICAL MODEL

Guymon and others (4) briefly review the current literature related to modeling frost heave and heat and moisture transport in freezing soils and present most of the details of the development of the mathematical model. Although it is recognized that in many situations a two-dimensional or even a three-dimensional process is involved, a one-dimensional approach was taken in order to simplify the computational problem and concentrate on demonstrating the validity of the modeling concept. In fact, at the time the research was begun in 1975, the modeling approach was regarded as a relatively high-risk research effort. At that time, only Harlan (5) and Guymon and Luthin (6) had shown modest success in modeling coupled heat and moisture movement in freezing soils. They assumed moisture movement in freezing soils could be approximated by unsaturated flow theory, and they did not consider ice segregation and associated frost heave.

Our model is based on the one-dimensional equations of moisture and heat transport in a vertical soil column. Assuming Darcy's law applies and inserting it into the continuity equation yield

$$(\partial/\partial x)(K_H \partial\phi/\partial x) = (\partial\theta_u/\partial t) + M_s \quad (1)$$

where

- x = vertical coordinate (positive downward);
- K_H = hydraulic conductivity = $K_H(\theta, \theta_i)$;
- ϕ = total hydraulic head = $\psi - x$, where ψ equals the pore-water-pressure head;
- θ_u = volumetric water content;
- t = time; and
- M_s = a moisture sink due to ice formation = $\rho_i \partial\theta_i / \rho_w \partial t$, where ρ is ice and water density and θ_i is ice content.

The coupled heat transport equation for a freezing soil column is given by

$$(\partial/\partial x)(K_T \partial T/\partial x) - C_w v(\partial T/\partial x) = C_m(\partial T/\partial t) - LM_s \quad (2)$$

where

- K_T = thermal conductivity of the soil-ice-water mixture,
- T = temperature,
- C_w = volumetric heat capacity of water,
- v = liquid water velocity flux,
- C_m = volumetric heat capacity of the soil-water-ice mixture, and
- L = volumetric latent heat of fusion of water.

The linearized moisture transport and heat transport equations were independently verified for simple equations (2). The equations of moisture transport and heat transport are coupled through the parameters that arise in their derivation, and these coupled nonlinear equations can only be verified by comparison with laboratory or field data. Parameters such as thermal conductivity and volumetric heat capacity of soil-water-ice mixtures are computed by using the DeVries relations (7) or similar methods. Solution of the moisture transport equation requires a functional relation between pore-water pressure and water content [e.g., Gardner's relation (8)].

A significant aspect of this model is the manner in which phase-change effects are handled and ice segregation is assumed to occur. We have assumed an isothermal freezing process in which a heat budget for a finite volume of freezing soil is established (9). The soil is considered entirely frozen only

when latent heat effects are satisfied for the amount of water present in excess of an unfrozen water content factor (θ_n); i.e., the water that would remain unfrozen at a preselected subfreezing temperature (10). This method of handling phase change is tantamount to computing small changes in heat evolution rather than solving the heat transport equation for small changes in temperature. Because phase-change processes dominate the thermal process, this manner of computing phase-change effects provides certain numerical advantages by permitting large spatial discretization and large computational time steps. Ice segregation is assumed to occur if, within a finite volume of soil, the frozen water plus the unfrozen water content factor exceed the original porosity of the soil. Figure 1 shows the computational algorithm and the formation of segregated ice (θ_s) during a certain time level.

The θ_n parameter establishes the pore-water pressure at the freezing front for the solution of the moisture transport equation. The lower hydraulic boundary condition is usually the water table. Overburden effects (ψ_o), which tend to restrain frost heave, are modeled by adjusting the pore-water pressure at the ice segregation front by the weight of the overlying material and surcharge, thereby limiting the amount of water drawn toward the freezing front.

This model of the complex freezing and ice segregation process is a macroscopic lumped thermodynamic model that ignores the complicated and poorly understood microprocesses that occur in the freezing zone. Such processes as regelation and problems associated with water-ice film pressures are not included in our model. In summary, the model is based on macrophysics equations. Specifically, it is assumed that:

1. Moisture transport in the unfrozen zone is governed by the unsaturated flow equation based on Darcy's law.
2. Moisture flow is via liquid movement and vapor flow is negligible.
3. Moisture flow in the frozen zone is negligible.

Figure 1. Typical model simulation result at given simulation time level.

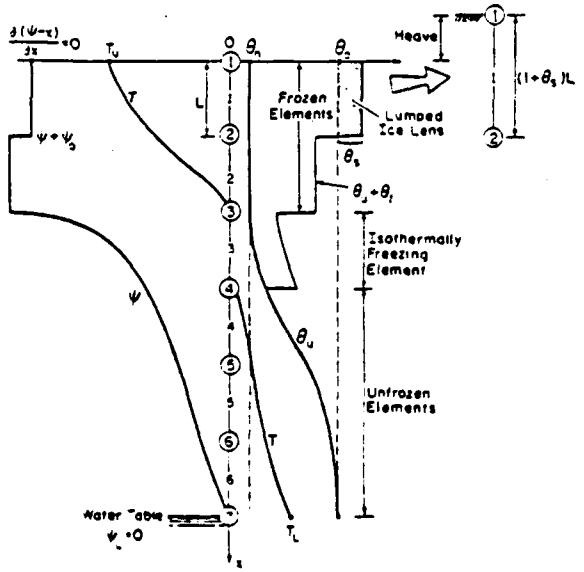

4. The unfrozen zone is nondeformable.
5. Soil pore-water pressures in the freezing zone are governed by an unfrozen water content factor.
6. All processes are single valued; i.e., there is no hysteresis.
7. Heat transport in the entire soil column is governed by the sensible heat transport equation, including a convective term.
8. The frozen zone is deformable for determining thermal parameters.
9. Salt exclusion processes are negligible; i.e., the freezing-point depression of water is constant.
10. Phase-change effects and moisture effects can be modeled as decoupled processes.
11. Freezing is an isothermal process.
12. Constant parameters are constant with respect to time.

Numerical solution of the governing equations discussed above, subject to their respective boundary and initial conditions, is by either the subdomain method or the finite element method (3,11). The one-dimensional solution domain is divided into a number of variable-length "finite elements", where parameters are assumed temporarily constant but may vary from element to element and from time to time. The state variable in each element is assumed to be described by a linear basis function in such a way that the state variable is continuous throughout the solution domain (3). The time domain solution is by the well-known Crank-Nicolson method (12). The governing equations are reduced to a set of explicit algebraic equations that may be solved on the "mini" class of computers (e.g., the PDP 11/34). One of our main objectives is to provide a mathematical model that is efficient and capable of operating on readily available small computers.

Application of the model requires the following soil hydraulic and thermal parameters:

1. Relation between water content and pressure (unfrozen soil),
2. Relation between unsaturated hydraulic conductivity and pore pressure (unfrozen soil),
3. Hydraulic conductivity correction factor for partly frozen soil,
4. Soil porosity,
5. Soil density,
6. Relation between subfreezing temperature and unfrozen water content for the soil,
7. Soil thermal conductivity,
8. Soil heat capacity, and
9. Soil-water freezing-point depression.

Thermal parameters for water and ice are included in the model. The above-required parameters must be determined in the laboratory, or values must be assumed in order to use the computer model. In addition, the model requires the following auxiliary conditions:

1. Initial conditions for pore pressure, ice content, and temperature;
2. Soil-surface boundary conditions for pore pressure and temperatures (may vary with time); and
3. Lower boundary conditions for pore-water pressure and temperature (may vary with time).

To conduct a computer simulation of frost heave, a column length must be specified (e.g., 1 m), and the total length must be divided into sublengths (finite elements) that are on the order of 1 cm. Time solution factors are specified, such as time-step size and total simulation time.

VERIFICATION RESULTS

Preliminary verification of the model is discussed elsewhere (2,4). The model verification work will be expanded on here, and additional results will be presented.

The primary emphasis of our verification has been to compare simulated values of frost heave, soil pore-water pressures, and soil-water-ice temperatures with corresponding actual values measured in a laboratory soil column. Berg and others (1) describe the soil column and present data for Fairbanks silt, which is the primary test soil considered to date.

The test column filled with Fairbanks silt was subjected to various boundary conditions, and frost heave was measured while a 15-cm length was frozen. The lower portions of the column were unfrozen with a water table initially approximately 45 cm below the top of the column. Laboratory analyses of Fairbanks silt were conducted to determine soil hydraulic properties. These parameters and boundary conditions were approximated as input data for the mathematical model simulations. Two cases were used for comparison. The first case was a 110-day simulation for nearly unrestrained heave in which a nominal surcharge of 3.4 kPa was applied to the top of the soil column. This case was also used for an extensive sensitivity analysis of the parameters. The second case considered was a problem of restrained heave in which a 34.5-kPa surcharge was applied to the top of the laboratory column.

Figure 2 shows a comparison of measured and simulated heave for the small-surcharge case. Pore-water pressures and locations of the 0°C isotherm were also compared (4), and good agreement was obtained between the model and the soil column (see Table 1). The simulated frost heave shown in Figure 2 was achieved *before* incorporation of a correction factor for the hydraulic conductivity in the freezing zone. Slight (within 10 percent) adjustment of the laboratory-derived soil moisture characteristic curve (soil water pressure versus water content) was required in order to achieve the results shown in Figure 2 and given in Table 1. As Figure 2 shows, the rate of heave during the initial 25-day period is accurately computed. Total heave is simulated relatively well for the entire test. The laboratory soil column had essentially ceased heaving when the test ended at 40 days, and the model also exhibited no additional heaving after about 40 days. Parameters in the model were varied singly and in pairs to test their sensitivity for the early 25-day period, which showed the maximum heave rate. For Fairbanks silt, the unfrozen water content factor was the most

Figure 2. Simulated versus measured heave in vertical column of Fairbanks silt with nominal surcharge.

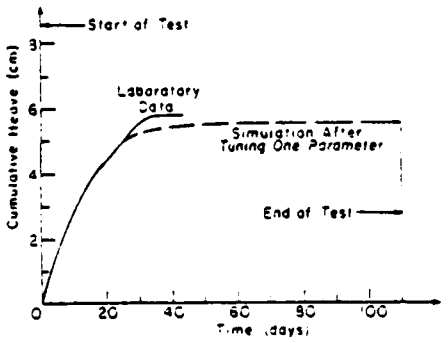

Table 1. Comparison of simulated and measured frost-heave data for 3.4-kPa surcharge.

Type of Data	5 Days	10 Days	15 Days
Laboratory			
Frost heave (cm)	1.6	2.8	4.0
0°C isotherm depth (cm)	6	11	11
Moisture tension at 24-cm depth (cm of water)	≈200	≈200	≈200
Simulated			
Frost heave (cm)	1.5	2.9	3.9
0°C isotherm depth (cm)	4.5-7.5	7-10	10-12.5
Moisture tension at 24-cm depth (cm of water)	100	130	150

critical parameter. Sensitivity analysis disclosed that the model is highly sensitive to pore-water pressure versus water content and hydraulic conductivity parameters and is less sensitive to thermal parameters. A fairly substantial variation in thermal parameters does not significantly affect simulated frost heave because the thermal process is dominated by the phase-change process and sensible heat conduction and convection do not play predominant roles. Processes occurring in the freezing zone dominate the soil-heaving process where the supply of water and the rate of heat extraction are the most significant factors.

In an effort to combine the sensitivity of various hydraulic parameters into one parameter and also to improve the accuracy of model prediction, a correction factor for hydraulic conductivity in the freezing zone was included in the model. This factor accounts for the decreased hydraulic conductivity due to ice formation in soil pores and is defined as

$$K(\Psi, \theta_i) = K(\Psi) \cdot 10^{-E\theta_i} \quad (3)$$

where $E\theta_i \geq 0$ and $K(\Psi)$ is determined from the relation between hydraulic conductivity and pore pressure for unfrozen soil. Currently, the E factor must be determined by calibration for a given soil. When we have more experience with application of the model to a range of soils, it may be possible to select a suitable value without calibration or testing.

Figure 3 shows a plot of frost heave versus time for the small-surcharge Fairbanks silt case (also shown in Figure 2) for the first 25 days. With no tuning of the various parameters, and with E selected equal to 8, the simulated heave almost exactly duplicated the experimentally measured heave. Figure 3 also shows the effect of varying the E parameter. When this parameter is included, other parameters such as $K(\Psi)$ and θ_n show less sensitivity. The sensitivity of thermal parameters remains negligible.

Figure 4 shows the results of a 25-day simulation of restrained heave (34.5-kPa surcharge) compared with laboratory heave data. As can be seen, simulated heave closely approximated the laboratory data. Exact comparison is somewhat difficult because of the need to use approximate boundary conditions in the simulation.

Model simulations were also compared with data from the Tomakomi field site in Japan (13). Soil properties determined from laboratory data, together with approximate boundary conditions, were used to simulate frost heave, which is compared with measured frost heave (Figure 5). The first five days of the heave process were used to calibrate the E parameter to a value of 5. As can be seen, fair agreement was achieved without adjusting the other parameters. Further attempts to more accurately compute frost heave and frost depth were considered

Figure 3. Simulated versus measured frost heave in vertical column of Fairbanks silt with nominal surcharge showing effect of ±20 percent variation in E parameter (dashed lines).

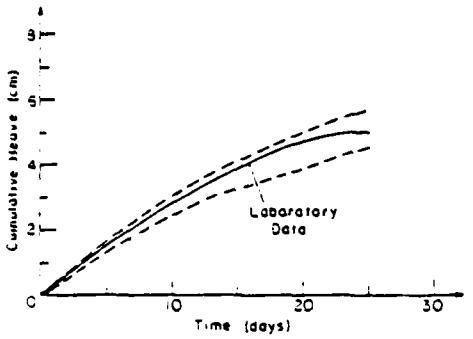

Figure 4. Simulated versus measured restrained heave (34.5-kPa surcharge) in vertical column of Fairbanks silt.

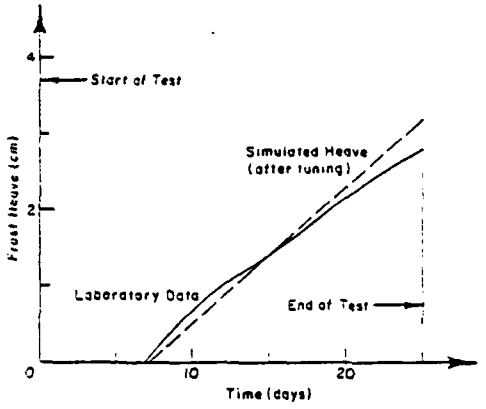

unwarranted because the upper temperature boundary condition was not accurately known. Very limited sensitivity analyses for this case were performed. It appears that the Tomakomi silt is much less sensitive to hydraulic parameters than the Fairbanks silt.

To further verify the model, it is also being applied to other field data. Several sets of field data were obtained from the Winchendon test area in northwestern Massachusetts. Figure 6 shows measured and computed frost heaves and frost depths for Ikalanian silt during the 1978-1979 winter. Laboratory-determined values of hydraulic conductivity and other parameters required by the model were used in the simulation. Boundary conditions and initial conditions for the 1978-1979 winter were estimated or determined from the field data and were applied to the model. Periods from 50 to 70 days were used to calibrate the E parameter. As Figure 6 shows, computed frost heave does not compare with measured frost heave as well as in previous simulations. Simulated frost depths are about the same as those measured in the field except during the spring thaw period (day 70 and beyond), when predicted frost penetration is too shallow. The discrepancy may be due to rather large elements (10 cm) used on the bottom of a 1-m simulation column. Several periods of thaw during the 1978-1979 winter are also approximated by the model. In particular, the spring thaw from day 90 on was approximated accurately in terms

Figure 5. Simulated versus measured frost heave and frost penetration for field tank with Tomakomi silt.

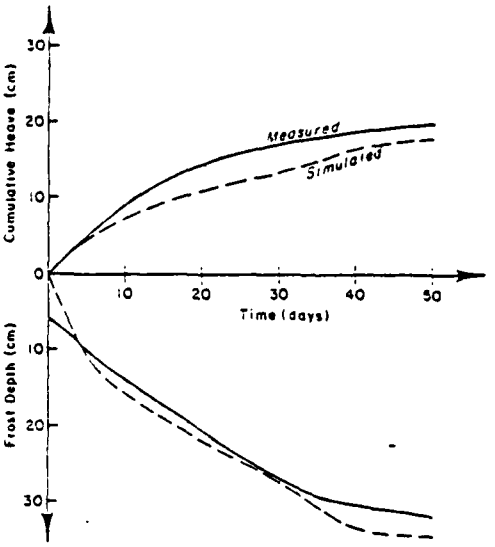

of both thaw consolidation and thaw depth. The difficulty in accurately simulating the entire record is probably due to the fact that there were a number of freeze-thaw cycles during the year. Cyclic freezing and thawing causes parameters to change with respect to time, but the model assumes parameters that are invariant with respect to time.

DISCUSSION OF RESULTS

Development of the frost-heave model has progressed to the point where both restrained and unrestrained heave can be simulated in relatively well-controlled cases. Further study is, however, required to improve or extend the model.

The sensitivity problem needs further study. The fact that the model is sensitive to certain parameters should not be a surprise, since the frost-heave process itself is highly sensitive. Slight differences in environmental and/or soil conditions cause markedly different results. More complete physics-based information on the ice segregation process may reduce some of the sensitivity. If such information should become available, it can be included in the model; however, it is probable that purely deterministic simulations will never be adequate no matter how complete our knowledge. It therefore seems inevitable that some form of a probabilistic model must be associated with the deterministic model. In other words, a deterministic simulation can be performed and then simulated frost heave would be presented in terms of confidence bands based on given or anticipated variations in parameters and boundary conditions. Research on this aspect of the problem has already commenced and will be reported at a later date.

The model needs to be extended to include thaw weakening. We will develop an algorithm for estimating temporal variations in the resilient modulus (or some other parameter reflective of the strength of the pavement system), especially during periods of thaw weakening.

The third area of concern is the dissemination of the model and its use by engineers. The model is somewhat complex and will not be readily understood

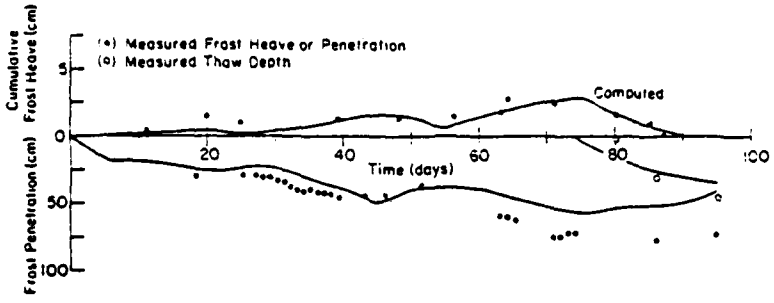

Figure 6. Simulated versus measured frost heave, frost penetration, and thaw depth for Ikalarian silt during 1978-1979 winter at Winchendon, Massachusetts, field site.

by many practicing engineers. We are attempting to simplify the code to provide a model that is versatile and usable on small, readily available computers. During the next year or more, a major effort will be to make the model more readily usable by the practicing engineer.

ACKNOWLEDGMENT

The research reported in this paper was partly supported by the U.S. Army Research Office by means of a research grant to the University of California, Irvine. Soil samples and experimental data from the Tomakomi field site were furnished by S. Kinosita of the Institute of Low-Temperature Science, Sapporo, Japan.

REFERENCES

1. R.L. Berg, J.I. Ingersoll, and G.L. Guymon. Frost Heave in an Instrumented Soil Column. Cold Regions Science and Technology, Vol. 3, 1980, pp. 211-221.
2. R.L. Berg, G.L. Guymon, and T.C. Johnson. Mathematical Model to Correlate Frost Heave of Pavements with Laboratory Predictions. U.S. Army Cold Regions Research and Engineering Laboratory, Hanover, NH, Rept. 80-10, 1980.
3. D.L. Townsend and T.I. Csathy. Soil Type in Relation to Frost Action. Ontario Joint Highway Program, Queen's Univ., Kingston, Ontario, Canada, Rept. 15, 1963.
4. G.L. Guymon, T.V. Hromadka II, and R.L. Berg. A One-Dimensional Frost Heave Model Based upon Simulation of Simultaneous Heat and Water Flux. Cold Regions Science and Technology, Vol. 3, 1980, pp. 253-262.
5. R.L. Harlan. Analysis of Coupled Heat: Fluid Transport in Partially Frozen Soil. Water Resources Research, Vol. 9, No. 5, 1973, pp. 1314-1323.
6. G.L. Guymon and J.N. Luthin. A Coupled Heat and Moisture Transport Model for Arctic Soils. Water Resources Research, Vol. 10, No. 5, 1974, pp. 995-1001.
7. D.A. DeVries. Thermal Properties of Soils. In Physics of Plant Environment (W.E. Van Wijk, ed.), North-Holland Publishing Co., Amsterdam, The Netherlands, 1966, pp. 210-235.
8. W.R. Gardner. Some Steady-State Solutions of the Unsaturated Moisture Flow Equation with Application to Evaporation from a Water Table. Soil Science, Vol. 85, 1958, pp. 228-232.
9. T.V. Hromadka II, G.L. Guymon, and R.L. Berg. Some Approaches to Modeling Phase Change in Freezing Soils. Cold Regions Science and Technology (in preparation).
10. D.M. Anderson, A.R. Tice, and H.L. McKim. The Unfrozen Water and the Apparent Specific Heat Capacity of Frozen Ground. Proc., 2nd International Conference on Permafrost, North American Contribution, National Academy of Sciences, Washington, DC, 1973, pp. 289-294.
11. T.V. Hromadka II and G.L. Guymon. Nodal Domain Integration Model of One-Dimensional Advection-Diffusion. Advances in Water Resources (in preparation).
12. C.S. Desai. Elementary Finite Element Method. Prentice-Hall, Inc., Englewood Cliffs, NJ, 1979.
13. S. Kinosita and others. Observations of Frost Heaving Action in the Experimental Site, Tomakomi, Japan. Proc., 3rd International Conference on Permafrost, National Research Council of Canada, Ottawa, Ontario, Vol. 1, 1978.

Publication of this paper sponsored by Committee on Frost Action.

Evaluation of a Self-Refrigerated Unit for Frost-Heave Testing

K.J. LOMAS AND R.H. JONES

The British Transport and Road Research Laboratory (TRRL) frost-heave test, in which specimens are frozen from the top downward in an open system for 250 h, is specified in terms of a cold room but is more often undertaken in a self-refrigerated unit (SRU). In both units the air temperature above the specimens is maintained at -17°C and the water bath at +4°C. The maximum permitted heave is 13 mm in England and 18 mm in Scotland. A comparative study involving six aggregates of 40-mm maximum size and covering a range of geological types and gradings was undertaken to estab-

TECHNICAL NOTES

Numerical approximation of linear two-dimensional advection–diffusion processes in rectangular spatial domains

T. V. HROMADKA II and G. L. GUYMON

Department of Civil Engineering, School of Engineering, University of California, Irvine, Ca 92717, USA

INTRODUCTION

Numerical solutions of two-dimensional linear and non-linear partial differential equations such as occur in the theory of advection–diffusion processes are generally limited to solution by the finite difference or Galerkin finite element methods. Finite difference approximations, such as described by Spalding[9], can be derived for regular and irregular rectangular two-dimensional subdomains. The Galerkin finite element approach[8] can also be applied to irregular rectangular domains. Both numerical methods are often compared to each other for numerical 'efficiency' or other descriptions of superiority[1].

Recently, Hromadka and Guymon[2–6] have developed a new numerical approach called the nodal domain integration method which has been applied to one-dimensional linear and non-linear problems. From this numerical model, the finite difference, subdomain, and Galerkin finite element methods are included in a single numerical statement.

In this note, the nodal domain integration method is applied to a two-dimensional irregular rectangular element domain. As special cases, the Galerkin finite element, subdomain, and finite difference numerical models are determined by the appropriate specification of a single parameter in the resulting nodal domain integration numerical statement.

The first objective of this note is to present a basic description of the nodal domain integration procedure as applied to the class of partial differential equations generally encountered in the theory of advection–diffusion processes. Detailed mathematical derivations and applications of this numerical approach for a one-dimensional problem are contained in other papers[2–6]. The theoretical foundations of this numerical method are based on the well-known subdomain technique of the finite element weighted residuals approach.

The second objective is to develop a simple numerical statement which can represent the finite element Galerkin statement, subdomain numerical statement, finite difference integrated control volume statement, and the nodal domain integration numerical statement, by the specification of a single parameter in the resulting nodal domain integration numerical approximation.

Hromadka and Guymon[5] used the nodal domain integration approach to numerically approximate the one-dimensional advection diffusion process

$$\frac{\partial}{\partial x}\left[D\frac{\partial\theta}{\partial x}-U\theta\right]=\frac{\partial\theta}{\partial t},\quad x\in\Omega \tag{1}$$

where D and U are the diffusion and advection parameters respectively; θ is the state variable; x, t are spatial and temporal coordinates; and Ω is the spatial domain of definition. For constant parameters, equation (1) can be rewritten into the linear form:

$$D\frac{\partial^2\theta}{\partial x^2}-U\frac{\partial\theta}{\partial x}=\frac{\partial\theta}{\partial t},\quad x\in\Omega \tag{2}$$

Discretizing the spatial domain Ω by m nodal points into m subdomains, R_j, Hromadka and Guymon[6] use the subdomain version of the weighted residuals method to develop a one-dimensional numerical statement for each nodal point value:

$$\frac{D_0}{2\Delta}\left[\theta^2_{j+1}-2\theta^2_j-\theta^2_{j-1}-\theta^1_{j+1}-2\theta^1_j-\theta^1_{j-1}\right]-$$

$$\frac{U_0}{2}\left[\theta^2_{j+1}-\theta^2_{j-1}+\theta^1_{j+1}-\theta^1_{j-1}\right] \tag{3}$$

$$=\frac{1}{2\Delta t(n-1)}\left[\theta^2_{j+1}-2\eta\theta^2_j-\theta^2_{j-1}-\theta^1_{j+1}-2n\theta^1_j-\theta^1_{j-1}\right]$$

where nodal value $\theta^k_j=\theta(x_j,t_k)$, $x_j=j\Delta x$, $t_k=k\Delta t$. It was shown that the η term in equation (3) can vary between R_j and with respect to time in order to approximate a higher order or more complex trial function for the state variable, θ. It was also shown that for a linear polynomial trial function for θ and a Crank–Nicolson time advancement approximation, equation (3) represents the Galerkin finite element, subdomain integration, and finite difference numerical approximations for constant η values of 1, 2, ∞, respectively.

In the following, the one-dimensional numerical statement of equation (3) will be extended to the case of a two-dimensional irregular rectangular subdomain. The problem domain, Ω, is descretized into a set of nodal domains, Ω_j, defined by the intersection of a finite element cover, $\hat{\Omega}_j$, and subdomain cover, R_j, of Ω. Integrating the governing partial differential equations with respect to both space and time on each nodal domain results in a numerical contribution which can be combined with other nodal domain contributions to form a finite difference statement or a finite element matrix system. Similar to the one-dimensional case, the resulting nodal domain integration numerical statement will be shown to also represent the Galerkin finite element, subdomain integration, and finite difference numerical statements by the appropriate specification of a single parameter.

NODAL DOMAIN DISCRETIZATION OF SOLUTION DOMAIN

Consider the partial differential operation:

$$A(\varphi)=f;\ (x,y)\in\Omega,\ \Omega=\Omega\cup\Gamma \tag{4}$$

with boundary condition types of Dirichlet or Neumann specified on boundary Γ. A m-nodal point distribution can be defined in Ω with arbitrary density (Fig. 1) such that an approximation $\hat{\varphi}$ for φ is defined in Ω by:

$$\hat{\varphi}=\sum_{j=1}^{m} N_j(x,y)\varphi_j;\ (x,y)\in\Omega \tag{5}$$

where $N_j(x,y)$ are linearly independent global shape functions and φ_j are assumed values of the state variable, φ, at nodal point j. In equation (5) it is assumed that:

$$\lim_{m\to\infty}\hat{\varphi}=\lim_{\max(x_j,y_j)\to 0}\hat{\varphi}=\varphi,\ (x,y)\in\Omega \tag{6}$$

$$(x_j,y_j)\in R_j;\ (x_k,y_k)\in R_k,\ j=k$$

A closed connected spatial subset R_j is defined for each nodal point j such that:

$$\Omega=\bigcup_{j=1}^{m} R_j \tag{7}$$

with supplementary conditions of:

$$(x_j,y_j)\in R_j;\ (x_k,y_k)\in R_k,\ j=k \tag{8}$$

and

$$R_j=R_j\cup B_j \tag{9}$$

where (x_j,y_j) are the spatial coordinates of node j and B_j is the boundary of R_j. It is assumed that every subdomain is disjoint except along shared boundaries, i.e.

$$R_j\cap R_k=B_j\cap B_k \tag{10}$$

The subdomain method of the finite element weighted residuals approach approximates equation (4) by solving the m equations:

$$\int_{\Omega}(A(\varphi)-f)w_j\,d\Omega=0 \tag{11}$$

where

$$w_j=\begin{cases}1, & (x,y)\in R_j\\ 0, & (x,y)\notin R_j\end{cases} \tag{12}$$

A second cover of Ω is defined by the finite element method with:

$$\Omega=\cup\hat{\Omega}_e \tag{13}$$

where $\hat{\Omega}_e$ is the closure of finite element domain $\hat{\Omega}_e$ and its boundary $\hat{\Gamma}_e$.

Let S_e be the set of nodal points defined by:

$$S_e\equiv\{j\mid\hat{\Omega}_e\cap R_j\neq\{\varnothing\}\} \tag{14}$$

Then a set of nodal domains Ω_j is defined for each finite element domain $\hat{\Omega}_e$ by:

$$\Omega_j=\hat{\Omega}_e\cap R_j,\ j\in S_e \tag{15}$$

The subdomain method of weighted residuals as expressed by equation (11) can be rewritten in terms of the subdomain cover of Ω by:

$$\int_{\Omega}(A(\varphi)-f)w_j\,d\Omega=\int_{R}(A(\varphi)-f)\,d\Omega \tag{16}$$

With respect to the finite element discretization of Ω,

$$\int_{R}(A(\varphi)-f)\,d\Omega=\int_{R\cap\Omega_e}(A(\varphi)-f)\,d\Omega \tag{17}$$

where for each finite element domain $\hat{\Omega}_e$,

$$\int_{\Omega_e\cap R}(A(\varphi)-f)\,d\Omega=\int_{\Omega_e}(A(\varphi)-f)\,d\Omega,\ j\in S_e \tag{18}$$

From the above subset definitions and set covers of Ω, application of the usual subdomain method to the governing partial differential operation of equation (4) is accomplished by an integration of the governing equations over the nodal domains interior of each finite element, resulting in a finite element matrix system similar to that determined by the Galerkin finite element method. The spatial definition of each nodal domain Ω_j depends on the definition of both the finite element and subdomain covers of Ω, and is therefore somewhat arbitrary. A convenient criterion is to define the nodal domains such that the resulting finite element matrix system is symmetric. This symmetry property is used for the definition of finite element nodal domains in the following model development of a two-dimensional advection-diffusion process.

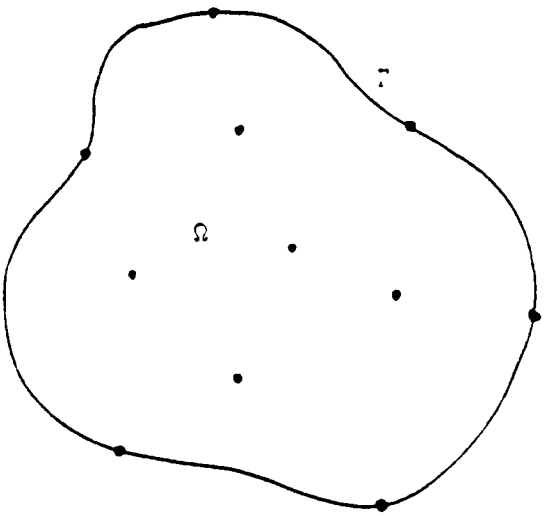

Figure 1. Distribution of nodal points in two-dimensional domain Ω with boundary Γ

NODAL DOMAIN INTEGRATION PROCEDURE

A two-dimensional advection–diffusion process similar to equation (1) is given by:

$$\frac{\partial}{\partial x}\left[D\frac{\partial\theta}{\partial x}-U\theta\right]+\frac{\partial}{\partial z}\left[D\frac{\partial\theta}{\partial z}-W\theta\right]=\frac{\partial\theta}{\partial t},\ (x,z)\in\Omega \quad (19)$$

where Ω is a two-dimensional rectangular spatial domain of definition; (U,W) are advection parameters in the (x,z) directions respectively; and $D\equiv D(x,z)$.

An operator relationship for the two-dimensional advection–diffusion process of equation (19) is defined by:

$$A(\theta)-f=\frac{\partial}{\partial x}\left[D\frac{\partial\theta}{\partial x}-U\theta\right]+\frac{\partial}{\partial z}\left[D\frac{\partial\theta}{\partial z}-W\theta\right]-\frac{\partial\theta}{\partial t} \quad (20)$$

Substituting equation (20) into equation (18) gives the finite element matrix system for $\hat{\Omega}_e$ (Fig. 3).

$$\left\{\int_{\hat{\Omega}}\left(\frac{\partial}{\partial x}\left[D\frac{\partial\theta}{\partial x}-U\theta\right]+\frac{\partial}{\partial z}\left[D\frac{\partial\theta}{\partial z}-W\theta\right]-\frac{\partial\theta}{\partial t}\right)\mathrm{d}A\right\}_j=\{0\}_j,\quad j\in S_e \quad (21)$$

Expanding equation (21) gives:

$$\left\{\int_{\Gamma_j\cap\Gamma_e}\left(D\frac{\partial\theta}{\partial n}-\hat{C}\theta\right)\Big|_{\Gamma_j}\mathrm{d}s\right\}+\left\{\int_{\Gamma_j-\Gamma_j\cap\Gamma_e}\left(D\frac{\partial\theta}{\partial n}-\hat{C}\theta\right)\Big|_{\Gamma_j}\mathrm{d}s\right\}=\left\{\int_{\hat{\Omega}_e}\frac{\partial\theta}{\partial t}\mathrm{d}A\right\}_j,\quad j\in S_e \quad (22)$$

where the first term of equation (22) cancels due to flux contributions form neighbouring finite elements (Fig. 4) or satisfies zero-flux natural boundary conditions on Γ_e and where (n,s) are outward normal and tangential vector components on B_j, Γ_j and $\hat{\Gamma}_e$, and $\hat{C}$ is an advection parameter notation for (U,W) in Γ.

The finite element discretization of Ω is assumed to be composed of rectangles with vertex-located nodal points associated to each finite element domain $\hat{\Omega}_e$ (Fig. 2).

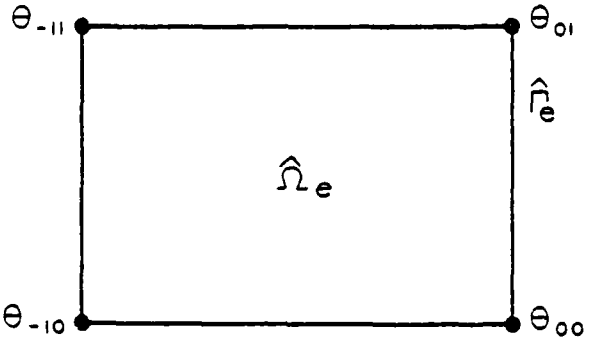

Figure 2. Finite element $\hat{\Omega}_e$ with vertex located nodal points

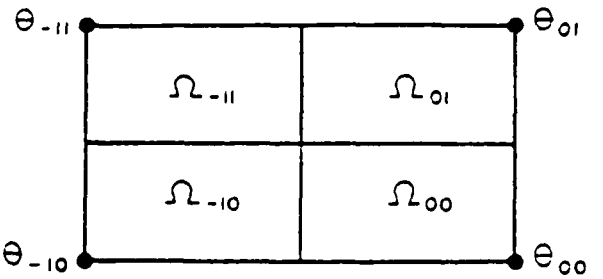

Figure 3. Nodal domain cover of finite element $\hat{\Omega}_e$

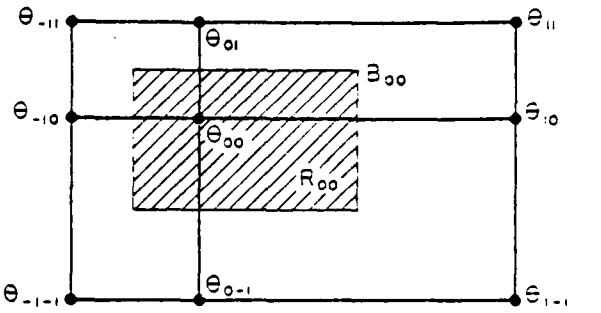

Figure 4. Subdomain R_j as the union of all nodal domains associated to nodal point j

Integration of the governing flow equation on each Ω_e involves the definition and integration of non-linear parameters D and $\hat{C}$. Hromadka and Guymon[4] expand the non-linear parameters by Taylor series and integrate the expanded infinite series expression resulting in an equivalent numerical approximation as a function of the assumed trial function nodal point values. Another approach to handling the non-linearity problem is to approximately linearize the governing flow equation by assuming the non-linear parameters to be uniform in the finite element[5] for small durations of time, Δt. Some methods of determining quasi-constant values for non-linear parameters are examined for a one-dimensional problem in Hromadka and Guymon[3]. Using quasi-constant values of $D^{(e)}$, $\hat{C}^{(e)}$ for the non-linear parameters of the governing flow equation for a small time step Δt simplifies the finite element matrix system of equation (22) to:

$$\left\{\int_{\Gamma_j-\Gamma_j\cap\Gamma_e}\left(D^{(e)}\frac{\partial\theta}{\partial n}-\hat{C}^{(e)}\theta\right)\Big|_{\Gamma_j}\mathrm{d}s\right\}=\left\{\frac{\partial}{\partial t}\int_{\hat{\Omega}}\theta\,\mathrm{d}A\right\}_j;\ 0\le t\le\Delta t,\quad j\in S_e \quad (23)$$

The nodal domain integration method solves equation (23) for each $\hat{\Omega}_e$ by defining functions for a Δt timestep[5,6]

$$\int_{\hat{\Omega}}\theta\,\mathrm{d}A\equiv\int_{\hat{\Omega}}f_j(\theta_j,t)\,\mathrm{d}A,\quad j\in S_e \quad (24)$$

$$\int_{\Gamma_j-\Gamma_j\cap\Gamma_e}\left(\frac{\partial\theta}{\partial n}\right)_{\Gamma_j}\mathrm{d}s\equiv f_j(\theta)\int_{\Gamma_j-\Gamma_j\cap\Gamma_e}\left(\frac{\partial\theta}{\partial n}\right)_{\Gamma_j}\mathrm{d}s,\quad j\in S_e \quad (25)$$

where $f_i(\theta_k,t)$ is a function of time and finite element domain $\hat{\Omega}_e$ associated nodal points, correction factor $c_i(t)$ is a function of time, and $\tilde{\theta}$ is a linear trial function for θ in Ω. The above function definitions are extensions of a similar set of function definitions determined for a one-dimensional flow problem[4,5]. In the study of one-dimensional problems, it was concluded that the $f_i(\theta_k,t)$ functions had a far greater effect on model accuracy than did the $c_i(t)$ functions and that the simplifying definition could be made:

$$c_i(t)=1 \tag{26}$$

for many problems. This conclusion is valid for both first and second order polynomial trial functions where the finite element discretization is composed of nodal domains satisfying the matrix symmetry criterion.

For the assumed rectangular finite element discretization of Ω, a definition of nodal domains Ω_i is required in order to evaluate the $f_i(\theta_k,t)$ functions. Using matrix symmetry as a criterion, element nodal domains are defined by the intersection of perpendicular bisectors (Fig. 3) partitioning the rectangle into four equal areas. The definition of $f_i(\theta_k,t)$ used for each nodal domain Ω_i is given by extending the one-dimensional function definitions to obtain:

$$f_i(\theta_k,t)=\left[\frac{\Sigma\eta_k(t)\theta_k}{\Sigma\eta_k(t)}\right]\frac{A^{(e)}}{4};\ i,k\in S_e \tag{27}$$

where $A^{(e)}$ is the area of rectangle $\hat{\Omega}_e$. In order to provide element matrix symmetry,

$$f_i(\theta_k,t)\equiv f_i(\bar{\eta}_i(t),\ \theta_k);\ i,k\in S_e \tag{28}$$

where $\bar{\eta}_i(t)$ is the average of the $\eta_k(t)$ in finite element $\hat{\Omega}_e$ given by:

$$\bar{\eta}_i(t)=\frac{1}{4}\Sigma\eta_k(t);\ k\in S_e \tag{29}$$

NODAL DOMAIN INTEGRATION NUMERICAL MODEL

For constant advection–diffusion parameters, equation (19) reduces to the linear partial differential equation:

$$D_0\frac{\partial^2\theta}{\partial X^2}+D_1\frac{\partial^2\theta}{\partial Z^2}-U_0\frac{\partial\theta}{\partial X}-W_0\frac{\partial\theta}{\partial Z}=\frac{\partial\theta}{\partial t};\ (X,Z)\in\Omega \tag{30}$$

where (D_0,D_1,U_0,W_0) are constant throughout Ω. Pinder and Gray[5] develop a Galerkin finite element analogue for equation (30). Also, equation (30) is readily approximated by the well known finite difference method[9], and the subdomain version of the weighted residuals method.

A comparison of the Galerkin finite element (linear trial function), finite difference, and subdomain integration numerical statements to the nodal domain integration numerical statement indicates that the nodal domain integration analogue can represent each of the above methods.

For the x-direction diffusion term $D_0\partial^2\theta/\partial X^2$, the Galerkin, subdomain integration, and finite difference modeling statement for a linear polynomial trial function are given by:

$$\frac{D_0\Delta Z}{6}\left\{\frac{\theta_{11}-\theta_{01}}{\beta\Delta X}-\frac{\theta_{01}-\theta_{-11}}{\Delta X}\right\}-$$

$$2(1-\alpha)\left\{\frac{\theta_{10}-\theta_{00}}{\beta\Delta X}-\frac{\theta_{00}-\theta_{-10}}{\Delta X}\right\}-$$

$$\alpha\left\{\frac{\theta_{1-1}-\theta_{0-1}}{\beta\Delta X}-\frac{\theta_{0-1}-\theta_{-1-1}}{\Delta X}\right\}_t^{t+\Delta t} \tag{31}$$

$$\frac{D_0\Delta Z}{8}\left\{\frac{\theta_{11}-\theta_{01}}{\beta\Delta X}-\frac{\theta_{01}-\theta_{-11}}{\Delta X}\right\}-$$

$$3(1-\alpha)\left\{\frac{\theta_{10}-\theta_{00}}{\beta\Delta X}-\frac{\theta_{00}-\theta_{-10}}{\Delta X}\right\}-$$

$$\alpha\left\{\frac{\theta_{1-1}-\theta_{0-1}}{\beta\Delta X}-\frac{\theta_{0-1}-\theta_{-1-1}}{\Delta X}\right\}_t^{t+\Delta t} \tag{32}$$

$$\frac{D_0\Delta Z}{2}(1-\alpha)\left\{\frac{\theta_{10}-\theta_{00}}{\beta\Delta X}-\frac{\theta_{00}-\theta_{-10}}{\Delta X}\right\} \tag{33}$$

and the nodal domain integration statement is:

$$\frac{D_0\Delta Z}{2(\eta-1)}\left\{\frac{\theta_{11}-\theta_{01}}{\beta\Delta X}-\frac{\theta_{01}-\theta_{-11}}{\Delta X}\right\}-$$

$$\eta(1-\alpha)\left\{\frac{\theta_{10}-\theta_{00}}{\beta\Delta X}-\frac{\theta_{00}-\theta_{-10}}{\Delta X}\right\}-$$

$$\alpha\left\{\frac{\theta_{1-1}-\theta_{0-1}}{\beta\Delta X}-\frac{\theta_{0-1}-\theta_{-1-1}}{\Delta X}\right\}_t^{t+\Delta t} \tag{34}$$

where equations (31), (32) and (33) are the numerical statements determined by the Galerkin finite element, subdomain integration, and finite difference methods, respectively. The nodal domain integration model of equation (34) is an equivalent statement for the three models considered for $\eta=(2,3,\infty)$, respectively.

The x-direction advection term $U_0\partial\theta/\partial X$ numerical statements are given by:

$$U_0\frac{\Delta Z}{12}(\theta_{11}-\theta_{-11})-2(1-\alpha)\theta_{10}-\theta_{-10})-$$

$$\alpha(\theta_{1-1}-\theta_{-1-1})_t^{t+\Delta t} \tag{35}$$

$$U_0\frac{\Delta Z}{16}(\theta_{11}-\theta_{-11})-3(1-\alpha)\theta_{10}-\theta_{-10})-$$

$$\alpha(\theta_{1-1}-\theta_{-1-1})_t^{t+\Delta t} \tag{36}$$

$$U_0\frac{\Delta Z}{4}(1-\alpha)\theta_{10}-\theta_{-10}) \tag{37}$$

$$\frac{U_0\Delta Z}{4(\eta-1)}(\theta_{11}-\theta_{-11})-\eta(1-\alpha)\theta_{10}-\theta_{-10})-$$

$$\alpha(\theta_{1-1}-\theta_{-1-1})_t^{t+\Delta t} \tag{38}$$

where equations (35), (36) and (37) are determined from the Galerkin finite element, subdomain integration, and finite difference methods, respectively. The nodal domain integration model of equation (39) is an equivalent statement for equations (35), (36) and (37) for $\eta = 1, 2, 3, \infty$.

Finally, the capacitance (time derivative) term $\partial\theta/\partial t$ numerical statements are:

$$\frac{\partial}{\partial t}\frac{\Delta X \Delta Z}{36}\{\theta_{-1,-1} + 2(1-\beta)\theta_{01} + \beta\theta_{11} + 2(1-\alpha)\theta_{-1,0} + 4(1-\alpha)(1-\beta)\theta_{00} + 2\beta(1-\alpha)\theta_{10} + \alpha\theta_{-1,1} + 2\alpha(1-\beta)\theta_{0,-1} + \alpha\beta\theta_{1,-1}\} \quad (39)$$

$$\frac{\partial}{\partial t}\frac{\Delta X \Delta Z}{64}\{\theta_{-1,-1} + 3(1-\beta)\theta_{01} + \beta\theta_{11} + 3(1-\alpha)\theta_{-1,0} + 9(1-\alpha)(1-\beta)\theta_{10} + 3\beta(1-\alpha)\theta_{10} + \alpha\theta_{-1,1} + 3\alpha(1-\beta)\theta_{0,-1} + \alpha\beta\theta_{1,-1}\} \quad (40)$$

$$\frac{\partial}{\partial t}\frac{\Delta X \Delta Z}{4}(1-\alpha)(1-\beta)\theta_{00} \quad (41)$$

$$\frac{\partial}{\partial t}\frac{\Delta X \Delta Z}{[2(\eta-1)]^2}\{\theta_{-1,-1} + \eta(1-\beta)\theta_{01} + \beta\theta_{11} + \eta(1-\alpha)\theta_{-1,0} + \eta^2(1-\alpha)(1-\beta)\theta_{00} + \eta\beta(1-\alpha)\theta_{10} + \alpha\theta_{-1,1} + \eta\alpha(1-\beta)\theta_{0,-1} + \alpha\beta\theta_{1,-1}\} \quad (42)$$

where equations (39), (40) and (41) are determined from the Galerkin finite element, subdomain integration, and finite difference methods, respectively. The nodal domain integration model of equation (42) is an equivalent statement for equations (39), (40) and (41) for $\eta = 1, 2, 3, \infty$.

The remaining z-direction terms can be determined similar to the above. The resulting nodal domain integration numerical statement for equation (30) on Ω_{00} (Fig. 2) is given by:

$$\frac{D_0 \Delta Z}{2(\eta-1)}\left\{\left[\frac{\theta_{11}-\theta_{01}}{\beta\Delta X} - \frac{\theta_{01}-\theta_{-11}}{\Delta X}\right] - \left(\frac{\theta_{10}-\theta_{00}}{\beta\Delta X} - \frac{\theta_{00}-\theta_{-10}}{\Delta X}\right)\eta(1-\alpha) - \left(\frac{\theta_{1,-1}-\theta_{0,-1}}{\beta\Delta X} - \frac{\theta_{0,-1}-\theta_{-1,-1}}{\Delta X}\right)\alpha\right\} -$$

$$\frac{D_0 \Delta X}{2(\eta-1)}\left\{\left(\frac{\theta_{11}-\theta_{10}}{\Delta Z} - \frac{\theta_{10}-\theta_{1,-1}}{\alpha\Delta Z}\right)\beta + \left(\frac{\theta_{01}-\theta_{00}}{\Delta Z} - \frac{\theta_{00}-\theta_{0,-1}}{\alpha\Delta Z}\right)\eta(1-\beta) - \left(\frac{\theta_{-11}-\theta_{-10}}{\Delta Z} - \frac{\theta_{-10}-\theta_{-1,-1}}{\alpha\Delta Z}\right)\right\} -$$

$$\frac{U_0 \Delta Z}{4(\eta-1)}(\theta_{11}-\theta_{-1,-1}) - \eta(1-\alpha)\theta_{10} - \theta_{-10}) -$$

$$\alpha\theta_{1,-1} - \theta_{-1,-1}) -$$

$$\frac{W_0 \Delta X}{4(\eta-1)}\beta(\theta_{11}-\theta_{-1,1}) + \eta(1-\beta)\theta_{01} - \theta_{0,-1}) + \beta(\theta_{11}-\theta_{-1,1}) +$$

$$\alpha(\theta_{1,-1}-\theta_{-1,-1})\Big\} =$$

$$\frac{\partial}{\partial t}\frac{\Delta X \Delta Z}{[2(\eta-1)]^2}\{\theta_{-1,-1} + \eta(1-\beta)\theta_{01} + \beta\theta_{11} + \eta(1-\alpha)\theta_{-1,0} + \eta^2(1-\alpha)(1-\beta)\theta_{00} + \eta\beta(1-\alpha)\theta_{10} + \alpha\theta_{-1,1} + \eta\alpha(1-\beta)\theta_{0,-1} + \alpha\beta\theta_{1,-1}\} \quad (43)$$

where the Galerkin finite element, nodal domain integration, and finite difference methods are given by $\eta = 1, 2, 3, \infty$ respectively. Equation (43) can be directly compared to the Galerkin finite element results in Pinder and Gray[9], (Table IV.2).

Other constant values of η in equation (43) represent other numerical approximations. For example, $\eta = 1.1$ represents an approximation based on the subdomain method of weighted residuals for a "second order polynomial trial function[3]. Additionally, by use of the function definitions of equations (24) and (25), a variable η between subdomains (or finite element matrices) and with respect to time can be obtained.

CONCLUSIONS

The nodal domain integration numerical approach has been used to determine a numerical analogue which incorporates the Galerkin finite element, subdomain, and integrated finite difference methods as special cases. The resulting numerical statement involves the same computational requirements as does the Galerkin finite element procedure. Thus, a computer program may be prepared based on the nodal domain integration numerical approximation which inherently contains the Galerkin finite element, subdomain integration, and finite difference numerical approximations for the considered class of partial differential equations.

ACKNOWLEDGEMENT

This research was supported by the US Army Research Office (Grant No. DAAG29-79-C-0080).

REFERENCES

1. Haghoe, H. N. Study of relative efficiency of finite difference and Galerkin techniques for modeling soil-water transfer. *Water Resour. Res.* 1978, 14, 97.
2. Hromadka II, T. V. and Guymon, G. L. Some effects of linearizing the unsaturated soil-moisture transfer diffusion model. *Water Resour. Res.* 1980, 16, 659.
3. Hromadka II, T. V. and Guymon, G. L. Numerical mass balance for soil-moisture transfer problems. *Int. Water Resour.* 1980, 3, 37.
4. Hromadka II, T. V. and Guymon, G. L. Technical note on time integration of soil-moisture transport. *Int.* 1980, 3, 51.
5. Hromadka II, T. V. and Guymon, G. L. Improved linear shape function model of soil moisture transport. *Water Resour. Res.* 1981, 17, 504.
6. Hromadka II, T. V. and Guymon, G. L. Nodal domain integration model of one-dimensional advection diffusion. *Int. Water Resour.* 1982, 5, 9.
7. Myers, G. E. *Analytical Methods in Conduction Heat Transfer*. McGraw-Hill, New York, 1971.
8. Pinder, G. F. and Gray, W. G. *Finite Element Simulation in Surface and Subsurface Hydrology*. Academic Press, New York, 1977.
9. Spalding, D. B. A novel finite-difference formulation for differential expressions involving both first and second derivatives. *Int. J. Num. Methods Eng.* 1972, 4, 551.

WATER RESOURCES RESEARCH, VOL. 17, NO. 5, PAGES 1425–1430, OCTOBER 1981

Nodal Domain Integration Model of Unsaturated Two-Dimensional Soil-Water Flow: Development

T. V. HROMADKA II, G. L. GUYMON, AND G. C. PARDOEN

Department of Civil Engineering, University of California, Irvine, California 92717

The nodal domain integration method is applied to a two-dimensional unsaturated soil water flow problem where the solution domain is discretized into irregular triangular elements and the state variable is approximated by a spatial linear trial function within each triangular element. The resulting element matrices incorporate the well-known Galerkin finite element, subdomain, and integrated finite difference numerical statements as special cases of the nodal domain integration numerical statement.

INTRODUCTION

Numerical solutions of two-dimensional nonlinear partial differential equations such as those that occur in the theory of unsaturated ground water flow are generally limited to solution by the finite difference or finite element methods. Finite difference approximations, such as those described by *Spalding* [1972], can be derived for rectangular and also for irregular two-dimensional domains. Finite element methods [*Pinder and Gray*, 1977] can also be applied to irregular two-dimensional domains. Both methods are often compared to each other for numerical 'efficiency' or other descriptions of superiority [*Hayhoe*, 1978].

Recently, *Hromadka and Guymon* [1980*a*, *b*, *c*] have developed a new numerical approach called the nodal domain integration method, which has been applied to one-dimensional linear and nonlinear problems. From this numerical model, the finite difference, subdomain, and Galerkin finite element methods are included in a single numerical statement.

In this paper, the nodal domain integration method is applied to the two-dimensional triangular finite element. As special cases, the Galerkin finite element, subdomain, and finite difference numerical models are determined by the appropriate specification of a single parameter in the resulting nodal domain integration numerical statement. Thus all three numerical approaches are included in one numerical statement similar to the usual Galerkin finite element matrix system.

The purpose of this paper is twofold. The first objective is to present a basic description of the nodal domain integration procedure as applied to the class of partial differential equations generally encountered in the theory of unsaturated groundwater flow. Detailed mathematical derivations and applications of this numerical approach for a one-dimensional problem are contained in other papers [*Hromadka and Guymon*, 1980*b*, *c*]. The theoretical foundations of this numerical method are based on the well-known subdomain technique of the finite element weighted residuals approach. The second objective is to develop a numerical statement which represents the finite element Galerkin statement, subdomain numerical statement, finite difference integrated control volume statement, and the nodal domain integration statement by the specification of a single parameter in the resulting triangle element matrix system.

Paper number 1W0810.
0043-1397/81/001W-0810$01.00

GOVERNING EQUATIONS

Two-dimensional unsaturated Darcian soil water flow in a nondeformable homogeneous porous media is assumed described by the partial differential equation

$$\frac{\partial}{\partial x}\left(K_x \frac{\partial \phi}{\partial x}\right) + \frac{\partial}{\partial y}\left(K_y \frac{\partial \phi}{\partial y}\right) = \frac{\partial \theta}{\partial t} \qquad (x, y) \in \Omega \tag{1}$$

$$K_x = K_x(x, y, \psi, t) \tag{2}$$

where K_x are anisotropic hydraulic conductivity values in the (x, y) directions, respectively, ϕ is the total hydraulic energy head ($\phi = \psi + y$), ψ is the soil water pore pressure head, and θ is the volumetric water content. In (1), water content is assumed to be a single valued function of soil water pore pressure according to the usual soil drying curve with hysteresis effects neglected. Thus

$$\begin{aligned} \theta &= \theta(\psi) \qquad \psi < 0 \\ \theta &= \theta_0 \qquad \psi \geq 0 \end{aligned} \tag{3}$$

where θ_0 is assumed constant. A volumetric water content to pore pressure gradient is defined by

$$\begin{aligned} \theta^* &= \frac{\partial \theta}{\partial \psi} \qquad \psi < 0 \\ \theta^* &= 0 \qquad \psi \geq 0 \end{aligned} \tag{4}$$

For the above assumptions, (1) is rewritten as

$$\frac{\partial}{\partial x}\left[K_x \frac{\partial \phi}{\partial x}\right] + \frac{\partial}{\partial y}\left[K_y \frac{\partial \phi}{\partial y}\right] = \theta^* \frac{\partial \phi}{\partial t} \qquad (x, y) \in \Omega \tag{5}$$

NODAL DOMAIN DISCRETIZATION OF SOLUTION DOMAIN

Consider the partial differential operation

$$A(\phi) = f \qquad (x, y) \in \Omega \quad \Omega = \Omega \cup \Gamma \tag{6}$$

with boundary condition types of Dirichlet or Neumann specified on boundary Γ. An m-nodal point distribution can be defined in Ω with arbitrary density (Figure 1) such that an approximation $\hat{\phi}$ for ϕ is defined in Ω by

$$\hat{\phi} = \sum_{i=1}^{m} N_i(x, y)\phi_i \qquad (x, y) \in \Omega \tag{7}$$

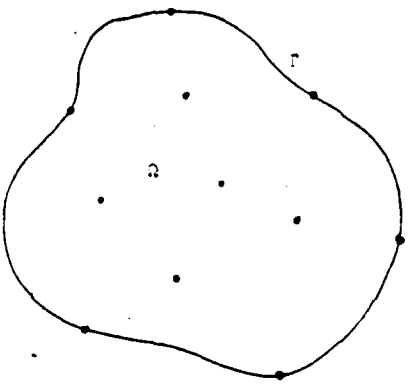

Fig. 1. Distribution of nodal points in two-dimensional domain Ω with boundary Γ.

where $N_j(x, y)$ are linearly independent global shape functions and ϕ_j are assumed values of the state variable ϕ at nodal point j. In (7) it is assumed that

$$\lim_{m\to\infty} \tilde{\phi} = \lim_{\max\|(x_j,y_j)-(x_k,y_k)\|\to 0} \tilde{\phi} = \phi \qquad (x, y) \in \Omega \tag{8}$$

The nodal domain integration approach uses the topology of sets resulting from the discretization procedure associated with the well known finite element and integrated finite difference methods. Generally, the global domain Ω is discretized into finite elements or control volumes and subdomains, depending on whether the finite element or integrated finite difference approach is used. These two discretizations share a common nodal domain discretization of Ω, consequently, the resulting numerical approximations form the various numerical methods which can be defined by a single unifying analog. In the following a subdomain R_j and a finite element Ω_e, a discretization of the global domain Ω, is defined. From these two set covers of Ω a unifying nodal domain cover of Ω is defined. A closed connected spatial subset R_j is defined for each nodal point j such that

$$\Omega = \bigcup_{j=1}^{m} R_j \tag{9}$$

with supplementary conditions of

$$(x_j, y_j) \in R_j \qquad (x_j, y_j) \notin R_k \qquad j \neq k \tag{10}$$

$$R_j = R_j \cup B_j \tag{11}$$

where (x_j, y_j) are the spatial coordinates of node j and B_j is the boundary of R_j. It is assumed that every subdomain is disjoint except along shared boundaries, i.e.,

$$R_j \cap R_k = B_j \cap B_k \tag{12}$$

The subdomain method of the finite element weighted residuals approach approximates (6) by solving the m equations

$$\int_\Omega (A(\phi) - f) w_j \, dA = 0 \tag{13}$$

where

$$w_j = 1 \qquad (x, y) \in R_j$$
$$w_j = 0, \qquad (x, y) \notin R_j \tag{14}$$

A second cover of Ω is defined by the finite element method with

$$\Omega = \cup \, \Omega_e \tag{15}$$

where Ω_e is the closure of finite element domain Ω_e and its boundary Γ_e.

Let S_e be the set of nodal points defined by

$$S_e = \{j | \Omega_e \cap R_j \neq \{0\}\} \tag{16}$$

Then a set of nodal domains Ω_j is defined for each finite element domain Ω_e by

$$\Omega_j = \Omega_e \cap R_j \qquad j \in S_e \tag{17}$$

The subdomain method of weighted residuals as expressed by (13) can be rewritten in terms of the subdomain cover of Ω by

$$\int_\Omega (A(\phi) - f) w_j \, dA = \int_{R_j} (A(\phi) - f) \, dA \tag{18}$$

With respect to the finite element discretization of Ω,

$$\int_{R_j} (A(\phi) - f) \, dA = \int_{R_j \cap \Omega_e} (A(\phi) - f) \, dA \tag{19}$$

where for each finite element domain Ω_e,

$$\int_{\Omega_e \cap R_j} (A(\phi) - f) \, dA = \int_{\Omega_j} (A(\phi) - f) \, dA \qquad j \in S_e \tag{20}$$

From the above subset definitions and set covers of Ω, application of the usual subdomain method to the governing partial differential operation of (6) is accomplished by an integration of the governing equations over the nodal domains interior of each finite element, resulting in a finite element *matrix system similar* to that determined by the Galerkin finite element method. The spatial definition of each nodal domain Ω_j depends on the definition of both the finite element and subdomain covers of Ω and is therefore somewhat arbitrary. A convenient criterion is to define the nodal domains such that the resulting finite element matrix system is symmetric. This symmetry property is used for the definition of finite element nodal domains in the following model development of two-dimensional unsaturated soil water flow.

Nodal Domain Integration Model

The operator relationship for the two-dimensional unsaturated soil water flow model of (5) is

$$A(\phi) - f = \frac{\partial}{\partial x}\left[K_h \frac{\partial \phi}{\partial x}\right] + \frac{\partial}{\partial y}\left[K_h \frac{\partial \phi}{\partial y}\right] - \theta^* \frac{\partial \phi}{\partial t} \tag{21}$$

Substituting (21) into (20) gives the finite element matrix system for Ω_e (Figure 3)

$$\left\{\int_{\Omega_e} \left(\frac{\partial}{\partial x}\left[K_h \frac{\partial \phi}{\partial x}\right] + \frac{\partial}{\partial y}\left[K_h \frac{\partial \phi}{\partial y}\right] - \theta^* \frac{\partial \phi}{\partial t}\right) dA\right\} = \{0\} \qquad j \in S_e \tag{22}$$

Expanding (22) gives

$$\left\{\int_{\Gamma_e - \Gamma \cap \Gamma_e} \left|K_h \frac{\partial \phi}{\partial n}\right|_{\Gamma_e} ds\right\} + \left\{\int_{\Gamma - \Gamma \cap \Gamma_e} \left|K_h \frac{\partial \phi}{\partial n}\right|_{\Gamma} ds\right\} = \left\{\int_{\Omega_e} \theta^* \frac{\partial \phi}{\partial t} \, dA\right\} \qquad j \in S_e \tag{23}$$

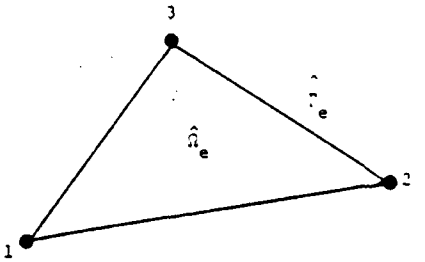

Fig. 2. Subdomain R_j as the union of all nodal domains associated to nodal point j.

where the first term of (23) cancels due to flux contributions from neighboring finite elements (Figure 2) or satisfies zero-flux natural boundary conditions on Γ and where (n, s) are normal and tangential vector components on B_r, Γ_r, and Γ_e. The finite element discretization of Ω is assumed to be composed of triangles with three vertex-located nodal points associated to each finite element domain Ω_e (Figure 3).

Integration of the governing flow equation on each Ω_j involves the definition and integration of nonlinear parameters K_h and θ^*. *Hromadka and Guymon* [1980c] expand the nonlinear parameters by Taylor series and integrate the expanded infinite series expression resulting in an equivalent numerical approximation as a function of the assumed trial function nodal point values. Another approach to handling the nonlinearity problem is to approximately linearize the governing flow equation by assuming the nonlinear parameters to be uniform in the finite element [*Myers*, 1971] for small durations of time, Δt. Some methods of determining quasiconstant values for nonlinear parameters are examined for the one-dimensional unsaturated soil water flow problem by *Hromadka and Guymon* [1980a]. Using quasiconstant values of $(K_h^{(e)}, \theta^*(e))$ for the nonlinear parameters of the governing flow equation for a small time step Δt simplifies the finite element matrix system of (23) to

$$\left\{\int_{\Gamma_j-\Gamma_j\cap\Gamma_e}\left|K_h^{(e)}\frac{\partial\phi}{\partial n}\right|_{\Gamma_j} ds\right\} = \left\{\theta^*(e)\frac{\partial}{\partial t}\int_{\Omega_j}\phi\, dA\right\} \quad (24)$$
$$0 \le t \le \Delta t \qquad j \in S_e$$

The nodal domain integration method solves (24) for each Ω_e by defining functions for a Δt timestep:

$$\int_{\Omega_j}\phi\, dA = \int_{\Omega_j} f_j(\phi_k, t)\, dA \qquad \{j, k \in S_e\} \quad (25)$$

$$\int_{\Gamma_j-\Gamma_j\cap\Gamma_e}\left|\frac{\partial\phi}{\partial n}\right|_{\Gamma_j} ds = c_j(t)\int_{\Gamma_j-\Gamma_j\cup\Gamma_e}\left|\frac{\partial\tilde{\phi}}{\partial n}\right|_{\Gamma_j} ds \qquad j \in S_e \quad (26)$$

where $f_j(\phi_k, t)$ is a function of time and finite element domain $\hat{\Omega}_e$ associated nodal points; correction factor $c_j(t)$ is a function of time; and $\tilde{\phi}$ is a linear trial function for ϕ in $\hat{\Omega}_e$. The above function definitions are extensions of a similar set of function definitions determined for a one-dimensional soil water flow problem [*Hromadka and Guymon*, 1981]. In the study of one-dimensional problems it was concluded that the $f_j(\phi_k, t)$ functions had a far greater effect on model accuracy than did the $c(t)$ functions and that the simplifying definition

$$c_j(t) = 1 \quad (27)$$

could be made for many problems. This conclusion is valid for both first- and second-order polynomial trial functions where the finite element discretization is composed of nodal domains satisfying the matrix symmetry criterion.

For the assumed triangular finite element discretization of Ω, a definition of nodal domains Ω_j is required in order to evaluate the $f_j(\phi_k, t)$ functions. Using matrix symmetry as a criterion, element nodal domains are defined by the intersection of triangle finite element medians (Figure 4) partitioning the triangle into three equal areas. The definition of $f_j(\phi_k, t)$ used for each nodal domain Ω_j is

$$f_j(\phi_k, t) = \left[\frac{(\eta_j(t)\phi_j + \sum_{k\neq j}\phi_k)}{2 + \eta_j(t)}\right]\frac{A^{(e)}}{3} \qquad (j, k) \in S_e \quad (28)$$

where $A^{(e)}$ is the area of triangle $\hat{\Omega}_e$. In order to provide element matrix symmetry,

$$f_j(\phi_k, t) = f(\bar{\eta}(t), \phi_k) \qquad (j, k) \in S_e \quad (29)$$

where

$$\bar{\eta}(t) = \frac{1}{3}\sum \eta_j(t) \qquad j \in S_e \quad (30)$$

For finite element domain $\hat{\Omega}_e$, the above gives the element capacitance $\mathbf{P}^{(e)}$ matrix approximation

$$\mathbf{P}^{(e)}[\bar{\eta}(t)] = \frac{\theta^*(e)A^{(e)}}{3(\bar{\eta}(t)+2)}\begin{bmatrix}\bar{\eta}(t) & 1 & 1\\ 1 & \bar{\eta}(t) & 1\\ 1 & 1 & \bar{\eta}(t)\end{bmatrix} \quad (31)$$

For $c(t) = 1$, the element conduction matrix $\mathbf{K}^{(e)}$ for $\hat{\Omega}_e$ is determined from (24) and (26). From (26) the state variable flux term $\partial\phi/\partial n$ is approximated on $(\Gamma_j - \Gamma_j \cap \Gamma_e)$ by assuming ϕ to be described in $\hat{\Omega}_e$ by a linear trial function.

In order to evaluate the spatially integrated flux terms of (26) for each nodal domain of a triangular finite element, the triangle geometry is defined by a system of vectors as shown in Figure 5. For the assumed linear trial function variation of the state variable ϕ in the finite element triangle, the spatially integrated flux term contribution to nodal domain Ω_1 is geometrically determined by Figure 6. Flux must contribute to Ω_1 through the boundaries of Ω_1 and can be calculated by the flux vector through state variable ϕ values ϕ_1 (at node 1) and ϕ' as shown in the figure where

$$\phi' = \frac{1}{L}(\phi_2 d_1 + \phi_3 d_2) \quad (32)$$

The integration of the spatial boundary of Ω_1 normal to the considered flux vector is $L/2$ as shown in Figure 6. From

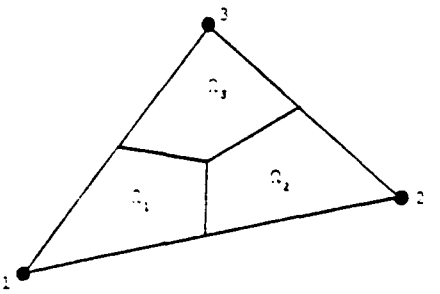

Fig. 3. Finite element $\hat{\Omega}_e$ with three vertex-located nodal points.

Darcy's Law, the efflux for a linear polynomial function approximation is

$$-\frac{K_h^{(e)}[\phi_2(d_1/L)+\phi_3(d_2/L)-\phi_1]}{h} \tag{33}$$

and the integrated efflux (discharge) contribution from Ω_1 is

$$-\frac{K_h^{(e)}}{2hL}[\phi_2 d_1 L+\phi_3 d_2 L-L^2\phi_1] \tag{34}$$

which is obtained by multiplying $L/2$ with (33). From Figure 5 the geometric constants in (34) are

$$L^2=\bar{r}_{23}\bar{r}_{23}=x_{23}^2+y_{23}^2 \tag{35}$$

$$d_1L=\bar{r}_{13}\bar{r}_{23}=x_{13}x_{23}+y_{13}y_{23} \tag{36}$$

$$d_2L=-\bar{r}_{12}\bar{r}_{23}=-(x_{12}x_{23}+y_{12}y_{23}) \tag{37}$$

where $x_{23}=x_3-x_2$. Using matrix notation, (34) may be written as follows:

$$\frac{K_h^{(e)}}{4A^{(e)}}[x_{23}^2+y_{23}^2),\ -(x_{13}x_{23}+y_{13}y_{23}),\ (x_{12}x_{23}+y_{12}y_{23})]\begin{Bmatrix}\phi_1\\ \phi_2\\ \phi_3\end{Bmatrix} \tag{38}$$

Combining the finite element nodal domain equations, the element conduction matrix $\mathbf{K}^{(e)}$ for Ω_e is

$$\mathbf{K}^{(e)}=\frac{K_h^{(e)}}{4A^{(e)}}\begin{bmatrix}(x_{23}^2+y_{23}^2), & -(x_{13}x_{23}+y_{13}y_{23}), & (x_{12}x_{23}+y_{12}y_{23})\\ (\text{symmetric}) & (x_{13}^2+y_{13}^2), & -(x_{12}x_{13}+y_{12}y_{13})\\ & & (x_{12}^2+y_{12}^2)\end{bmatrix} \tag{39}$$

The approximation of (24) by the nodal domain integration element matrix system for Ω_e is

$$\mathbf{K}^{(e)}\phi_j+\mathbf{P}^{(e)}[\bar{\eta}(t)]\,\dot{\phi}_j=\{0\} \qquad j\in S_e \tag{40}$$

where ϕ_j and $\dot{\phi}_j$ are the vector of nodal point values and time derivative of nodal point values associated to finite element domain Ω_e.

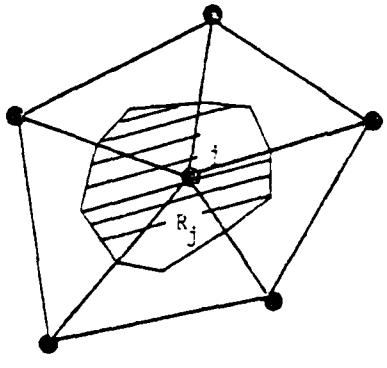

Fig. 4. Finite element partitioned into nodal domains.

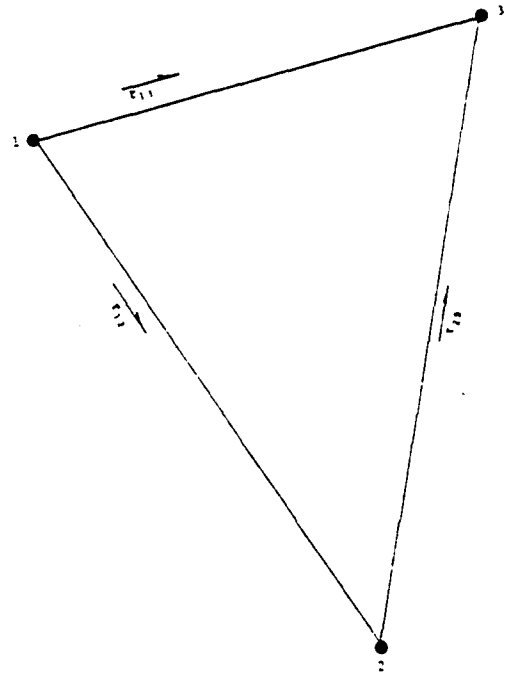

Fig. 5. Vector description of triangle finite element geometry.

SIMILARITY OF NODAL DOMAIN INTEGRATION MODEL TO OTHER NUMERICAL MODELS

In this section the finite element subdomain and *Galerkin* techniques of the weighted residuals method [*Pinder and Gray*, 1977] and the integrated finite difference method as developed by *Spalding* [1972] will be applied to the assumed linearized soil water flow equation. The models derived from these numerical approaches will be compared to the nodal domain integration model and an appropriate $\bar{\eta}(t)$ determined such that the element matrix system of (40) also represents these other various modeling approaches.

Integrated Finite Difference Method

By using a control volume defined by the union of all nodal domains associated to a particular nodal point (Figure 2), the integrated finite difference approach can be derived. The control volume CV_j is defined by

$$CV_j=\cup\Omega_e \tag{41}$$

The integrated influx to the control volume along the boundary is the sum of influx contributions from each interior nodal domain Ω_e. The nodal domain Ω_e efflux contribution from CV_j (by means of the boundary Γ_j) is determined from (38). The total integrated efflux from CV_j would be row j of the assembled global conduction matrix derived by the usual sum of element conduction matrices of (39).

The integrated finite difference model assumes that ϕ is constant-valued in CV_j. Consequently,

$$\int_{CV}\phi\,dA=\phi_j\int_{CV_j}dA \tag{42}$$

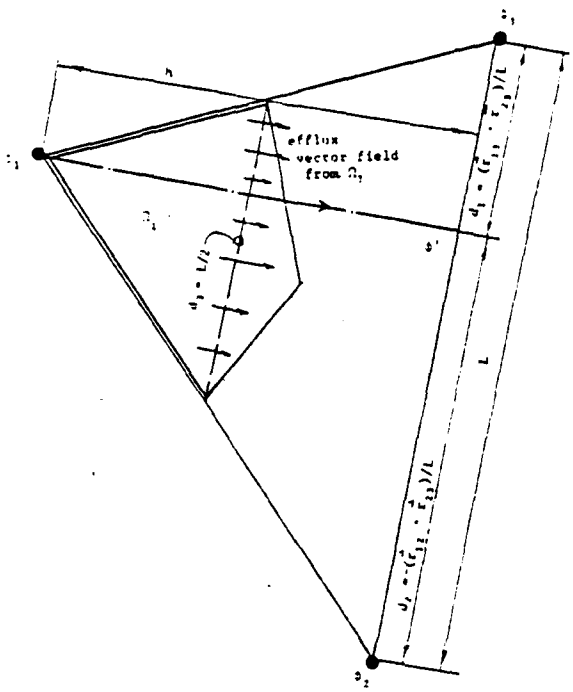

Fig. 6. Geometric solution of flux distribution (for nodal domain Ω_1) for assumed linear trial function distribution of state variable.

Holding ϕ constant in each Ω_j gives

$$\int_{\Omega_j} \phi \, dA = \phi_j \int_{\Omega_j} dA = \phi_j \frac{A^{(e)}}{3} \tag{43}$$

The element capacitance matrix of (31) includes the integrated finite difference statement of (43) by

$$\lim_{\bar{\eta}(t)\to\infty} \mathbf{P}^{(e)}[\bar{\eta}(t)] = \frac{\theta^*(e)A^{(e)}}{3} \begin{bmatrix} 1 & 0 & 0 \\ 0 & 1 & 0 \\ 0 & 0 & 1 \end{bmatrix} \tag{44}$$

Therefore the integrated finite difference model for the linearized soil water flow problem is

$$\lim_{\bar{\eta}(t)\to\infty} (\mathbf{K}^{(e)}\phi_j + \mathbf{P}^{(e)}[\bar{\eta}(t)]\dot{\phi}_j = \{0\}) \qquad j \in S_e \tag{45}$$

Subdomain Method of Weighted Residuals

A subdomain model for the assumed linearized soil water flow problem can be derived from the nodal domain integration model by prescribing the trial function $\hat{\phi}$ to be linear in each finite element domain Ω_e. Using a linear trial function $\hat{\phi}$ in Ω_e allows a direct integration of $\dot{\hat{\phi}}$ in each Ω_j (Figure 7). Therefore a subdomain approximation in Ω_1 is

$$\int_{\Omega_1} \dot{\hat{\phi}} \, dA = \frac{A^{(e)}}{108} [22\dot{\phi}_1 + 7\dot{\phi}_2 + 7\dot{\phi}_3] \tag{46}$$

By comparison to the integrated finite difference model,

$$R_j = CV_j \tag{47}$$

Therefore the element capacitance matrix $\mathbf{P}^{(e)}[\bar{\eta}(t)]$ includes a subdomain model

$$\mathbf{P}^{(e)} \begin{bmatrix} 22 \\ 7 \end{bmatrix} = \frac{\theta^*(e)A^{(e)}}{108} \begin{bmatrix} 22 & 7 & 7 \\ 7 & 22 & 7 \\ 7 & 7 & 22 \end{bmatrix} \tag{48}$$

The integrated efflux from subdomain R_j through boundary B_j is given by the jth row of the assembled global conduction matrix. Therefore a subdomain model for the linearized soil water flow problem is

$$\left(\mathbf{K}^{(e)}\phi_j + \mathbf{P}^{(e)} \begin{bmatrix} 22 \\ 7 \end{bmatrix} \dot{\phi}_j = \{0\}\right) \qquad j \in S_e \tag{49}$$

Galerkin Method of Weighted Residuals

The Galerkin finite element approach applied to the linearized soil water flow problem for triangular elements and a linear trial function [*Myers*, 1971] is included in the nodal domain integration model by

$$(\mathbf{K}^{(e)}\phi_j + \mathbf{P}^{(e)}[2]\dot{\phi}_j = \{0\}) \qquad j \in S_e \tag{50}$$

Nodal Domain Integration Method

From the above the nodal domain integration model includes the integrated finite difference, subdomain, and Galerkin finite element models for constant values of $\bar{\eta}(t) = (2, 22/7, \infty)$. Consequently, a computer model based on the nodal domain integration element matrix systems also includes the above numerical models by the specification of a single constant for $\bar{\eta}(t)$. These results can be compared to the one-di-

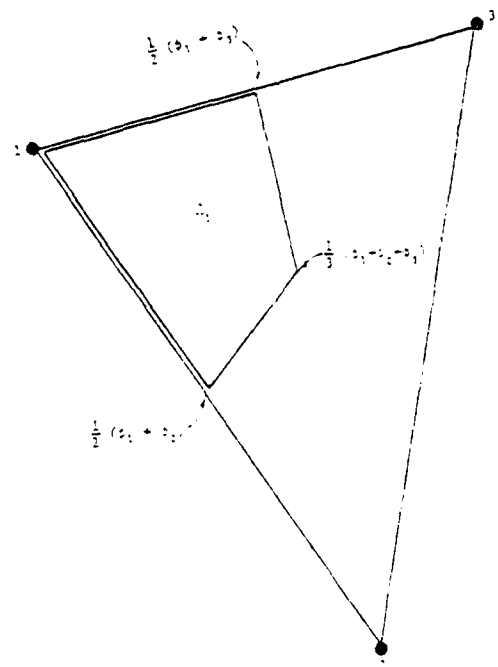

Fig. 7. Linearly distributed state variable values in nodal domain partition Ω_1.

mensional nodel domain integration model [*Hromadka and Guymon*, 1980*a*] which represents the finite element, subdomain, and finite difference models for $\eta = (2, 3, \infty)$, respectively.

CONCLUSIONS

The nodal domain integration numerical approach has been used to determine a numerical analog which incorporates the Galerkin finite element, subdomain, and integrated finite difference methods as special cases. The resulting numerical statement involves the same computational requirements as does the Galerkin finite element procedure. Thus computer programs may be prepared based on the nodal domain integration procedure which inherently contains the Galerkin finite element, subdomain, and finite difference techniques. A powerful method of comparing the accuracy of various numerical techniques is provided which eliminates uncertainty of effects between codes used for comparison.

Theoretically, the so-called 'nodal domain integration' method contains all numerical subsets in addition to those derived; i.e., finite element, finite difference, and subdomain methods. For instance, this method would include linear basis function approximations of higher order basis functions. The method proposed here can be extended to include the case where a single computational problem can be allowed to select a spatially and temporarily varying η function to achieve optimal spatial accuracy.

Acknowledgments. This work was supported by the U.S. Army Research Office (Research Grant DAAG24-79-C-0080). The second author was on sabbatical leave at the U.S. Army Cold Regions Research and Engineering Laboratory, Hanover, N. H. during the preparation of this paper.

REFERENCES

Hayhoe, H. N., Study of relative efficiency of finite difference and Galerkin techniques for modeling soil-water transfer, *Water Resour. Res.*, *14*(1), 97–102, 1978.

Hromadka, T. V., II, and G. L. Guymon, Some effects of linearizing the unsaturated soil moisture transfer diffusion model, *Water Resour. Res.*, *16*(4), 643–650 1980*a*.

Hromadka, T. V., II, and G. L. Guymon, Numerical mass balance for soil-moisture transfer problems, *Advan. Water Resour.*, *3*, 107, 1980*b*.

Hromadka, T. V., II, and G. L. Guymon, Note on time integration of soil moisture transport, *Advan. Water Resour.*, *3*, 181–186, 1980*c*.

Hromadka, T. V., II, and G. L. Guymon, Improved linear shape function model of soil moisture transport, *Water Resour. Res.*, *17*(3), 504–512, 1981.

Myers, G. E., *Analytical Methods in Conduction Heat Transfer*, McGraw-Hill, New York, 1971.

Pinder, G. F., and W. G. Gray, *Finite Element Simulation in Surface and Subsurface Hydrology*, Academic, New York, 1977.

Spalding, D. B., A novel finite-difference formulation for differential expressions involving both first and second derivations, *Int. J. Numer. Methods Eng.*, *4*, 551, 1972.

(Received November 24, 1980;
revised April 27, 1981;
accepted May 5, 1981.)

Correction to 'Nodal Domain Integration Model of Unsaturated Two-Dimensional Soil-Water Flow: Development'

In the paper 'Nodal Domain Integration Model of Unsaturated Two-Dimensional Soil-Water Flow: Development' by T. V. Hromadka II, G. L. Guymon, and G. C. Pardoen [*Water Resources Research*, *17*(5), 1425–1431, 1981], Figures 2, 3, and 4 have been switched and should appear as shown here.

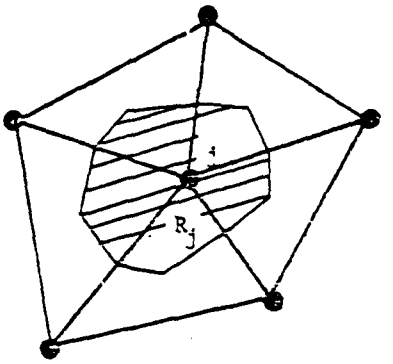

Fig. 2. Subdomain R_j as the union of all nodal domains associated to nodal point j.

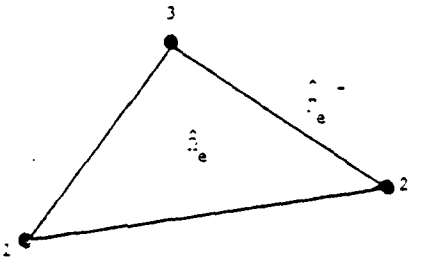

Fig. 3. Finite element Ω_e with three vertex-located nodal points.

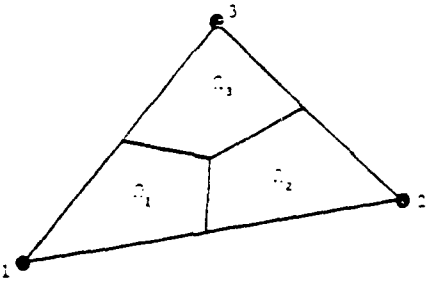

Fig. 4. Finite element partitioned into nodal domains.

(Received December 15, 1981)

Paper number 1W1897
0043-1397/82/001W-1897$02.00/0

Cold Regions Science and Technology, 5 (1981) 127–140
Elsevier Scientific Publishing Company, Amsterdam – Printed in The Netherlands

A PROBABILISTIC-DETERMINISTIC ANALYSIS OF ONE-DIMENSIONAL ICE SEGREGATION IN A FREEZING SOIL COLUMN

G.L. Guymon
School of Engineering, University of California, Irvine, CA (U.S.A.)

M.E. Harr
School of Civil Engineering, Purdue University, West Lafayette, IN (U.S.A.)

R.L. Berg
U.S. Army Cold Regions Research and Engineering Laboratory, Hanover, NH (U.S.A.)

T.V. Hromadka, II
School of Engineering, University of California, Irvine, CA (U.S.A.)

(Received March 13, 1981; accepted in revised form, May 19, 1981)

ABSTRACT

A deterministic model of frost heave based upon simultaneous analysis of coupled heat and moisture transport is cascaded with a probabilistic model of parameter variations. The multiparameter, deterministic model is based upon submodels of moisture transport, heat transport, and lumped isothermal freezing processes. The probabilistic model is based upon Rosenblueth's method which only requires knowledge of parameter means and their coefficients of variation. The deterministic model is relatively insensitive to thermal parameter variations because the phase change process dominates the thermal regime of a freezing moist soil. The model is sensitive to hydraulic parameters which control the rate mobile liquid water is drawn into the freezing soil region. Four hydraulic parameters were varied within reported and assumed levels of parameter variation for two soils; a frost-susceptible silt and a marginally frost-susceptible dirty gravel for which laboratory data on parameters and frost heave were available. The resulting frost heave variations were fit to a beta distribution and confidence limits of at least 95% were predicted within two sigma bounds. The coefficient of variation of unfrozen hydraulic conductivity primarily determines the coefficient of variation of simulated frost heave. Comparison of these results with two detailed field cases indicates a close comparison with beta distribution parameters.

INTRODUCTION

Attempts to develop mathematical models of frost heave have centered on continuum-deterministic approaches which are sometimes referred to as conceptual or physics based approaches. Guymon et al. (1980) and Hopke (1980) review these efforts. Generally, mathematical models have included simultaneous heat and moisture transport in a one-dimensional column. While there is almost total agreement that these two processes must somehow be included in any model of frost heave, there is considerable uncertainty and disagreement on the ice segregation processes itself. The processes occurring in the freezing zone are, unfortunately, poorly understood. There also are somewhat divergent objectives in developing these models as explicitly or implicitly viewed by the various authors, and these differences in objectives have led to differences in approaches. One purpose of this paper is to present a more systematic basis for viewing or judging the frost heave modeling exercise.

0165-232X/81/0000–0000/$02.50

Guymon et al. (1981) have questioned the fundamental concept of using deterministic models because of uncertainty concerning model parameters and modeling concepts of the ice segregation process. They suggest that probabilistic concepts should be coupled with deterministic approaches.

Chamberlain (1980) has recently conducted comprehensive studies of field frost heave for a small section of roadway in Hanover, NH, with sandy silts as the base material. The variations of frost heave were carefully measured at 455 discrete points and were fitted to a beta-probability distribution, suggesting that frost heave can be evaluated as a probabilistic process. Chamberlain observed a coefficient of variation of about 72% and a maximum and minimum frost heave of about 3 and 2 standard deviations, respectively. The maximum mean frost heave he observed was 4.2 cm and frost penetration was 90 cm. Numerous "undisturbed" samples collected at this site for determining hydraulic parameters should be useful in defining the statistical properties of these parameters which may in turn be related to the observed frost heave variations. We have made similar measurements at 39 discrete points on a taxiway at the Albany County Airport in Albany, NY. A maximum mean heave of 1.65 cm was observed on 11 February 1980 when frost had penetrated less than 50 cm into the silty-sand sub-base material. A maximum 130% coefficient of variation for heave was obtained. Observed maximum and minimum heave values 3.35 cm and 0.9 cm are equivalent to approximately plus and minus two standard deviations. Cores of frozen ground where ice lensing has occurred also suggest a process exhibiting random features. Ice lenses will occur in a seemingly random pattern in a core only a few cm in diameter. Analysis of such a "one-dimensional" core uniformly frozen so that there would be a generally uniform distribution of ice, indicated little relation between the frequency of ice lenses along three vertical transects taken 4 cm apart. Ice lenses were on the order of 0.4 mm thick. An ice lens might occur on one horizontal transect and just 4 cm horizontally to the right or left no ice lens was visible.

A central objective of this paper is to develop a probabilistic concept of frost heave which includes the usual deterministic approaches but recognizes the inherent discrete nature of porous media. To do this, a new probabilistic approach will be presented which avoids the commonly used and sometimes expensive Monte Carlo method. Although a particular mathematical model will be used (Guymon et al., 1980) to develop a probabilistic-deterministic model, the theory developed here is generally applicable to deterministic models proposed by others.

SYSTEMS CONCEPTS

Figure 1 is an approach to viewing the modeling process. The prototype system S (e.g. a laboratory soil column) is subject to excitations, x (or inputs) which are spatially and temporarily distributed. Spatially and temporally distributed outputs are observed. Inputs or boundary conditions may be subfreezing temperatures, water table location, and surface surcharge (overburden). Outputs may be frost heave, y, or soil pore pressure, temperatures, or ice content. Because it is usually impossible to measure x exactly, subsystem X indicates a model process to determine an index, x', of x which has some error. In our case we are generally lumping x in space but are preserving, to the extent possible, any low-frequency dynamic characteristics of x. Since our deterministic model M is based upon the continuum assumption, certain parameters arise in the model derivation which purport to characterize S (e.g. thermal conductivity or hydraulic conductivity). Subsystem P indicates this modeling or sampling process which yields imperfectly known parameters, p_i. Model outputs, y', will therefore be imprecise but may be compared to imperfect observations of y for

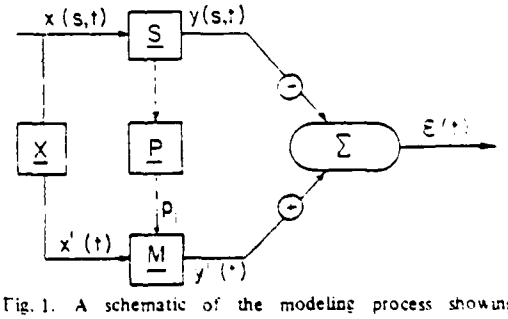

Fig. 1. A schematic of the modeling process showing modeling uncertainty

some bounded time period to determine model uncertainty, $\epsilon(t)$, where

$$\epsilon(t) = y'(t) - y(t) \quad (1)$$

We are considering y as lumped in order to make this computation. Modeling uncertainty is arbitrarily grouped into four general areas:

1. Errors α_1 due to the choice of M which includes the choice of a numerical analog.
2. Errors α_2 due to spatial and temporal discretization and averaging.
3. Errors α_3 due to boundary conditions (i.e. choice of X) and due to choice of initial conditions.
4. Errors α_4 due to the selection of p_i; i.e. choice of P.

The total model uncertainty is some function of the α_i errors

$$\epsilon(t) = \epsilon(\alpha_1, \alpha_2, \alpha_3, \alpha_4) \quad (2)$$

where the α_i errors may be interrelated and ϵ may be non-stationary. Because of approximations necessarily incorporated in the model there will obviously be some error or uncertainty in model predictions. Furthermore, the complex and nonlinear nature of the model requires comparison to prototype situations to evaluate its precision.

An investigation of errors associated with the choice of numerical methods (e.g. finite difference and finite element methods) and spatial and temporal discretization is the subject of a future paper. Boundary condition effects will also be investigated in a future paper.

The major thrust of this paper will concentrate on parameter errors associated with an assumed uniform soil profile. It is well known (Harr, 1977; Nielsen et al., 1973; Warrick and Nielson, 1980) that considerable variation is observed in field soils that are within a small geographical area and may be generally classed as the same soil. Moreover, most field soil profiles are layered (non-uniform) although they are often simplified to an "average" uniform soil profile for analysis. This usually unknown variability coupled with sampling and measuring errors is significant. Frost heave is an ideal process to study by probabilistic methods since it is sensitive to minor variations in soil properties and environmental conditions. Moreover, frost heave or ice segregation processes effectively integrate all hydraulic, thermal and chemical processes taking place in a finite column of soil so that by measuring one output, frost heave, all other processes are indirectly sampled. Frost penetration depths can also be accurately measured and they provide some indication of parameter variability effects.

BRIEF REVIEW OF DETERMINISTIC MODEL

Guymon et al. (1981) describe the deterministic model, and these details will not be repeated here. Only a general summary of the model will be presented.

The model is applicable to a saturated or unsaturated, one-dimensional, vertical, soil column which is subjected to time-dependent variations in upper and lower boundary temperature and pore water pressure conditions. The upper boundary condition is assumed to be a no-moisture flux condition if the soil surface is frozen. Additionally, a surface surcharge or overburden condition is accommodated by the model. Major assumptions employed in the model are:

1. Unsaturated moisture flow theory applies and Darcy's law is valid in the unfrozen zone and the freezing fringe.
2. Moisture movement is by liquid films driven by the total hydraulic head energy gradient.
3. Moisture movement in frozen zones is negligable.
4. The well known heat equation, including a sensible heat advection term, applies to the entire soil profile.
5. The unfrozen zone is nondeformable and the frozen zone is only deformable due to ice lens growth.
6. The fluid sink due to freezing and the latent heat process may be decoupled into an isothermal approach (i.e. a heat balance process).
7. Ice segregation occurs when moisture drawn into the freezing zone exceeds the soil porosity minus an unfrozen water content factor, corrected for volumetric ice expansion.
8. Hysteresis is not present and all functions are single valued and piece-wise continuous.
9. Overburden and surcharge effects are included

by adding these pressures to pore water pressures at ice segregation fronts only.

10. Salt transport effects are negligible; i.e. the freezing point depression of soil water is constant, and the unfrozen moisture content at a given temperature is constant.
11. Constant parameters are invariant with respect to time; i.e. they do not change in response to freeze–thaw cycles.

The model is based upon simultaneous solution of partial differential equations of heat and moisture flux in the unfrozen zone wherein it is assumed unsaturated flow is modeled by unsaturated flow theory

$$\frac{\partial[K_H(\partial\phi/\partial x)]}{\partial x} = \frac{\partial\theta_u}{\partial t} + \frac{\rho_w}{\rho_i}\frac{\partial\theta_i}{\partial t} \qquad (3)$$

and the well known sensible heat conduction–advection equation

$$\frac{\partial[K_T(\partial T/\partial x)]}{\partial x} - C_w\, v\,\frac{\partial T}{\partial x} = C_m\,\frac{\partial T}{\partial t} - L_a\frac{\rho_w}{\rho_i}\frac{\partial\theta_i}{\partial t} \qquad (4)$$

where

x = positive coordinate downward
t = time
ϕ = total head = $\psi - x$ (where ψ = pore pressure head)
θ_u = volumetric unfrozen water content
θ_i = volumetric ice content
ρ_w, ρ_i = density of water and ice respectively
K_H = $K(\psi)$ = hydraulic conductivity
T = temperature
K_T = thermal conductivity of soil–water–ice mixture
L_a = volumetric latent heat of fusion for bulk water
C_w = volumetric heat capacity of water
C_m = volumetric heat capacity of soil–water–ice mixture

The moisture sink and latent heat components of eqns. (3) and (4) are decoupled and are solved using an isothermal approximation (Hromadka et al., 1981). These components only exist in freezing or thawing zones of the soil profile.

Figure 2 illustrates the computation process at a specific time level. An overburden pressure (as head of water), ψ_o, is shown. Also the unfrozen water

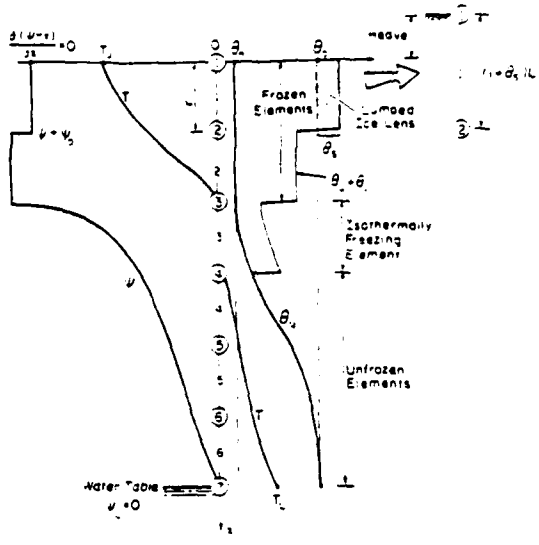

Fig. 2. Illustration of deterministic model results at a given time level (from Guymon et al., 1981).

content factor, ϑ_n, and soil porosity, θ_o, are shown. The primary variables ψ and T are computed from eqns. (3) and (4) and the secondary variables ϑ_u, ϑ_i, and θ_s (segregated ice) are computed. From this latter quantity, lumped heave is computed as shown in Fig. 2.

TABLE 1

Soil parameters required for the deterministic model

Parameter	Description
n, A_w	Characterize soil water versus pore pressure relationship for unfrozen soil
$K(\psi)$	Unfrozen hydraulic conductivity versus pore pressure relationship
E	Parameter to correct $K(\psi)$ for ice in freezing zone (as function of ϑ_i, ice content)
θ_o	Porosity
θ_n	Unfrozen water content factor
C_s	Volumetric heat capacity of soil
K_s	Thermal conductivity of soil
ρ_s	Soil density
T_f	Freezing point depression of soil water

Numerical solution is by the nodal domain integration method (Hromadka and Guyman, 1981) which requires a spatial discretization of the order of 1 cm. The time domain solution is by the Crank–Nicolson method which requires temporal discretization on the order of 0.5 h and a parameter update frequency on the order of 1.0 h. Equations are temporarily decoupled during discrete time periods and parameters are assumed constant within each discrete spatial solution domain.

The model is a multiparameter model and is highly nonlinear. Table 1 lists the soil parameters required by the model. The heat and fluid transport processes are coupled through the latent heat process and the parameters that must be employed in the derivations of eqns. (3) and (4). Fortunately, soil systems are usually highly damped, permitting reasonable approximations without employing costly iteration techniques. The model is efficient and can be solved on the miniclass computers using FORTRAN IV language.

PROBABILITY MODEL

Freeze (1975) and others have investigated the combination of stochastic and deterministic models. In particular, Freeze considered the problem of groundwater flow in a non-uniform one-dimensional homogeneous medium. On the basis of his study, Freeze had "doubts about the presumed accuracy of the deterministic conceptual models that are so widely used in groundwater hydrology." If he had doubts about a similar but simpler system, we must confess considerable pessimism about deterministic models of the more complex ice segregation processes. Only a few parameters were of concern to Freeze (1975), but we are considering the 10 parameters shown in Table 1. Values of the heat capacity, thermal conductivity, density and latent heat capacity of water and ice were obtained from standard tables.

Freeze's (1975) stochastic analysis was based upon the well known Monte Carlo technique (Harr, 1977) which requires an assumption of the statistical distribution of the stochastic variables. Freeze assumed porosity was normally distributed and saturated hydraulic conductivity was log-normally distributed, and used 500 Monte Carlo runs for each parameter. Values were randomly generated from an assumed probability distribution and were applied to a deterministic model. Typically, most investigations of this nature use a large number of runs, i.e. 500 or more. Because of the apparent need for many Monte Carlo runs, this type of stochastic analysis can be expensive, particularly if the variance is non-stationary for the type of dynamic problems being considered and if the variance should be significantly different for different soil types.

An alternative approach to the Monte Carlo method is proposed that is based upon Rosenblueth's (1973) method, but because this method is not widely known in the open literature, a heuristic derivation of the method will be presented for the case of one random variable. Suppose

$$y = f(x) \tag{5}$$

where $f(x)$ is an arbitrary, continuously differentiable frequency distribution of the random variable x. The usual procedure for determining the expectance or mean and the second moment or variance of y is to expand y around $\bar{x}$ (the mean of x) using a Taylor's series (Harr, 1977).

Alternatively, one may use Rosenblueth's method which is analogous to determining the required simple support forces for a statically stable weightless beam with an arbitrary load (Fig. 3). Now suppose $f(x)$ has been normalized so that the total load equals unity, i.e.

$$1 = \int_0^L f(x)dx \tag{6}$$

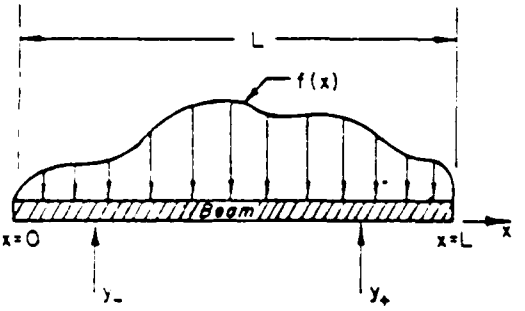

Fig. 3. Schematic illustrating Rosenblueth's method.

Also, suppose the mean value of x and its coefficient of variation are known for N discrete values of x, where these statistical properties are defined in the usual manner

$$E(x) = \bar{x} = \frac{1}{N}\sum_{i}^{N} x_i \tag{7a}$$

$$V_x = E(x^2) - [E(x)]^2 = \frac{1}{N}\sum_{i}^{N} (x_i - \bar{x})^2 \tag{7b}$$

where V_x is the variance of x. The coefficient of variation is given by

$$CV = S_x/\bar{x} \tag{8}$$

where S_x is the standard deviation and is equal to the positive square root of the variance. Adopting the notation

$$\begin{aligned} y_+ &= f(\bar{x} + S_x) \\ y_- &= f(\bar{x} - S_x), \end{aligned} \tag{9}$$

static equilibrium of the beam shown in Fig. 3 will be achieved if

$$\bar{y} = \frac{y_+ + y_-}{2} \tag{10a}$$

and

$$S_y = \frac{y_+ - y_-}{2}. \tag{10b}$$

This can be heuristically proven by noting that $f(x)$ can be expanded in Taylor's series (Harr, 1977) and the mean and variance calculated by

$$\bar{y} \approx f(\bar{x}) + \tfrac{1}{2} f''(\bar{x}) S_x^2 \tag{11a}$$

$$S_y^2 \equiv [f'(\bar{x})]^2 S_x^2 \tag{11b}$$

The validity of eqns. (10*a*) and (10*b*) can be demonstrated by assuming any arbitrary differentiable function $f(x)$, using eqn. 9 in eqns. (10*a*) and (10*b*), and showing the result equal to eqns. (11*a*) and (11*b*).

The simulated frost heave, y', is a function of many parameters, p_i including the input conditions x', i.e.

$$y' = f(p_1, p_2, \ldots, p_m, x'), \tag{12}$$

where for the moment it is assumed the p_i are uncorrelated. Similar to the heuristic proof above for one variate, Rosenblueth deduced the general relationship

$$E[(y')^N] = \frac{1}{2^m}\left[(y'_{+\cdots+m})^N + (y'_{+\cdots-m})^N + \ldots (y'_{-\cdots-m})^N\right] \tag{13}$$

where there are m parameters to be considered, and N is the exponent (moment) of y'. The notation $y'_{\pm\cdots m}$ indicates the use of all sign permutations of

$$y' = f(\bar{p}_1 \pm S_{p_1}, \bar{p}_2 \pm S_{p_2}, \ldots, \bar{p}_m \pm S_{p_m}) \tag{14}$$

where $\bar{p}_i$ is the mean of the ith parameter and S_{p_i} is the standard deviation of the parameter. The subscript sign is determined by the sign of S_p. The mean and variance of y' are computed in the usual fashion

$$\bar{y}' = E(y') \tag{15}$$

$$V_{y'} = E[(y')^2] - [E(\bar{y}')]^2. \tag{16}$$

Now suppose some or all of the p_i are correlated. Rosenblueth's method can be extended using the covariance (cov) statistic [Harr (1977)] as follows:

$$\rho_{g,h} = \rho_{h,g} = \frac{\mathrm{cov}(p_g, p_h)}{S_{p_g} S_{p_h}} \tag{17}$$

where ρ is the covariance measure and the subscripts denote there are m random variables (parameters) that are correlated a pair at a time. Define a q-function such that there will be M of these functions given by

$$q_{ij\cdots m} = 1 + \sum_{\substack{g=1 \\ h=1}}^{M} \frac{|gh|}{gh}\, \delta_{g,h}\, \rho_{g,h} \tag{18}$$

$$\delta_{g,h} = \begin{cases} 0, & g \geq h, \\ 1, & |g| < |h| \end{cases}$$

where the $ij\ldots m$ are all the permutations of the signs of the standard deviation of each parameter where each sign is attached to the subscript. The moments of y' are defined as

$$E[(y')^N] = \frac{1}{2^m}\sum_{0}^{M} (q_{ij\cdots m})(y'_{ij\cdots m})^N \tag{19}$$

and the first and second moments are computed as in eqns. (15) and (16). Equation (19) reduces to eqn. (13) in the event all ρ are zero (i.e. the p_i are all uncorrelated and $q = 1$).

Rosenblueth's method is a powerful tool that is ideally suited to the type of problem being considered. No prior assumptions are required concerning the probability distribution of the parameter variables. Only an estimate of parameter mean and coefficient of variation are necessary. This method requires only that the functional relationship between y' and x' need be specified, i.e. the deterministic model. The method is general, however, and is applicable to any deterministic model. Instead of the many costly simulations required by the commonly employed Monte Carlo method, only 2^m simulations are required using the present modification of Rosenblueth's method.

Given a measure of parameter variability the first and second moments of predicted frost heave can be readily computed, giving useful statistical information to establish a range of possible frost heave rather than a single deterministic value. While higher moments can be obtained to give some indication of skewness and peakedness, this information is not of great significance to the present objective.

The capability of extending knowledge by supposing we know nothing about the distribution of frost heave follows from Chebeshev's inequality

$$P[\bar{y} - hS_y \leq y \leq \bar{y} - hS_y] \geq 1 - \frac{1}{h^2} \qquad (20)$$

For example, if two standard deviations are used ($h=2$), the probability that y is bounded by $\pm hS_y$ is greater than or equal to 75%. Now if it is assumed y is symmetrically distributed, Gauss' inequality may be applied

$$P[\bar{y} - hS_y \leq y \leq \bar{y} + hS_y] \geq 1 - \frac{4}{9h^2} \qquad (21)$$

which says for $h=2$ there is a greater or equal probability of 89% that y is so bounded. Finally, given additional information the distribution of y can be further narrowed. A versatile distribution to assume is the beta distribution (Harr, 1977):

$$f(y) = \frac{\alpha!\beta!(b-a)^{\alpha+\beta+1}}{(\alpha+\beta+1)!}(y-a)^{\alpha}(b-y)^{\beta} \qquad (22)$$

where to find the α and β parameters one needs to know $\bar{y}$, S_y, and a and b, the lower and upper bounds of the distribution. The parameters $\bar{y}$ and S_y are generated by Rosenblueth's method. The a and b parameters may be estimated by data such as Chamberlain (1980) has developed. He found that $a = \bar{y} - 2S_y$ and $b = \bar{y} + 3S_y$ for one field study. Once a beta distribution is determined, confidence limits and other desired statistical properties of $f(y)$ can be established (Harr, 1977).

Questions yet to be resolved include the question of stationarity, or in other words, how will the statistical properties of $f(y)$ vary with time? The second question concerns the nature of $f(y)$ for various soils. Can a single beta-distribution be found that is applicable to a class of soils, such as the so-called "frost-susceptible soils"?

APPLICATION OF MODEL

The model was applied to a set of laboratory data obtained from a vertical soil column equipped with temperature and water level control and instrumentation to measure soil temperatures and pore water pressures (described by Berg et al., 1980; Ingersoll and Berg, 1981). Two different uniform soils were placed in the column to obtain comparison data: a well known frost susceptible soil, Fairbanks silt, and a weakly frost-susceptible dirty gravel, West Lebanon gravel. Guymon et al. (1981) reported on comparisons of simulated frost heave and measured laboratory frost heave for both restrained and unrestrained cases using Fairbanks silt among other soils.

The simulation procedure consists of determining hydraulic parameters using remolded samples of the same soil employed in the frost heave column. Porosity and density are determined using standard techniques. A modified Tempe cell, as described by Ingersoll and Berg (1981), was used to determine the soil characteristic drying curve and the unsaturated hydraulic conductivity relationship. An average characteristic curve of two tests on Fairbanks silt is shown in Fig. 4 together with the parameters used to describe this curve in the model where

$$\theta_e = \frac{\theta_0}{A_w \psi^n + 1} \qquad (23)$$

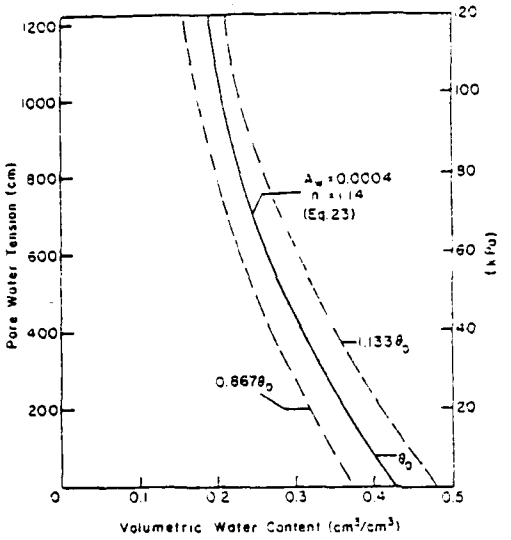

Fig. 4. Soil–water characteristic for Fairbanks silt (average of two tests).

These parameters fit the actual curve with less than a ±0.03 error. Unfrozen hydraulic conductivity versus pore water pressure, $K(\psi)$, for a sample of Fairbanks silt during a drying cycle, is shown in Fig. 5. The solid line fits data obtained from the modified Tempe cell and the broken line fits data obtained from a volumetric pressure plate extractor. The deterministic model uses unfrozen hydraulic conductivity data as a discrete table where intermediate values are determined by linear interpolation. The partly frozen soil hydraulic conductivity correction factor, E, where

$$K(\psi,\theta_i) = K(\psi)\cdot 10^{-E\theta_i} \qquad (24)$$

was determined by calibration such that a deterministic simulation of frost heave closely approximated measured frost heave in the laboratory freezing column. Other parameters in Table 1 such as the thermal parameters, were assumed. Table 2 lists the parameters used in the "best" deterministic simulation of measured frost heave for both Fairbanks silt and West Lebanon gravel. It is assumed that these parameters represent the mean parameter values for the soil in the laboratory freezing column.

Boundary and initial conditions applied to the laboratory column were approximated as closely as possible in the deterministic model simulations. Because there is inherently some uncertainty concerning boundary conditions, a precise simulation was not expected or attempted.

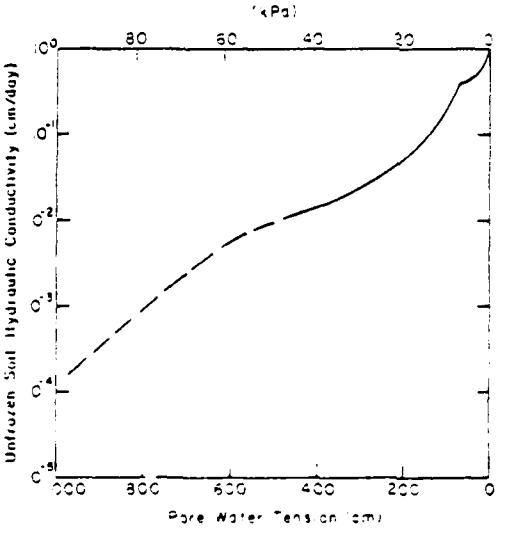

Fig. 5. Unfrozen hydraulic conductivity for Fairbanks silt (solid line derived for modified tempe cell, broken line derived from volumetric pressure plate extractor).

TABLE 2

Mean soil parameters used in model simulations

Parameter	Soil	
	Fairbanks silt	W. Lebanon gravel
A_w	0.0004 [a,f]	0.119 [a]
n	1.14 [a,f]	0.50 [a]
$K(\psi=0)$	0.04 cm h^{-1} [a,d]	0.42 cm h^{-1} [a,e]
E	8 [b]	20 [b]
θ_n	0.150 [c]	0.082 [b]
θ_o	0.425 [a]	0.27 [a]
ρ_s	1.6 [a]	1.99 [a]
T_f	0°C [c]	0°C [c]
K_s	17 cal cm^{-1}°C^{-1} h^{-1} [c]	17 cal cm^{-1}°C^{-1} h^{-1} [c]
C_s	0.3 cal cm^{-3}°C^{-1} [c]	0.3 cal cm^{-3}°C^{-1} [c]

[a] Measured in laboratory.
[b] Determined by model calibration.
[c] Assumed.
[d] See Fig. 5 for complete relationship.
[e] Complete relationship not shown herein.
[f] Average of two laboratory tests.

TABLE 3

Comparison of measured unrestrained and simulated frost heave varying soil parameters for Fairbanks silt (cm)

Day	Measured	Best simulation	$T_f = -0.005$	$0.82\,K_s$	$1.33\,C_s$	$1.3\,K(\psi)$	$1.15\,\theta_n$	$1.13\,\theta_o$	$1.1\,E$
5	1.6	1.5	1.5	1.5	1.5	1.6	1.6	1.5	1.5
10	2.8	2.6	2.6	2.6	2.7	2.8	2.8	2.7	2.6
15	3.9	3.5	3.5	3.6	3.6	3.7	3.7	3.7	3.5
20	4.4	4.4	4.4	4.4	4.4	4.6	4.6	4.6	4.3
25	5.0	5.1	5.1	5.2	5.2	5.3	5.3	5.4	5.0
30	5.6	5.7	5.8	5.9	5.8	6.0	6.0	6.1	5.7

Table 3 compares simulated and measured unrestrained cumulative frost heave for the Fairbanks silt case. To evaluate the effect of a single-parameter variation while holding all other parameters at their assumed mean value, seven additional simulations are shown in Table 3. Although a substantial variation in K_s shows some sensitivity, it was assumed that thermal parameters would have a minor effect on frost heave simulation results for Fairbanks silt under the conditions of the laboratory tests. The reason for this is that phase change processes overshadow sensible heat processes in a freezing soil. Although not shown, parameter variations for Fairbanks silt have an insignificant effect on simulated frost penetration which very closely approximated measured frost penetration. Frost heave showed marked sensitivity to hydraulic parameter variations. Consequently, these parameters were selected for a more detailed analysis using Rosenblueth's method. The most sensitive parameters are porosity, unfrozen water content factor, and unfrozen hydraulic conductivity.

Varying porosity within reasonable bounds affects the results by modifying the mass accumulation term in the moisture transport equation (3) by modifying the available pore space in the soil for ice to develop without ice segregation occurring, and by modifying the soil–water characteristics (eqn. (23)). Varying porosity can also account for hysteresis (Fig. 4) which is not considered in the deterministic model. To include this phenomenon would necessitate the incorporation of memory into the model, significantly increasing the computation effort and probably not markedly improving the computation precision or certainty. Figure 4 shows a plus and minus 13.3% variation effect on the characteristic curve. Numerous measurements we have made on silts and similar soils suggest that hysteresis effects would be adequately bounded by such an approach. We believe there is now no reason to explicity include hysteresis in any soil phenomena related model. This process can be adequately dealt with by incorporation of a probabilistic model.

The so-called "unfrozen water content factor" controls the available space for pore ice to develop before ice segregation occurs. In the deterministic model, this parameter also determines the unrestrained pore water pressure at the bottom of the frozen zone (Fig. 2), thereby determining the hydraulic gradient and the rate water is drawn into the freezing zone. The balance between the rate of heat extraction and water importation to this zone is the controlling factor in the ice segregation processes as the deterministic model is conceived. For this reason, the hydraulic conductivity of the soil system is obviously an important, if not the most significant, parameter, although it is difficult to measure accurately for unsaturated fine-grained soils and is subject to considerable uncertainty. Very little work has been done on measuring hydraulic conductivity for partly frozen soils in the range of temperatures found in field soils under winter conditions.

The "best" simulation results for measured frost heave of West Lebanon gravel are shown in Figs. 6 and 7. The laboratory results for a slightly restrained soil (i.e. 0.5 lbf/in^2 or 3.45 kPa surcharge) were used for parameter calibration (see Table 2); the results are shown in Fig. 6. A restrained (i.e. 5.0 lbf/in^2 or 34.5 kPa surcharge) laboratory case with identical boundary conditions to the slightly restrained case was

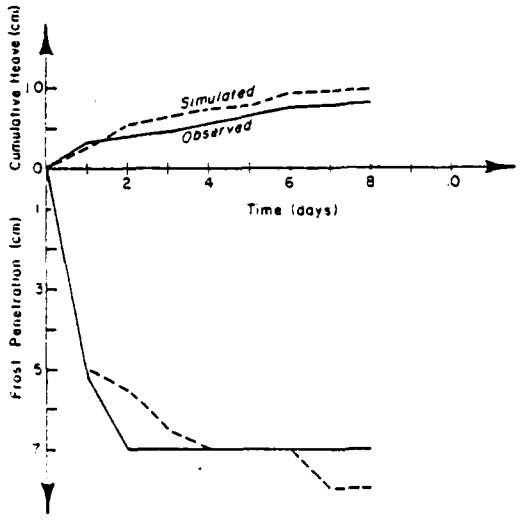

Fig. 6. Observed and simulated frost heave and frost penetration for West Lebanon gravel with a 0.5 lbf/in² (3.45 kPa) surcharge.

simulated without adjusting parameters. As can be seen from Fig. 7, the results are satisfactory.

The effect of soil density variations was not studied because this parameter has a minor effect on overburden pressures for shallow freezing cases with

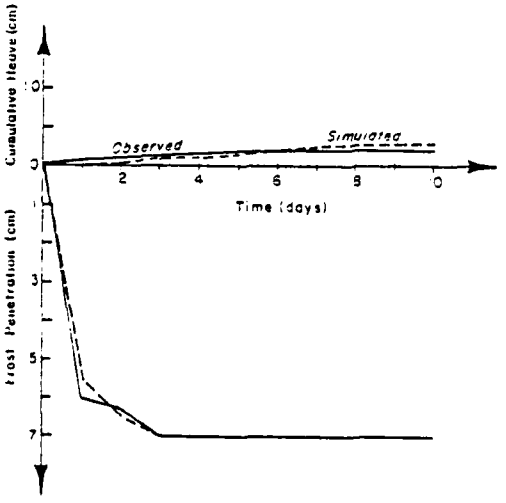

Fig. 7. Observed and simulated frost heave and frost penetration for West Lebanon gravel with a 5.0 lbf/in² (34.5 kPa) surcharge.

which we are concerned. Obviously density variations are highly important since porosity and the hydraulic parameters are closely correlated to density.

Freeze (1975) reviews some references that deal with porosity and hydraulic conductivity variations and Harr (1977) reviews some of the available literature on these and other soil parameter statistics. Warrick and Nielson (1980) review their own data as well as those of others for soil density, water content, particle size, and hydraulic conductivity variations. Schultze (1972) obtained a coefficient of variation for porosity of silt of 13.3% while Nielsen et al. (1973) obtained an average coefficient of variation of 10.0% for a clay–loam soil. They also obtained a coefficient of variation for the same soil for soil–water characteristics that ranged from 10% at low tensions to about 24% at moderate tensions (i.e. 200 cm of water). We know of no similar data for the unfrozen water content factor; however, we assume a similar range of behavior as for porosity. A coefficient of variation of 15% is probably adequate to describe most frost susceptible soils. Nielsen et al. (1973) performed extensive analysis on the variability of unsaturated hydraulic conductivity for clay–loam soil. They report a coefficient of variation that ranges from 100 to 450% for field variations. Laboratory measured variations for the same soil might be on the lower end of this range (i.e. 100%). Very little work has been done on determining partially frozen soil hydraulic conductivity, let alone determining measurement or sampling errors and field variability. It is probably safe to assume considerably more variability for frozen soil than for an unfrozen soil. For lack of more definitive data, we assume a coefficient of variation of 500% for frozen soil hydraulic conductivity. If the E-factor varies by 10%, about a 500% coefficient of variation in frozen soil hydraulic conductivity is obtained when we couple the E-factor variation to the unfrozen hydraulic conductivity variation.

Although there may be some autocorrelation between hydraulic parameters, the correlation coefficient was taken to be zero (i.e. $\rho = 0$, eqn. 17)). Limited attempts to correlate parameters showed a very weak correlation between porosity and hydraulic conductivity; however, sufficient data were not available to draw definitive conclusions.

Equations (13)–(16) were used as previously

described to generate the mean and variance of simulated heave due to parameter variation. Four parameters were used in the procedure where $m = 4$ in eqn. (13) and

$$\left.\begin{aligned} \theta_0 &= (1 \pm CV)\,\bar{\theta}_0 \\ \theta_n &= (1 \pm CV)\,\bar{\theta}_n \\ K(\psi) &= (1 \pm CV)\,\bar{K}(\psi) \\ E &= (1 \pm CV)\,\bar{E} \end{aligned}\right\} \qquad (25)$$

where the bar denotes the assumed mean value used in the "best" calibration simulation. All other parameters were held constant.

Boundary conditions measured in the laboratory were closely approximated in the simulations. Boundary condition errors were effectively eliminated by using the same boundary and initial conditions for each separate simulation. However, because there are boundary condition errors we can only comment on variations around a mean and cannot comment on simulation error (eqn. (1)), resulting from parameter variability.

Table 4 presents results for a 30-day simulation assuming parameter coefficients of variation for θ_0, θ_n, E, and $K(\psi)$ of 13.3, 15, 10, and 30%, respectively, and using parameters for unrestrained Fairbanks silt. As can be seen the mean frost heave using Rosenblueth's method closely approximates the "best" simulation shown in Table 3. The coefficient of variation of simulated frost heave derived from employing Rosenblueth's method is essentially stationary after some possible initial numerical instability. Although we have not attempted longer simulations using Rosenblueth's method, it is reasonable to expect a stationary coefficient of variation. Based upon field data obtained by Chamberlain (1980), we have assumed a beta-distribution lower bound of three standard deviations (Chamberlain actually obtained two) and an upper bound of four standard deviations. The α and β parameters of the beta-distribution are derived after Harr (1977) and are listed for each simulation day tabulated.

As can be seen, α approximately equals a constant 3.2, and β about equals a constant 4.8 in the last two-thirds of the simulation. The probability confidence limits are also shown in Table 4 for two standard deviations. The results are slightly skewed since we deliberately choose a slightly skewed distribution (Harr, 1977). Other confidence bounds can be easily obtained by integrating eqn. (22) between any desired limits.

Additional simulations were performed for unrestrained Fairbanks silt and slightly restrained and restrained West Lebanon gravel. A summary of the normalized results is shown in Table 5. The results shown in Table 4 are normalized and repeated in Table 5 on the first line. Similar to the results shown in Table 4, the coefficient of variation of simulated frost heave becomes essentially stationary after the first five days. As can be seen from Table 5, there is considerable variation in the coefficient of variation depending on the soil simulated, the magnitude of parameter variations, and the surcharge condition. Nevertheless, the α and β parameters of the beta-

TABLE 4

Simulated frost heave for unrestrained Fairbanks silt using Rosenblueth's method and varying $\theta_0 \pm 13.3\%$, $\theta_n \pm 15\%$, $E \pm 10\%$, and $K(\psi) \pm 30\%$

Day	Mean cumulative frost heave (cm)	Standard deviation	Coefficient of variation (%)	$a=\bar{y}-3S_y$	$b=\bar{y}+4S_y$	α	β	$P[y \leq \bar{y}+2S_y]$	$P[y \geq \bar{y}-2S_y]$
5	1.5	0.16	11	1.0	2.1	3.55	4.47	0.96	0.97
10	2.6	0.24	9	1.9	3.6	3.85	5.93	0.97	0.99
15	3.5	0.31	9	2.6	4.7	3.24	4.65	0.96	0.98
20	4.3	0.38	9	3.2	5.8	3.24	4.78	0.97	0.99
25	5.1	0.44	9	3.8	6.9	3.24	4.87	0.96	0.98
30	5.8	0.51	9	4.3	7.8	3.29	4.72	0.96	0.98

TABLE 5

Simulated frost heave statistics using Rosenblueth's method and an assumed beta-distribution for unrestrained Fairbanks silt and unrestrained and restrained West Lebanon gravel

Soil	Parameter coefficient of variation				Normalized simulated frost heave			a/y	b/y	α	β	$P[\bar{y}-2S_y \leq y \leq \bar{y}+2S_y]$
	θ_0	θ_n	E	$K(\psi)$	CV (%)	Min	Max					
Fairbanks silt	13.3	15	10	30	9	0.86	1.12	0.74	1.34	3.3	4.8	96
Fairbanks silt	20	20	20	50	17	0.76	1.24	0.48	1.66	3.6	5.5	97
Fairbanks silt	13.3	15	10	100	95	0.05	2.10	−1.84 [a]	4.79	3.7	5.3	97
W. Lebanon gravel – 0.5 psi surcharge	13.3	15	10	30	20	0.67	1.33	0.39	1.81	3.7	5.3	97
W. Lebanon gravel – 5.0 psi surcharge	13.3	15	10	30	107	0	2.91	−2.21 [a]	5.28	3.4	5.2	97
W. Lebanon gravel – 0.5 psi surcharge	13.3	15	10	100	103	0	2.45	−2.09 [a]	5.12	3.4	4.9	97

[a] A minus value used to derive beta distribution parameters.

distribution are quite similar, suggesting a universal frequency distribution is applicable to the model we are employing. An α of about 3.5 and a β of about 5.0 will generally reproduce the same coefficient of variation tabulated, using the correct a and b limits, with only a minor difference in results. The last column of Table 5 lists the smallest percent probability that the computed heave will lie within two standard deviations of the mean. Recall from Table 4 that confidence limits are slightly skewed. To derive a meaningful beta-distribution it was necessary to assume a lower limit a that was negative in several cases. Obviously, the lowest possible value of frost heave must be zero.

TABLE 6

Comparison of simulated heave for non-uniform and uniform soil profiles with average parameters derived from non-uniform profile

Day	Cumulative frost heave (cm)	
	Uniform profile	Non-uniform profile
5	2.0	2.1
10	3.1	3.2
15	3.9	3.9
20	4.4	4.4
25	4.8	4.8
30	5.0	5.0

Although the results are not presented here, parameter variations were found to have little direct effect upon simulated frost penetration. The reason for this is that latent heat effects dominate the thermal process and we assume that the thermal coefficient of phase change is a constant and equal to the value for bulk water. The computation of frost penetration is influenced by the amount of frost heave estimated. Thus, an error in computed frost heave will influence the estimate of frost penetration.

A non-uniform soil profile situation was examined to demonstrate the feasibility of modeling a layered soil profile as an averaged uniform profile. Because we have not conducted laboratory studies of non-uniform, layered, soil profiles, we assumed a situation similar to the case represented in Table 4. Slightly different boundary conditions were used since the computer code for the layered case uses a somewhat different boundary condition simulator. First it was

assumed that the soil profile from surface down was a 5 cm layer of sandy soil, a 5 cm layer of silty soil, a 5 cm layer of clayey silt soil, and finally a 30 cm layer of silty soil. Representative hydraulic parameters were applied and frost heave simulated for 30 days of real time. The resulting heave was compared to a similar simulation using exactly the same boundary conditions but assuming a uniform soil profile with hydraulic parameters about equal to the average of those used in the layer simulation. The results of both simulations are shown in Table 6. In view of the often used approximations to represent a prototype soil profile (i.e. simplify a layered soil by assuming a homogeneous uniform soil profile), the results of Table 6 can be viewed with some optimism. The simulated frost depth at the end of the simulation was more than 17 cm below the original ground surface so that freezing had completely penetrated through the first three layers of the soil profile. Both results are almost identical and the non-uniform variation is certainly well within the confidence limits shown for the uniform soil parameter variability studies.

DISCUSSION

A powerful general tool is offered to evaluate the effects of parameter variability upon deterministic computations of any process in which parameters have a known variation. The method was applied to the frost heave simulation or analysis problem.

It was shown that thermal parameter variations had a less important effect upon simulated frost heave than hydraulic parameters. The reason for this is that thermal processes are dominated by the phase change process.

Table 5 indicates that the most important parameter variation is hydraulic conductivity. For gravels, the coefficient of variation of frost heave will about equal the coefficient of variation of unfrozen hydraulic conductivity. For silts, the coefficient of variation for simulated frost heave will be less than half of that for gravels at smaller variations of unsaturated hydraulic conductivity and is about the same as for gravels at larger variations of unsaturated hydraulic conductivity. The results obtained for West Lebanon gravel with a 5.0 lbf/in^2 (34.5 kPa) surcharge should be viewed as a special case since West Lebanon gravel is marginally frost-susceptible and a 5.0 lbf/in^2 surcharge is about the critical pressure to restrain frost heave completely. In this situation frost heave is much more sensitive to parameter variations than when the system is only moderately restrained.

It appears that a conservative universal approach to defining the coefficient of variation of simulated deterministic heave would be to use an assumed coefficient of variation for hydraulic conductivity, use an assumed number of standard deviations of variation to compute the lower beta-distribution bound, use the definition of mean and variance of the beta-distribution as defined by Harr (1977), and compute the coefficient of variation of frost heave assuming $\alpha = 3.5$ and $\beta = 5.0$. One could safely be assured that computed heave would lie within two standard deviations with a 95% probability. Such a computation would not apply to a critically restrained soil.

Comparing the simulation results to Chamberlain's (1980) data and the Albany County Airport data we have collected shows some striking similarities. If one assumes −3 and +4 standard deviations for the beta distribution minimum and maximum, as was assumed for simulated heave, similar α and β parameters for the beta-distribution are obtained. For Chamberlain's data, $\alpha = 3.6$ and $\beta = 5.2$ were obtained and for the Albany County Airport data, $\alpha = 3.8$ and $\beta = 5.4$ were obtained. This similarity to the simulated frost heave results suggests a strong justification for our results and our contention that deterministic solutions alone are not adequate. A probabilistic model coupled with a deterministic model is required. Furthermore, the results strongly suggest that the deterministic approach advocated is valid.

ACKNOWLEDGMENTS

This work was partly supported by an U.S. Army Research Office grant to the University of California, Irvine (Grant No. DAAG24-79-C-0080). The Federal Highway Administration, Federal Aviation Administration and U.S. Army, Corps of Engineers jointly funded research work at USACRREL. The first author was on leave at USACRREL during the 1980–81 academic year when this paper was prepared.

REFERENCES

Berg, R.L., Ingersoll J. and Guymon G.L., 1980, Frost heave in an instrumented soil column. Cold Regions Sci. Technol., 3(2+3): 211–221.

Chamberlain, E.J., 1980. Determining differential frost heave by the probabilistic method, USACRREL Manuscript.

Freeze, R.A., 1975, A stochastic-conceptual analysis of one-dimensional groundwater flow in nonuniform homogeneous media, Water Resources Res ., 11(5): 725–741.

Guymon, G.L., Hromadka II, T.V. and Berg R.L., 1980, A one-dimensional frost heave model based upon simulation of simultaneous heat and water flux, Cold Regions Sci. Technol., 3(2+3): 253–262.

Guymon, G.L., Berg R.L., Johnson T.C. and Hromadka II, T.V., 1981, Results from a mathematical model of frost heave, Transportation Res. Board (accepted for publication).

Harr, M.E., 1977, Mechanics of Particulate Media, a Probabilistic Approach, McGraw-Hill, New York.

Hopke, S.W., 1980, A model for frost heave including overburden, Cold Regions Sci. Technol., 3(2+3): 111–147.

Hromadka II, T.V., Guymon G.L. and Berg R.L., 1980, Some approaches to modeling phase change in freezing soils, Cold Regions Sci. Technol., 4: 137–145.

Hromadka II, T.V. and Guymon G.L., 1980, Nodal domain integration model of one-dimensional advection-diffusion, Adv. Water Resources (in press).

Ingersoll, J. and Berg R.L., 1981, Simulating frost action using an instrumented soil column, Transportation Res. Board (accepted for publication).

Nielsen, D.R., Biggar J.W. and Erb K.T., 1973, Spatial variability of field-measured soil–water properties, Hilgardia, 42(7).

Rosenblueth, E., 1973, Point estimates for probability moments, Proc. Nat. Acad. Sci., USA, 72(10): 3812–3814.

Schultze, E., 1972, Frequency distributions and correlations of soil properties, Statistics and Probability in Civil engineering, Hong Kong Univ. Press (Dist. by Oxford Univ. Press, London).

Warrick, A.W. and Nielsen D.R., 1980, Spatial variability of soil physical properties in the field, in Applications of Soil Physics by D. Hillel, Academic Press, New York.

COLD REGIONS SCI & TECH (IN PRESS)

SENSITIVITY OF FROST HEAVE MODEL TO THE METHOD OF NUMERICAL SIMULATION

T. V. Hromadka II[1], G. L. Guymon[2], R. L. Berg[3]

SUMMARY

A unifying numerical method is developed for solution of frost heave in a vertical freezing column of soil. Within one general computer code a single unifying parameter can be preselected to employ the commonly used Galerkin finite element, subdomain weighted residual, or finite difference methods as well as several other methods developed from the Alternation Theorem. Comparing results from the various numerical techniques in the computation of frost heave to measured frost heave in a laboratory column indicates there is little advantage of one numerical technique over another. One numerical technique, the subdomain methid, was used to investigate discretization errors. The model is relatively insensitive to spatial discretization but is significantly sensitive to temporal discretization. The primary reason for this is that an updating procedure, rather than a more accurate iterative procedure, is used to evaluate nonlinear parameters that arise in the moisture transport and heat transport equations.

1 Assistant Research Engineer/Lecturer, University of California, Irvine

2 Associate Professor, University of California, Irvine

3 Research Civil Engineer, U. S. Army Cold Regions Research and Engineering Laboratory, Hanover, NH 03755

INTRODUCTION

Guymon et al (1980) and Hopke (1980) review much of the recent efforts to develop comprehensive mathematical models of frost heave. These models can generally be classed as conceptual (or deterministic) models which are developed from physics based knowledge or assumptions. Generally, most modeling efforts include a simultaneous computation of heat and moisture transport in a freezing soil. Models, however, differ significantly in the manner latent heat effects are estimated and in the manner ice segretation is assumed to occur. The more advanced efforts to model frost heave have demonstrated that numerical modeling is a feasible tool for analysis of frost heave.

This paper will examine the choice of a numerical analog of the conceptual physics based equations used in a particular model; i.e., the model investigated by Guymon et al (1980) will be used as a test case. In order to systematically carry out this purpose, a unifying numerical analog is developed so that appropriate comparisons between numerical methods can be made using identical computer code. Because most models presented in the literature assume the same flow equations, the results presented here are generally applicable. The unifying numerical method that will be used is the nodal domain integration method which represents the subdomain integration method and the common Galerkin finite element and finite difference methods by the specification of a single constant parameter in the resulting spatial discretization matrix system. The nodal domain integration method has been developed for linearized one-dimensional transport equations (Hromadka and Guymon, 1981) and has been extended to two-dimensions using linear trial functions (Hromadka et al, 1981). These references include evaluation of numerical errors when comparing to exact solutions. Hromadka and Guymon (1980) examine some effects of linearizing nonlinear equations. In this paper, the nodal domain integration method is applied to a non-linear coupled heat and moisture transport problem. The application of nodal domain integration to such problems is a new contribution.

Furthermore, the application of numerical solution techniques to the frost heave problem is a rather new endeavor and one aspect of the problem, the choice of numerical technique, deserves examination.

Previously, Guymon et al (1981) discussed model errors and examined in detail errors associated with parameters of a deterministic model of frost heave. Four arbitrary groups of errors were identified:

1. Model errors including numerical analog errors.
2. Spatial and temporal discretization errors.
3. Boundary and initial condition errors.
4. Parameter errors.

Numerical analog errors may be investigated in simple cases by linearizing a problem and comparing a numerical solution to an analytic or so-called "exact" solution. In the case of our multiparameter model, it is highly nonlinear and heat and moisture transport are coupled through the parameters arising from the conceptual assumptions employed. Furthermore, several ancillary equations are used to estimate parameters and processes involved. The only realistic way of evaluating errors is to compare model output with prototype output. This approach is highly effective in this case where lumped frost heave represents or integrates all the complicated processes occurring in a freezing soil. A set of data obtained in the laboratory for Fairbanks silt is used for comparison with numerical solutions.

A particular deterministic model of one-dimensional frost heave in a vertical saturated or partly-saturated soil column is used herein (Guymon et al, 1980). Details of this model will not be repeated here. The modeling concept is shown in Table 1. Symbols used in this table are defined under "Notation." Moisture flow in a partly-saturated column toward a freezing frost is assumed to obey continuity and Darcy's law. Sensible heat flow in both the frozen and unfrozen zones is estimated. Complicated processes in the freezing zone are lumped into an assumed isothermal freezing process. This process controls the

rate and magnitude of frost heave in the model and integrates all other model processes.

NUMERICAL MODELING APPROACH

In this section, the nodal domain integration numerical method is briefly reviewed for the reader's convenience. By using the subdomain version of the weighted residuals method defined on subsets of a finite element discretization (nodal domains) an element matrix system is derived similar to the element matrix system developed for a Galerkin finite element analog. The nodal domain integration element matrix system is found to be a function of a single parameter where the Galerkin finite element, subdomain integration, and finite difference methods are represented as special cases. Consequently, the development of a numerical model based on the nodal domain integration method also results in a numerical model based on the more popular Galerkin finite element, subdomain integration, and finite difference methods.

$$A(C) = f;\ x\varepsilon\Omega,\ \Omega \equiv \Omega' \cup \Gamma \tag{1}$$

with boundary condition types of Dirichlet or Neumann specified on boundary Γ. A n-nodal point distribution can be defined on Ω with arbitrary density(Fig. 1) such that an approximation $\hat{C}$ for C is defined in Ω by

$$\hat{C} = \sum_{j=1}^{n} N_j(x) C_j;\ x\varepsilon\Omega \tag{2}$$

where $N_j(x)$ are the usual linearly independent global shape functions (Zienkiewicz, 1977) and C_j are values of the state variable, C, at nodal points j.

In Eq. 2 it is assumed that

$$\lim_{n\to\infty} \hat{C} = \lim_{\max ||x_j, x_k|| \to 0} \hat{C} = C, \quad x\in\Omega \tag{3}$$

A cover of Ω is defined by

$$\Omega = \bigcup_{j=1}^{n} R_j \tag{4}$$

where a closed connected subset R_j is defined for each nodal point j such that

$$x_j \in R_j; \; x_j \notin R_k, \; j\neq k \tag{5}$$

and

$$R_j = R_j \cup B_j \tag{6}$$

where x_j is the spatial coordinate of node j, and B_j is the boundary of subdomain R_j. It is also assumed that

$$R_j \cap R_k = B_j \cap B_k \tag{7}$$

The subdomain version of the finite element method of weighted residuals approximates Eq. 1 on Ω by solving the n equations

$$\int_{\Omega} (A(C) - f)\, w_j \, dx = 0 \tag{8}$$

where

$$w_j = \begin{cases} 1, & x \in R_j \\ 0, & x \notin R_j \end{cases} \tag{9}$$

A second cover of Ω is given by the usual finite element discretization

$$\Omega = \bigcup \Omega^e \tag{10}$$

where Ω^e is the closure of finite element and its boundary Γ^e.

A set of nodal domains Ω_j^e is defined for each finite element Ω^e by

$$\Omega_j^e = \Omega^e \cap R_j, \quad j \in S_e \tag{11}$$

where S_e is the set of nodal point numbers defined by

$$S_e = \left\{ j \;\middle|\; \Omega^e \cap \Omega_j^e \neq \{\phi\} \right\} \tag{12}$$

That is, S_e is the nodal point numbers associated with Ω_e. The subdomain integration numerical model of Eq. 8 can be rewritten in the terms of the subdomain cover of Ω by

$$\int_{\Omega} (A\,(C) - f)\, w_j dx = \int_{R_j} (A\,(C) - f)\, dx \tag{13}$$

With respect to the finite element discretization of Ω

$$\int_{R_j} (A\,(C) - f)\, dx = \int_{R_j \cap U\Omega^e} (A\,(C) - f)\, dx \tag{14}$$

where for each finite element domain Ω^e

$$\int_{\Omega^e \cap R_j} (A\,(C) - f)\, dx = \int_{\Omega_j^e} (A\,(C) - f)\, dx. \tag{15}$$

From Eq. 15, the subdomain method of weighted residuals determines an element matrix system for each finite element Ω^e by the integration of the governing equation on each member of the nodal domain cover Ω_j^e. The spatial definition of each nodal domain Ω_j^e depends on the definition of both the finite element and subdomain discretization of Ω, and is therefore somewhat arbitrary. A convenient criterion is to define the nodal domains such that the resulting finite element matrix system is symmetric. This symmetric property is used for the definition of the subdomain cover R_j of Ω in the following model development of an one-dimensional advection

diffusion type process. Extension of the one-dimensional nodal domain integration procedure to two-dimensional problems are contained in (Hromadka et al, 1981).

The government heat and soil water flow equations can be written in the operator relationship

$$A\,(C) - f = \frac{\partial}{\partial x}\left[k_1 \frac{\partial C}{\partial x}\right] - \frac{\partial}{\partial x}\left[k_2\, C\right] - k_3 \frac{\partial C}{\partial t}\;;\; x \in \Omega \qquad (16)$$

where all parameters are assumed to be continuous in Ω, and where for the heat flow process k_1 = thermal conductivity; $k_2 = C_w v$ $k_3 = C_m$; and C = temperature, T. For the soil water flow equation $k_1 = K_H$; $k_2 = 0$; $k_3 = \frac{\partial \theta}{\partial \psi}$ and C = ψ. The ice content terms of both flow processes are not needed in Eq. 16 due to the isothermal phase change approximation used by Guymon et al (1980). Therefore, Eq. 16 is solved for heat and soil water flow processes during a small timestep Δt; then, the computed values of unfrozen water content, ice content and temperature are recalculated to accommodate isothermal phase change of available soil water. Substituting the operator relationship of Eq. 16 into the integration statement of Eq. 15 gives an element matrix system for finite element Ω^e

$$\int_{\Omega_j^e} \left(\frac{\partial}{\partial x}\left[k_1 \frac{\partial C}{\partial x}\right] - \frac{\partial}{\partial x}\left[k_2\, C\right] - k_3 \frac{\partial C}{\partial t}\right) dx = 0; \quad j \in S_e \qquad (17)$$

Expanding Eq. 17 gives the element matrix components for the conduct[illegible], vection, and mass terms of the operator relationship

$$\left(k_1 \frac{\partial C}{\partial x}\right)_j^e - \left(k_2\, C\right)_j^e + \left(k_1 \frac{\partial C}{\partial x} - k_2\, C\right)_j^e = \int_{\Omega_j^e} k_3 \frac{\partial C}{\partial t}\, dx$$

AD-A118 264 CALIFORNIA UNIV IRVINE F/G 8/13
TWO-DIMENSIONAL NUMERICAL MODEL OF COUPLED HEAT AND MOISTURE TR--ETC(U)
AUG 82 G L GUYMON, T V HROMADKA DAAG29-79-C-0080
UNCLASSIFIED ARO-16278.25-65 NL

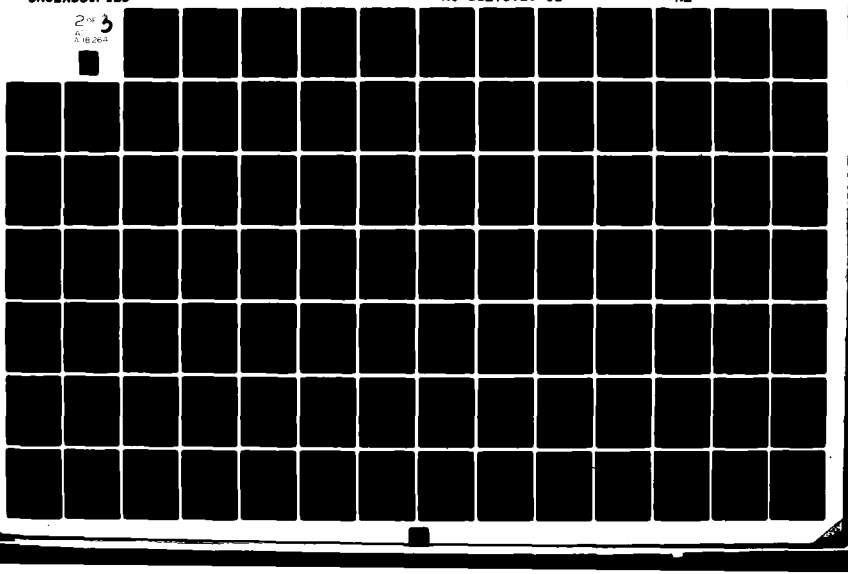

The first matrix term of Eq. 18 cancels due to flux contributions from neighboring finite elements or satisfies zero flux (Dirichlet) boundary conditions on Γ. In order to develop the element matrices for Ω^e from Eq. 18, a definition of a subdomain and finite element discretization of domain Ω is required.

A cover of spatial domain Ω is given by the set of n closed connected subdomains R_j defined by

$$\begin{aligned} R_1 &\equiv \{x|\ 0 = x_1 \leq x \leq (x_1+x_2)/2\} \\ R_2 &\equiv \{x|\ (x_1+x_2)/2 < x \leq (x_2+x_3)/2\} \\ R_n &\equiv \{x|\ (x_{n-1}+x_n)/2 < x \leq x_n = L\} \end{aligned} \tag{19}$$

where x_j is the spatial coordinate associated to nodal point value C_j. In Eq. 19, C_j represents nodal point values of temperature and total hydraulic head for the heat and soil water flow equations, respectively. In the following, the definition of the subdomain discretization of Ω given in Eq. 19 will be shown to result in symmetrical element conduction and element mass matrices.

The finite element discretization of domain Ω is assumed to be composed of one-dimensional elements defined by

$$\begin{aligned} \Omega^1 &\equiv \{x|x_1 \leq x \leq x_2\} \\ \Omega^2 &\equiv \{x|x_2 \leq x \leq x_3\} \\ \Omega^{n-1} &\equiv \{x|x_{n-1} \leq x \leq x_n\} \end{aligned} \tag{20}$$

The nodal domain cover of global domain Ω is defined by the intersection of the finite element and subdomain covers of Ω (Fig. 2)

$$\begin{aligned} \Omega_1^1 &\equiv \{x|x_1 \leq x \leq x_1/2\} \\ \Omega_2^1 &\equiv \{x|x_1/2 \leq x \leq x_2\} \\ \Omega_n^{n-1} &\equiv \{x|(x_{n-1}+x_n)/2 \leq x \leq x_n\} \end{aligned} \tag{21}$$

For the assumed finite element discretization of Ω, the element matrix system for the finite element Ω^e is given from Eq. 18 as

$$\left\{k_1 \frac{\partial C}{\partial x}\right\}\Big|_{\Gamma_j^e - \Gamma_j^e \cap \Gamma^e} - \left\{k_2\, C\right\}\Big|_{\Gamma_j^e \cap \Gamma^e} - \left\{k_2\, C\right\}\Big|_{\Gamma_j^e - \Gamma_j^e \cap \Gamma^e} = \left\{\int_{\Omega_j^e} k_3 \frac{\partial C}{\partial t}\, dx\right\},\ j \in S_e \qquad (22)$$

where for an interior finite element ($e \neq 1, n-1$), $S_e = \{e, e+1\}$. Thus, Eq. 22 can be rewritten for an interior Ω^e and an assumed linear trial function, $\bar{C}$, on Ω^e

$$\begin{bmatrix} (k_1 \frac{\partial \bar{C}}{\partial x})\Big|_{(x_e + x_{e+1})/2} \\ -(k_1 \frac{\partial \bar{C}}{\partial x})\Big|_{(x_e + x_{e+1})/2} \end{bmatrix} - \begin{bmatrix} (k_2\, \bar{C})\Big|_{(x_e + x_{e+1})/2} \\ -(k_2\, \bar{C})\Big|_{(x_e + x_{e+1})/2} \end{bmatrix} = \begin{bmatrix} \int_{\Omega_e^e} k_3 \frac{\partial \bar{C}}{\partial t}\, dx \\ \int_{\Omega_{e+1}^e} k_3 \frac{\partial \bar{C}}{\partial t}\, dx \end{bmatrix} \qquad (23)$$

where the second term of Eq. 22 cancels due to neighboring finite elements. Hromadka and Guymon (1981) show that for a first order polynomial trial function $\bar{C}$ for the state variable C in each finite element, and for the assumed definitions of the subdomain and finite element discretization of problem domain Ω, the Galerkin finite element, subdomain integration, and finite difference numerical analogs can be represented by a single element matrix system similar to Eq. 23 for finite element Ω^e

$$-\frac{k_1}{\ell_e}\begin{bmatrix} 1 & -1 \\ -1 & 1 \end{bmatrix}\begin{Bmatrix} C_e \\ C_{e+1} \end{Bmatrix} + \frac{k_2}{2}\begin{bmatrix} 1 & -1 \\ 1 & -1 \end{bmatrix}\begin{Bmatrix} C_e \\ C_{e+1} \end{Bmatrix} = \frac{\ell_e k_3}{2(\eta+1)}\begin{bmatrix} \eta & 1 \\ 1 & \eta \end{bmatrix}\begin{Bmatrix} \frac{\partial C_e}{\partial t} \\ \frac{\partial C_{e+1}}{\partial t} \end{Bmatrix} \qquad (24)$$

where $\eta = (2, 3, \infty)$ gives the Galerkin finite element, subdomain integration, and finite difference models, respectively. In Eq. 24, the nonlinear parameters (k_1, k_2, k_3) are assumed constant for a small duration of time Δt; ℓ_e is the length of finite element Ω^e; and C_e is the nodal point value. Generally, convection is assumed to be negligible in Eq. 24 and the k_2 parameter is set to zero. For this study, however, convection is maintained but approximated as a constant for a small duration of time Δt.

From Eq. 24, a single model can be developed which can represent the Galerkin finite element, subdomain integration, and finite difference methods for approximating the governing heat and soil water flow equations. The method of linearizing the governing flow equations is to assume all nonlinear parameters to be constant during a small timestep Δt. From the above, the element matrix system used to approximate the governing flow equations in finite element Ω^e becomes

$$-\frac{k_1}{\ell_e}\begin{bmatrix}1 & -1\\ -1 & 1\end{bmatrix}\begin{Bmatrix}C_e\\ C_{e+1}\end{Bmatrix} = \frac{\ell_e k_3}{2(\eta+1)}\begin{bmatrix}\eta & 1\\ 1 & \eta\end{bmatrix}\begin{Bmatrix}\frac{\partial C_e}{\partial t}\\ \frac{\partial C_{e+1}}{\partial t}\end{Bmatrix} - \frac{k_2}{2}\begin{bmatrix}1 & -1\\ 1 & -1\end{bmatrix}\begin{Bmatrix}\bar{C}_e\\ \bar{C}_{e+1}\end{Bmatrix} \qquad (25)$$

where $\{\bar{C}_e, \bar{C}_{e+1}\}$ are temporally-averaged nodal values during timestep Δt. The Crank-Nicolson time advancement approximation can be used to integrate Eq. 25 with respect to time giving

$$(\underset{\sim}{H}(\eta) + \frac{\Delta t}{2}\underset{\sim}{G})\,\underset{\sim}{C}^{(k+1)\Delta t} = (\underset{\sim}{H}(\eta) - \frac{\Delta t}{2}\underset{\sim}{G})\,\underset{\sim}{C}^{k\Delta t} - \underset{\sim}{\beta}\Delta t \qquad (26)$$

where $\underset{\sim}{C}$ is the vector of nodal point values at time $(k+1)\Delta t$ and $k\Delta t$; $\underset{\sim}{\beta}$ is an assumed constant value for convection in Ω^e during timestep Δt; and the element matrices are given by

$$\underset{\sim}{G} = \frac{k_1}{\ell_e}\begin{bmatrix}1 & -1\\ -1 & 1\end{bmatrix} \qquad (27)$$

$$\underset{\sim}{H}(\eta) = \frac{k_3\ell_e}{2(\eta+1)}\begin{bmatrix}\eta & 1\\ 1 & \eta\end{bmatrix} \qquad (28)$$

Hromadka and Guymon (1981) also examined two methods of approximating a higher order or more complex family of trial functions by a linear polynomial trial function. One method used the Alternation Theorem (Cheney, 1966) to determine an optimum linear polynomial estimate of a higher order approximator.

Using an adjusted linear trial function $\bar{C}$ approximation of a higher order trial function $\hat{C}$ approximation of the state variable C in each finite element Ω^e (Fig. 3), it was shown that the gradient terms due to conduction were given by Eq. 27, but the integrated mass matrix term was given by Eq. 28 with values of η depending on the function definition of $\hat{C}$. For example, given a sinusoidal trial function $\hat{C}$ in each Ω^e, an optimum linear approximation $\bar{C}$ of $\hat{C}$ in Ω^e results in a value of $\eta = 5.9$. For a parabola trial function $\hat{C}$ in Ω^e, Eq. 28 is determined to be given by $\eta = 7$ when $\hat{C}$ is approximated by a linear trial function in each Ω^e. Additionally, by assuming $\hat{C}$ to be given by second order polynomials in each subdomain R_j, integration of the governing flow equations result in $\eta = 11$. The various submethods of the nodal domain integration concept (using the Alternation Theorem) derived to date are listed in Table 2.

A second method of approximating a higher order or more complex family of trial functions $\hat{C}$ for the state variable C is by use of correction functions for both the integration and differentiation of C in each subdomain R_j. This approach was found to give the best numerical accuracy for the problems tested, and resulted in a numerical statement similar to Eq. 26 but with η a function of time, and variable between finite elements. This approach is reviewed in the following:

Let $\bar{C}$ be a linear approximation function of a higher order approximation $\hat{C}$ of C in an interior subdomain R_j where the spatial gradients of $\bar{C}$ on B_j are defined by

$$\left\{ \frac{\partial \bar{C}}{\partial x} \right\}_{B_j} \equiv \frac{(C_{j+1} - C_j)}{\ell_j} - \frac{(C_j - C_{j-1})}{\ell_{j-1}}, \quad \ell_j \equiv \| \quad \| \tag{29}$$

A spatial gradient adjustment function h(x,t) is defined by

$$h(x,t) \equiv \begin{cases} \dfrac{\partial \hat{C}}{\partial x} \Big/ \dfrac{\partial \bar{C}}{\partial x} ; & 0<h<\infty \\ 1 ; & \text{otherwise} \end{cases} \tag{30}$$

It is assumed that

$$k_1 \frac{\partial \hat{C}}{\partial x} = k_1 \, h \frac{\partial \bar{C}}{\partial x} \tag{31}$$

where

$$\left\{ k_1 \frac{\partial \hat{C}}{\partial x} \right\} \Bigg|_{B_j} = \left\{ k_1 \, h \frac{\partial \bar{C}}{\partial x} \right\} \Bigg|_{B_j} \tag{32}$$

On B_j, define

$$k_1 \, h = A(t); \; k\Delta t \leq t \leq (k+1)\Delta t \tag{33}$$

such that

$$A(k\Delta t+\varepsilon) = \sum_{i=0}^{\infty} A^{(i)}(k\Delta t) \frac{\varepsilon^i}{i!} ; \; 0 \leq \varepsilon \leq \Delta t \tag{34}$$

where (i) represents the i-th order temporal partial differential operator. Then

$$\left\{ k_1 \frac{\partial \hat{C}}{\partial x} \right\} \Bigg|_{B_j} = \left\{ \sum_{i=0}^{\infty} A^{(i)}(k\Delta t) \frac{\varepsilon^i}{i!} \frac{\partial \bar{C}}{\partial x} \right\} \Bigg|_{B_j} \tag{35}$$

A function $\eta(t)$ is defined by

$$\int_{R_j} \hat{C}dx = \frac{\bar{\ell}}{2[\eta(t)+1]} [C_{j-1} + 2C_j\ \eta(t) + C_{j+1}] \tag{36}$$

where $\bar{\ell} = ||R_j||$, and

$$\eta(t) \neq -1 \tag{37}$$

The value of $\eta=3$ in Eq. 36 corresponds to a first order polynomial $\hat{C}$ function subdomain approximation for C, whereas $\eta(t) = 2$ corresponds to a Galerkin finite element model, and $\eta(t) = \infty$ determines a finite difference model.

The $\bar{C}$ approximator is also defined to have the property

$$\int_{R_j} \bar{C}\ dx \equiv \int_{R_j} \hat{C}\ dx,\ \eta(t) \neq -1 \tag{38}$$

Substituting Eqs. 35 and 36 into Eq. 22 gives the modeling statement (for convection $\underset{\sim}{\beta}$ quasi-constant during timestep Δt)

$$\int_{\Delta t} \left\{ \sum_{i=0}^{\infty} A^{(i)}(k\Delta t) \frac{\varepsilon^i}{i!} \frac{\partial \bar{C}}{\partial x} \right\}\Big|_{B_j} d\varepsilon =$$

$$k_3(k\Delta t+\Delta t)\ \frac{\bar{\ell}[C^*_{j-1} + 2C^*_j\ \eta(k\Delta t+\Delta t) + C^*_{j+1}]}{2[\eta(k\Delta t+\Delta t) + 1]} \tag{39}$$

$$- k_3(k\Delta t)\ \frac{\bar{\ell}[C'_{j-1} + 2C'_j\ \eta(k\Delta t) + C'_{j+1}]}{2[\eta(k\Delta t) + 1]} + \underset{\sim}{\beta}\Delta t$$

where $C_j^* = C_j(k\Delta t+\Delta t)$; $C_j' = C_j(k\Delta t)$; and where k_j is assumed uniform in R_j, and

$$\eta(k\Delta t+\varepsilon) = \sum_{i=0}^{\infty} \eta^{(i)}(k\Delta t)\,\frac{\varepsilon^i}{i!}\;;\quad 0\le\varepsilon\le\Delta t \tag{40}$$

Integrating the conduction term in Eq. 39 on Ω^e gives

$$\left.\begin{aligned} \bar{\bar{A}}(\lambda) &= \frac{1}{\ell_e}\sum_{i=0} \frac{A^{(i)}(\lambda)(\Delta t)^{i+1}}{i!(i+2)} \\ \bar{A}(\lambda) &= \frac{1}{\ell_e}\sum_{i=0}^{\infty} \frac{A^{(i)}(\lambda)(\Delta t)^{i+1}}{(i+2)!} \end{aligned}\right\} \quad \lambda \in B_j\ ,\ \lambda \in \hat{\Omega}_e \tag{41}$$

The nodal domain integration element matrix system similar to Eq. 26 is given by

$$(\underset{\sim}{\bar{\bar{H}}} + \underset{\sim}{\bar{\bar{G}}})\ \{\underset{\sim}{C}\}^{(k+1)\Delta t} = (\underset{\sim}{\bar{H}} - \underset{\sim}{\bar{G}})\ \{\underset{\sim}{C}\}^{k\Delta t} - \underset{\sim}{\beta}\Delta t \tag{42}$$

where

$$\left.\begin{aligned} \underset{\sim}{\bar{\bar{G}}} &= \bar{\bar{A}}(\lambda)\begin{bmatrix} 1 & -1 \\ -1 & 1 \end{bmatrix} \\ \underset{\sim}{\bar{G}} &= \bar{A}(\lambda)\begin{bmatrix} 1 & -1 \\ -1 & 1 \end{bmatrix} \\ \underset{\sim}{\bar{\bar{H}}}(\eta) &= \frac{\ell_e}{2(\bar{\bar{\eta}}+1)}\begin{bmatrix} \bar{\bar{\eta}} & 1 \\ 1 & \bar{\bar{\eta}} \end{bmatrix} \\ \underset{\sim}{\bar{H}}(\eta) &= \frac{\ell_e}{2(\bar{\eta}+1)}\begin{bmatrix} \bar{\eta} & 1 \\ 1 & \bar{\eta} \end{bmatrix} \end{aligned}\right\} \tag{43}$$

and where $\bar{\bar{\eta}} = \eta(k\Delta t+\Delta t)$, $\bar{\eta} = \eta(k\Delta t)$, $\ell_e = ||\Omega^e||$, and λ is the midpoint of Ω^e.

RESULTS

The numerical models of Eqs. 26 and 42 were used to solve the governing heat and soil water flow equations as used in the Guymon et al (1980) frost heave model. Since the only variation of the numerical model required to determine a Galerkin finite element, subdomain integration, finite difference, or nodal domain integration analog is the adjustment of the η term in Eq. 26, a single computer code may be used. As a result variability normally inherent between computer programs is entirely eliminated, giving a precise comparison of numerical methods. A Fairbanks silt vertical soil freezing column test as described in Berg et al (1980) is used as the test case for determining the sensitivity of the frost heave model to the method of numerical simulation. The laboratory test used is for a soil column freezing case in which frost penetrated at an approximately uniform rate until a depth of 15 cm was reached at about 25 days after initiation of the test. Frost heave proceeded at a more or less uniform rate during this test. During the test all components of the system were in a dynamic state.

Using identical problem initial and boundary conditions, a twenty-five day duration computer simulation was made varying timestep and element discretization magnitudes as well as varying constant values of η given in Table 2. Values of timesteps used in the temporal numerical integration (Crank-Nicolson time advancement approximation) are Δt = (0.1, 0.2, 0.4, 1.0, 2.0 hours). Constant finite element sizes used are $\Delta x \equiv ||\Omega^e|| = (\frac{1}{2}, 1, 1.5, 3.0$ cm). For each combination of (Δx,Δt) values, constant value of η=(2,3,5.9,7,11,10000) were tested representing a linear trial function Galerkin finite element, subdomain integration, nodal domain integration linear approximation of a sinusoidal and parabola trial function, subdomain integration model of parabola trial function, and finite difference numerical analogs, respectively.

Figure 4 shows the results of varying timestep and spatial discretization using the sudomain method (n=3). Simulated heave is compared to measured heave for a laboratory column and error in percent is computed by taking the difference and dividing by measured heave after 25 days. Similar results to Fig. 4 are obtained for shorter durations of time. As can be seen, there is slight sensitivity to spatial discretization, and marked sensitivity to timestep size for advancing the solution in time. A timestep of about 0.5 hr. gives the best result. It is important to note that the method proposed by Guymon et al (1980) uses a simple update procedure to adjust nonlinear parameters rather than a possibly more accurate iteration procedure normally employed with nonlinear equations.

Table 3 compares computed frost heave for a timestep size and update frequency of 2 hours and a spatial uniform discretization of 3 cm. Results shown in Table 3 are typical of results obtained using choice of different timesteps and mesh sizes. As can be seen there is initially some sensitivity in the numerical method; however after 10 days, differences between numerical methods are slight. Errors associated with the choice of numerical model for the one-dimensional problem considered here are much less than errors introduced by parameter uncertainty (Guymon et al 1981) and by boundary condition uncertainty.

CONCLUSIONS

A frost heave model is examined in an effort to determine the sensitivity of predicted frost heave values to the choice of numerical method used to solve the governing heat and soil water flow equations. A computer code based on the nodal domain integration method accommodates several other numerical analogs by the specification of a single constant parameter n in the resulting element matrix contributions; consequently, sensitivity of the frost heave model to the method of numerical simulation can be determined by the variation of the single parameter n.

From the simulation results, the Guymon, et al frost heave model shows negligible sensitivity to the numerical approach used to solve the governing flow equations. Although sensitivity is observed initially for a large time-step choice, all frost heave evolution curves are found to merge at the end of the twenty-five day simulation. Since freezing soil problems are generally subjected to freezing temperatures for durations in excess of twenty-five days, it is concluded that negligible sensitivity occurs due to the numerical approach chosen to model the heat and soil-water flow equations in the considered frost heave model. One numerical method is as good as another. Variations between the variously proposed models (e.g. as reviewed by Hopke, 1980) will primarily depend upon efficiency of code and user orientated features; there seems to be little point in debating the virtues of a particular numerical method. We conclude that modeling errors that can be associated with model choice (Eq. 1) will primarily be related for the choice of governing equations and ancillary assumptions used in a model. Whether we can definitely isolate errors associated with the choice of such equations and assumptions will depend on our ability to isolate the other errors we have identified.

The type of model investigated by Guymon, et al (1980) shows minor sensitivity to spatial discretiation while there is significant sensitivity to temporal discretization. This is largely due to the nonlinear nature of the problem we are dealing with and the updating method of adjusting nonlinear problems. True iterative techniques would probably show less sensitivity to temporal discretization but would require considerably more solution time.

Our results suggest that solutions are reasonably bounded. Consequently, the fact that our model does not account for all processes occurring at the freezing front is not a significant concern from an engineering applicability criterion. Provided boundedness can be defined, the model can be employed with a certain level of confidence in the statistical sense.

ACKNOWLEDGEMENTS

This research was supported by the U.S. Army Research Office (Grant No. DAAG29-79-C-0080) and by the U.S. Army, Cold Regions Research and Engineering Laboratory, Hanover, New Hampshire, where the second author was on sabbatical leave during 1980-81.

REFERENCES

Berg, R. L., J. Ingersoll, and G. L. Guymon, "Frost Heave in an Instrumented Soil Column," Cold Regions Science and Technology, 3(2&3), 211-221, 1980.

Cheney, E. W., Introduction to Approximation Theory, McGraw-Hill, 1966.

Guymon, G. L., T. V. Hromadka II, and R. L. Berg, "A One Dimensional Frost Heave Model Based Upon Simulation of Simultaneous Heat and Water Flux," Cold Regions Science and Technology, Elsevier, 3(2&3), 253-262, 1980.

Guymon, G. L., M. E. Harr, R. L. Berg, and T. V. Hromadka II, "A Probabilistic-Deterministic Analysis of One-Dimensional Ice Segregation in a Freezing Soil Column," Cold Regions Science and Technology, (in-press), (1981).

Hopke, S. S., "A Model for Frost Heave including Overburden," Cold Regions Science and Technology, Elsevier, 3(2&3), 111-127, 1980.

Hromadka II, T. V., and G. L. Guymon, "Some Effects of Linearizing the Unsaturated Soil-Moisture Transfer Diffusion Model," Water Resources Research, (16), 633-640, 1980.

Hromadka II, T. V., and G. L. Guymon, "Improved Linear Shape Function Model of Soil Moisture Transport," Water Resources Research, 17(3), 504-521, 1981.

Hromadka II, T. V., and G. L. Guymon, "Nodal Domain Integration Model of One Dimensional Advection-Diffusion," Advances in Water Resources (in-press), (1981).

Hromadka II, T. V., G. L. Guymon, and G. C. Pardoen, "Nodal Domain Integration Model of Unsaturated Two-Dimensional Soil Water Flow: Development," (in-press), (1981).

Zienkiewicz, O. C., "The Finite Element Method," McGraw-Hill, 1977.

NOTATION

The following symbols are used in this paper:

$A(\ )$ = partial differential operator

C_m = volumetric heat capacity of soil-water-ice mixture

C_w = volumetric heat capacity of water

K_H = Darcy hydraulic conductivity

K_T = Thermal conductivity of soil-water-ice mixture

n = number of nodal points

$N_j(x)$ = shape function

$\underset{\sim}{H}$ = finite element capacitance matrix

$\underset{\sim}{G}$ = finite element stiffness matrix

t = time

Δt = timestep of numerical temporal integration

T = temperature of soil-water-ice mixture

C = state variable, ϕ or T

v = Darcy flux

x = spatial coordinate

ϕ = total hydraulic head, $\phi = \psi - x$ (x measured downwards)

ψ = pore water pressure head

Ω = global domain of definition

Ω^e = finite element domain

R_j = subdomain

Ω_j^e = nodal domain

Γ = boundary of global domain

Γ^e = finite element boundary

Γ_j^e = nodal domain boundary

B_j = subdomain boundary

$\underset{\sim}{\xi}$ = quasi-constant value of convection term during timestep Δt

x = coordinate downward

t = time

T = temperature

T_f = freezing point depression of water

T_u = soil surface temperature boundary condition

T_L = column bottom temperature boundary condition

Ψ = pore water pressure in hydraulic head units

Ψ_L = column bottom pore pressure boundary condition

Ψ_o = surcharge plus overburden pressure expressed as hydraulic head

ϑ_o = porosity

ϑ_n = volumetric unfrozen water content factor

θ_u = volumetric unfrozen water content

θ_i = volumetric ice content

ρ_i = density of ice

ρ_w = density of liquid water

L = latent heat of fusion

K_H = hydraulic conductivity

K_T = thermal conductivity of soil-water-ice mixture

K_i = thermal conductivity of ice

K_w = thermal conductivity of water

K_s = thermal conductivity of soil

C_m = volumetric heat capacity of soil-water-ice mixture

C_i = volumetric heat capacity of ice

C_w = volumetric heat capacity of water

C_s = volumetric heat capacity of soil

ℓ = length of finite volume of soil

k = timestep increment number, $k \geq 0$.

k_1, k_2, k_3 = nonlinear operator parameters

$\bar{L}$ = length of subdomain

ℓ_e = length of finite element

C = state variable

$\hat{C}$ = higher order trial function

$\bar{C}$ = linear polynomial trial function

C_j = nodal point values of state variable C at node j.

$C_j^* = C_j(k\Delta t+\Delta t)$

$C_j' = C_j(k\Delta t)$

Table 2. Nodal Domain Integration
η-factor Representations

η factor	Numerical Method
2	Galerkin finite element (linear trial function)
3	Subdomain (linear trial function)
5.9	Linear trial function approximation of sine function
7	Linear trial function approximation of parabolic function
11	Subdomain (Second order polynomial trial function)
∞ (e.g., 10,000)	Finite difference

Table 3. Comparison of Results for
Various Numerical Methods
(Timestep = 2 hr, Δx = 3cm)

	Cumulative Frost Heave for Indicated Day				
η	5	10	15	20	25
2	.61	2.22	2.85	3,52	4.46
3	.66	2.26	2.88	3.52	4.46
7	.72	2.29	2.90	3.49	4.44
11	.74	2.29	2.90	3.48	4.43
∞	.77	2.29	2.90	3.46	4.41

LIST OF FIGURES

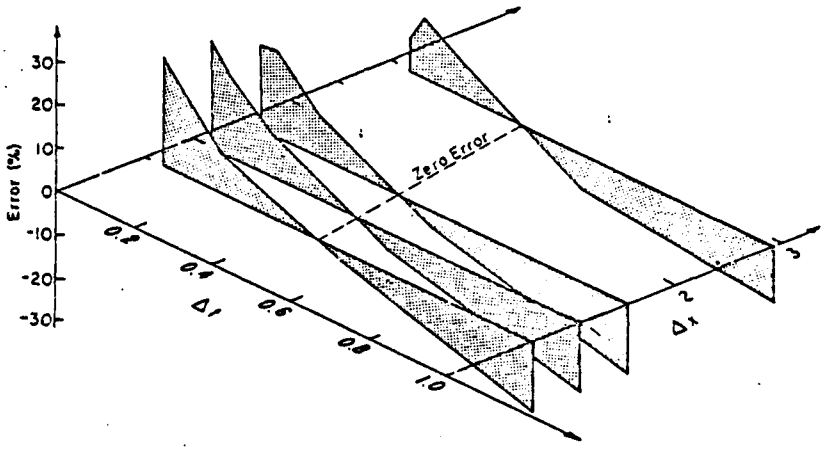

Fig. 4. Frost heave simulation error as a function of spatial and temporal discretization.

Numerical Heat Transfer, vol. 5, pp. 223-232, 1982

TECHNICAL NOTE

A NOTE ON APPROXIMATION OF ONE-DIMENSIONAL HEAT TRANSFER WITH AND WITHOUT PHASE CHANGE

T. V. Hromadka II and G. L. Guymon
Department of Civil Engineering, University of California, Irvine, California 92717

A numerical model is developed for the one-dimensional heat transfer equation with and without phase change. The numerical model is based on the nodal dimain integration method, which can represent the well-known integrated finite-difference method, the subdomain integration and Galerkin weighted residual methods, and an infinity of other finite-element lumped-mass models by the single numerical analog. A variable-order polynomial trial function is used to approximate the temperature within each finite element. Accurate solutions were obtained for the test problems considered, and the computer model requirements are small, allowing the numerical model to be accommodated with a hand-held programmable calculator.

INTRODUCTION

The technique of solving partial differential equations (PDEs) by numerical approximation is becoming increasingly attractive with the greater availability of digital computers such as current mini- and microcomputers. For some specialized problems, numerical approximation is feasible for even hand-held programmable calculators.

In this paper a numerical model of the well-known one-dimensional parabolic PDE that mathematically describes heat transfer is developed. The governing PDE is assumed to be expressed by

$$\frac{\partial}{\partial x}\left(K\frac{\partial \phi}{\partial x}\right) - C\frac{\partial \phi}{\partial t} = 0 \qquad x \in \Omega \tag{1}$$

where ϕ is the dependent variable, temperature; x and t are space and time; and K and C are the thermal conduction and capacitance terms, respectively, both assumed constant in global domain Ω. A sophisticated version of Eq. (1) including isothermal phase change of soil moisture in a freezing soil is also considered in this paper.

A review of the literature showing the current trends in numerical approximation of moisture phase change problems, such as the well-known Stefan problem, is contained in Lynch and O'Neill [1] and will not be repeated here. Usually, either the Galerkin finite-element method or an integrated finite-difference method is used to numerically solve the governing PDE. In other papers, soil moisture and heat transport models based on the control volume or subdomain integration method have been found to produce

Calculator programming was provided by Mr. Bill Burchard, Williamson & Schmid, Irvine, California.

This research was supported by the U.S. Army Research Office (grant DAAG29-79-C-0080).

0149-5720/82/020223-09$2.75

more accurate results than the Galerkin finite-element method (Hromadka and Guymon [2], Narasimhan and Witherspoon [3], Narasimhan et al. [4], Baliga and Patankar [5]). Hromadka and Guymon [2] examine the various numerical approaches and conclude that for problems where analytical solutions exist, the approximation error is not minimized by any of these approaches. In fact, they show that to minimize the approximation error, the method of numerical solution must change as the simulation progresses in modeled time.

Using the nodal domain integration method, Hromadka and Guymon [2] develop a finite-element matrix system that can represent the Galerkin, subdomain integration, and integrated finite-difference methods by the specification of a single mass weighting factor. For a linear trial function estimate within each finite element, the resulting element matrix systems for each of the above numerical approaches are identical except for a variation in mass weighting of the element capacitance matrix. Consequently, a unifying numerical analog is easily developed and is expressed by

$$\mathbf{A}^e(\eta) = \mathbf{S}^e\phi^e + \mathbf{P}^e(\eta)\dot{\phi}^e \tag{2}$$

where $\mathbf{A}^e$ is the finite-element matrix system for the approximation of Eq. (1) in local element Ω^e; ϕ^e and $\dot{\phi}^e$ are the element nodal state variable values and time derivative of nodal state variable values; and $\mathbf{S}^e$ and $\mathbf{P}^e(\eta)$ are element matrices defined by

$$\mathbf{S}^e \equiv \frac{K}{l^e}\begin{bmatrix} 1 & -1 \\ -1 & 1 \end{bmatrix} \tag{3}$$

$$\mathbf{P}^e(\eta) = \frac{Cl^e}{2(\eta+1)}\begin{bmatrix} \eta & 1 \\ 1 & \eta \end{bmatrix} \tag{4}$$

where l^e is the length of element Ω^e and η is a mass weighting factor. From Eq. (2), the Galerkin, subdomain integration, and integrated finite-difference methods are given by $\eta = (2, 3, \infty)$, respectively.

Thus it is seen that from Eq. (2) an infinite of mass weighting models exist. However, no single mass weighting model (including Galerkin, finite difference, and subdomain integration) provides the best numerical approximation. The optimum definition of η that minimizes the approximation error is a function of time, such that

$$A^e(\eta) = A^e[\eta(t)] \tag{5}$$

In this paper a modification of the unifying nodal domain integration model of Eq. (2) is used to numerically approximate the two-phase Stefan problem as defined for a freezing soil. The definition of the model mass weighting factor is given by the integration of a variable-order polynomial trial function within each finite element. Because the proposed trial function family can approximate both smooth and steep function surfaces, the number of necessary finite elements is reduced, and this significantly reduces computer memory requirements.

GOVERNING EQUATIONS

A two-phase Stefan moving-boundary problem in a freezing soil is defined by

$$C_1 \frac{\partial T}{\partial t} = \frac{\partial}{\partial x} K_1 \frac{\partial T}{\partial x} \text{ in } R_1 \qquad C_2 \frac{\partial T}{\partial t} = \frac{\partial}{\partial x} K_2 \frac{\partial T}{\partial x} \text{ in } R_2 \tag{6}$$

where C_1 and K_1 are the volumetric heat capacity and thermal conductivity of frozen soil and C_2 and K_2 are the appropriate unfrozen thermal parameters. The problem domain of definition is divided into the regions R_1 and R_2 by a moving boundary S, defined by

$$L \frac{dS}{dt} = K_1 \frac{\partial T}{\partial x}\bigg|_{S^-} - K_2 \frac{\partial T}{\partial x}\bigg|_{S^+} \tag{7}$$

where L is the volumetric latent heat of fusion of the soil water available for freezing.

The one-dimensional freezing soil problem is further defined by the boundary conditions of a freezing and subfreezing temperature imposed on respective ends of the problem domain, with the initial condition of the soil-water mixture being specified at a thawed temperature.

Without phase change, the governing heat equations can be reduced to the well-known normalized problem with conditions

$$\begin{gathered} \xi(t=0) = 1 \qquad 0 \leqslant x \leqslant 1 \\ \xi(x=0, t>0) = \xi(x=1, t>0) = 0 \end{gathered} \tag{8}$$

where ξ is a normalized variable substitution for the dependent variable temperature, and the problem domain of definition is redefined as $\{x : 0 \leqslant x \leqslant 1\}$.

Both heat transfer problems described above will be modeled by the numerical methods presented in the following sections. For the normalized heat transfer problem with conditions of Eq. (8), symmetry is used to redefine the problem with a zero-flux (Neumann) boundary condition at the midpoint of the domain, and then one finite element is used to approximate the temperature profiles as the solution progresses in time. For the two-phase Stefan problem, specified boundary temperatures (Dirichlet) at the endpoints of the problem and at the freezing front are used as follows:

$$\left.\begin{array}{lll} T = T_F & x = 0 & \\ T = T_U & x = \infty & T_F < 0^\circ\text{C} < T_U \\ T = T_U & t = 0 & \end{array}\right\} \tag{9}$$

where the freezing point temperature is 0°C. For the phase change problem, two finite elements are used with nodal points defined at the freezing front and at $x = \{0, x_0\}$, where x_0 is arbitrarily large to approximate the second condition stated in Eq. (9).

The trial functions $\hat{\phi}^e$ to be used in each local finite element Ω^e are the two families defined on ϕ^e by

$$\hat{\phi}^e \equiv \begin{cases} N_1 \phi_1^e + N_2 \phi_2^e & \dfrac{\partial \hat{\phi}^e}{\partial t} \leqslant 0 \\ M_1 \phi_1^e + M_2 \phi_2^e & \dfrac{\partial \hat{\phi}^e}{\partial t} \geqslant 0 \end{cases} \tag{10}$$

where the $\{N_i, M_i\}$ trial function family depends on whether there is accumulation of heat within the finite element Ω^e and the subscripts denote a concave-down or concave-up function. The definitions of $\{N_i, M_i\}$ used are

$$[N_1, N_2] \equiv [(1 - \hat{y}^n), \hat{y}^n] \tag{11}$$

$$[M_1, M_2] = [(1 - \hat{y})^n, 1 - (1 - \hat{y})^n] \tag{12}$$

where $\hat{y}$ is a finite-element local coordinate for a two-endpoint-node element with nodes at $\hat{y} = (0, 1)$. The order n of the shape functions is determined by the numerical model as part of the problem solution. Consequently, knowledge of the nodal values and the order of the trial function polynomial gives a significantly better estimate of the solution interior to each finite element than is obtained by the linear trial functions often used.

NUMERICAL METHOD

The local element matrix systems for finite element Ω^e are given by

$$\mathbf{S}^e\boldsymbol{\phi}^e \equiv \begin{Bmatrix} \left(K \dfrac{\partial \phi}{\partial x}\right)\Big|_{Z_e} \\ * \\ * \\ \left(K \dfrac{\partial \phi}{\partial x}\right)\Big|_{Z_e} \end{Bmatrix} \quad \mathbf{P}^e \equiv \begin{bmatrix} \displaystyle\int_0^{Z_e} N_1 \, d\hat{y} & \displaystyle\int_0^{Z_e} N_2 \, d\hat{y} \\ \displaystyle\int_{Z_e}^{0} N_1 \, d\hat{y} & \displaystyle\int_{Z_e}^{0} N_2 \, d\hat{y} \end{bmatrix} \tag{13}$$

where * indicates the evaluation of flux at finite-element boundaries and Z_e is chosen such that $\mathbf{P}^e$ is symmetric. That is,

$$\int_0^{Z_e} N_2 \, d\hat{y} \equiv \int_{Z_e}^{1} N_1 \, d\hat{y}$$

defines Z_e for each local finite element Ω^e.

From Eq. (13),

$$Z_e = \frac{n}{n+1} : N_i \text{ family} \qquad Z_e = \frac{1}{n+1} : M_i \text{ family} \tag{14}$$

where n is the order of the N_i shape function family. For the N_i trial functions the variable lumped-mass capacitance matrix is given by

$$\mathbf{P}^e = \frac{Cl^e}{n+1}\begin{bmatrix}(n-\alpha) & \alpha \\ \alpha & (1-\alpha)\end{bmatrix} \qquad \alpha = Z_e^{n+1} \tag{15}$$

The conduction matrix is also a function of time and is given by

$$\mathbf{S}^e = \frac{Kn(n/n+1)^{n-1}}{l^e}\begin{bmatrix}1 & -1 \\ -1 & 1\end{bmatrix} \tag{16}$$

where for nonlinear problems K is the thermal conductivity evaluated at $\hat{\gamma} = Z_e$.

Examination of the local element matrix systems indicates that a time-dependent lumped-mass scheme has been developed in which the element conduction and capacitance matrices change as the solution progresses in time. The element matrix variability, however, needs to be defined so that the matrices can be developed. Initially, the order of the trial function is specified based on knowledge of the initial conditions of the problem.

For modeling purposes, an explicit finite-difference approximation is used to approximate

$$\left(\frac{\partial}{\partial x} K \frac{\partial \phi}{\partial x} - C\frac{\partial \phi}{\partial t}\right)\Bigg|_{Z_e} = 0 \tag{17}$$

where for the normalized heat transfer problem, Eq. (17) is approximated with

$$\left(\frac{\phi^{i+1} - \phi^i}{\Delta t}\right)\Bigg|_{Z_e} = \left(\frac{\partial^2 \hat{\phi}^e}{\partial x^2}\right)\Bigg|_{Z_e} \tag{18}$$

where the superscripts are time step notation. In Eq. (18), $\hat{\phi}^e$ is the trial function in local element Ω^e, and the second derivative is evaluated based on the most recent assumed order of the trial function. From Eq. (18),

$$\phi^{i+1}(Z_e) = \phi^i(Z_e) + \Delta t \left(\frac{\partial^2 \hat{\phi}^e}{\partial x^2}\right)\Bigg|_{Z_e} \tag{19}$$

where Δt is the time step size, which is also determined as part of the problem solution.

To evaluate the time step, the model assumes the usual explicit method stability criteria, i.e.,

$$\frac{\Delta t}{(\Delta x)^2} \leqslant \frac{1}{2} \qquad \Delta x = \min\left[l^e(1 - Z_e), l^e Z_e\right] \tag{20}$$

From Eqs. (19) and (20), $\phi^{i+1}(Z_e)$ is approximated. From Eq. (2), the nodal values φ^e are approximated. Updated values of the trial function order n are determined by passing a trial function through the new ϕ^e values and $\phi^{i+1}(Z_e)$ for each successive time step advancement.

MODEL APPLICATIONS

Problems of heat transfer with and without soil water phase change in a freezing soil were numerically modeled by the proposed methods. To begin the model solution, an initial condition is defined to closely approximate the actual initial conditions of the problem. For example, a polynomial trial function of arbitrarily high order ($n = 100$) was used for the initial trial function approximation of temperature in the finite element for the heat transfer problem without phase change. The well-known Crank-Nicolson time advancement method is used to solve for the time derivative of temperature. The model determines the time advancement time step size Δt, subsequent trial function polynomial orders n, and mass-lumped matrix symmetry local coordinates Z_e as part of the model solution according to the equations given above.

Because of the simple computer coding and minimal requirements for model variable storage, both test problems were numerically approximated with a programmable hand-held calculator. A Texas Instruments 58A calculator was used in this study, but other programmable calculators are equally suitable for problems of this level of complexity.

Figure 1 shows computed normalized temperature profiles at various unit time levels along with the analytical solution profiles for the normalized heat transfer problem without phase change. Approximation profiles were plotted by using the single (midpoint) nodal temperature values from the finite-element model and incorporating the approximated polynomial trial function. Figure 2 shows the modeled parameter variations of n, Z_e, and Δt plotted against the model time step number. From Fig. 2, the initially high-order polynomial trial function model utilizes a small time step size. As the solution progresses in time, the polynomial order approaches the limiting value $n = 1.66$; the model time step Δt and other model parameters also approach limiting values, as shown in Fig. 2.

For the two-phase Stefan problem, Fig. 3 shows modeled and analytical values of

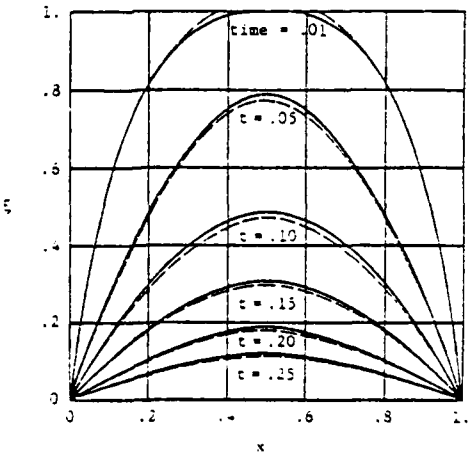

Fig. 1 Analytical solution (dashed line) and approximation results (solid line) for normalized heat transfer problem with a one-finite-element model.

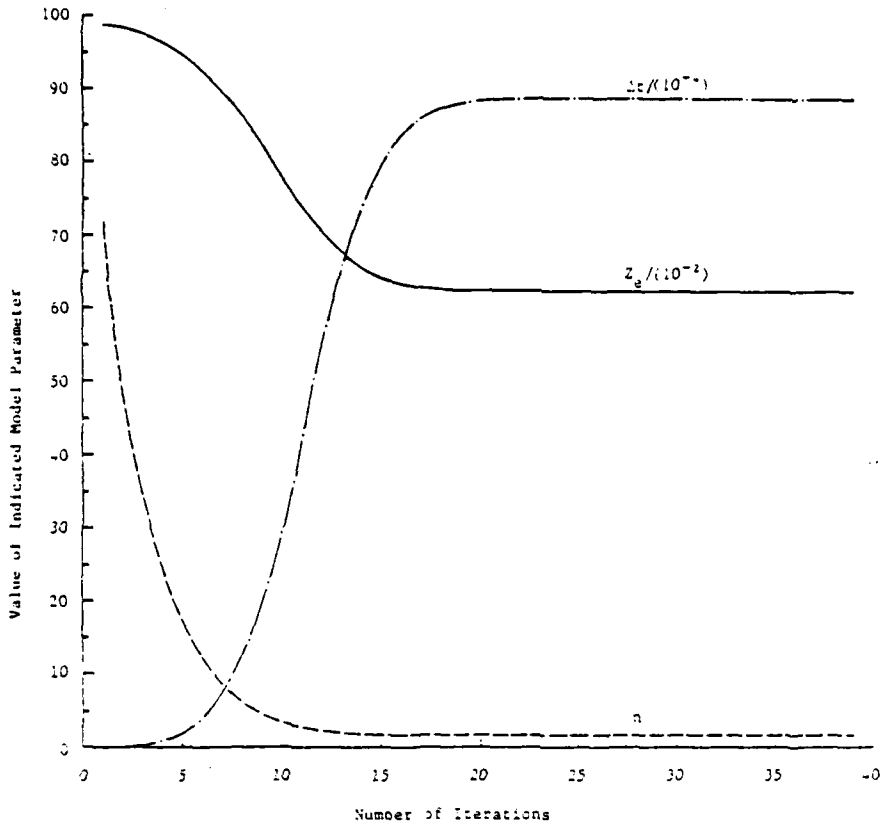

Fig. 2 Plot of model variables Δt, Z_e, and trial function order n in approximation of normalized heat transfer problem.

the freezing front penetration into a soil column. Values of 0.62 cal/cm^3 for C, 9.6 $\times$ 10^{-3} cal/cm·s·°C^{-1} for K, and 17.68 cal (per cubic centimeter of soil) for L were used, which are appropriate for a water-saturated, dense sand. The same problem was considered by Lynch and O'Neill [1]. Figure 3 shows that good agreement is obtained in the prediction of freezing front penetration when the two-element numerical model is used. Only the initial portion of the numerical model results is shown in Fig. 3 because of the continued close agreement between approximated and analytical results. The results from the proposed model closely match the numerical modeling results from Lynch and O'Neill, who used a computationally more elaborate method based on a Galerkin finite-element convection-diffusion type of model with a deforming one-dimensional grid approximation, which also required 10 Hermitian cubic elements in the finite-element model.

CONCLUSIONS

A new efficient numerical method has been employed with the classical two-phase Stefan problem. The proposed method is based on the nodal domain integration (variable

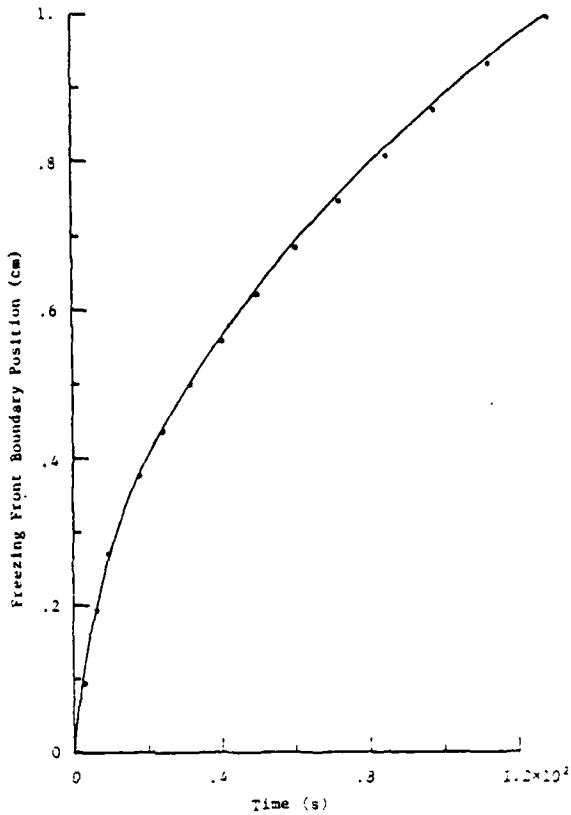

Fig. 3 Analytic solution (solid line) and approximation results (points) in model of two-phase Stefan problem.

lumped-mass finite-element) method, and incorporates a sophisticated variable-order polynomial trial function within each finite element. Some advantages of this family of "smart" trial functions are as follows:

1. Reduces the need for fine discretization of the one-dimensional domain near the freezing front.
2. Reduces the need to use a moving-boundary variable finite-element mesh.
3. Reduces the number of finite elements needed to produce similar levels of approximation accuracy.
4. Provides supplemental trial function information, which can be used to accurately analyze the function surface within large finite elements.
5. Models a sharp function surface or interface with a minimum of finite elements.

Although the test problems presented in this paper are simple, an extension to more general one-dimensional problems should result in more efficient codes, especially for problems that involve interface or sharp function surfaces in the solution. Extension of the method to multidimensional problems is not obvious and requires further research.

REFERENCES

1. D. R. Lynch and K. O'Neill, Continuously Deforming Finite Elements for the Solution of Parabolic Problems, with and without Phase Change, *Int. J. Numer. Methods Eng.*, vol. 17, pp. 81–96, 1981.
2. T. V. Hromadka II and G. L. Guymon, Nodal Domain Integration Model of One-dimensional Advection-Diffusion, *Adv. Water Resour.*, vol. 5, pp. 9–16, 1982.
3. T. N. Narasimhan and P. A. Witherspoon, An Integrated Finite Difference Method for Analyzing Fluid Flow in Porous Media, *Water Resour. Res.*, vol. 12, pp. 57–64, 1976.
4. T. N. Narasimhan, S. P. Neuman, and P. A. Witherspoon, Finite Element Method for Subsurface Hydrology using a Mixed Explicit-implicit scheme, *Water Resour. Res.*, vol. 14, p. 5, 1978.
5. B. R. Baliga and S. V. Patankar, A New Finite-Element Formulation for Convection-Diffusion Problems, *Numer. Heat Transfer*, vol. 3, pp. 393–409, 1980.

Received October 1, 1981
Accepted February 5, 1982

Requests for reprints should be sent to G. L. Guymon.

MASS LUMPING MODELS OF THE LINEAR DIFFUSION EQUATION

T. V. Hromadka II[1] and G. L. Guymon[2]

ABSTRACT

The nodal domain integration method is used to develop a numerical model of the linear diffusion equation. The nodal domain integration approach is shown to represent an infinity of finite element mass matrix lumping schemes including the Galerkin and subdomain integration versions of the weighted residual method and an integrated finite difference method. Neumann, Dirichlet and mixed boundary conditions are accommodated analogous to the Galerkin finite element method. In order to reduce overall integrated approximation relative error, a mass matrix lumping formulation is developed which is based on the Crank-Nicolson time advancement approximation. The optimum mass lumping factors are found to be strongly related to the model timestep size.

---

1 Assistant Research Engineer/Lecturer, Civil Engineering, University of California, Irvine.

2 Associate Professor, Civil Engineering, University of California, Irvine.

INTRODUCTION

Engineers and scientists are increasing their reliance on numerical methods to approximately solve differential equations of boundary and/or initial value problems such as occur in the study of transport processes. Usually, the numerical approaches of finite difference or finite elements are employed. These techniques discretize an assumed continuum-domain of definition into finite elements or control volumes, and the governing partial differential equation (PDE) is approximated in the continuum by trial functions which fully or partially satisfy the PDE boundary conditions. Choosing suitable points called "nodes" within the several finite elements or control volumes, the variable in the PDE is written as a linear combination of specified interpolation functions and the values of the variable or its various derivatives at the nodal points. Using variational or weighted residual methods, the governing flow process PDE is approximated by a system of linear equations as functions of nodal point values.

There are numerous numerical approaches available; however, usually either the Galerkin finite element or finite difference methods are used to solve PDE's such as diffusion problems (Bear, 1979). Alternative numerical approaches have been investigated by serveral workers. Narasimhan (1976, 1978a,b) examined fluid flow in porous media and the diffusion problem by a control volume approach which is based on a finite difference method. Patankar (1980) also presented a triangular finite difference control volume model for a heat transfer diffusion problem. Both modeling efforts can be expressed in a finite element matrix form such as described in Hromadka et al. (1981).

The control volume models are analogous to finite element mass matrix lumping models such as described by Kikuchi (1974). That is, the control volume approach essentially results in the formulation of a finite element

mass matrix which is lumped or diagonal. Fried and Malkus (1974) use numerical integration to form mass matrix lumping schemes with the optimal rate of energy convergence retained. Other formulations include a consistent diagonal mass matrix finite element model (Schreyer, 1978) which also produces a diagonal mass matrix similar to the lumped class. This type of formulation is extended to two-dimensional finite elements using orthogonal base functions (Schreyer, 1979). Another examination of mass lumped and consistent mass matrices is given by Surana (1981) for the special problem of a three dimensional structural beam element.

The above mass lumping models and control volume approches can be shown to be essentially analogous to the basic integrated finite difference method developed by Spalding (1972) for transport problems. The integrated finite difference method is oftentimes acclaimed for its ease of model development and simple solution of the integrated version of the governing PDE (Baliga and Patankar, 1980). Additionally for many problems, the finite difference method (often referred to as the control volume approach) may produce "better" results than the Galerking finite element method (Ramadhyani and Patankar, 1980) although the opposite can be true depending on the class of problem being solved (Hayhoe, 1978). The subdomain integration method is also referred to as the control volume approach and can be shown to result in another mass matrix which is consistent (Zienkiewicz, 1977), but yet is not diagonal. Thus the modeler is left to choose between several different numerical modeling methods which are in reality essentially similar to each other when written in a simple finite element matrix form.

The main objectives of this paper are twofold. First, this paper will briefly review the development of a one-dimensional nodal domain integration numerical model of the diffusion problem. This model development is derived in detail in previous papers (Hromadka and Guymon, 1981a, 1982), and only the

major steps of the derivation are included in this paper for the reader's convenience. Extension of the one-dimensional model to a two and three dimensional formulation follows from the one-dimensional model derivation. Each of the resulting numerical models are shown to represent the often-used Galerkin and subdomain integration models and an integrated finite difference model as well as an infinity of other nodal weighting schemes. The global matrix systems are shown to satisfy both Dirichlet, Neumann, and mixed boundary conditions similar to the Galerkin approach.

The second objective of this paper is to determine a nodal weighting relation which has a high probability of reducing integrated relative error. The proposed nodal weighting (mass lumping) method was determined by curve-fitting numerous optimized mass-lumping factors developed by trial and error in the comparison of approximation results to analytical results for several classical linear PDE boundary value problems where analytical solutions exist. Based on the comparison of modeled results and corresponding errors, general patterns were identified which may lead to the best numerical solution to the general problem.

The proposed mass lumped scheme is based on the subdomain integration (control volume) approach as applied to an actual solution trial function of the governing PDE. The trial function assumed is the principal eigen-function of the Fourier series expansion solution to a special case of the diffusion problem which approximates the control volume in the global model. Since all but one of the eigenfunctions essentially disappear in the solution of the PDE after a short time, the resulting model solution generally produces better approximations for the diffusion problem than any of the more popular domain numerical methods. The diffusion problems considered are only for the linear class of PDE. Extension of nonlinear problems is not straightforward due to the evaluation of a nonlinear diffusivity at the

boundary of the control volume. Further research is required to extend these methods to nonlinear problems.

All of the above models can be written in terms of a single nodal domain integration numerical statement for each nodal point value. The numerical statement is written as a function of a single mass matrix lumping factor η, and results in a representation of domain models in finite element matrix form.

DOMAIN APPROXIMATIONS OF PARABOLIC EQUATIONS

In this section, a brief summary of domain numerical model derivations is presented for the well known Galerkin finite element and the integrated finite difference models. Also presented is the subdomain integration model derivation. Although the derivations are well known, some particular steps are presented here in order to determine some of the many similarities between the various models. Each numerical model is then written in a finite element matrix form which indicates the degree of mass lumping each model involves. All of the models are then combined into one unifying finite element matrix formulation (or nodal domain integration model) as a function of the degree of mass matrix diagonalization. The resulting NDI statements represent an infinity of possible mass matrix lumping models of which the more popular domain methods are but special cases. In the following section, an improved nodal weighting scheme is developed which, for the problems tested, reduce integrated relative error for one-dimensional linear diffusion problems.

Galerkin Method of Weighted Residuals

The general parabolic equation describing a linear one-dimensional diffusion process is

$$a\frac{\partial \phi}{\partial t} - \frac{\partial^2 \phi}{\partial x^2} = 0 \ , \ x \in \Omega \qquad (1)$$

where ϕ is the volumetric concentration; (x,t) are spatial and temporal coordinates; α is a diffusivity parameter; and Ω is the problem global domain with global boundary Γ.

The finite element approach (Pinder and Gray, 1977) discretizes the global domain into the union of finite elements by

$$\Omega \equiv \bigcup \Omega^e \tag{2}$$

The domain is expressed as the union of domain and boundary

$$\Omega \equiv \Omega \cup \Gamma \tag{3}$$

$$\Omega^e \equiv \Omega^e \cup \Gamma^e \tag{4}$$

where

$$\Omega^e \cap \Omega^{e+1} \equiv \Gamma^e \cap \Gamma^{e+1} \tag{5}$$

The PDE variable ϕ is assumed approximated in each Ω^e by a linear trial function ϕ^e defined by

$$\phi^e \equiv \sum N_j(x)\ \phi_j^e \tag{6}$$

where $N_j(x)$ is an assumed linear polynomial shape function of nodal point j and ϕ_j^e is a nodal point value associated to element Ω^e. The Galerkin weighted residual process approximates (1) in each Ω^e by setting

$$\int_{\Omega^e} \left(\frac{\partial^2 \phi}{\partial x^2} - \alpha \frac{\partial \phi}{\partial t} \right) N_j d\Omega \equiv 0, \quad e = 1,2,\ldots \tag{7}$$

where boundary conditions of Neumann or Dirichlet are assumed on global boundary Γ. Integrating (7) by parts gives

$$\int_{\Omega^e} \left(\frac{\partial^2 \phi}{\partial x^2} - \alpha \frac{\partial \phi}{\partial t} \right) N_j d\Omega = \left(\frac{\partial \phi}{\partial x} N_j \right) \Big|_{\Gamma^e} - \int_{\Omega^e} \left(\frac{\partial \phi}{\partial x} \frac{dN_j}{dx} + \alpha \frac{\partial \phi}{\partial t} N_j \right) d\Omega \tag{8}$$

To conserve mass-flux continuity between Ω^e, it is assumed that

$$\sum_e \left(\frac{\partial \phi}{\partial x} N_j \right) \Big|_{\Gamma^e} \equiv \left(\frac{\partial \phi}{\partial x} \right) \Big|_{\Gamma} \tag{9}$$

For a Neumann (natural) boundary condition on global boundary Γ,

$$\left(\frac{\partial \phi}{\partial x} \right) \Big|_{\Gamma} \equiv 0 \tag{10}$$

For Neumann or Dirichlet boundary conditions specified on global domain Γ, the Galerkin analog for local element Ω^e reduces to

$$\int_{\Omega^e} \left(\frac{\partial^2 \phi}{\partial x^2} - \alpha \frac{\partial \phi}{\partial t} \right) N_j d\Omega = - \int_{\Omega^e} \left(\frac{\partial \phi}{\partial x} \frac{dN}{dx} j + \alpha \frac{\partial \phi}{\partial t} N_j \right) d\Omega \tag{11}$$

For the linear trial function ϕ^e in Ω^e,

$$\phi \cong \phi^e = \left(\frac{\ell^e - v}{\ell^e} \right) \phi_e + \left(\frac{v}{\ell^e} \right) \phi_{e+1} \tag{12}$$

where y is a local coordinate in Ω^e, dy = dx; $\ell^e = (x_{e+1} - x_e)$; $(\phi_e, \phi_{e+1}) \equiv \underset{\sim}{\phi}^e$; and x_e is the spatial coordinate of node e. Substituting (12) into (11) gives a Galerkin analog for local element Ω^e

$$0 \equiv \int_{\Omega^e} \left(\frac{\partial \phi^e}{\partial x} \frac{dN_j}{dx} + \alpha^e \frac{\partial \phi^e}{\partial t} N_j \right) d\Omega, \quad j = e, e+1 \tag{13}$$

For ϕ^e linear, all gradients are constant giving

$$\underset{\sim}{0} \equiv \frac{\partial \phi^e}{\partial x} \int_{\Omega^e} \frac{dN_j}{dx} d\Omega + \alpha^e \frac{\partial}{\partial t} \int_{\Omega^e} \phi^e N_j d\Omega, \quad j = e, e+1 \tag{14}$$

In matrix notation, the linear system of equations approximating the governing PDE in local element Ω^e is

$$\underset{\sim}{S}^e\underset{\sim}{\phi}^e + \underset{\sim}{P}^e[2]\,\dot{\underset{\sim}{\phi}}^e = \frac{\partial\phi^e}{\partial x}\int_{\Omega^e}\frac{dN_j}{dx^j}\,d\Omega + \alpha^e\frac{\partial}{\partial t}\int_{\Omega^e}\phi^e N_j\,d\Omega \qquad (15)$$

where

$$\underset{\sim}{S}^e = \frac{1}{\ell^e}\begin{bmatrix}1 & -1\\ -1 & 1\end{bmatrix} \qquad (16)$$

$$\underset{\sim}{P}^e[2] = \frac{\alpha^e\ell^e}{6}\begin{bmatrix}2 & 1\\ 1 & 2\end{bmatrix} \qquad (17)$$

and $\dot{\underset{\sim}{\phi}}^e = \frac{\partial}{\partial t}\left(\underset{\sim}{\phi}^e\right)$.

Subdomain Integration

The subdomain integration method discretizes the global domain Ω into subdomains (control volumes) where

$$\Omega = \bigcup R_j \qquad (18)$$

Generally, the subdomains are defined such that R_j is somewhat centered about nodal point j and

$$x_j \in R_j \qquad (19)$$

$$x_k \notin R_j, \quad k\neq j \qquad (20)$$

$$R_j \cap R_k = \Gamma_j \cap \Gamma_k \qquad (21)$$

$$R_j \equiv R_j \cup \Gamma_j \qquad (22)$$

For the one-dimensional parabolic PDE problem, Ω is discretized into subdomains which overlap contiguous finite elements from midelement to midelement.

The subdomain integration weighted residual approach averages the approximation error in estimating the governing PDE in R_j by the formulation

$$\int_{\Omega}\left(\frac{\partial^2\phi}{\partial x^2} - \alpha \frac{\partial\phi}{\partial t} \right) \omega_j d\Omega \equiv 0 \tag{23}$$

where boundary conditions of Neumann or Dirichlet are specified on global boundary Γ. From the discretization of Ω,

$$\int_{\Omega}\left(\frac{\partial^2\phi}{\partial x^2} - \alpha \frac{\partial\phi}{\partial t} \right)\omega_j d\Omega = \int_{R_j}\left(\frac{\partial^2\phi}{\partial x^2} - \alpha \frac{\partial\phi}{\partial t} \right)\omega_j d\Omega \tag{24}$$

where

$$\omega_j \equiv \begin{cases} 1, & x \in R_j \\ 0, & \text{otherwise} \end{cases} \tag{25}$$

Thus,

$$\int_{\Omega}\left(\frac{\partial^2\phi}{\partial x^2} - \alpha \frac{\partial\phi}{\partial t} \right)\omega_j d\Omega = \int_{R_j}\left(\frac{\partial^2\phi}{\partial x^2} - \alpha \frac{\partial\phi}{\partial t} \right) d\Omega \tag{26}$$

The subdomain and finite element discretization of Ω can be rewritten in terms of a nodal domain Ω_j^e discretization of Ω by

$$\Omega_j^e \equiv \Omega^e \cap R_j \tag{27}$$

A one-dimensional discretization of global domain Ω by each of the three approaches are shown in Fig. 1. From the definition of the nodal domain, a subdomain R_j would be the union of each Ω_j^e, that is

$$R_j = \cup \Omega_j^e \tag{28}$$

and the finite element Ω^e is given by

$$\Omega^e = \bigcup \Omega_j^e, \quad j \in S^e \tag{29}$$

where S^e is the set of nodal point numbers associated to finite element Ω^e

$$S^e \equiv \left\{ j : \Omega^e \cap \Omega_j^e \neq \{\emptyset\} \right\} \tag{30}$$

Consequently, a finite element matrix system can be determined for a sub-domain integration model by noting that

$$\iint_{R_j} \left(\frac{\partial^2 \phi}{\partial x^2} - \alpha \frac{\partial \phi}{\partial t} \right) d\Omega = \int_{\Omega_j^e} \left(\frac{\partial^2 \phi}{\partial x^2} - \alpha \frac{\partial \phi}{\partial t} \right) d\Omega \tag{31}$$

In terms of finite element Ω^e,

$$\iint_{\Omega^e} \left(\frac{\partial^2 \phi}{\partial x^2} - \alpha \frac{\partial \phi}{\partial t} \right) w_j \, d\Omega = \int_{\Omega_j^e} \left(\frac{\partial^2 \phi}{\partial x^2} - \alpha \frac{\partial \phi}{\partial t} \right) d\Omega, \quad j \in S^e \tag{32}$$

Integrating (32) by parts gives

$$\begin{aligned} \iint_{\Omega_j^e} \left(\frac{\partial^2 \phi}{\partial x^2} - \alpha \frac{\partial \phi}{\partial t} \right) d\Omega = & \left(\frac{\partial \phi}{\partial x} \right) \Big|_{\Gamma_j^e \cap \Gamma^e} + \left(\frac{\partial \phi}{\partial x} \right) \Big|_{\Gamma^e - \Gamma_j^e \cap \Gamma^e} \\ & - \int_{\Omega_j^e} \alpha \frac{\partial \phi}{\partial t} \, d\Omega \quad , j \in S^e \end{aligned} \tag{33}$$

where $S^e = (e, e+1)$; and Γ_j^e is the boundary of nodal domain Ω_j^e.

Similar to the Galerkin approach, flux continuity is assumed between finite elements and Neumann or Dirichlet boundary conditions are assumed on global boundary Γ giving

$$\sum_e \left(\frac{\partial \phi}{\partial x} \right) \Big|_{\Gamma_j^e \cap \Gamma^e} \equiv \left(\frac{\partial \phi}{\partial x} \right) \Big|_{\Gamma} \tag{34}$$

Thus, the subdomain integration analog in local element Ω^e reduces to

$$\int_{\Omega_j^e}\left(\frac{\partial^2\phi}{\partial x^2}-\alpha\frac{\partial\phi}{\partial t}\right)d\Omega \overset{*}{=} \left(\frac{\partial\phi}{\partial x}\right)\Big|_{\Gamma^e-\Gamma_j^e\cap\Gamma^e} - \int_{\Omega_j^e}\alpha\frac{\partial\phi}{\partial t}\,d\Omega, \quad j=(e,e+1) \tag{35}$$

where the $\overset{*}{=}$ notation in (35) implies an equality due to (34).
For $(\alpha,\phi) = (\alpha^e, \phi^e)$ in Ω^e during a small interval of time Δt,

$$\int_{\Omega_j^e}\left(\frac{\partial^2\phi}{\partial x^2}-\alpha\frac{\partial\phi}{\partial t}\right)d\Omega \overset{*}{=} \left(\frac{\partial\phi^e}{\partial x}\right)\Big|_{\Gamma^e-\Gamma_j^e\cap\Gamma^e} - \alpha^e\frac{\partial}{\partial t}\int_{\Omega_j^e}\phi^e d\Omega, \quad j=(e,e+1) \tag{36}$$

giving the element matrix system

$$\underset{\sim}{S}^e\underset{\sim}{\phi}^e + \underset{\sim}{P}^e[3]\dot{\underset{\sim}{\phi}}^e = \left(\frac{\partial\phi^e}{\partial x}\right)\Big|_{\Gamma^e-\Gamma_j^e\cap\Gamma^e} - \alpha^e\frac{\partial}{\partial t}\int_{\Omega_j^e}\phi^e d\Omega, \quad j=(e,e+1) \tag{37}$$

where $\underset{\sim}{S}^e$ is as defined in (16), and

$$\underset{\sim}{P}^e[3] = \frac{\alpha^e\ell^e}{8}\begin{bmatrix}3 & 1\\ 1 & 3\end{bmatrix} \tag{38}$$

Integrated Finite Difference

The integrated finite difference approach is analogous to the subdomain integration approach for a linear trial function ϕ^e in each element Ω^e except that

$$\int_{\Omega_j^e}\phi^e d\Omega \equiv \phi_j\int_{\Omega_j^e}d\Omega \tag{39}$$

Consequently, the element matrix system for solution of the governing PDE in Ω^e is

$$\underset{\sim}{S}^e\underset{\sim}{\phi}^e + \underset{\sim}{P}^e[\infty]\dot{\underset{\sim}{\phi}}^e = \left.\left(\frac{\partial\phi^e}{\partial x}\right)\right|_{\Gamma^e-\Gamma_j\,\cap\,\Gamma^e} - \alpha^e\int_{\Omega_j^e}\frac{\partial\phi^e}{\partial t}\,d\Omega, j\epsilon S^e \tag{40}$$

where $\underset{\sim}{S}^e$ is defined by (16), and

$$\underset{\sim}{P}^e[\infty] = \frac{\alpha^e\ell^e}{2}\begin{bmatrix}1 & 0\\ 0 & 1\end{bmatrix} \tag{41}$$

Nodal Domain Integration

For the one-dimensional parabolic PDE, the three domain numerical approaches derived above can be represented by a single element matrix system (Hromadka and Guymon, 1980)

$$\underset{\sim}{S}^e\underset{\sim}{\phi}^e + \underset{\sim}{P}^e[\eta_e]\dot{\underset{\sim}{\phi}}^e = \frac{1}{\ell^e}\begin{bmatrix}1 & -1\\ -1 & 1\end{bmatrix}\begin{Bmatrix}\phi_e\\ \phi_{e+1}\end{Bmatrix} + \frac{\alpha^e\ell^e}{2[\eta_e+1]}\begin{bmatrix}\eta_e & 1\\ 1 & \eta_e\end{bmatrix}\begin{Bmatrix}\dot{\phi}_e\\ \dot{\phi}_{e+1}\end{Bmatrix} \tag{42}$$

where η_e is an element mass lumping factor and determines the Galerkin, subdomain integration, and integrated finite difference domain analogs for $\eta_e = (2,3,\infty)$.

For the linear trial function ϕ^e in an irregular triangle and tetrahedron finite elements, the appropriate element matrix systems for two and three dimensional linear diffusion problems are readily determined (Hromadka, et al 1981b). In the two-dimensional triangle element matrix system, Fig. 2, the two-dimensional element matrix system is

$$\underset{\sim 2}{S}^e\underset{\sim}{\phi}^e + \underset{\sim 1}{P}^e[\eta_e]\,\dot{\underset{\sim}{\phi}}^e \equiv \underset{\sim}{0} \tag{43}$$

where the subscript notation indicates a two-dimensional matrix system, and

where $S_{\sim 2}^{e}$ is a Galerkin approximation for the diffusion component in element Ω^{e}, and

$$P_{\sim 2}^{e}\ [\eta_e] = \frac{\alpha^e A^e}{3[\eta_e+2]} \begin{bmatrix} \eta_e & 1 & 1 \\ 1 & \eta_e & 1 \\ 1 & 1 & \eta_e \end{bmatrix} \tag{44}$$

where A^e = area of triangle element, and where $\eta_e = (2,22/7,\infty)$ gives the Galerkin, subdomain integration, and integrated finite difference analogs. As in the one-dimensional problem, Dirichlet and Neuman boundary conditions are accommodated analogous to the Galerkin method.

For the three-dimensional tetrahedrom element, (Fig. 3) the appropriate element capacitance matrix is given by

$$P_{\sim 3}^{e}\ [\eta_e] = \frac{\alpha^e V^e}{4[\eta_e+3]} \begin{bmatrix} \eta_e & 1 & 1 & 1 \\ 1 & \eta_e & 1 & 1 \\ 1 & 1 & \eta_e & 1 \\ 1 & 1 & 1 & \eta_e \end{bmatrix} \tag{45}$$

where V^e = volume of the tetrahedron element, and where $\eta_e = (2,75/23,\infty)$ gives the Galerkin, subdomain integration, and integrated finite difference analogs. The element diffusion component is given by the usual Galerkin approximation in element Ω^e.

IMPROVED MASS MATRIX LUMPING FACTOR

In the previous section, a NDI model is developed for several of the common finite element configurations. The NDI statement is found to represent several numerical approaches by the variation of a mass lumping factor. Numerous mass lumping factors can be determined depending on the approach used to approximate the PDE. Zienkiewicz (1977) discusses mass lumping systems and also includes discontinuous trial function approximations in each finite element.

A brief examination of stability and convergence considerations for the family of domain models is given in Appendix A. From Appendix A it is concluded that if a Galerkin analog ($n=2$) and an integrated finite difference analog ($n=\infty$) are stable and convergent, then so is the entire range of mass lumped matrix finite element models ($2 \leq n < \infty$).

Approximating complex finite element trial functions with a lower order trial function generates a complete spectrum of possible domain finite element models which can be included into the variable mass lumped formulation. For example, two common approximation norms used in developing such lower order trial function models are the relative error and inner-product norms. Both of these approximation norms can be used to formulate numerous specialized mass lumped finite element models based on some assumed function configuration within each element. Such considerations suggest that an infinity of possible domain numerical models may be produced, each model perhaps providing the "best" approximation to a particular PDE or a specific class of boundary value problems.

Hromadka and Guymon (1981a) developed a variable mass-lumped matrix model which allowed a variation of the mass lumping factor with respect to time and between finite elements. However this variable n scheme involves frequent global matrix regeneration, which results in a relatively high increase in computational effort over a constant n-factor model. Consequently with an infinite number of potential constant-n domain models to choose from, the selection of the constant mass-lumping factor which has the highest probability of producing the best numerical approximation for diffusion problems is needed.

This is the main objective of the paper: to develop such a constant n factor which has the highest probability of reducing relative approximation error. It can be easily shown that any n-factor model provides a "best" approximation for some region of a problem domain or for some portion of the simulation. For example, Fig. 4 shows the relative error from various mass-lumped models in the

approximation of a classical linear diffusion problem. It can also be shown that these approximations fail or succeed to be the "best" depending on the problem being considered.

In this paper, the approach used to determine an optimum mass weighting factor for the one-dimensional NDI model of (42) is based on the Fourier series expansion of an assumed boundary value problem in each control volume of the global domain. For a finite interval R_j (control volume), the usual processes of normalization reduces the governing PDE to the solution of an equivalent PDE on a normalized unit interval

$$\frac{\partial^2 \theta}{\partial x^2} = \frac{\partial \theta}{\partial t} \quad , \; x \in [0,1] \tag{46}$$

where θ is a normalized variable for the PDE state variable, and (x,t) is now defined as normalized space and time. It is assumed in (46) that $\theta(x=0) = \theta_{j-1}$, $\theta(x=.5) = \theta_j$, and $\theta(x=1) = \theta_{j+1}$ where θ_k are the usual nodal values.

The NDI model is based on the well known Crank-Nicolson time advancement procedure to approximate the time derivative of (46). The nodal equation for solution of θ_j is therefore

$$\frac{\Delta t}{2||R_j||}\left[\left(\theta_{j-1}^{i+1} - 2\theta_j^{i+1} + \theta_{j+1}^{i+1}\right) + \left(\theta_{j-1}^{i} - 2\theta_j^{i} + \theta_{j+1}^{i}\right)\right] =$$

$$\frac{||R_j||}{2(n_j+1)}\left[\left(\theta_{j-1}^{i+1} - \theta_{j-1}^{i}\right) + 2n_j\left(\theta_j^{i+1} - \theta_j^{i}\right) + \left(\theta_{j+1}^{i+1} - \theta_{j+1}^{i}\right)\right] \tag{47}$$

where the normalized length, $||R_j|| = \frac{1}{2}$; i is the timestep number; and n_j is constant during normalized timestep Δt. Equation (47) evaluates all modeled flux terms at the midtimestep. For other time derivative approximations, such as forward or backward step differencing, a similar PDE finite difference

statement can be developed. An exact solution of the governing PDE at this midtimestep is

$$\hat{\theta}(x,\varepsilon) = -\frac{1}{2}\left(\bar{\theta}_{j-1} - 2\bar{\theta}_j + \bar{\theta}_{j+1}\right)\sin \pi x e^{-\pi^2\varepsilon} + \left(\bar{\theta}_{j+1} + \bar{\theta}_{j-1}\right) x + \bar{\theta}_{j-1} \tag{48}$$

where ε is normalized time measured from the midtimestep; and where $\bar{\theta} = \frac{1}{2}\left(\theta_j^i + \theta_j^{i+1}\right)$. Equation (48) is a solution to the governing PDE. If it is assumed that all effects of a moving boundary value at x=(0,1) are equivalent to holding θ constant at the midtimestep boundary values, then (48) represents an exact solution to the assumed boundary value problem.

The exact Fourier series expansion solution to the proposed boundary value problem, (48), is a good approximation for diffusion problems where the initial condition is a sinusoidal curve. Additionally, (48) is the principal eigenfunction of the boundary value problem since the remaining series terms quickly reduce to zero (Myers, 1971).

Holding the boundary values of $\hat{\theta}$ constant at the midtimestep allows a simplification of the NDI nodal equation to

$$\frac{\Delta t}{||R_j||}\left[\left(\bar{\theta}_{j-1} + \bar{\theta}_{j+1}\right) - \left(\theta_j^i + \theta_j^{i+1}\right)\right] = \frac{||R_j||}{2(\eta_j+1)}\left[2\eta_j\left(\theta_j^{i+1} - \theta_j^i\right)\right] \tag{49}$$

Since (48) is assumed exact,

$$\theta_j^i = \hat{\theta}\left(\frac{1}{2}, \frac{-\Delta t}{2}\right) = -\frac{1}{2}\left(\bar{\theta}_{j-1} - 2\bar{\theta}_j + \bar{\theta}_{j+1}\right)e^{-\pi^2\Delta t/2} + \frac{1}{2}\left(\bar{\theta}_{j-1} + \bar{\theta}_{j+1}\right) \tag{50}$$

$$\theta_j^{i-1} = \hat{\theta}\left(\frac{1}{2}, \frac{\Delta t}{2}\right) = -\frac{1}{2}\left(\bar{\theta}_{j-1} - 2\bar{\theta}_j + \bar{\theta}_{j+1}\right)e^{-\pi^2\Delta t/2} - \frac{1}{2}\left(\bar{\theta}_{j-1} + \bar{\theta}_{j+1}\right)$$

Substituting (50) into (49) and simplifying gives the NDI mass lumping factor

$$\eta_j(\Delta t) = \left\{ \frac{4\Delta t\ (1+e^{-\pi^2\Delta t})}{1 - e^{-\pi^2\Delta t} - 4\Delta t\ (1+e^{-\pi^2\Delta t})} \right\} \tag{51}$$

where the normalized timestep Δt is related to the global model timestep $\overline{\Delta t}$ by

$$\Delta t = \frac{\overline{\Delta t}\alpha}{4||R_j||^2} \tag{52}$$

Normally Δt is assumed constant for the entire numerical simulation and a single η_j is determined for each finite element. Should Δt vary, then new η_j values may be required according to (51).

From (51), the mass lumping factor varies by

$$8/(\pi^2-8) \leq \eta_j(\Delta t) < \infty \tag{53}$$

Equation (51) can be derived by a similar argument applied to other normalized boundary value problems. Inclusion of a time variable (linear polynomial variation) boundary condition adds additional terms to the numerator and denominator of (51), but adds little to change η for small Δt values. Although (51) is a function of the model timestep size, a mass lumped model using the $\eta_j(\Delta t)$ function would be constant with respect to η_j unless the timestep size is changed during the problem simulation.

Comparison of the proposed $\eta_j(\Delta t)$ mass lumped model to other values of mass lumping (e.g. Galerkin, subdomain integration, finite difference) models in the solution of classical boundary value linear diffusion problems will not be presented due to the unavoidable biased selection procedure. That is, it is perhaps more meaningful to express the success of a numerical method in terms of a probability as determined from numerous simulations, rather than demonstrating the success of the method for a single problem.

A general overview of using the $\eta_j(\Delta t)$ model can be summarized based on the comparison of over 300 computer simulations of several one-dimensional linear diffusion problems using various timestep and element size combinations, as well as different types of boundary conditions (McWhorter and Sunada, 1977). In diffusion problems where the state variable varies rapidly or where a sharp profile exists, a standard lumped mass finite difference analog produces the best results. For slower variations in the state variable and for smoother profiles, the proposed $\eta_j(\Delta t)$ model generally gave the best results. For the fast nodal variation problems, the basic assumptions in deriving the $\eta_j(\Delta t)$ model fail in that the exact solution includes several eigenfunctions beyond the principal eigenfunction used in the $\eta_j(\Delta t)$ model. For the slower nodal variation problems, the Fourier series of eigenfunctions essentially reduces to the principal eigenfunction which is modeled by the assumed boundary value problem in each control volume.

Figure 5 shows a plot of the experimentally determined probability of the $\eta_j(\Delta t)$ model producing the minimum integrated relative error in the solution of several linear diffusion problems. The accuracy of the $\eta_j(\Delta t)$ model was found to decrease as the normalized timestep increases; this observation may be explained by the inaccurate boundary conditions assumed for each control volume problem. It should be noted that although the $\eta_j(\Delta t)$ model was not consistently the best model, in the problems examined where $\eta_j(\Delta t)$ was not the optimum mass lumping factor the resulting model error was generally less than from either the Galerkin finite element or the integrated finite difference models.

The consequences of the above results is that use of the proposed $\eta_j(\Delta t)$ factor should result in a linear diffusion mass matrix lumped finite element model which has a significantly higher occurrance of being the best numerical model. This is important due to the uncertainty of accuracy in any numerical

model in the approximation of a PDE where the exact solution is unknown. Once a computer code is prepared based on the NDI variable lumped mass matrix system, it is relatively easy to simulate the particular PDE by each of the more popular domain methods and also by the $\eta_j(\Delta t)$ approach. Such a comparison should aid the analyst in determining a more appropriate discretization of the domain or an adjustment of the timestep in order to reduce the discrepancy between the various mass lumped models and ultimately increase the level of confidence in the final approximation results.

CONCLUSIONS

The major conclusions from this research are the following:

1. A unifying numerical model can be developed for many finite element configurations including the one-dimensional, triangle, and tetrahedron, finite elements. The unifying model is based on the straight forward nodal domain integration method. The resulting model is found to have the capability of representing the Galerkin finite element, subdomain integration, and integrated finite difference methods by the specification of a single mass matrix lumping factor, η.
2. The global matrix system composed of the sum of all NDI elements accommodates Dirichlet, Neumann, and mixed boundary conditions.
3. An infinity of possible domain numerical methods are possible. Two methods of developing various mass lumping models are based on the well known relative error and inner-product norms as applied to polynomial trial functions. These models can all be represented by the NDI model for specific values of η.
4. A computer code based on the Galerkin finite element method can easily be modified to allow a variable mass lumped matrix system and, consequently, represent an integrated finite difference, subdomain integration, and an infinity of other domain methods.

5. An improved mass lumping factor exists which apparently minimizes approximation error more often than any other domain method. The probability of the proposed optimum mass lumping system being the best numerical method is approximately 85 percent for small normalized timestep sizes. The improved method is developed based on a linear trial function model and a Crank-Nicolson time advancement approximation. Extension to higher order polynomial trial functions and other time advancement approximations should follow similarly. Although only the one-dimensional problem is considered extension of the approach to multidimensional problems is straightforward.

APPENDIX A: STABILITY & CONVERGENCE CONSIDERATIONS

Definition: The governing partial differential equation is defined by the description variable Φ as

$$\Phi \equiv \frac{\partial^2 \Theta}{\partial x^2} - \frac{\partial \Theta}{\partial t} \; ; \; x \in \Omega \tag{A-1}$$

where $\Phi = 0$ is the problem being studied, and initial and boundary conditions are assumed specified according to (46) and (47).

Definition: The $\left\{ \underset{\sim}{S}, \underset{\sim}{P}(\eta) \right\}$ matrices are defined as follows:

$$\underset{\sim}{S} \equiv \frac{1}{\ell^e} \begin{bmatrix} 1 & -1 \\ -1 & 1 \end{bmatrix} \tag{A-2}$$

$$\underset{\sim}{P}(\eta) \equiv \frac{\ell^e}{2(\eta+1)} \begin{bmatrix} \eta & 1 \\ 1 & \eta \end{bmatrix} \tag{A-3}$$

Definition: The matrix system operation $A(\eta, \underset{\sim}{\phi})$ is defined by

$$A(\eta, \underset{\sim}{\phi}) \equiv \underset{\sim}{P}(\eta) \frac{(\underset{\sim}{\phi}^{i+1} - \underset{\sim}{\phi}^{i})}{\Delta t} + \underset{\sim}{S} \frac{(\underset{\sim}{\phi}^{i+1} + \underset{\sim}{\phi}^{i})}{2} \tag{A-4}$$

where $\underset{\sim}{\phi}^{k}$ are vectors of nodal values at time k. $A(\eta, \underset{\sim}{\phi})$ describes a Galerkin, subdomain and finite difference

approximation for $\eta = (2,3,\infty)$ respectively, for the approximation of Φ in Ω.

Theorum: If A(2) and A(∞) are convergent algorithms to Φ, then $A(\eta)$ is convergent to Φ for $\eta \geq 2$.

Proof: From the definition of $\underset{\sim}{P}(\eta)$

$$\underset{\sim}{P}(\eta) = \left(\frac{3}{\eta+1}\right) \underset{\sim}{P}(2) + \left(\frac{\eta-2}{\eta+1}\right) \underset{\sim}{P}(\infty) \tag{A-5}$$

Or

$$\underset{\sim}{P}(\eta) \equiv a_1\underset{\sim}{P}(2) + a_2\underset{\sim}{P}(\infty); \quad a_1+a_2=1 \tag{A-6}$$

Therefore

$$A(\eta) = a_1A(2) + a_2A(\infty) \tag{A-7}$$

and

$$\lim_{\substack{\Delta x\to 0\\ \Delta t\to 0}} A(\eta) = a_1 \lim_{\substack{\Delta x\to 0\\ \Delta t\to 0}} A(2) + a_2 \lim_{\substack{\Delta x\to 0\\ \Delta t\to 0}} A(\infty) \tag{A-8}$$

where A(2) and A(∞) are Galerkin and finite difference approximations.

Thus

$$\lim_{\substack{\Delta x\to 0\\ \Delta t\to 0}} A(\eta) = a_1\Phi + a_2\Phi = \Phi \tag{A-9}$$

Theorum: Consider the approximation $A(\eta) = 0$ where η is constant in Ω. Then $A(\eta)$ is stable.

Proof: Rewrite $A(\eta)=0$ as

$$\left(a_1\underset{\sim}{P}(2) + a_2\underset{\sim}{P}(\infty) + \frac{\Delta t}{2}\underset{\sim}{S}\right)\underset{\sim}{\Phi}^{i+1} = \left(a_1\underset{\sim}{P}(2) + a_2\underset{\sim}{P}(\infty) - \frac{\Delta t}{2}\underset{\sim}{S}\right)\underset{\sim}{\Phi}^{i} \tag{A-10}$$

or in global matrix notation

$$\underset{\approx}{G}\underset{\sim}{\Phi}^{i+1} = \underset{\approx}{H}\underset{\sim}{\Phi}^{i} \tag{A-11}$$

For ℓ^e constant in Ω, $a_1 \underset{\approx}{P}(2)$ determines a tridiagonal matrix

$$a_1 \underset{\approx}{P}(2) = \frac{a_1 \ell^e}{6} \begin{bmatrix} 2 & 1 & & & \\ 1 & 4 & 1 & & \\ 0 & 1 & 4 & 1 & \\ \cdots & \cdots & \cdots & \cdots & \cdots \\ & & & & \\ & & 1 & 4 & 1 \\ & & 0 & 1 & 2 \end{bmatrix} \tag{A-12}$$

and

$$\frac{\Delta t}{2} \underset{\approx}{S} = \frac{\Delta t}{2 \ell^e} \begin{bmatrix} 1 & -1 & & & \\ -1 & 2 & -1 & & \\ 0 & -1 & 2 & -1 & \\ \cdots & \cdots & \cdots & \cdots & \cdots \\ & & & & \\ & & -1 & 2 & -1 \\ & & & -1 & 1 \end{bmatrix} \tag{A-13}$$

Likewise,

$$a_2 \underset{\approx}{P}(\infty) = \frac{a_2 \ell^e}{2} \begin{bmatrix} 1 & 0 & & & \\ 0 & 2 & 0 & & \\ 0 & 0 & 2 & 0 & \\ \cdots & \cdots & \cdots & \cdots & \cdots \\ & & & & \\ & & 0 & 2 & 0 \\ & & & 0 & 1 \end{bmatrix} \tag{A-14}$$

For $\gamma = \dfrac{\Delta t}{(\ell^e)^2}$,

$$\underset{\approx}{G} = \begin{bmatrix} \left(\frac{a_1}{3} + \frac{a_2}{2} + \frac{\gamma}{2}\right) & \left(\frac{a_1}{6} + \frac{-\gamma}{2}\right) & & \\ \left(\frac{a_1}{6} - \frac{\gamma}{2}\right) & \left(\frac{2a_1}{3} + a_1 + \gamma\right) & \left(\frac{a_1}{6} - \frac{\gamma}{2}\right) & \\ \cdots & \cdots & \cdots & \cdots \\ & & & \end{bmatrix} \tag{A-15}$$

and

$$\underset{\sim}{H} = \begin{bmatrix} \left(\frac{a_1}{3} + \frac{a_2}{2} - \frac{\gamma}{2}\right) & \left(\frac{a_1}{6} + \frac{\gamma}{2}\right) & & \\ \left(\frac{a_1}{6} + \frac{\gamma}{2}\right) & \left(\frac{2}{3}a_1 + a_2 - \gamma\right) & \left(\frac{a_1}{6} + \frac{\gamma}{2}\right) & \cdots \\ \cdots\cdots\cdots\cdots\cdots\cdots\cdots\cdots\cdots\cdots & & & \end{bmatrix} \tag{A-16}$$

For the specified boundary conditions of Φ: $\Theta(x=0,L;t>0)=0$, the $(\underset{\sim}{G},\underset{\sim}{H})$ matrix system becomes a regular tridiagonal matrix system. To show stability, the largest eigenvalue of

$$\underset{\sim}{G}^{-1}\underset{\sim}{H} \tag{A-17}$$

must be less than 1.

For the $\underset{\sim}{G}$ matrix,

$$\lambda_G = \left(\frac{2}{3}a_1 + a_2 + \gamma\right) + 2\left(\frac{a_1}{6} - \frac{\gamma}{2}\right)\cos\frac{S\pi}{N-1} \tag{A-18}$$

where N+1 nodal points are designated between x=0 and x=L.

Then

$$\lambda_G = 1 - 2\left(\frac{a_1}{3} - \gamma\right)\sin^2\left(\frac{S\pi}{2(N-1)}\right) \tag{A-19}$$

For the $\underset{\sim}{H}$ matrix

$$\lambda_H = \frac{2}{3}a_1 + a_2 - \gamma + \left(\frac{a_1}{3} + \gamma\right)\cos\left(\frac{S\pi}{N-1}\right) \tag{A-20}$$

or

$$\lambda_H = 1 - \left(\frac{a_1}{3} + \gamma\right)\left[2\sin^2\left(\frac{S\pi}{2(N-1)}\right)\right] \tag{A-21}$$

and

$$\underset{\sim}{H} = \begin{bmatrix} \left(\frac{a_1}{3} + \frac{a_2}{2} - \frac{\gamma}{2}\right) & \left(\frac{a_1}{6} + \frac{\gamma}{2}\right) & & \\ \left(\frac{a_1}{6} + \frac{\gamma}{2}\right) & \left(\frac{2}{3}a_1 + a_2 - \gamma\right) & \left(\frac{a_1}{6} + \frac{\gamma}{2}\right) & \cdots \\ \cdots & \cdots & \cdots & \cdots \end{bmatrix} \tag{A-16}$$

For the specified boundary conditions of Φ: $\Theta(x=0,L;t>0)=0$, the $(\underset{\sim}{G},\underset{\sim}{H})$ matrix system becomes a regular tridiagonal matrix system. To show stability, the largest eigenvalue of

$$\underset{\sim}{G}^{-1}\underset{\sim}{H} \tag{A-17}$$

must be less than 1.

For the $\underset{\sim}{G}$ matrix,

$$\lambda_G = \left(\frac{2}{3}a_1 + a_2 + \gamma\right) + 2\left(\frac{a_1}{6} - \frac{\gamma}{2}\right)\cos\frac{S\pi}{N-1} \tag{A-18}$$

where N+1 nodal points are designated between x=0 and x=L.

Then

$$\lambda_G = 1 - 2\left(\frac{a_1}{3} - \gamma\right)\sin^2\left(\frac{S\pi}{2(N-1)}\right) \tag{A-19}$$

For the $\underset{\sim}{H}$ matrix

$$\lambda_H = \frac{2}{3}a_1 + a_2 - \gamma + \left(\frac{a_1}{3} + \gamma\right)\cos\left(\frac{S\pi}{N-1}\right) \tag{A-20}$$

or

$$\lambda_H = 1 - \left(\frac{a_1}{3} + \gamma\right)\left[2\sin^2\left(\frac{S\pi}{2(N-1)}\right)\right] \tag{A-21}$$

Thus

$$\lambda_{\underset{\sim}{G}^{-1}\underset{\sim}{H}} = \frac{1-2\left(\frac{a_1}{3}+\gamma\right)\sin^2(\alpha)}{1+2\left(\frac{a_1}{3}+\gamma\right)\sin^2(\alpha)} \quad , \; S=1,2,\ldots,N-1 \tag{A-22}$$

where $\alpha = (S\pi)/2(N-1)$

From the above

$$\left| \lambda_{\underset{\sim}{G}^{-1}\underset{\sim}{H}} \right| \text{ is } \leq 1 \text{ for all } \gamma \text{ if } a_1 \geq 0.$$

Theorum: $A(\eta)$ is stable for any distribution of $\eta \geq 1$ in Ω.

Proof: This proof will be developed for a nodal point (subdomain) approximation of Φ. For any row p of $A(\eta)$, the following linear equation is determined for solution of nodal value ϕ_p:

$$\left[\left(\underset{\sim}{P}(\eta) + \frac{\Delta t}{2}\,\underset{\sim}{S}\right)\underset{\sim}{\phi}^{q+1} = \left(\underset{\sim}{P}(\eta) - \frac{\Delta t}{2}\,\underset{\sim}{S}\right)\underset{\sim}{\phi}^{q}\right]_p \tag{A-23}$$

where p designates nodal values contributing to row p of $A(\eta)$.

For row p

$$\underset{\sim}{P}(\eta)\underset{\sim}{\phi} \equiv \frac{\ell}{2(\eta+1)}\left[\phi_{p-1}+2\eta\phi_p+\phi_{p+1}\right] \tag{A-24}$$

and

$$\underset{\sim}{S}\underset{\sim}{\phi} \equiv \frac{1}{\ell}\left[-\phi_{p-1}+2\phi_p-\phi_{p+1}\right] \tag{A-25}$$

Thus, the above gives

Thus

$$\lambda_{\underset{\sim}{G}^{-1}\underset{\sim}{H}} = \frac{1-2\left(\frac{a_1}{3}+\gamma\right)\sin^2(\alpha)}{1+2\left(\frac{a_1}{3}+\gamma\right)\sin^2(\alpha)} \quad , \; S=1,2,\ldots,N-1 \tag{A-22}$$

where $\alpha = (S\pi)/2(N-1)$

From the above

$$\left| \lambda_{\underset{\sim}{G}^{-1}\underset{\sim}{H}} \right| \text{ is } \leq 1 \text{ for all } \gamma \text{ if } a_1 \geq 0.$$

Theorum: $A(\eta)$ is stable for any distribution of $\eta \geq 1$ in Ω.

Proof: This proof will be developed for a nodal point (subdomain) approximation of ϕ. For any row p of $A(\eta)$, the following linear equation is determined for solution of nodal value ϕ_p:

$$\left[\left(\underset{\sim}{P}(\eta) + \frac{\Delta t}{2}\,\underset{\sim}{S}\right)\underset{\sim}{\phi}^{q+1} = \left(\underset{\sim}{P}(\eta) - \frac{\Delta t}{2}\,\underset{\sim}{S}\right)\underset{\sim}{\phi}^{q}\right]_p \tag{A-23}$$

where p designates nodal values contributing to row p of $A(\eta)$.

For row p

$$\underset{\sim}{P}(\eta)\underset{\sim}{\phi} \equiv \frac{\ell}{2(\eta+1)}\left[\phi_{p-1} + 2\eta\phi_p + \phi_{p+1}\right] \tag{A-24}$$

and

$$\underset{\sim}{S}\underset{\sim}{\phi} \equiv \frac{1}{\ell}\left[-\phi_{p-1} + 2\phi_p - \phi_{p+1}\right] \tag{A-25}$$

Thus, the above gives

$$\frac{1}{2(\eta+1)}\left[\phi_{p-1,q+1}+2\eta\phi_{p,q+1}+\phi_{p+1,q+1}\right]+$$

$$\frac{\Delta t}{2\ell^2}\left[-\phi_{p-1,q+1}+2\phi_{p,q+1}-\phi_{p+1,q+1}\right]=$$

$$\frac{1}{2(\eta+1)}\left[\phi_{p-1,q}+2\eta_{p,q}+\phi_{p+1,q}\right]-$$

$$\frac{\Delta t}{2\ell^2}\left[-\phi_{p-1,q}+2\phi_{p,q}-\phi_{p+1,q}\right] \qquad \text{(A-26)}$$

Let $\mu = (\eta+1)\Delta t/\ell^2$

and define an error at node p and time q by a Fourier distribution term

$$E_{p,q} \equiv e^{i\beta p h_\xi q} \qquad \text{(A-27)}$$

Substituting $E_{p,q}$ into the above gives

$$\left[e^{i\beta(p-1)h_\xi q+1}+2\eta e^{i\beta p h_\xi q+1}+e^{i\beta(p+1)h_\xi q+1}\right]$$

$$+\mu\left[-e^{i\beta(p-1)h_\xi q+1}+2e^{i\beta p h_\xi q+1}-e^{i\beta(p+1)h_\xi q+1}\right]=$$

$$\left[e^{i\beta(p-1)h_\xi q}+2\eta e^{i\beta p h_\xi q}+e^{i\beta(p+1)h_\xi q+1}\right] \qquad \text{(A-28)}$$

$$+\mu\left[e^{i\beta(p-1)h_\xi q}-2e^{i\beta p h_\xi q}+e^{i\beta(p+1)h_\xi q}\right]$$

Dividing thru by $e^{i\beta ph}\xi^{q}$ gives

$$\xi\left[\, e^{-i\beta h}+2\eta+e^{i\beta h}\,\right]-\mu\xi\left[\, e^{-i\beta h}-2+e^{i\beta h}\,\right]= \tag{A-29}$$

$$\left[e^{-i\beta h}+2\eta+e^{i\beta h}\right]+\mu\left[e^{-i\beta h}-2+e^{i\beta h}\right]$$

But $\cos\beta h = (e^{i\beta h} - e^{-i\beta h})/2$; thus

$$\xi[2\cos\beta h + 2\eta] - \mu\xi[2\cos\beta h - 2] = [2\cos\beta h + 2\eta] + \mu[2\cos\beta h-2] \tag{A-30}$$

giving

$$\xi = \frac{(\cos\beta h+\eta) - \mu(1 - \cos\beta h)}{(\cos\beta h+\eta) + \mu(1 + \cos\beta h)} \tag{A-31}$$

Stability requires $|\xi| \leq 1$

where in the above, $\mu \equiv \frac{(n+1)\Delta t}{\ell^2}$

and β is a value of $\beta_n \equiv \frac{n\pi}{Nh}$, $Nh=L$.

Thus,

$$\xi = \frac{(\cos\beta h+\eta) - 2\mu\sin^2\left(\frac{\beta h}{2}\right)}{(\cos\beta h+\eta) + 2\mu\sin^2\left(\frac{\beta h}{2}\right)} \tag{A-32}$$

The condition $|\xi| \leq 1$ requires

$$\left|(\cos\beta h + \eta) - 2\mu\sin^2\left(\frac{\beta h}{2}\right)\right| \leq \left|(\cos\beta h+\eta) + 2\mu\sin^2\left(\frac{\beta h}{2}\right)\right. \tag{A-33}$$

But for $\cos\beta h+\eta\geq 0$, η is greater or equal to one which causes the NDI algorithm to be stable.

REFERENCES

1. Baliga, B. R., and Patankar, W. V., A New Finite-Element Formulation for Convection-Diffusion Problems, Numerical Heat Transfer, Vol. 3, 393-409, 1980.

2. Bear, Jacob, Hydraulics of Groundwater Flow, McGraw-Hill, (1979).

3. Cheney, E. W., Introduction to Approximation Theory, McGraw-Hill, 1966.

4. Fried, Isaac, and Malkus, D.S., Finite Element Mass Matrix Lumping by Numerical Integration with no Convergence Rate Loss, Int. J. Solids Structures, (11),461-466, 1974.

5. Hromadka II, T. V., and G. L. Guymon, Improved Linear Shape Function Model of Soil Moisture Transport, Water Resources Research, Vol. 17, No. 3, 504-521, 1981(a).

6. Hromadka II, T. V., and G. L. Guymon, A Note on Numerical Approximation of Advection-Diffusion Processes in Rectangular Domains, Advances in Water Resources, Vol. 5, 55-60, 1982.

7. Hromadka II, T. V., and G. L. Guymon, Some Effects of Linearizing the Unsaturated Soil-Moisture Transfer Diffusion Model, Water Resources Research (1980c), (16), 643-650.

8. Hromadka II, T. V., G. L. Guymon, G. Pardoen, Nodal Domain Integration Model of Unsaturated Two-Dimensional Soil-Water Flow: Development, Water Resources Research, Vol. 17, No. 5, 1425-1430, 1981(b).

9. Kikuchi, Fumio, Notes on the Lumped Mass Approximation for Vibration Problems, Proceedings of the 24th Japan National Congress for Applied Mechanics, University of Tokyo, Japan, 1974.

10. McWhorter, D. B., and Sunada, D. K., Groundwater Hydrology and Hydraulics, Water Resources Publications, 1977.

11. Myers, G. C., Analytical Methods in Conduction Heat Transfer, McGraw-Hill, (1971).

12. Narasimhan, T. N., and P. A. Witherspoon, An Integrated Finite Difference Method for Analyzing Fluid Flow in Porous Media, Water Resources Research, (12), 57-64, 1976.

13. Narasimhan, T. N., A Perspective on Numerical Analysis of the Diffusion Equation, Advances in Water Resources, (1), 3, 1978.

14. Narasimhan, T. N., S. P. Neuman, and P. A. Witherspoon, Finite Element Method for Subsurface Hydrology using a Mixed Explicit-Implicit Scheme, Water Resources Research, (14), 5, 1978.

15. Pavlin, V., and Perrone, N., Finite Difference Energy Techniques for Arbitrary Meshes Applied to Linear Plate Problems, Int. J. Num. Meth. in Eng., (14), 647-664, (1979).

16. Pinder, G. F., and W. G. Gray, Finite Element Simulation in Surface and Subsurface Hydrology, Academic Press, 1977.

17. Ramadhyani, S., and S. V. Patankar, Solution of the Poisson Equation: Comparison of the Galerkin and Control-Volume Methods, 1st Journal for Num. Methods in Eng., (15), 1395-1418, 1980.

18. Schreyer, H. L., Consistent Diagonal Mass Matrices and Finite Element Equations for One-Dimensional Problems, Int. J. Num. Meth. in Eng. (12), 1171-1184, (1978).

19. Schreyer, H. L., Fedock, J. J., Orthogonal Base Functions and Consistent Diagonal Mass Matrices for Two-Dimensional Elements, Int. J. Num. Meth. in Eng., (14), 1379-1398, (1979).

20. Spalding, D. B., A Novel finite-difference formulation for differential expressions involving both first and second derivations, Int. Journal Num. Methods in Eng., (4), 551, 1972.

21. Surana, K. S., Consistent Mass Matrices for Three Dimensional Beam Element Due to Distributed and Lumped Non-Structural Mass Systems Acting on its Span, Computers and Structures, (13), 515-524, 1981.

22. Zienkiewicz, O.C., The Finite Element Method in Engineering Science, McGraw-Hill, 1977.

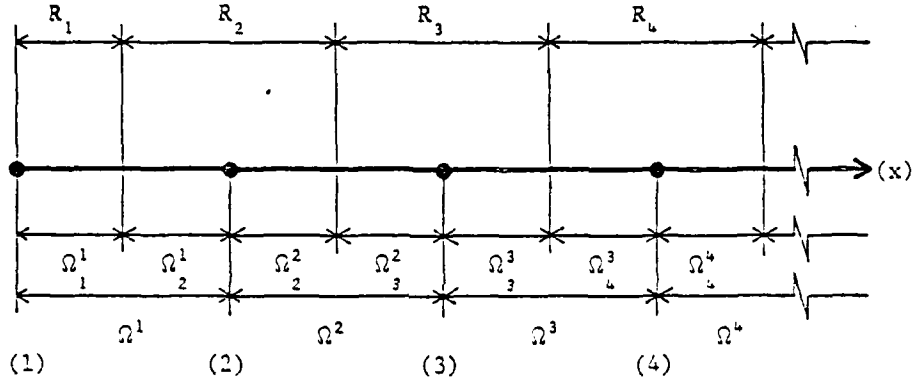

Fig. 1. - One Dimensional Discretization of Global Domain Ω showing nodal points (1), finite elements Ω^e, subdomains R_j, nodal domains Ω^e_j, and nodes •.

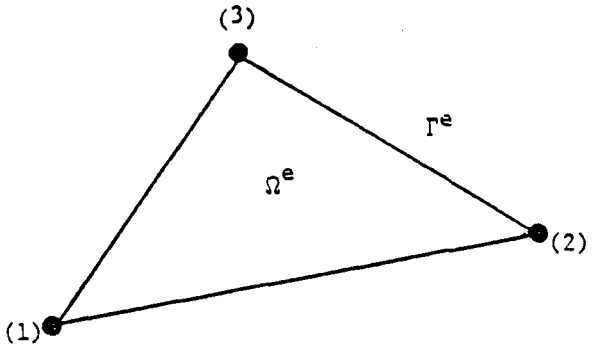

Fig. 2a. Finite Element Ω^e With Three Vertex Located Nodal Points

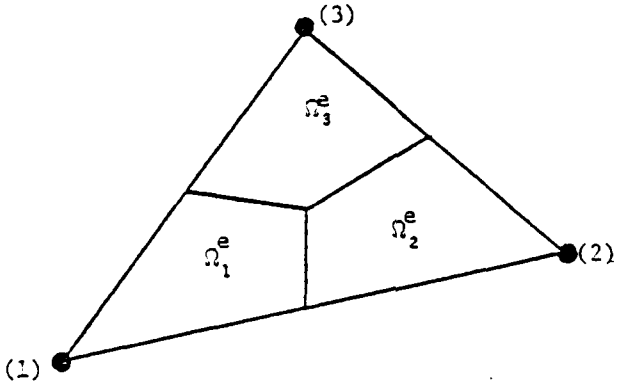

Fig. 2b. Finite Element Partitioned into Nodal Domains

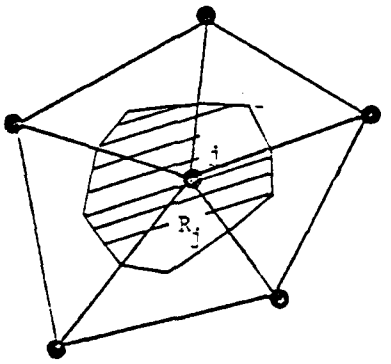

Fig. 2c. Subdomain R_j as the Union of all Nodal Domains Associated to Nodal Point j.

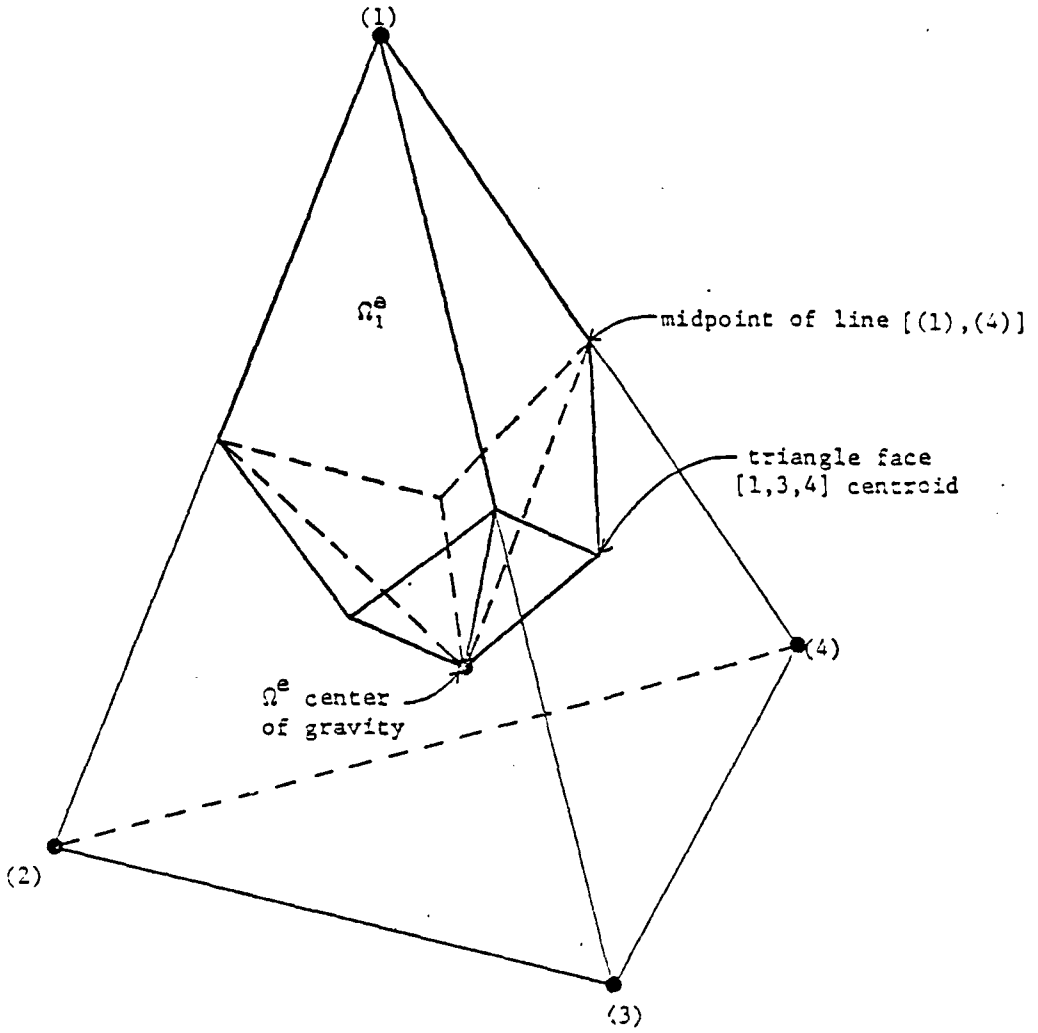

Fig. 3 - Nodal Domain Ω_1^e Geometric Definition in Finite Element Ω^e.

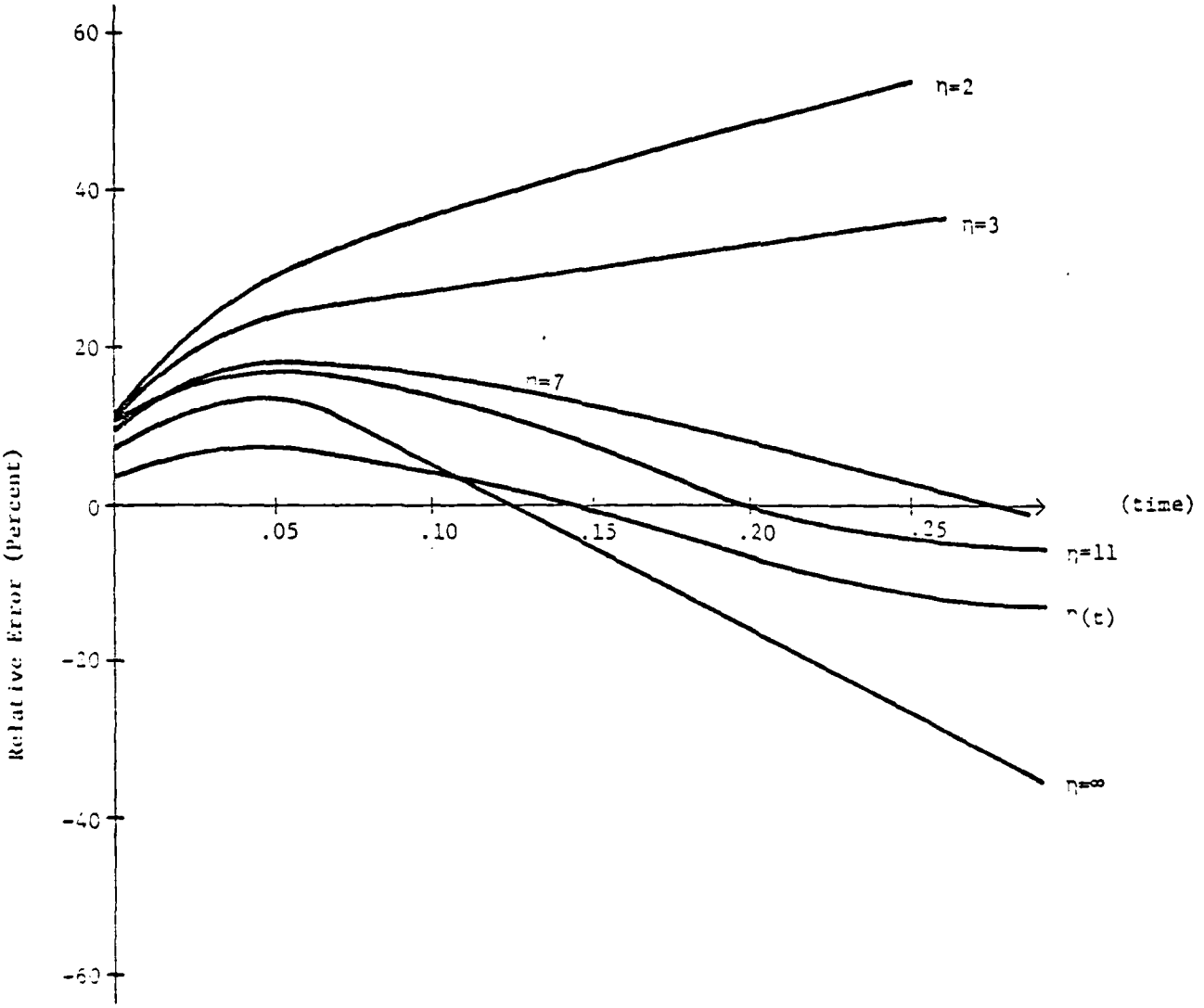

Fig. 4 - Example Integrated Relative Error in Modeling One-Dimensional Diffusion Problem (n=2 : Galerkin; n=3: subdomain integration; n=∞ : finite difference, n(t) = variable NDI model after Hromadka and Guymon, 1980a).

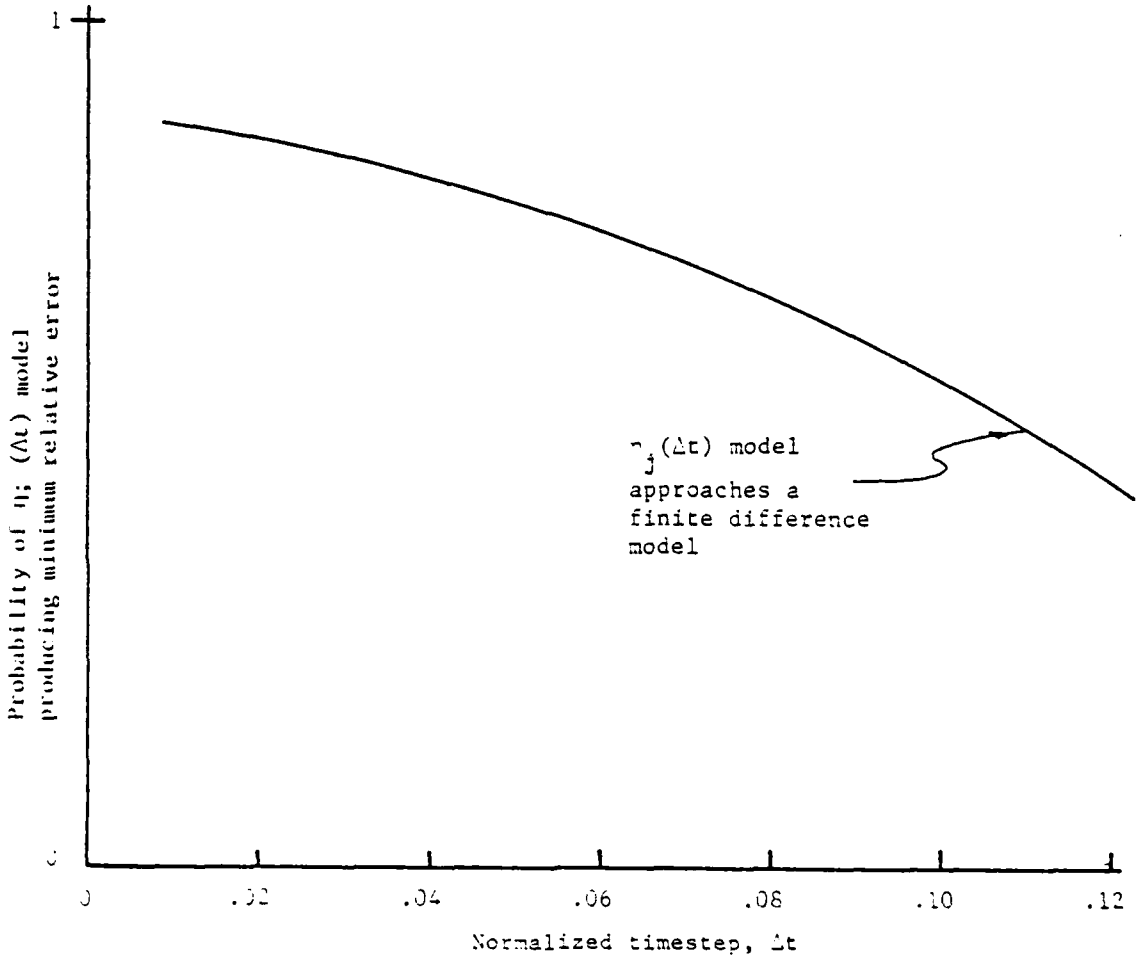

Fig. 5 - Estimated Probability of the $\eta_j(\Delta t)$ Model Producing Minimum Integrated Relative Error for Linear Diffusion Problems (Sample of 300 computer simulations)

APPLICATION OF A BOUNDARY INTEGRAL EQUATION TO PREDICTION OF FREEZING FRONTS IN SOIL

T. V. Hromadka II and G. L. Guymon
Civil Engineering,
University of California, Irvine, CA 92717

ABSTRACT

A boundary integral equation formulation based on the complex Cauchy integral theorem is applied to two-dimensional soil-water phase change problems encountered in algid soils. The model assumes that potential theory applies in the estimation of heat flux along a freezing front of differential thickness and that quasi-steady-state temperatures occur along the problem domain boundary. Application of the boundary integral formulation to two-dimensional problems results in predicted locations of the freezing front which are highly accurate. Although the proposed formulation is based on the Cauchy integral theorem, similar models may be developed based on other forms of integration equation methods.

INTRODUCTION

The purpose of this paper is to apply well known potential theory to the solution of soil-water freezing or thawing problems wherin the temperature is a harmonic function. For problems where phase change latent heat effects dominate the heat transport process, the heat balance equations may be approximated by the Laplace equations coupled with the boundary conditions modified to include the effects of phase change. To do this, tne dynamic component of the classical heat transport equation is assumed neglible compared to the latent heat term when freezing or thawing a soil-region. Moreover, it is necessary to assume an isotrophic, homogeneous solution domain. However, by means of a suitable coordinate transformation for relatively geometrically simple regions, anisotropic or even heterogenious domains may be transformed into a region in which potential theory may apply. As a result, boundary integral equation techniques may be applied which, for the test problems considered, significantly reduce computer storage and execution times when compared to classical domain methods. Generally, in freezing problems we are interested primarily in the location of the freezing front and in the estimation of heat flux values normal to the freezing front. Boundary integral equation methods (B.I.E.M.) focuses on these two types of problems directly. Additionally, the B.I.E.M. based models can significantly reduce the computational effort involved in producing mesh generations and manipulations, besides allowing very small mesh relocation except along a moving freezing front boundary. In this paper, we will develop a model based on a sophistication of a boundary integral equation method utilizing Cauchy's integral theorem for analytic functions as presented by Hunt and Isaacs (1981), and show results that support its use in geothermal problems involving freezing or thawing that are associated with geotechnical problems typical to areas where there is significant penetration of the freezing isotherm.

The application of potential theory is illustrated by considering a heat flow problem defined on a connected domain Ω with an exterior boundary described by a simple closed contour Γ. The heat flux across a surface located in the interior of Ω is given by

$$\vec{Q} = -K\vec{\nabla}\phi \tag{1}$$

where ϕ is the temperature-potential, and K is the thermal conductivity which is assumed isotropic and constant in Ω.

For two-dimensional problems the heat flux may be represented by complex variable notation as

$$Q = Q_x + iQ_y = -K\frac{\partial\phi}{\partial x} - iK\frac{\partial\phi}{\partial y} \tag{2}$$

where $i = \sqrt{-1}$

For an arbitrary simple closed contour C interior of Ω

$$\oint_C Q_n \, ds = \oint_C Q_t \, ds = 0 \tag{3}$$

where Q_n and Q_t are outward normal and tangential components of the heat flux on C and steady state conditions are assumed in Ω with no thermal sources or sinks. Equation (3) defines ϕ as harmonic, satisfying the Laplace equation in Ω. The harmonic conjugate ψ exists in Ω and is related to ϕ by the Cauchy-Riemann equations (Dettman, 1969). The complex temperature $\xi(z)$ is defined by

$$\xi(z) = \phi(x,y) + i\psi(x,y) \tag{4}$$

where $\psi(x,y) = k_o$ represents constant heat flux lines and $\phi(x,y) = k_o$ represents an isothermal potential where ϕ is constant along each potential.

Classes of problems which can be described in terms of a complex function such as (4) include ideal fluid flow, heat flow, electrostatics and porous media flow in isotropic, homogeneous domains. For approximate solutions, domain numerical approximations are generally employed such as the finite element, finite difference, or nodal domain integration methods. For homogeneous problems, boundary integral equation methods are reported superior to the domain numerical methods (Liggett, 1977; Liggett and Liu, 1979; Lennon, et al, 1980).

In this paper, a boundary integral method is used to solve for the temperature distribution on the problem boundary Γ where two types of boundary conditions are approximated simultaneously on $\Gamma_1 + \Gamma_2 = \Gamma$

$$\begin{aligned} \phi(x,y) &= \phi_o(x,y), \ (x,y) \in \Gamma_1 \\ \psi(x,y) &= \psi_o(x,y), \ (x,y) \in \Gamma_2 \end{aligned} \tag{5}$$

and isothermal phase change is defined on $\Gamma_3 \ \Gamma_1$ such that

$$L \frac{ds}{dt} = \sum_i Q_{n_i} \tag{6}$$

where the subscript i is a summation indice, and where s and Q_{n_i} are normal spatial and heat flux terms, respectively.

Equation 6 indicates that the rate of boundary movement (freezing front) due to isothermal phase change is directly related to the net heat efflux on the boundary of Γ_3. Additionally, the sum of normal heat flux terms along Γ_3 is defined in algebraic sign according to the freezing/thawing direction. In eq. (6), the volumetric latent heat of fusion for soil-water is used for L where the class of problems to be studied is the prediction of the freezing

front location within a homogeneous isotropic (or regional homogeneous isotropic) freezing/thawing soil where soil-water transport is assumed negligible. From eq. (6), the freezing front contour Γ_3 is redefined in (x,y) coordinates after each time advancement. An approach used to calculate new Γ_3 (x,y) coordinates is to displace the nodal points (located at the midpoint of each boundary element) normal to the heat flux direction such that the total Γ_3 movement balances the total heat efflux integrated with respect to time along Γ_3. The normal heat flux values are calculated along Γ_3 by the Cauchy-Riemann relations for analytic (complex variable) functions. For the examples considered, results indicate that the nodal x-coordinates vary considerably less than the y-coordinates and that carefully defined subregions of two-dimensional problems may be compared to one-dimensional model results to check modeling accuracy.

The approach used to develop a two-dimensional soil-water freezing/thawing model is to approximate a two-dimensional dynamic temperature field with a time-stepped steady state temperature distribution in Ω by means of a complex boundary integral formulation. In soil-water phase change problems where latent heat effects dominate the transient heat evolution, a quasi-steady state type problem can be formulated for many real world situations where a steady state heat flux estimation is a good approximation for the time-averaged dynamic heat flux values.

Such an approach includes the advantage of a precisely defined freezing front location in a two-dimensional domain Ω without the use of finite element deforming grid method (such as used in Lynch and O'Neill, 1981) or a multi-dimensional finite element model. Consequently, the proposed model may be ideal for many homogeneous soil freezing/thawing problems in geotechnical engineering where computer capability is limited, such as can be obtained on present day microcomputers.

FORMULATION

A discussion of the current trends in cold-regions thermal numerical models is contained in Guymon et al (1980) and a review of current boundary integral methodologies is contained in Hunt and Isaacs (1981). The general trend in algid-soil numerical models is to use domain methods to approximate the dynamic heat flow equation and to include a soil-water phase change model incorporating an isothermal or apparent heat capacity approximation. These domain numerical models allow the ease of solving for problems which have a spectrum of dissimilar materials and anisotropy. However for problems which are homogeneous, a B.I.E.M. formulation may be used to estimate the heat flux values within the problem, resulting in a numerical model which, for the test problems considered, is a fraction of the size of the domain model. However, because the B.I.E.M. model develops a fully populated N^{th} order matrix for a N nodal point discretization, the global model size can quickly exceed a domain model's requirements when a fine mesh is used on the problem boundary.

THEORY

Figure 1 shows an assumed problem to be studied which consists of a roadway embankment. A constant temperature is specified for t_U and t_L with the sides of the roadway embankment problem being specified with values of $t = t_L$ and t_R. For a boundary integral formulation, Neumann boundary conditions can be used on the left and right sides rather than determining t_L and t_R or an equivalent t_L and t_R. Any of the usual boundary integral approaches can be used for this problem; a complex formulation is used in this study due to the ease in contour integration which results from the well known Cauchy's integral theorem.

Assuming the freezing front location to be defined at some time t_o, the dynamic heat evolution problem is approximated by solving the Laplace relations (Fig. 1) to estimate the mean heat flux values along the freezing front location during a large timestep, Δt. For example, in the problems studied, timesteps of one-week are used with good results. From the estimated heat flux values, the change in the freezing front is calculated from eq. 6. That is, a method to calculate the change in the freezing front coordinates is to calculate the change in the nodal point coordinates in the direction of net normal heat flux. For nodal points located at the midpoint of boundary elements (Brebbia, 1978), the determination of new coordinates at the freezing front may be estimated by a simple balance between the volume of soil frozen, and the time-integrated heat evolved. Due to the model's basic assumption of phase change effects dominating the entire heat transport process the freezing front evolution is relatively slow, and the simple freezing front evolution model described above was found to be adequate for the problems tested. The new freezing front location at time $t_o+\Delta t$ is then used to obtain a better estimate of average heat evolution balance using heat flux approximations for time $t_o+\Delta t/2$.

To solve the Laplace equations, $\xi(z)$ is solved on the boundary of each subproblem to determine simultaneous heat flux values at each nodal point along the freezing front. From Cauchy's theorem,

$$\xi(z_o) = \frac{1}{2\pi i} \oint_{\Gamma} \frac{\xi(z)\, dz}{(z - z_o)} \tag{7}$$

where z ($z=x+iy$) $\in \Gamma$, and z_o is in the interior of Ω. Integration is performed in the usual counterclockwise fashion on boundary Γ.

By definition of the contour integral

$$\oint_{\Gamma} \frac{\xi(z)\, dz}{(z - z_o)} = \int_{\Gamma_{j,j+1}} \frac{\xi(z)\, dz}{(z - z_o)} \tag{8}$$

where $\Gamma_{j,j+1}$ is the contour between nodes z_j and z_{j+1}. For z_j on Γ,

$$\xi(z_j) = \frac{P}{\theta i} \int_{\Gamma} \frac{\xi(z)\, dz}{(z - z_j)} \tag{9}$$

where P is the Cauchy Principal Value, and θ is the interior angle between line segments $\Gamma_{j,j-1}$ and $\Gamma_{j,j+1}$ (Fig.2). On the boundary Γ of each subproblem, either $\psi(z_j)$ or $\phi(z_j)$ is defined at each boundary nodal point $z_j \in \Gamma$. Consequently from eq. (9), N equations result for the N unknown variables for a N-nodal point discretization of Γ. The integrations on Γ are approximated by means of combining eqs. 8 and 9.

The numerical integrations from solving eqs. 8 and 9 are arrived at by assuming $\xi(z)$ to be piecewise linear between nodal points, that is

$$\hat{\xi}(z) \equiv \left(\frac{z - z_j}{z_{j+1} - z_j}\right) \xi_{j+1} + \left(\frac{z_{j+1} - z}{z_{j+1} - z_j}\right) \xi_j \tag{10}$$

where $\hat{\xi}(z)$ is the approximation of $\xi(z)$ on $\Gamma_{j,j+1}$; and ξ_j is a nodal point value at node z_j.

The numerical integrations result in a complex logarithm formulation which is given in Hunt and Isaacs (1981) and is summarized in the following:

$$P \int_{z_{j-1}}^{z_{j+1}} \frac{\xi(z)}{(z - z_j)}\, dz = \xi_{j+1} - \xi_{j-1} + \xi_j \ln \left|\frac{z_{j+1} - z_j}{z_{j-1} - z_j}\right| \tag{11}$$

for $z_j \in \Gamma$. For boundary nodal points $z_o \neq j,j+1$

$$\int_{j,j+1} \frac{\xi(z)\,dz}{(z - z_o)} = \xi_{j+1}\left[1 + \left(\frac{z_o - z_j}{z_{j+1} - z_j}\right) \ln\left(\frac{z_{j+1} - z_o}{z_j - z_o}\right)\right] - \xi_j\left[1 + \left(\frac{z_o - z_{j+1}}{z_{j+1} - z_j}\right) \ln\left(\frac{z_{j+1} - z_o}{z_j - z_o}\right)\right] \tag{12}$$

The contour integrations result in the equation system

$$\xi_j = \frac{\xi_{j+1} - \xi_{j-1} + \sum_{k \neq j,j+1} \int_{k,k+1} \frac{\xi(z)\,dz}{(z - z_j)}}{\ln\left|\frac{z_{j-1} - z}{z_{j+1} - z_j}\right| + i\theta} \tag{13}$$

The full system is written in matrix form

$$\underset{\sim}{K}\,(\underset{\sim}{\phi}, \underset{\sim}{\psi}) = \underset{\sim}{0} \tag{14}$$

where $\underset{\sim}{K}$ is a fully populated matrix of known coefficients from eq. 13 and $(\underset{\sim}{\phi}, \underset{\sim}{\psi})$ is the array of (ϕ_j, ψ_j) values of the complex temperature ξ_j. Heat flux values can be estimated by determining a ξ_o interior of Ω and calculating the normal temperature gradient values using each $\phi_o(\phi_o = 0°C)$ value along the freezing front, Γ_3, or directly from the Cauchy-Riemann equations.

Since the problem domain is assumed homogeneous and isotropic, parameter estimations are not required on a control volume basis because the soil-mixture is assumed either entirely frozen (with some predetermined unfrozen water content typical of these problem freezing temperatures) or thawed on either size of the freezing front, Γ_3. In comparison to a finite element fixed grid model, thermal parameters are constantly changing as the control volume ice content values change with time, necessarily causing frequent domain method global matrix regenerations due to the linearized approximations of the governing nonlinear heat flow equation.

For an anisotropic homogeneous problem, the above methodology can be utilized by simply rescaling the global problem to accommodate the ratio of horizontal-to-vertical thermal conductivity values (Myers, 1971), and solving the modified problem in the new $(\hat{x},\hat{y})$ space.

For nonhomogeneous problems, complexities arise in an effort to simultaneously solve for the unknowns of ξ_j shared on the boundaries of homogeneous regions. The resulting extra manipulations oftentimes overshadow the benefits of the proposed geothermal model, especially when comparing the effort required for problem data-input preparation between a domain method formulation and the boundary integral formulation. Additionally, in the approximation of heat evolution in a nonhomogeneous problem several nodal points are required interior of Ω along the boundaries of the defined homogeneous regions, resulting in a significant increase in computational effort due to the fully populated matrix requirements of a boundary integral formulation.

For computational efficiency and model comparison purposes, a B.I.E.M. numerical model (Brebbia, 1978) was also used for the approximation of nodal temperatures and heat flux values on the freezing front boundary. Both the complex temperature formulation and the "boundary element method" were applied to identical nodal placements and definitions for each test problem studied. Comparison of computational results indicate that either approach produces similar values of heat flux on the freezing front boundary and, therefore, predict nearly identical freezing front locations. An advantage of the complex temperature formulation is the relative straightforward contour integrations summed along the boundary Γ. An advantage of the boundary element formulation is the direct computation of heat flux values along the freezing front nodal points.

APPLICATIONS

The boundary integral equation method (B.I.E.M.) geothermal model was applied to the roadway embankment problem schematically defined in Fig. 1. The first problem studied assumed that a constant -10°C temperature is uniformly imposed along the top surface of the domain with the rest of the domain initially set at +0.1°C; that is,

$$\phi_U = -10°C$$

$$\phi_B = +0.1°C$$

$$(\phi_R, \phi_L) = \text{Linear variation from } (\phi_U, \phi_B) \text{ to } \Gamma_3$$

For the subproblem $\nabla^2 T_1 = 0$, a frozen thermal conductivity value of ice is used whereas an unfrozen thermal conductivity of water is used for subproblem $\nabla^2 T_2 = 0$. The freezing front Γ_3 is initially assumed at a location of 50 cm below the top ground surface. Figure 3 shows several plots of predicted freezing front locations from the geothermal model.

To test the accuracy of the model, three quasi one-dimensional problems were identified (labeled A-A, B-B, C-C) in the two-dimensional problem domain of Fig. 3, and the one-dimensional analytical solutions compared to the two-dimensional geothermal model results. The geothermal model was found to give good results (Fig. 4) when compared to the well known one-dimensional semi-infinite Stefan problem solution.

To examine the effects of model timestep size, the geothermal model was tested for variations in the prediction of the freezing front location as a function of the length of the timestep size. The variation in results are shown in Fig. 4 which indicates that the geothermal model results vary in accuracy less than 2-percent between timestep sizes of 6-hours and 1-week.

Due to the small computer memory requirements for matrix solution and the relatively simple coding necessary for the B.I.E.M. or boundary element (B.E.M.) approaches, the freezing front locations plotted in Fig. 3 were obtained from a well known 64 K byte microcomputer capability (FORTRAN language). Consequently, sophisticated two-dimensional problems may be analyzed economically by currently available low-cost "household" digital computers.

As a second example problem, the effects of a buried pipeline maintained at subfreezing temperatures was studied. In this problem the freezing front model used in the first example problem was utilized along with a radially defined freezing front from the buried pipeline (Fig. 5).

Three subproblem domains were defined in order to estimate a net efflux of heat along each freezing front. To verify the model approximations, one-dimensional problem solutions were compared to both the horizontal-plane freezing front and the radial freezing front problems. The problem simulation time was for a 6-month duration and required less than 10 CPU seconds on a Data General Eclipse mini-computer system (using a model timestep size of one-week). Model accuracy was found to be in error less than 2-percent from the one-dimensional Stefan problem analytical solutions. On a 64K byte (FORTRAN) microcomputer system, computer requirements cost approximately 2 CPU minutes for the same 6-month simulation. From Fig. 5, it can be noted that a peat layer is approximated by rescaling the global model and neglecting horizontal heat flux effects and assuming only a vertical freezing front penetration in the peat (the modeled results verified this assumption). Heat flux was assumed to be zero on the left and right sides of the global problem domain. Computer solution of the steady state heat flux problems were obtained by the B.I.E.M. (Brebbia) in order to directly obtain heat flux values along the radial freezing front.

REFERENCES

1. Brebbia, C.A., "The Boundary Element Method for Engineers," Pentech Press, 1978.

2. Dettman, J. W., "Applied Complex Variables," McMillan Co., 1969.

3. Guymon, G. L., T. V. Hromadka II, and R. L. Berg, "A One-Dimensional Frost Heave Model Based upon Simulation of Simultaneous Heat and Water Flux," Cold Regions Science and Technology, 3, 1980.

4. Hunt, B. and L. T. Isaacs, "Integral Equation Formulation for Groundwater Flow," Journal of Hydraulics Division, ASCE, 107, (10), 1981.

5. Lennon, G. P., P. L. F. Liu, and J. A. Liggett, "Boundary Integral Solutions to Three-Dimensional Unconfined Darcy's Flow," Water Resour. Res., (16) 651-658, (1980).

6. Liggett, J. A., "Location of Free Surface in Porous Media," Journal of Hydraulics Division, ASCE, 103, (4), 1977.

7. Liggett, J. A., and P. L. F. Liu, "Unsteady Free Surface Flow Through a Zoned Dam using Boundary Integration," Proceedings of the Symposium on App. of Comp. Methods in Eng., 1979.

8. Lynch, D. R., and K. O'Neill, "Continuously Deforming Finite Elements for the Solution of Parabolic Problems with and without Phase Change," Int. Journal Num. Methods in Eng., 1979.

9. Myers, G. C., "Analytical Methods in Conduction Heat Transfer," McGraw-Hill, 1971.

CONCLUSIONS

A soil-water freezing geothermal model is developed which is based on a complex variable boundary integral equation method using Cauchy's theorem. The geothermal model provides good results in the prediction of soil-water freezing fronts in two-dimensional problems. Since the latent heat effects of soil-water phase change are assumed to dominate the total heat evolution budget, quasi steady-state temperature distributions may be used to estimate total net heat flux values along the soil-water freezing fronts. The computer coding requirements are small, enabling the model to be accommodated on currently available home microcomputers for many two-dimensional freezing/thawing soil problems.

ACKNOWLEDGMENTS

This work was supported by the U.S. Army Research Office (Grant No. DAAG29-79-C-0080).

TABLE OF FIGURES

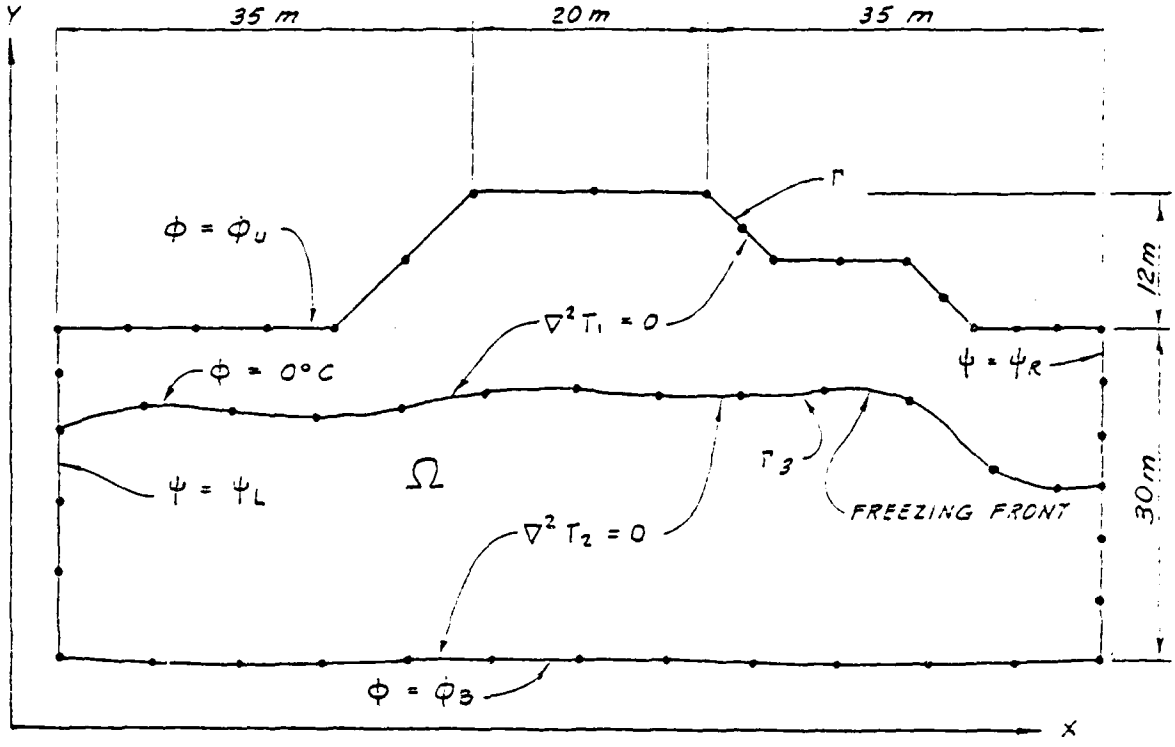
Y
35 m
20 m
35 m
Γ
$\phi = \phi_U$
12m
$\nabla^2 T_1 = 0$
$\phi = 0°C$
$\psi = \psi_R$
$\psi = \psi_L$
Ω
Γ_3
FREEZING FRONT
30m
$\nabla^2 T_2 = 0$
$\phi = \phi_B$
X

Figure 1

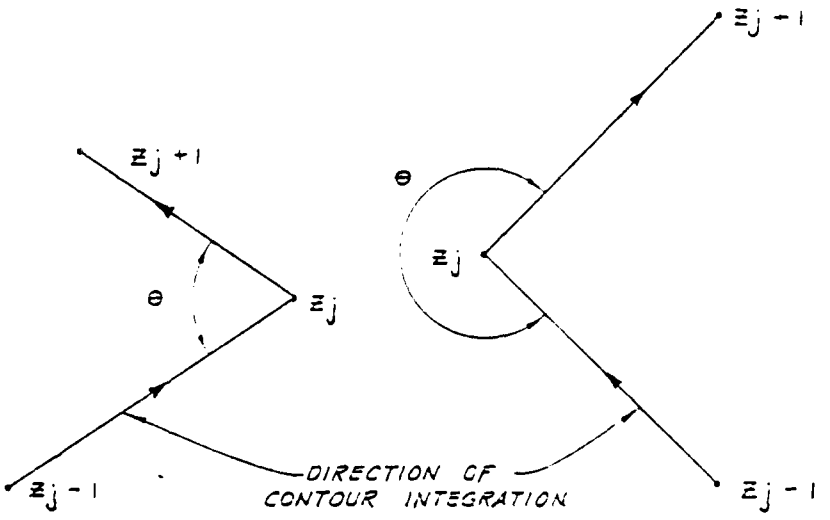
z_{j+1}
θ
z_j
z_{j-1}
DIRECTION OF
CONTOUR INTEGRATION
z_{j-1}
θ
z_j
z_{j-1}

Figure 2

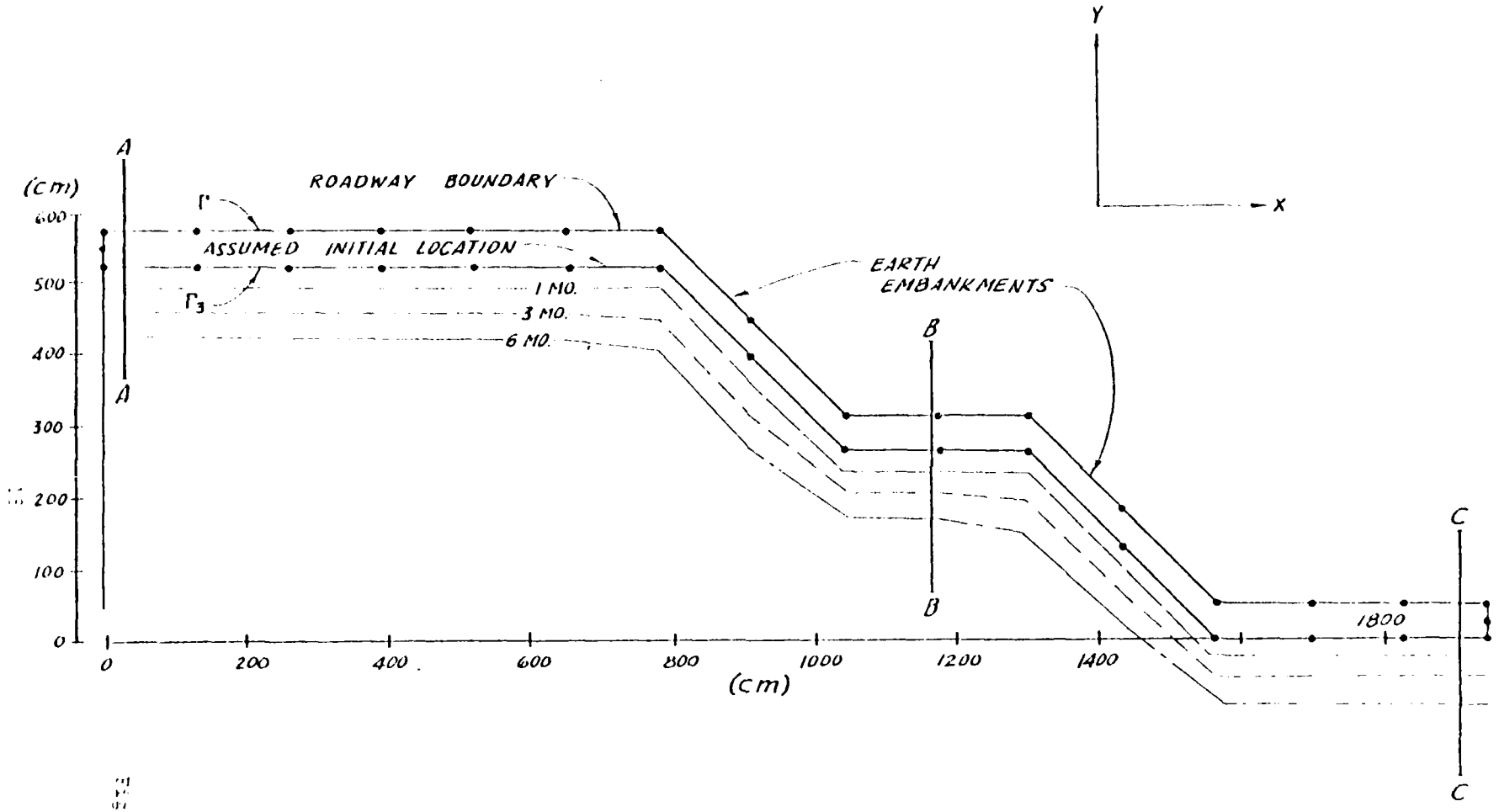
Y
X
A
A
(cm)
600
500
400
300
200
100
0
ROADWAY BOUNDARY
ASSUMED INITIAL LOCATION
Γ
Γ_3
1 MO.
3 MO.
6 MO.
EARTH EMBANKMENTS
B
B
C
C
1800
0
200
400
600
800
1000
1200
1400
(cm)

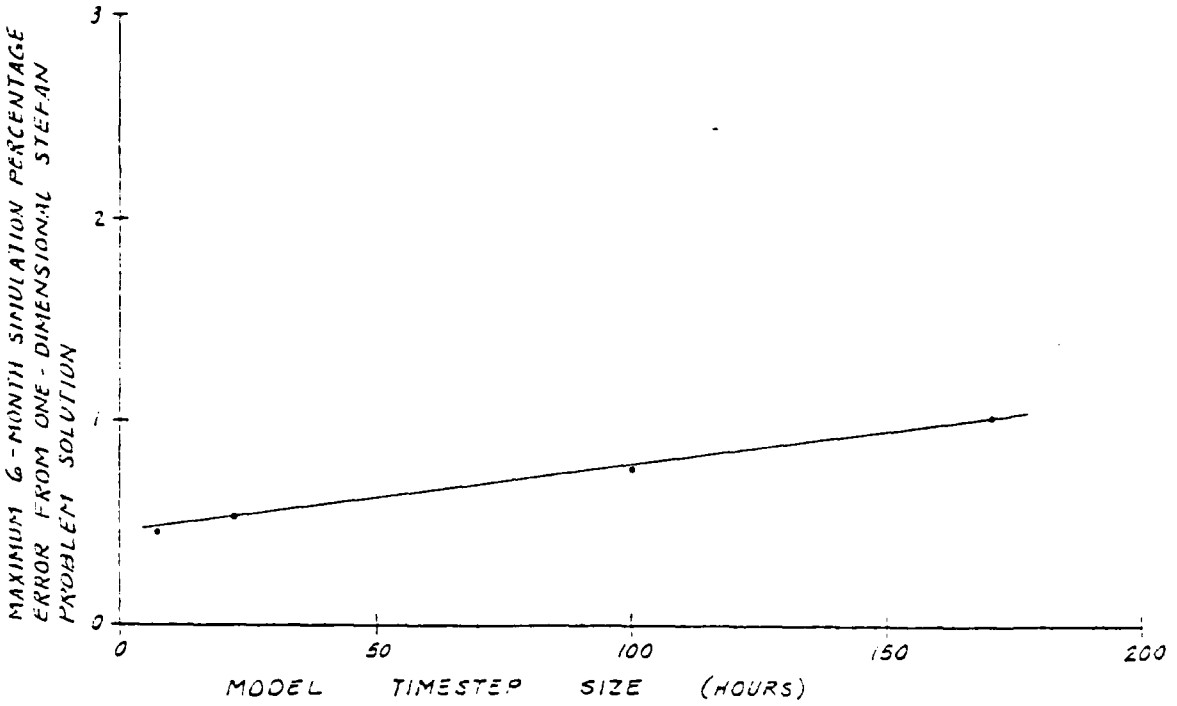
MAXIMUM 6-MONTH SIMULATION PERCENTAGE ERROR FROM ONE-DIMENSIONAL STEFAN PROBLEM SOLUTION
3
2
1
0
0
50
100
150
200
MODEL TIMESTEP SIZE (HOURS)

Figure -

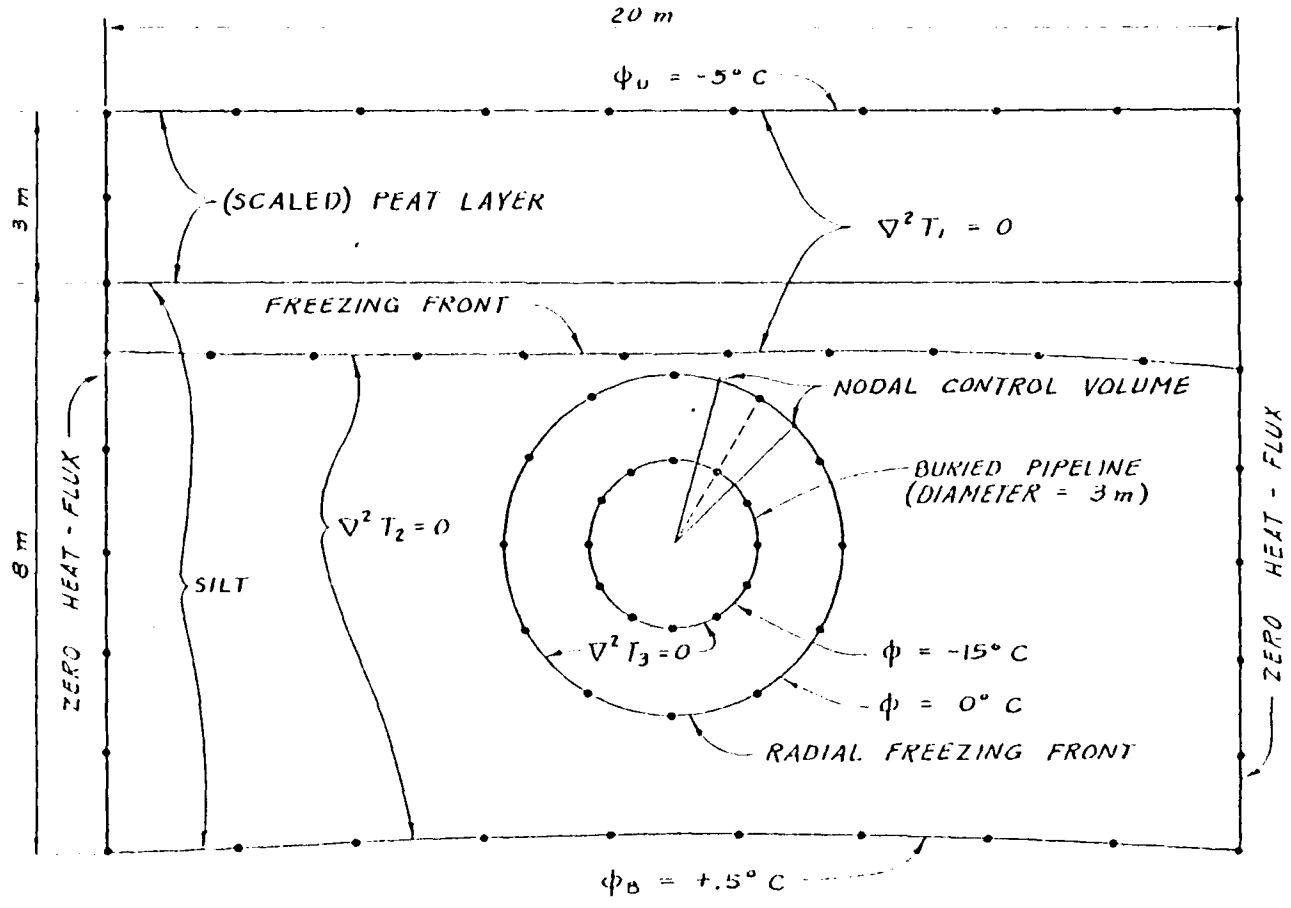
20 m
ϕ_U = -5° C
3 m
(SCALED) PEAT LAYER
$\nabla^2 T_1 = 0$
FREEZING FRONT
NODAL CONTROL VOLUME
BURIED PIPELINE
(DIAMETER = 3 m)
8 m
ZERO HEAT - FLUX
SILT
$\nabla^2 T_2 = 0$
$\nabla^2 T_3 = 0$
ϕ = -15° C
ϕ = 0° C
RADIAL FREEZING FRONT
ZERO HEAT - FLUX
ϕ_B = +.5° C

Figure 5

TWO-DIMENSIONAL MODEL OF COUPLED HEAT AND MOISTURE TRANSPORT IN FROST HEAVING SOILS

G. L. Guymon and T. V. Hromadka II
Civil Engineering
University of California, Irvine, CA, 92717, USA

INTRODUCTION

Numerical modeling of coupled heat and moisture transport in freezing and thawing soils has been the subject of a number of investigations generally beginning in the mid-1970's (Harlan, 1974 and Guymon and Luthin, 1975). Modeling efforts reported in the open literature primarily deal with one-dimensional heat and moisture transport. These models and numerical models of frost heave are reviewed by Guymon, et al (1980) and Hopke (1980) among others. While one-dimensional models of soil freezing or thawing are adequate for a large number of applications, at least two-dimensional models are required for many problems, e.g. buried pipelines, roadway berm problems, and embankments on permafrost.

Several well known two-dimensional geothermal models applicable to freezing or thawing soils have been developed, e.g. the Exxon EPR model. These models are proprietary and are generally not reported in the open literature. For many applications, it is permissible to assume that soil moisture is immobile, allowing one the luxury of dealing with heat tranport and moisture phase change alone. On the other hand, a great many soil freezing problems may involve unsteady moisture transport, which may modify the thermal regime of the soil over a long period of time, or may be substantially dependent on moisture transport as is the case when frost heave is occurring.

The purpose of this paper is to present a dynamic two-dimensional numerical model of coupled heat and moisture transport which is generally applicable to freezing and thawing soils. The model includes the ability to estimate frost heave and thaw consolidation for simple but useful geometries. Some of the problems associated with such modeling exercises are reviewed.

THEORY

The theory of heat transport in freezing soils and their thermal properties have been the subject of investigation since before the turn of the century, e.g. Stefan (1891). Recent definitive works on this topic are Lunardini (1981) and Farouki (1981). As a result, the deterministic equations of heat transport in moist soils are well established; i.e., in two-dimensions

$$\frac{\partial}{\partial x}\left[K_T \frac{\partial T}{\partial x}\right] + \frac{\partial}{\partial y}\left[K_T \frac{\partial T}{\partial y}\right] = C_m \frac{\partial T}{\partial t} - L \frac{\rho_i}{\rho_w} \frac{\partial \theta_i}{\partial t} + C_w v_x \frac{\partial T}{\partial x} + C_w v_y \frac{\partial T}{\partial x} \quad (1)$$

where x and y = cartesian coordinates, t = time, T = soil-water-air-ice mixture temperature, θ_i = volume of of ice per unit total volume of soil, K_T = thermal conductivity of soil-water-air-ice mixture, C_m = volumetric heat capacity of soil-water-air-ice mixture, L = volumetric latent heat of fusion of bulk water, ρ_i = ρ_w = density of ice and water, respectively, C_w = volumetric heat capacity of water, and v_x and v_y = the x and y velocity flux components. Obviously, the density parameters are relatively precisely temperature and salinity can be assumed to be constant for dilute solutions with temperatures less than -20°C (Anderson, et al, 1973). The latent heat term only contributes to (1) when soil regions are undergoing freezing or thawing. The remaining parameters, K and C_m, are functions of the volumetric proportions of each material constituent and soil structure, among other factors. There is some

variation in computed parameters depending upon the method of measurement or computation. DeVries (1966) method of estimating these parameters is often used, e.g. for C_m

$$C_m = \Sigma\, C_j\, \theta_j \tag{2}$$

where C_j = volumetric heat capacity of j^{th} constituent and θ_j = volumetric fraction of j^{th} constituent. A similar equation is used with and without a particle contact function for thermal conductivity. Equation (1) is nonlinear since the K_T and C_m parameters depend upon the amount of ice and water coexistant in a freezing and thawing soil. Additionally, (1) is coupled to equations describing the moisture state of a soil and soil freezing characteristic relationships such as discussed by Anderson, et al (1973).

Similarly the theory of water movement in unfrozen isothermal soils is well advanced; e.g. Bear (1979). A deterministic equation for moisture transport in nondeformable saturated or unsaturated porous media is

$$\frac{\partial}{\partial x}\left[K_H \frac{\partial \phi}{\partial x}\right] + \frac{\partial}{\partial y}\left[K_H \frac{\partial \phi}{\partial y}\right] = \frac{\partial \theta_u}{\partial t} + S \tag{3}$$

where ϕ = total hydraulic head, K_H = extended Darcy hydraulic conductivity, θ_u = volumetric water content, and S = moisture sink. In unsaturated soils K_H is a function of negative pore water pressures (soil water tension) and hence (3) is nonlinear. Depending on the orientation of the x and y coordinates, the temporal term in (3) may be zero or a function of the total saturated thickness multiplied by a storage coefficient. The moisture sink

term for a freezing soil accounts for the conversion of liquid water to ice; i.e.

$$S = L \frac{\rho_i}{\rho_w} \frac{\partial \theta_i}{\partial t} \tag{4}$$

One must consider three general regions in a freezing or thawing soil to apply (3). The unfrozen zone, which for instance may be between an advancing freezing front and a water table, will be adequately described by (3) assuming moisture movement is by connected liquid water films (in this case $S = 0$). In the freezing zone, a zone of finite width depending on material type and perhaps other factors, (3) may apply and $S \neq 0$. A major difficulty in applying (3) in a freezing region is determining the hydraulic conductivity parameter. Nakano et al, (1982) has demonstrated that the presence of ice in soil pores significantly effects the transport of water in soils. The hydraulic conductivity of partially frozen soil is much less than for unfrozen soil. Jame (1978) and Taylor and Luthin (1978) using data developed by Jame, indicated that unfrozen hydraulic conductivity had to be reduced in a freezing zone in order to adequately model the thermal and soil moisture regime of freezing horizontal columns. They assumed a phenomenological relationship of the form

$$K = K_H \, 10^{-E\theta_i} \tag{5}$$

where K = freezing soil hydraulic conductivity, K_H = unfrozen soil hydraulic conductivity, θ_i = volumetric ice content, and E = a calibration factor such that $E\theta_i \geq 0$. For fully frozen soil, it is generally believed that unfrozen water may move as liquid water films primarily in response to hydraulic gradients. In this case it may be assumed that $S = 0$. Whether this flow may be represented by Darcy's law is not established nor are there definitive data available on frozen soil hydraulic conductivity.

Because unsaturated soils are a common freezing and thawing problem, some means of relating unfrozen water content and total hydraulic head or pore pressure is required. This is accomplished by developing the usual soil moisture characteristics which for clays and silts is hysteretic. For convenience, it is usually desirable for modeling purposes to assume that this relationship is single valued, removing the problem of incorporating memory in models. Further, it is convenient to express this experimental relationship as some form of mathematical function. While numerous such relationships have been proposed, we have found that Gardner's (1958) relationship fits many soils we are interested in, i.e. the so-called frost susceptible soils. Water content is related to pore pressure as follows:

$$\theta = \frac{\theta_o}{A|u|^n+1} \qquad 6)$$

where θ_o = porosity, u = pore water pressure (expressed as hydraulic head) and A and n = regression fit coefficients which depend on soil type, density, and other factors.

Thermodynamic processes occurring in freezing zones, employing static thermodynamic theory, are relatively well developed. Applications to dynamic states are not as well known with the result that agreement is not widespread on how freezing zone processes should be modeled. In the event ice segregation occurs lenses of ice form deforming the soil surface approximately an equal amount (frost heave), and a dynamic process is involved between the rate latent heat is extracted and the rate moisture is supplied to the freezing zone. The micro-processes in this zone determine ice and pore water pressures and hence the ability to form segregated distinct ice lenses. Early attempts to relate these pressures resulted in the so-called capillary model, for example see Penner (1957) and Everett (1961). Changes in freezing temperature and pore water pressures have been evaluated using the Claperon equation, for instance

see Williams (1967). While both of these concepts are well established, there is a wide variation in how these concepts are utilized in frost heave models. The principal difficulty is relating estimated pore water pressures to ice pressures which may be assumed to equal the overburden stress and surcharge loading (Williams, 1967). Further, one needs a relationship between ice lens formation and the development of heave forces for many practical geotechnical problems. Surcharge loading is analogous to the formation of heave forces. If one were only interested in total unrestrained frost heave for relatively shallow freezing, a simple model of heat evolution and moisture transport might suffice; for example see Outcalt, (1980) and Arakawa (1966) for such models.

As a result of uncertainty concerning physical and thermodynamic mechanisms in freezing zones, and perhaps more significantly the uncertainty as how to incorporate what is known about these processes into complicated numerical models, deterministic numerical models are incomplete. While such incompleteness adds a degree of discomfort to a numerical modeling approach from the standpoint of confidence in the model results, there is still the need to develop such models to aid in geotechnical design studies.

MODEL DEVELOPMENT

While certain soil freezing and thawing processes are well understood, others are not. Furthermore, there is considerable choice in modeling the well established physics based equations presented in the previous section and the incorporation of ancillary relationships describing parameters and processes. The best approach to formulating a comprehensive model utilizing the present knowledge of the several individual processes is unclear (Morgenstern, personal communication). The problem is further compounded by the coupled nature of soil freezing process and the nonlinearity of the equations that purportedly describe these processes. These uncertainties lead to considerable difficulty in the choice of the several approximation models to solve the overall system problem. Current numerical techniques require some form of decoupling of processes and linearization in order to obtain a solution. Consequently, the development of a model is necessarily somewhat complicated.

A conceptual engineering approach is to use available well established physics-based equations to model the processes that are perceived to be adequately defined. This includes heat transport in frozen and unfrozen zones and moisture transport in unfrozen zones. For processes not well understood, such as occur in freezing zones, one may use lumped phenomenological approaches. As a result of these two modeling approaches a deterministic multiparameter model will result which will require phenomenological parameters that can only be determined by model calibration. As a consequence, verification of the model may be somewhat compromised. Depending upon how such a model is formulated it may be modified as future research refines the phenomenological assumptions.

An economical way of proceeding with this task is to first develop a one-dimensional model to test and refine modeling concepts. This phase of the

research has essentially been completed. Since 1979 the U.S.Army, Cold Regions Research and Engineering Laboratory (Guymon et al, 1982) has been developing a model of frost heave, thaw consolidation and thaw weakening, applicable to roadways and airfields. A major objective of this model is that it be ultimately user oriented, available to geotechnical engineers, and that it generally require parameters that are economically obtainable in standard geotechnical laboratories. Development of this model has been reported upon as follows. Guymon, et al (1980) and Berg, et al (1980) represented the concepts of a modeling approach and presented early verification and sensitivity results. Subsequently, Guymon, et al (1981a) presented additional verification results, and Hromadka, et al (1982) presented a detailed evaluation of model sensitivity to the choice of numerical analog. Guymon, et al (1981b) evaluate parameter sensitivity and develop a probabilistic model which is cascaded with the deterministic one-dimensional model. Finally, Guymon, et al (1982) are preparing a detailed report of exhaustive laboratory and field verification results of the one-dimensional deterministic model. Any additional improvements in modeling frost heave will require different modeling strategies and better knowledge of the physics of dynamic ice segregation processes and moisture transport in frozen soil.

Assuming the one-dimensional modeling strategy is reasonable, the next step is the development of a two-dimensional model. Because the above cited references explain modeling concepts in detail, only a brief discussion of the two-dimensional model will be presented below. Model assumptions are as follows:

1. Moisture flow occurs in unfrozen zones by liquid water film driven by hydraulic gradients and may be estimated by Darcy's law.
2. Moisture flow in frozen zones is negligible.
3. Sensible heat transport in all zones is governed by the heat transport equation.

4. Phase change effects may be decoupled from the govern transport equations and approximated as an isothermal freezing process.
5. Unfrozen zones are nondeformable, and in freezing zones or frozen zones, deformation is due to ice segregation or lens thawing only.
6. Soil water pore pressures in freezing zones are governed by an unfrozen water content factor determined from soil freezing characteristics.
7. Hystereses is not present.
8. Salt exclusion processes are negligible.
9. Constant parameters (e.g. porosity) remain constant with respect to time; i.e. freeze-thaw cycles do not modify parameters.
10. Freezing and thawing processes in a two-dimensional medium occur in such a way so that there are no internal shear or stress forces developed between different zones.

The equations for the two-dimensional model are summarized in Table 1. The moisture flow equation is solved using total head at the state variable rather than using pore water pressure as is customary in much of the literature. The motivation for using energy head is that the numerical analog "stiffness" matrix will be symmetrical, reducing computer memory requirements. The convective terms of the heat transport equation

$$C_w \left(v_x \frac{\partial T}{\partial x} + v_y \frac{\partial T}{\partial y} \right)$$

are approximated as a space-time average from a previous solution timestep so that these terms may be included in the numerical analog load vector term.

Table 1. Deterministic equations for two-dimensional frost heave model *

Soil region	Energy state	Liquid moisture transport	Phase change	Sensible heat transport
Freezing surface boundary		$\partial\phi/\partial n = 0$		$T_u = T(t) \leq T_f$
Frozen	$T<T_f$ $u = u(\theta_n + \delta\sigma/\gamma)$ $\delta = \begin{cases} 1, \theta_l \geq \theta_o - \theta_n \\ 0\ \theta_l < \theta_o - \epsilon_n \end{cases}$	$\nabla \phi = 0$	$\frac{\partial \theta_i}{\partial t} = 0$	$K_T \nabla^2 T = C_m \frac{\partial T}{\partial t}$
Freezing or Thawing	$T = T_f$ $u(\theta_n) < u < 0$	$\frac{\partial \theta_u}{\partial t} = K_{ll} \nabla^2 \phi$	$-\frac{\rho_i}{\rho_w} \frac{\partial \theta_i}{\partial t}$ $L \frac{\rho_i}{\rho_w} \frac{\partial \theta_i}{\partial t}$	$+ K_T \nabla^2 T = C_m \frac{\partial T}{\partial t} + C_w \left[v_x \frac{\partial T}{\partial x} + v_y \frac{\partial T}{\partial y} \right]$
Unfrozen	$T>T_f$ $u(\theta_n) < u < u_L$	$\frac{\partial \theta_u}{\partial t} = K_{ll} \nabla^2 \phi$	$\frac{\partial \theta_i}{\partial t} = 0$	$K_T \nabla^2 T = C_m \frac{\partial T}{\partial t} + C_w \left[v_x \frac{\partial T}{\partial x} + v_y \frac{\partial T}{\partial y} \right]$
Unfrozen surface boundary		$u_L = u(t)$		$T_L = T(t) > T_f$

* See NOTATION for a definition of symbols. Ancillary relationships are described in text.

Thus, the numerical analog "stiffness" matrix will be symmetrical, reducing computer memory storage requirements. One of the objectives is to avoid the need of mainframe computers and develop a code that will run on the now widespread mini-class computers.

Latent heat terms are typically handled by the so-called apparent heat capacity approach (Luikov, 1966). While there are no apparent theoretical problems in using this approach for models that incorporate heat transfer alone, Hromadka, et al (1981) show that for coupled problems, the use of the apparent heat capacity concept may lead to inconsistent models with undesirable restraints on parameters. Also, the use of the apparent heat capacity concept appears to restrict numerical solutions to using undesirably small timesteps and spatial discretization. For these reasons, an isothermal approach is used to approximate phase change effects (Hromadka, et al, 1981). The algorithm is based on a simple control volume approach. A volume of freezing soil is not allowed to reach a subfreezing temperature until the latent heat of fusion of all available water for freezing in a control volume of soil is exhausted. However, if this procedure is used for a large region of soil, it is difficult to determine the location of the freezing or thawing isotherm. Because there is a large difference in mechanical strength properties between frozen and unfrozen soil, the locations of the freezing isotherm is important and the freezing or thawing isotherm must be relatively precisely defined. This is done by using a pseudo apparent heat capacity approach. The numerical analog mass matrix diagonal terms are weighted so that phase change effects are lumped at nodal points whose associated control volumes are undergoing soil water phase change.

A number of ancillary relationships are required in order to solve the two transport equations. DeVries (1966) relationship (2) is used to compute the heat capacity and thermal conductivity of the soil-water-air-ice mixture. Solution of (3) requires that the relationship between pore water pressure and water content be known where the temporal term is replaced by

$$\frac{\partial \theta_u}{\partial u} \frac{\partial \phi}{\partial t}$$

The partial, $\partial \theta_u / \partial u$, is determined from Gardner's (1958) relationship (6). Additionally, this same relationship is used to relate hydraulic conductivity to pore water pressure; i.e.

$$K_H(u) = \frac{K_o}{A_K |u|^m + 1} \tag{7}$$

where K_o = saturated hydraulic conductivity (permeability) and A_K and m are parameters for a given soil. Hydraulic conductivity in freezing zones is estimated by the phenomenological relationship, (5).

Pore water pressures at freezing fronts, which largely determine the hydraulic gradient toward a freezing front, are determined by

$$u = u(\vartheta_n) \tag{8}$$

where ϑ_n = a constant unfrozen water content factor. Although (8) is dependent on temperature (Anderson, et al, 1973) and perhaps pressure, a constant value is used in the current version of the model.

Pore pressures, particularly at freezing fronts, may be modified by total stresses, σ, and by excess pore pressures, u_e, if consolidation occurs. Total stresses are the sum of overburden and surcharge stresses. Excess pore pressures may be modeled by Terzagi's consolidation theory. Only total stresses

are considered, and these are only considered if ice segregation is occurring in a freezing zone. If ice segregation is not occurring, the total stress is assumed to be supported by the soil matrix. If ice segregation is occurring then negative pore water pressures given by (8) are modified by adding overburden and surcharge pressures u_o (expressed as equivalent hydraulic head), to (8); i.e.,

$$u_f = u(\theta_n) + u_o \tag{9}$$

where u_f is the pressure at the ice lens-water interface. The water film on the ice lens is presumed to support the total overburden and surcharge weight. While excess pore pressures, u_e, may be added to (9), we have found that these pressures are very small for frost susceptible silts and sandy silts and may conveniently be neglected. Equation (9) simulates the physical processes that are assumed to occur at ice segregation fronts. Overburden and surcharge stresses reduce negative pore water pressures given by (8), and thus reduce hydraulic gradients and moisture flow toward ice segregation fronts.

Auxiliary equations are required for boundary and initial conditions in order to solve the problem. Required initial conditions are soil-water temperatures, ice content, and pore water pressures. While any type of boundary conditions may be incorporated (e.g. a soil surface heat budget simulator) we have generally used a functional relationship for soil surface temperatures based upon the U.S.Army, Corps of Engineers n-factor approach (Berg, 1974). For pore pressure boundary conditions, the model assumes no moisture flux at frozen boundaries and uses a specified time-varying pore water pressure at other boundaries.

Parameters required in the multi-parameter model are summarized in Table 2. Other required parameters such as the latent heat of fusion of water, heat capacities of ice and water, and density of water are taken from standard thermodynamic tables.

Table 2. Parameters required for the two-dimensional frost heave model

Parameter	Description
n, A_w	characterize volumetric water content versus pore water pressure relationship for unfrozen soil
K_s	saturated hydraulic conductivity for unfrozen soil
m, A_K	characterize soil pore water pressure versus hydraulic conductivity relationship for unsaturated unfrozen soil
E	corrects unfrozen unsaturated hydraulic conductivity for hydraulic conductivity in partial frozen soil in freezing zone (a calibration factor)
θ_o	soil porosity
θ_n	unfrozen water content factor in freezing or frozen soil (minimum soil water content assumed to coexist with ice)
K_s	thermal conductivity of soil
ρ_s	density of soil
T_f	freezing point depression of soil water

AD-A118 264 CALIFORNIA UNIV IRVINE F/G 8/13
TWO-DIMENSIONAL NUMERICAL MODEL OF COUPLED HEAT AND MOISTURE TR--ETC(U)
AUG 82 G L GUYMON, T V HROMADKA DAAG29-79-C-0080
UNCLASSIFIED ARO-16278.25-GS NL

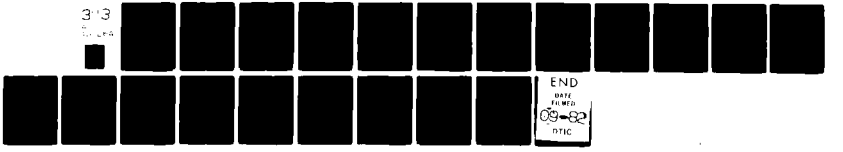

NUMERICAL ANALOG

The nodal domain integration method is used to solve the heat and moisture transport equations given in Table 1. This method has been presented in detail by Hromadka et al (1981) and elsewhere and will only be briefly reviewed here.

In order to develop a two-dimensional model which can be accommodated on mini-class computers and be used in studies cost effectively, extensive research in numerical methodology was undertaken. The main goal of this portion of research was to develop a numerical algorithm which produced a minimal level of relative error in approximation, and yet required a minimum computational effort. Due to the location of the freezing front being of primary interest in the total modeling approach, accurate calculation of temperature, soil water content, and other variables are required. As a result, the nodal domain integration approach was developed which adequately approximates the governing transport equations without the need of expensive expanding mesh algorithms or global system mesh regeneration requirements. In order to reduce computational requirements, numerical approximation simplifications are employed whenever possible.

The solution domain is discretized into finite elements, similar to the finite element procedure. For this model, we use triangular elements where the state variable is represented by linear trial functions. Depending upon how one defines a subdomain of integration for the partial differential operator, various numerical analogs may be developed; e.g. Galerkin finite element analog. Hromadka et al, (1981) show that an infinity of numerical analogs exist where the uncoupled linearized heat transport or moisture transport equations, given in Table 1, may be represented by the element matrix equation of the form

$$\underline{K}^e \phi_j + \underline{P}^e(n) \dot{\phi}_j = \{0\} \qquad (10)$$

where (10) is for the moisture transport equation and

where $\underline{K}^e$ = a symmetric banded conduction matrix identical to the usual stiffness matrix for linear trial function triangular elements (Zienkiewicz, 1977), $\underline{P}^e(\eta)$ = a symmetric banded capacitance matrix as a function of a mass weighting factor η, ϕ_j = a vector of unknown state variables at nodal points, and $\dot{\phi}_j$ = a vector of the time derivative of the unknown state variables. Matrix $\underline{P}^e(\eta)$ is given by

$$\underline{P}^e(\eta) = \frac{(\partial\theta_u/\partial u)^e A^e}{3(\eta + 2)} \begin{bmatrix} \eta & 1 & 1 \\ 1 & \eta & 1 \\ 1 & 1 & \eta \end{bmatrix} \qquad (11)$$

where e = a particular triangular element and A^e = the element area. When $\eta = 2$, the usual Galerkin finite element formulation is obtained for a linear trial function approximation. When $\eta = 22/7$ (approximately π), a subdomain integration formulation is obtained. When $\eta \to \infty$, an integrated finite difference formulation is obtained. Hromadka and Guymon (1982) show that η may be a function of time and that the best choice of a η depends upon the nature of the problem studied. For example, where sharp wetting fronts may occur in a porous media seepage problem, the integrated finite difference formulation generally results in less relative error than the Galerkin finite element formulation.

The derivation of (10) requires that parameters be held constant in each subdomain or element; however, parameters may vary from subdomain to subdomain. Additionally, each nonlinear partial differential equation is linearized where parameters are held constant for a small time interval. This procedure is in lieu of an iterative scheme to account for nonlinear parameters. This procedure is often valid for soil problems since the soil water phase change effects result in a damped system of partial differential equations.

For the entire solution domain, matrix (10) is assembled in an appropriate manner (Zienkiewicz, 1977) to form the system matrix equation

$$\underline{K}\,\phi_j + \underline{P}(n)\,\dot{\phi}_j = F_j \qquad (12)$$

where $\underline{K}$ and $\underline{P}(n)$ are square banded symmetric positive definite matrices, ϕ_j and $\dot{\phi}_j$ are, respectively, unknown nodal state variable and their temporal derivative, and F_j is a vector of known boundary conditions.

Solution of (12) is by a fully implicit approach which is required to solve problems where a free water surface exists within the solution domain (Neuman, 1973); i.e. (12) becomes

$$(\underline{K} + \underline{P}(n)/\Delta t)\phi_j^{t+\Delta t} - \underline{P}\,\phi_j^t/\Delta t = F_j^{t+\Delta t} \qquad (13)$$

where Δt = an appropriate timestep interval.

The solution procedure for both uncoupled equations of state (given in Table 1) is to use (13) to solve for the state variables ϕ and T. At specified intervals Δt^*, where $\Delta t^* \geq \Delta t$, all nonlinear parameters are recomputed, using the necessary ancillary relationships discussed previously, and the system matrices are "updated." Ice contents and secondary variables are computed at this time. Latent heat effects and total lumped ice segregation quantities are evaluated at each Δt timestep. Boundary condition information is updated at each Δt^* interval.

The numerical model, FROST2B, is coded in FORTRAN IV for use on mini-class computers. The model includes a front-end humanized, interactive data preparation program, PROTOØ, and a color graphics output program, ROAD. The model is coded in a modular form allowing easy modifications to a general class of problems. This version is for an arbitrary cross-section and does not permit the calculation of frost heave. A second version (D) is for a roadway embankment and permits frost heave calculations. FROST2D includes a mesh generator in order to keep track of differential frost heave at the roadway and embankment surface. All versions are capable of dealing with a layered soil profile.

MODEL VERIFICATION

Verification of a complex model, such as is presented above, is probably never complete. Each different application suggests some form of fine tuning of concepts or procedures imbedded in the model. In the case of the model developed here there are a number of submodels that require verification as well as the overall model system.

Guymon et al (1981) arbitrarily group frost heave modeling errors or uncertainty into four general categories:

1. Errors due to the choice of a model including the choice of a numberical analog
2. Errors due to spatial and temporal discretization and parameter averaging
3. Errors due to the choice of initial and boundary conditions
4. Errors due to the choice of parameters

The total modeling error is a function of the four general types of errors. Obviously, analytical solutions for comparison of model results are unavailable. Because of the nonlinear nature of the coupled problem and the model selected to represent frost heave, the only available method of verification is comparing model results to prototype data which may be a physical laboratory model or field situation. Even this approach is not entirely perfect because of uncertainty associated with boundary and initial conditions and parameters that arise in the model. While most of the parameters imbedded in the model have some presumed physical meaning and can be evaluated in a laboratory, the E-parameter can only be determined by calibration of the model. Sufficient calibration efforts may suggest a way of predetermining E in the future.

Linearized decoupled problems may be solved analytically to determine the accuracy of models. Because spatial and temporal discretiation interact with model errors, these problems need to be studied at the

same time. Most analytical solutions of freezing soil or bulk water are for one-dimensional columns. Thus, accuracy of a two-dimensional model may be studied by solving column problems oriented in the x-direction and then in the y-direction. This procedure was followed through several tests for both unsaturated soil moisture transport and heat transport, with and without phase change. For heat tranport alone, errors in the position of isotherms and particularly the freezing isotherm were less than 8 percent of relatively fine spatial discretization and fairly large timesteps. Errors could be reduced to less than 3 percent for smaller timesteps. Unsaturated soil moisture transport in a vertical column was evaluated by comparing to Philip's quasi-analytical solution as discussed in Guymon and Luthin (1974). Close agreement was obtained depending primarily on how frequent nonlinear hydraulic conductivity is updated in the model.

Additionally, the two-dimensional model was compared to one-dimensional model solutions and one-dimensional laboratory soil column tests. The one-dimensional model has been extensively verified against soil column data and field data (Guymon et al, 1981a; Guymon et al 1981b; and Guymon et al, 1982). Figure 1 shows an example comparison for a coupled heat and moisture transport problem involving Fairbanks silt. In this example, the column top was subjected to a -5°C temperature at time zero and the column bottom was maintained at the initial condition temperature of 1°C. A water table was maintained at the column bottom.

The two-dimensional model was tested against a number of isothermal unfrozen soil dam problems involving unsteady seepage with a free water surface. Figure 2 shows an example comparison of a model solution to experimental data and a solution of Vauclin et al (1975) for the phreatic surface for an unsteady ditch drainage problem. Experimental data and theoretical solutions compared favorably.

Figure 3 shows an example of a dam seepage problem where a dynamic model solution is compared to Unginchus' (1966) steady state theoretical solution.

Two-dimensional verification of the heat transport model has included comparison with field data for a freezing and thawing roadway embankment and a set of thawing data for a laboratory sand tank. In the first case model solutions were compared to sparce thermistor data for the summer and various winter times of the year at eight locations in a roadway. Boundary conditions were only approximately known and thermal properties of the different embankment materials were approximated from textural classification information. In all cases, estimated temperatures were within 1°C of measured temperatures. The position of the freezing isotherm was accurately estimated, errors being only a fraction of a foot in most cases.

The sand tank model consisted of a 3.92 m wide by 1.28 m deep tank of sandy silt that is over 4 m long to simulate two-dimensional thawing around a buried small diameter hot pipe. The embankment is initially frozen from the surface down by means of cold plates. Sides and bottoms are insulated to minimize heat loss. The upper boundary condition and pipe temperature boundary conditions are known. Side and bottom boundary conditions are assumed to be zero heat flux. Soil thermal parameters and initial soil ice contents were assumed. Because of symmetry only half the tank was analyzed, where at the pipe centerline, zero heat flux in the x-direction was assumed. A comparison of modeled and measured soil temperatures after one-day of initiating hot fluid flow in the buried pipe is shown in Figure 4. As time progresses, the solution at the bottom of the tank deviated somewhat from measured temperatures, primarily because of inaccurate representation of the bottom temperature and heat flux conditions.

Verification of the two-dimensional model for uncoupled moisture transport alone or uncoupled heat transport alone has demonstrated that these two important components of the overall model are accurately modeled. In particular, the isothermal freezing approach provides a relatively accurate and economical prediction of freezing and thawing phenomena. Rather large spatial discretization may be used. Unfortunately, we do not have a good data set for a two-dimensional frost heave prototype situation in order to further verify the model. However, one-dimensional data is available as described by Ingersoll and Berg, (1981). One-dimensional solutions using the two-dimensional model are identical to results achieved by the one-dimensional model which can accurately simulate unrestrained and restrained frost heave.

Evaluation of parameter errors and numerical analog errors have been extensively dealt with previously for the one-dimensional model (Guymon et al, 1981 and Hromadka et al, 1982). Similar to the one-dimensional model, the two-dimensional model is sensitive primarily to hydraulic conductivity parameters. Some success has been obtained in calibrating the E-parameter using split record tests. That is, the E-parameter may be calibrated using a one-year sequence of data, and without modification of parameters, a following one-year sequence of frost heave data may be reliably evaluated. Thermal parameters may be approximated without large error in results. This is primarily due to the fact that latent heat effects largely dominate the thermal regime of a freezing or thawing soil. It is emphasized that the model has been primarily tested against frost susceptible silts and dirty gravels. Additionally, the method of dealing with surcharge and overburden appears to only apply for relatively low overburden pressures (i.e., $u_o < 60$ kPa). The model tends to erroneously "cutoff" frost heave for large u_o.

EXAMPLE APPLICATIONS

The first problem considered is a buried chilled pipeline, 1.2 m in diameter. The problem domain is 4.3 m by 3.1 m in the horizontal and vertical dimensions, respectively. The soil is assumed to be a homogeneous Fairbanks silt with an initial homogeneous temperature of 0.5°C and pore pressure head of -70cm. Initial ice content is assumed to be zero throughout the soil region. The pipeline is assumed to be buried 1.2 m below the ground surface. The groundwater table effects are modeled by assuming a constant pore-pressure head of -70 cm 0.6 m below the bottom of the pipe. The solution is assumed to be symmetrical about the vertical centerline of the pipe. A constant thermal boundary condition of -2°C and .5°C is assumed at the top and bottom of the study region, respectively. The pipe surface is assumed to remain at a constant temperature of -.5°C. Overburden effects are not considered, and the total simulation is for 6 months. Estimated ice contents at the end of a 6-month period are plotted in Figure 5. Cross-hatched areas indicate regions in which ice contents exceed the assumed soil porosity and ice-segregation may be occurring. Dotted areas indicate where ice contents are approaching the assumed porosity.

Results of the two dimensional model are somewhat verified by assuming a one-dimensional problem at the vertical soil region furthest from the pipe. Comparison of one-dimensional model results to the pore pressures and temperatures computed by the two-dimensional version of the model were found to be in close agreement.

Frost heave is not estimated in this example because of the unknown effects of overburden and pipe interaction with the freezing soil. Also, the interaction between soil regions where ice segregation may be taking place and other soil regions is not known. For complicated geometry such as is considered in this example, only the heat transport and moisture transport aspects of the

model are valid. However, the tendency for ice segregation to occur can be qualitatively evaluated with the model.

A second example considered is a roadway embankment where it is assumed that soil interaction problems are minor and frost heave may be estimated. Figure 6 shows the soil solution domain for half of a roadway and the simulated frost heave at two different overburden values and for various days after initiation of freezing. Parameters for Fairbanks silt were assumed. A horizontal water table exists in the embankment as shown. Soil surface temperatures were assumed to be a constant -20°C and soil bottom temperatures were assumed to be a constant 1°C. Horizontal transport of moisture or heat at the solution domain sides was assumed to be zero.

As an approximate check, a one-dimensional solution, using the one-dimensional model, was compared to two-dimensional solution results at the roadway centerline and the right side of the solution domain. Centerline solutions compared very closely while right-side solutions using the one-dimensinal model were about 0.5 cm of heave greater than estimated with the two-dimensional model. However, the solutions were tending to converge after 30-days. The reason for this discrepancy may be that relatively large elements were used in the two-dimensional model.

Although this example is somewhat hypothetical, the results appear to be conceptually correct. The water table position strongly influences simulated heave. A rather small surcharge restrains frost heave somewhat. At the roadway edge, frost heave is reduced due to more rapid freezing caused by the surface geometry. At the embankment toe, frost heave is larger than for other areas for times up to 15-days because surface geometry results in less heat extraction.

DISCUSSION

A two-dimensional model of coupled heat and moisture transport in freezing or thawing soil is presented. For simple but useful geometries, frost heave or thaw consolidation may be estimated. The model is based upon well known transport equations to estimate heat and water transport for a soil freezing or thawing problem. Because the model is based upon incomplete theory for freezing zones, phenomenological relationships are also employed.

This results in a major limitation of the model since one phenomenological parameter (E) must be determined from laboratory freezing experiments or field data on a freezing soil. Guymon et al (1982) found that the E parameter may be reasonably evaluated for field cases provided a number of freeze-thaw cycles are included in the data.

Other parameters required for the model such as soil porosity and density can be routinely determined in the laboratory. However, hydraulic parameters such as unsaturated hydraulic conductivity and the unfrozen water content factor, θ_n, require specialized laboratories to determine them. Although there are such laboratories, their need is somewhat of a limitation to the routine employment of the model by the geotechnical cadre. In an effort to minimize this problem the U.S.Army-CRREL is attempting to analyze a large number of soils with the hope that this data may be of value in estimating sophisticated parameter without conducting costly tests. Some of this data is summarized in Guymon et al (1982).

The modeling approach used here is useful for problems involving dynamic coupled heat and moisture transport in which the primary variables of interest are soil temperature or water content (or pore water pressures) in frozen or unfrozen soils. We know of no other such two-dimensional model, reported in the open literature. The model is adaptable to a wide variety of problems and may be used for seepage problems alone or geothermal problems alone.

For simple but useful geometries, the proposed model may be used to estimate frost heave or thaw consolidation. Such estimates are only reasonably valid for geometries that do not involve appreciable interaction between soil masses where differential heave or thaw may be appreciable.

While we have experimented with different approaches of formulating numerical algorithms and believe we have assembled a good combination of these algorithms, we are by no means certain that we have assembled the best combination. We believe that this question should be the subject of continuing research.

As pointed out numerous times, the model we have investigated is incomplete from the standpoint of the thermodynamics of moisture in freezing zones. This drawback should not deter investigators in developing models which might be quite useful in a number of analysis problems. However, continued research to better define unknown areas should continue in order to improve analysis ability.

Finally, Guymon et al (1981) pointed out that purely deterministic models by themselves may never be adequate for modeling frost heave. Even if we had reasonably precise knowledge on all thermodynamic and physical processes involved, parameter uncertainty and perhaps boundary condition uncertainty requires some form of probabilistic approach. Assuming one reasonably formulates a deterministic model, as we believe we have done here, further model refinement may not yield better accuracy because parameter and boundary condition uncertainty may not permit more precise results. Most porous media flow models require some form of calibration and this is certainly true of the model we have presented here. Because both the one-dimensional model and two-dimensional model use identical parameters the one-dimensional model can be used to calibrate parameters (i.e. the E-factor) for each type of soil encountered in a two-dimensional problem.

ACKNOWLEDGMENTS

This research was supported by the U.S.Army Research Office (Grant No. DAAG29-79-C-0080). Mr. Chung-Cheng Yen assisted in verification analysis. Mr. David Esch of the Alaska Transportation and Public Facilities Department furnished temperature data on a roadway embankment, and the U.S.Army, Cold Regions Research and Engineering Laboratory, Hanover, New Hampshire furnished data on their sand tank model. We wish to particularly acknowledge the support and assistance of Dr. R. L. Berg, U.S.Army-CRREL.

SELECTED NOTATION

A_k, m = parameters describing unsaturated hydraulic conductivity of unfrozen soil

A_w, n = parameters describing soil moisture characteristics for unfrozen soil

C_m = volumetric thermal conductivity

C_w = volumetric heat capacity of water

E = calibration parameter

K_H = hydraulic conductivity for unfrozen soil

K_o = saturated hydraulic conductivity of unfrozen soil

K_T = thermal conductivity

L = volumetric latent heat of fusion of soil water (assumed to equal bulk water)

n = normal coordinate

ϕ = total hydraulic head

ρ_i = density of ice

ρ_w = density of water

t = time

T = temperature

T_t = freezing point depression of water

θ_i = volumetric ice content of soil

θ_n = unfrozen water content factor for frozen soil

θ_o = porosity of soil

θ_u = volumetric unfrozen water content of soil

u = pore water pressure expressed as hydraulic head

u_o = overburden pressure expressed a equivalent hydraulic head

v_x, v_y = velocity flux computed from Darcy's Law

x, y = Cartesian coordinates

REFERENCES

1. Anderson, D. M., Tice, A. R., and McKim, H. L., 1973. The unfrozen water and the apparent specific heat capacity of frozen ground. Second International Permafrost Conf., Yakutsk, U.S.S.R., North American Conference, National Acad. of Science, pp. 289-294.

2. Arakawa, K., 1966. Mathematical Model to Correlate Frost Heave of Pavements with Laboratory Predictions, U.S.Army, CRREL. Report 80-10.

3. Bear, J., 1979. Hydraulics of Groundwater. McGraw-Hill International Book Co.

4. Berg, R. L., 1974. Energy Balance on Paved Surface. U.S.Army, CRREL, Tech. Rpt. No. 226.

5. Berg, R. L., Guymon, G. L., and Johnson, T. C., 1980. Mathematical Model to Correlate Frost Heave of Pavements with Laboratory Predictions, U.S.Army, CRREL, Report 80-10.

6. DeVries, D. A., 1966. Thermal properties of soils. Physics of Plant Environment, (ed. by Van Wijk, W.R.). North-Holland, Amsterdam. pp. 210-235.

7. Everett, D. H., 1961. The thermodynamics of frost action in porous solids. Transactions of the Faraday Society, 57. pp. 1541-1551.

8. Farouki, O. T., 1981. Thermal properties of soil, U.S.Army, CRREL. Monograph 81-1.

9. Gardner, W. R., 1958. Some steady-state solutions of the unsaturated moisture flow equation with application to evaporation from a water table. Soil Science, 85. pp. 228-232.

10. Guymon, G. L., Berg, R. L., Johnson, T. C., and Hromadka II, T. V., 1982. Mathematical Model of Frost Heave in Pavements, U.S.Army, CRREL. Report under preparation.

11. Guymon, G. L., Berg, R. L., Johnson, T. C., and Hromadka II, T. V., 1981. Results from a mathematical model of frost heave. Transportation Research Record, 809. pp. 2-6.

12. Guymon, G. L., Harr, M. E., Berg, R. L., and Hromadka II, T. V., 1981. A probabilistic-deterministic analysis of one-dimensional ice segregation in a freezing soil column. Cold Regions Science and Technology, 5. pp. 127-140.

13. Guymon, G. L., Hromadka II, T. V., and Berg, R. L., 1980. A one-dimensional frost heave model based upon simulation of simultaneous heat and water flux. Cold Regions Science and Technology, 3. pp. 253-262.

14. Guymon, G. L., and Luthin, J. N., 1974. A coupled heat and moisture transport model for artic soils. Water Resources Research, 10(5). pp. 995-1001.

15. Harlan, R. L., 1974. Analysis of coupled heat: fluid transport in partially frozen soil. Water Resources Research, 9(5). pp. 1314-1323.

16. Hopke, S. W., 1980. A model for frost heave including overburden. Cold Regions Science and Technology, 3. pp. 111-147.

17. Hromadka II, T. V., and Guymon, G. L., 1982. Mass lumping models of the linear diffusion equation. Advances in Water Resources. In-press.

18. Hromadka II, T. V., Guymon, G. L., and Berg, R. L., 1982. Sensitivity of a frost heave model to the method of numerical simulation. Cold Regions Science and Technology. In-press.

19. Hromadka II, T. V., Guymon, G. L., and Berg, R. L., 1981. Some approaches to modeling phase change in freezing soils. Cold Regions Science and Technology, 4. pp. 137-140.

20. Hromadka II, T. V., Guymon, G. L., and Pardoen, G. C., 1981. Nodal domain integration model of unsaturated two-dimensional soil-water flow: development. Water Resources Research, 17(5). pp. 1425-1430.

21. Ingersoll, J., and Berg, R. L., 1981. Simulating frost action using an instrumented soil column. Transportation Research Record, 809. pp. 34-42.

22. Jame, Y. W., 1978. Heat and mass transfer in freezing unsaturated soil. Ph.D. Dissertation, Univ. of Saskatchewan, Saskatoon.

23. Luikov, A. V., 1966. Heat and Mass Transfer in Cappilary-Porous Bodies. Pergamon, New York.

24. Lunardini, V. J., 1981. Heat Transfer in Cold Climates. Van Nostrand Reinhold Co., New York.

25. Nakano, Y., Tice, A., Oliphant, J., and Jenkins, T., 1982. Transport of water in frozen soil, II. Effects of ice on the transport of water under isothermal conditions. Advances in Water Resources. In-press.

26. Neuman, S. P., 1973. Saturated-unsaturated seepage by finite elements. Journal of the Hydraulics Division, Amer. Soc. of Civil Engrs., 99 (HY12). pp. 2233-2250.

27. Outcalt, S. I., 1980. A numerical model of ice lensing in freezing soils.

28. Penner, E., 1957. Soil moisture tension and ice segregation. Highway Reserach Board. Bull. 168. pp. 50-64.

29. Stefan, J., 1891. Uber die theorie des eisbildung, insbesonder uber die die eishildung in polormete. Ann. Phys. u Chem. 42(2). pp. 269-286.

30. Taylor, G. S., and Luthin, J. N., 1978. A model for coupled heat and moisture transfer during soil freezing. Canadian Geotechnical Journal, 15. pp. 548-555.

31. Unginchus, N. N., 1966. Seepage through earth dams. Israel Program for Scientific Translations, Jerusalem.

32. Vauclin, M., Vachaud, G., and Khanji, J., 1975. Two-dimensional numerical analysis of transient water transfer in saturated-unsaturated soils. Computer Simulation of Water Resources, (ed. by Vanteenkiste, G. C.). North-Holland, Amsterdam. pp. 299-323.

33. Williams, P. J., 1967. Properties and Behavior of Freezing Soils. Norwegian Geotechnical Institute, Oslo, Norway.

LIST OF FIGURES

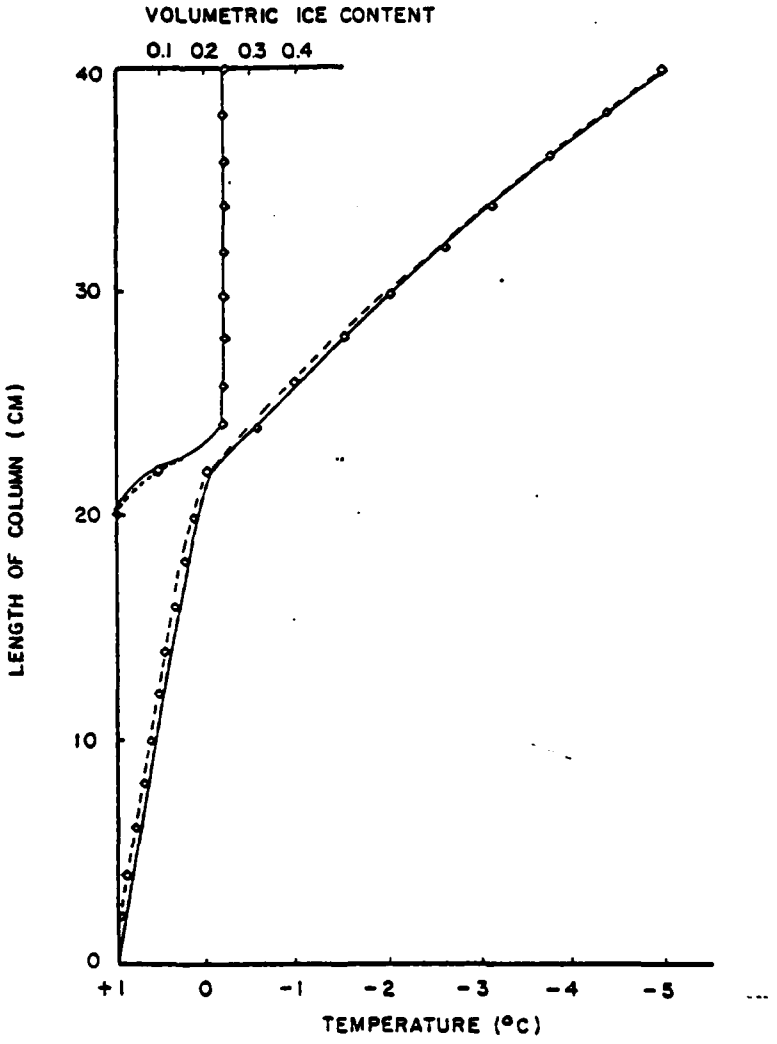
VOLUMETRIC ICE CONTENT
0.1 02 0.3 0.4
40
30
20
10
0
LENGTH OF COLUMN (CM)
+1 0 -1 -2 -3 -4 -5
TEMPERATURE (°C)

Figure 1

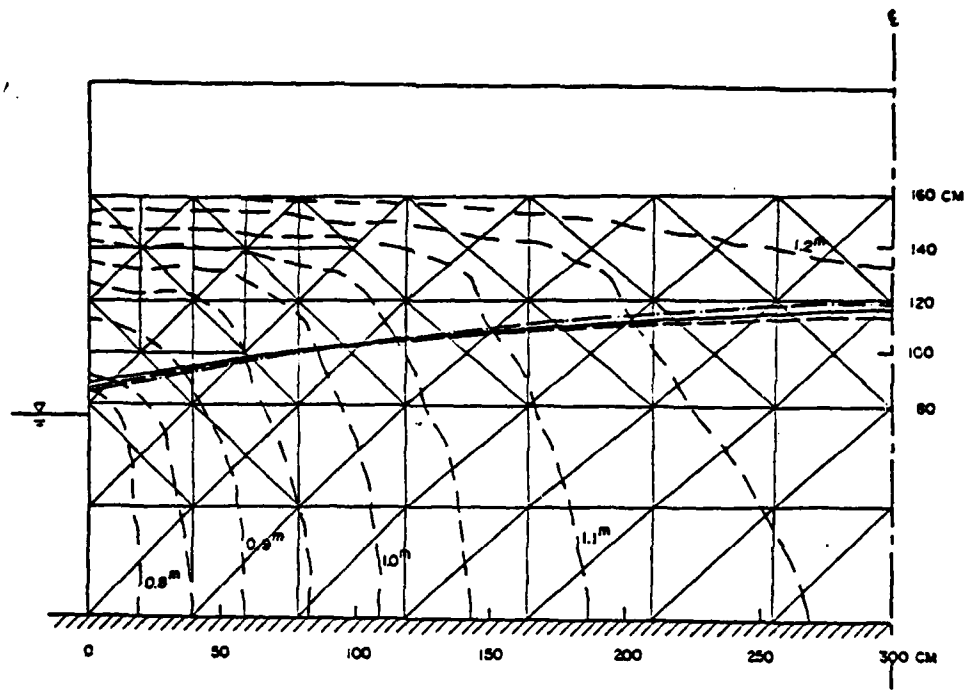

Figure 2

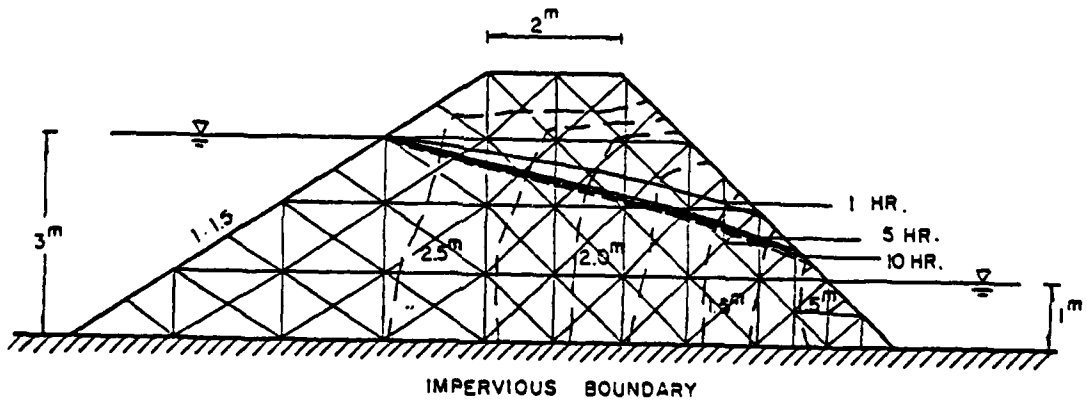

Figure 3

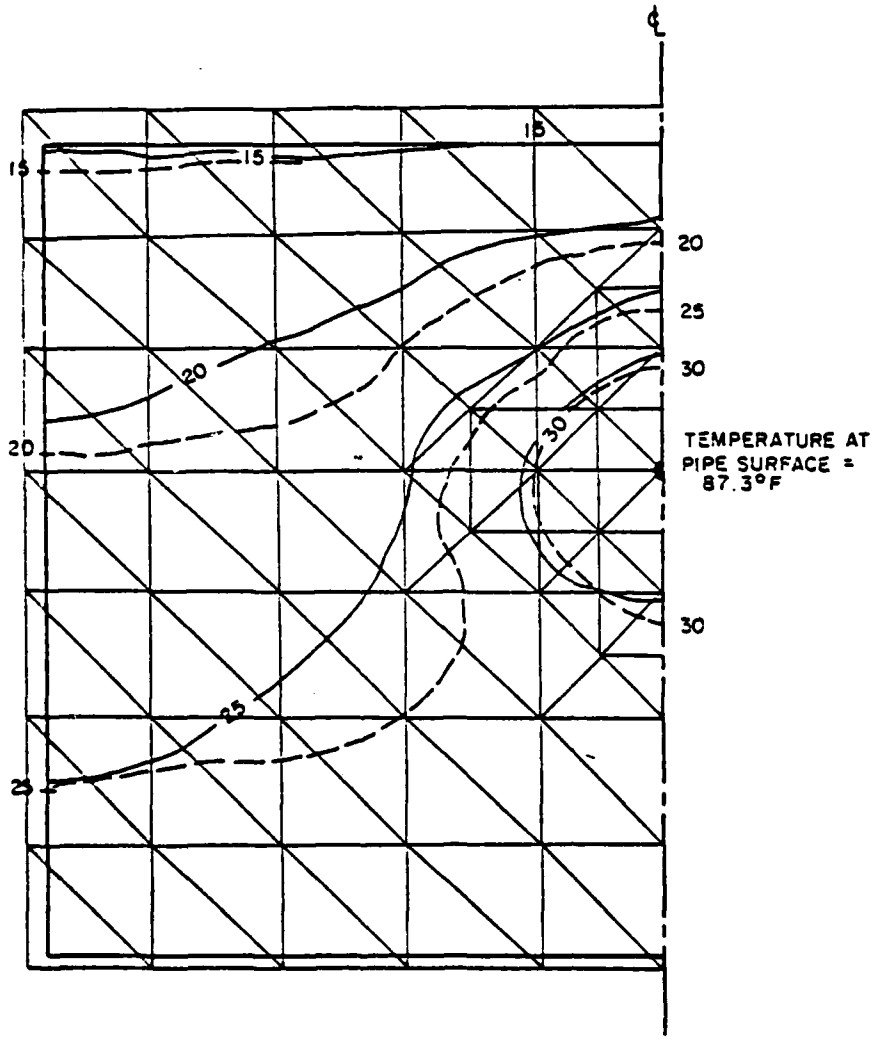

Figure 4

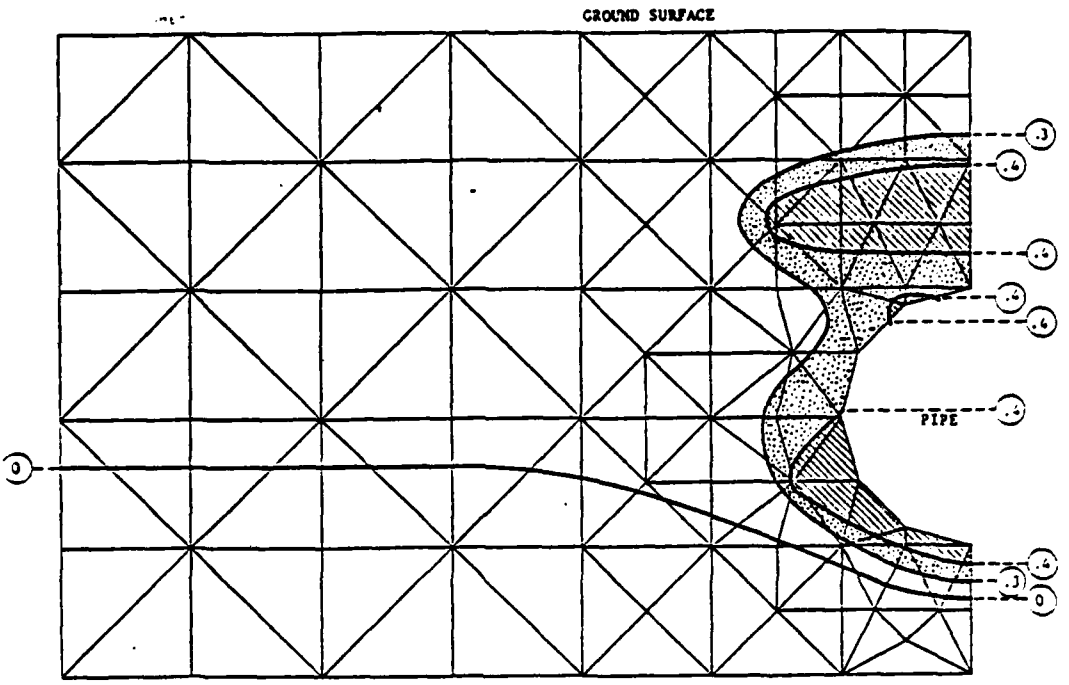

Figure 5

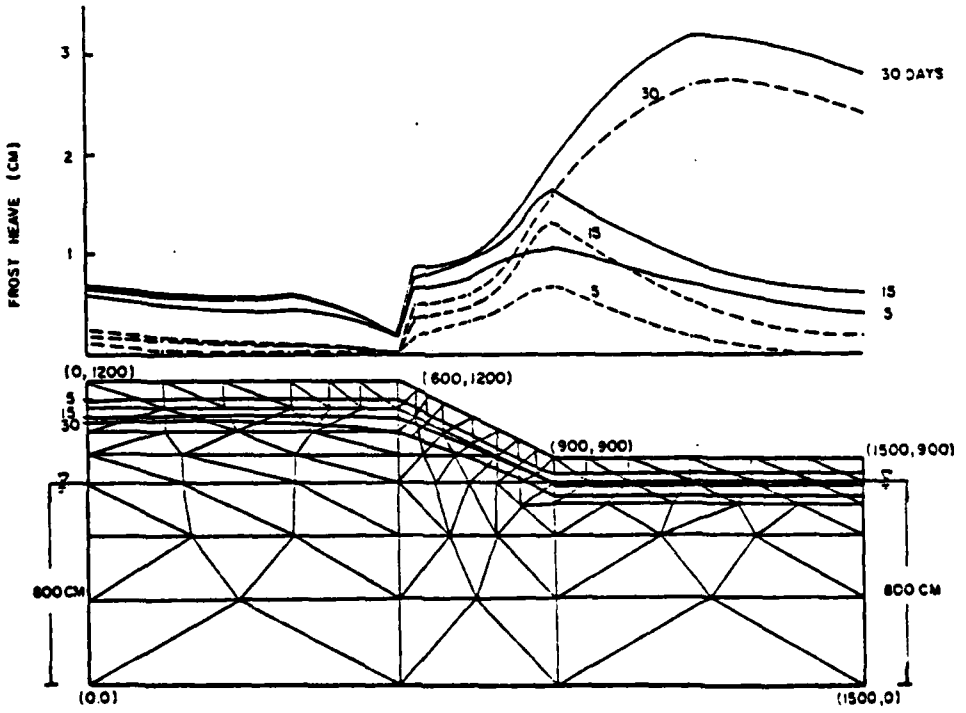

Figure 6

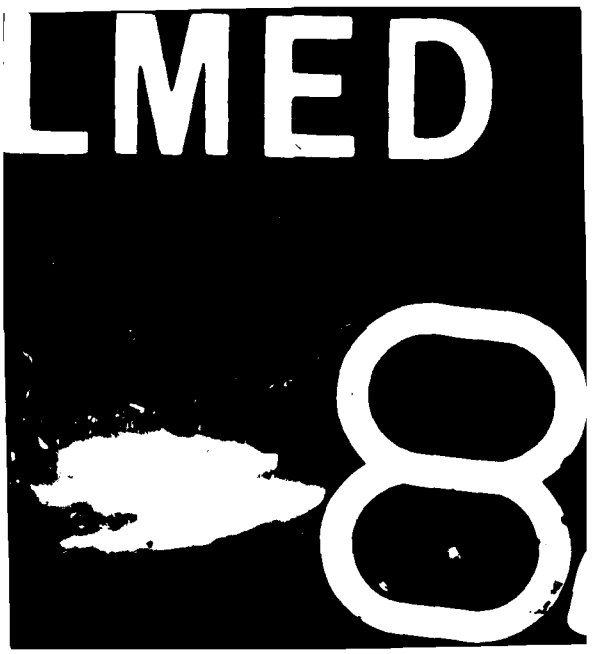
LMED
8